THE TETRAVALENT MANGANESE OXIDES: CLARIFICATION OF THEIR STRUCTURAL VARIATIONS AND RELATIONSHIPS AND CHARACTERIZATION OF THEIR OCCURRENCE IN THE TERRESTRIAL WEATHERING ENVIRONMENT AS DESERT VARNISH AND OTHER MANGANESE OXIDE CONCENTRATIONS

Thesis by

Russell Marsh Potter

In Partial Fulfillment of the Requirements

for the Degree of

Doctor of Philosophy

California Institute of Technology

Pasadena, California

1979

(Submitted November 8, 1978)

ACKNOWLEDGMENT

This thesis is not, of course, the product of my effort alone but the result of my interaction with a large number of people. Several I wish to thank especially. I count myself singularly fortunate to have had George Rossman as an adviser. Much of my growth in knowledge, in analytical and critical thought, and in verbal and written communication is a direct result of my interaction with him. He has provided guidance rather than a forced direction and has been a constant source of enthusiasm and interest in my work and that of those around me. Through guidance and discussion both in the field and in the office Bob Sharp has given me the benefit of his years of field experience; I am indebted to him for this and for his example as a man who, despite the many calls on his attention, nevertheless takes the time to provide help and encouragement to those around him. I wish to thank Heinz Lowenstam for this same thoughtfulness and encouragement.

Many people provided samples necessary for my work. I wish to thank them for their response to my requests and their interest in my work: Jim Bard, Al Bauman, George Brindley, Roger and Virginia Burns, Alice Corey, Skip Cunningham, Rock Currier, Marian Furst, Bernard Hallet, Julian Hayden, Arthur Jelinek, Tony Kampf, Edwin Larson, Vince Morgan, Ken Nealson, Gary Nowlan, Randy Perry, Jeri Rossman, Ron Stoessel, and John White, Jr.

Financial support was provided for Chapter 3 and parts of

Chapters 2 and 4 by the L.S.B. Leaky Foundation and the John S. McCarthy Foundation. I thank them for their support, without which this work could not have been done, and for the remarkable freedom from red tape.

My typist, Joanne Clark, has made the final stages of thesis preparation rather more of a joy than the drudgery I had expected. I expect that there are few typists who, finding themselves in a burning car, would give thought to the thesis in the back seat.

ABSTRACT

A number of structural problems in the mineralogy of the tetravalent manganese oxides have been addressed by infrared spectroscopy in conjunction with X-ray diffraction and chemical analysis. The first pyrolusite with proven orthorhombic symmetry is reported. Examination of pyrolusites with different degrees of orthorhombic distortion supports the view that this distortion is the result of micro-pores within the crystal. Pyrolusite infrared spectra exhibit variations which cannot be correlated to orthorhombic distortion, ramsdellite intergrowths, or other mineral impurity. The continuous structural variation of the nsutites from a ramsdellite end-member to a pyrolusite end-member has been confirmed although much of the variation in synthetic nsutites appears to be related to crystalline order. Ramsdellite has a single, crystallographically-ordered type of water, which appears to be an integral part of the structure. The only hydrous component of romanechite is water, which is located in the channels in a specific crystallographic site. The only hydrous component of lithiophorite is hydroxide ion, which is oriented perpendicular to the cleavage planes. Birnessite appears to have a layer structure on the basis of its infrared spectrum. Its identity with proposed synthetic analogs is confirmed. Todorokite is a valid mineral species which is not analogous to any synthetic phases or to any alteration products of them. It appears to have a layered structure. Rancieite probably has a layer structure related to birnessite.

It is possible to distinguish manganese oxides of different structural groups from one another by their spectra in the mid-infrared region, which is sensitive to the hydrous components and the manganese octahedral framework. Because of its sensitivity to short range order, infrared spectroscopy is often superior to X-ray diffraction for the determinative mineralogy of the manganese oxides, which often occur in a finely-particulate, poorly-crystalline state. Spectra in the region 4000 cm^{-1} to 200 cm^{-1} are presented for well-characterized manganese oxide samples in order to form a basis for identification of manganese oxide mineralogy. The following oxides are included: aurorite, birnessite, braunite, buserite, chalcophanite, coronadite, cryptomelane, groutite, hausmannite, hollandite, lithiophorite, manganite, manganosite, manjiroite, marokite, nsutite, partridgeite, pyrolusite, quenselite, ramsdellite, rancieite, romanechite (psilomelane), todorokite, and woodruffite.

This data base has been applied to the study of the mineralogy of manganese oxide concentrations of the terrestrial weathering environment. Through the integrated application of a variety of infrared spectroscopic, X-ray diffraction, electron optic, and chemical techniques, the characteristic mineralogy of desert varnish has been identified as birnessite, hematite, and mixed-layer illite-montmorillonite clay minerals. Clay minerals comprise greater than 70 percent of the varnish, the oxides constitute the bulk of the remainder and are in intimate physical association with the clays. An abrupt change in chemistry, mineralogy, and morphology exists at the varnish-rock interface. The origin of the

material is external to the rock which it coats. The clays are most likely transported by wind or water. The oxides appear to be transported by water. Clay minerals are necessary for varnish formation, probably through their influence on oxide concentration or deposition.

Morphological distinctions among desert varnish, manganese dendrites, river deposits and other manganese oxide concentrations of the terrestrial weathering environment have a sound basis in differences in their mineralogy. The manganese oxide in manganese dendrites is either romanechite or a hollandite group mineral. These are mixed with varying amounts of silicate minerals, which are a passive substrate for the oxide deposition. Manganese stream deposits are generally birnessite with minor amounts of silicate minerals; one nsutite stream deposit has been identified. Crack deposit mineralogy resembles that of manganese dendrites. Cave and subglacial deposit mineralogy resembles that of manganese stream deposits. No dendrite has been found to consist of pyrolusite. Hydropsilomelane concretions, which carry chemical remanent magnetization in sediments in Baja California, Mexico, consist of siltstone matrix minerals cemented by a manganese oxide having the chalcophanite structure. The high concentration of magnesium presumed to occur in the interlayer position of this mineral extends the known range of substitution in chalcophanite-structure minerals.

TABLE OF CONTENTS

page

CHAPTER 1
INTRODUCTION

THE PROBLEM

Manganese oxide concentrations are a common feature of the low-temperature environment. Examples can be found from most types of environments at the earth's weathering surface. Marine manganese nodules are of widespread occurrence on the sea floor; similar nodules are found in many freshwater lakes. Manganese concretions are common in soils and have been found in stream alluvium and young sediments. Manganese dendrites occur within and on the surfaces of rocks throughout the weathering environment. Rock surfaces in caves are frequently coated with manganese oxides. Desert varnish is a common feature on rock surfaces exposed in arid and semi-arid regions; and coatings of similar appearance occur in Antarctica, at high elevations in mountainous regions, in association with glaciers, and along streams in environments ranging from the tropical rain forests of South America to the arid southwestern United States.

Determination of the manganese mineralogy of many of these phenomena by X-ray diffraction has been difficult or impossible owing to the finely particulate and disordered nature of the manganese oxides and the presence of silicate phases as major components of the deposits. Consequently, little has been known of the mineralogy of the manganese oxide concentrations and the structural and genetic relationships among them. The distinctions between different types of concentrations has been based on the environment in which each is found and, sometimes, by its morphology. It has not been known

whether these distinctions reflect basic differences in structure and formation or whether each type of manganese oxide concentration represents a range of materials formed in various ways. One problem in dealing with the manganese oxide concentrations has thus been that of definition and classification. This problem lies primarily with the terrestrial deposits. The chemistry, mineralogy, form, and genesis of the marine manganese nodules have received much attention owing to their concentration of economically important metals.

Research into the structural and genetic nature of the terrestrial manganese oxide concentrations is prompted by three reasons besides the desire for order and understanding in widespread, natural phenomena: (1) Insight into the factors controlling the formation of marine manganese nodules and their absorption of metal cations may be gained through study of terrestrial manganese concentrations since some of them may be closely related to the nodules; (2) The trace element chemistry of terrestrial manganese oxide concentrations is gaining increasing study as a possible tool for geochemical prospecting. Efficient and reliable exploitation of their trace element chemistry requires an understanding of the concentrations' structures and formation processes; (3) Archeologists have hoped that a technique might be developed to determine the ages of surfaces coated with desert varnish based on measurement of some parameter of the varnish. Development of such a technique, even the assessment of its possibility, requires a knowledge of the structural and genetic nature of the varnish.

The problems encountered with the low-temperature manganese

deposits reflect basic complications in manganese oxide mineralogy. Those oxides which are of greatest importance in the weathering environment are commonly non-stoichiometric, of variable hydration state, and minute crystal size. Three-dimentional crystal structures have either not been possible or are in question, and there is confusion concerning the identity of natural materials with their synthetic analogs. Since these synthetic materials have been used to model the behavior of natural materials, their validity as structural analogs is important. Structural information on those oxides with unknown structures is important for understanding their cation absorption properties and their formation. Thus some aspects of the manganese oxide concentration problems require a more complete knowledge of manganese oxide mineralogy.

THE APPROACH

This thesis presents the results of research into the structural nature and relationships of the manganese oxides and of their concentrations in the terrestrial weathering environment. One major thrust of the work is in characterization of the concentrations themselves, particularly with respect to their mineralogy. The chemistry, mineralogy, and overall structural organization of the concentrations provide the most reliable constraints on possible formation mechanisms, and, as such, are a prerequisite for efficient investigation into the genetic relationships among the concentrations.

I focused my initial work on desert varnish. It is a striking and ubiquitous feature in the arid and semi-arid environment and combines potential for both geochemical prospecting and relative

age dating. The confusion in the literature regarding its formation mechanism and rate is a prime example of the effect of a lack of adequate characterization of the material itself. The difficulty in the mineralogical characterization of desert varnish is a direct result of three factors: its thin distribution on the rock surface, the finely-particulate and disordered nature of its oxide phases, and their intimate physical mixture with silicate phases. The sensitivity of infrared spectroscopy to amorphous materials and those with short-range order led to its use in studying desert varnish mineralogy. An approach integrating infrared spectroscopy, scanning electron microscopy, chemical analysis, and a number of chemical extraction techniques has proven effective in characterizing the chemistry, mineralogy, and overall structure of desert varnish.

Early in the work on desert varnish it became clear that manganese oxide infrared spectra in the literature were of insufficient quality and generality to allow reliable mineralogical identification. In addition, spectra of many of the manganese oxides were not available. Consequently, I began a compilation of spectra of well-characterized manganese oxides concurrently with the desert varnish research in order to determine the diagnostic infrared features of each of the manganese oxides. Emphasis was placed on the predominantly tetravalent manganese oxides, which are those most likely to be found in the weathering environment. As the compilation grew, I found that fundamental problems in manganese oxide mineralogy could be effectively addressed on the basis of infrared spectroscopy. The second major thrust of this thesis is an

investigation into the structural relationships among the tetravalent manganese oxides, their structural variations, and the use of infrared spectroscopy for their determinative mineralogy. Particular emphasis is placed on aspects which are closely related to manganese oxide concentrations of the low-temperature environment.

When my characterization studies of desert varnish were nearing completion, I expanded the scope of this research to include a wide range of low-temperature manganese oxide concentrations. This work is not a detailed study of chemistry, mineralogy, and overall structure as for desert varnish, but rather a survey designed to determine the degree to which morphology and environment are reflected in basic mineralogical differences among the concentrations and to suggest those areas which may be fruitful for further, more detailed investigation of the genetic and structural relationships among the concentrations.

Chapters 2-4, which contain the results of this research, are designed to be independent of one another although they are cross referenced when appropriate. Each has its own experimental section, appendixes, and set of references. Chapter 5 is devoted to concluding remarks based on all the chapters. It brings the conclusions into a coherent whole and, based on them, makes suggestions for future work.

CHAPTER 2

THE TETRAVALENT MANGANESE OXIDES: IDENTIFICATION, HYDRATION, AND STRUCTURAL RELATIONSHIPS BY INFRARED SPECTROSCOPY

1. INTRODUCTION

The finely-particulate and disordered nature of the manganese oxide in many of its concentrations in the weathering environment has made identification of its mineralogy difficult and sometimes impossible by means of X-ray diffraction, which is the traditional method of analysis. Characteristic X-ray powder diffraction lines are frequently broad, indistinct, or absent altogether and do not serve as a satisfactory basis for identification. The common occurrence of contaminating silicate phases in low-temperature manganese oxide deposits is an additional complication because their X-ray lines can sometimes be confused with those of the manganese oxides.

Problems of particle size and disorder are a characteristic of pure manganese oxides and have been responsible for the lack of understanding of manganese oxide crystal structures and structural relationships discussed in Chapter 1. X-ray powder diffraction patterns are the only structural data available on several of the oxides important in the weathering environment, and these generally show lines which are few in number, broad, and sometimes variable in position.

This work will show that infrared spectroscopy is often a necessary alternative and generally a useful supplement to X-ray diffraction for mineralogical analysis of the manganese oxides.

Because it is sensitive to amorphous components and those with short range order as well as to material with long range order, it yields a more complete and reliable description of materials such as the manganese oxides, where crystalline disorder may be expected. In addition, infrared spectroscopy is sensitive to the structural environment of the hydrous components, which is frequently diagnostic of the manganese oxide mineralogy.

Because infrared spectroscopy is not yet a primary structural technique like X-ray diffraction, it is necessary to "calibrate" it against well-crystallized materials whose mineralogy has been previously determined by X-ray diffraction. Once a mineral's characteristic infrared spectrum has been determined, it can then be used to identify this mineralogy in more disordered samples.

More than 20 predominantly tetravalent manganese oxide phases are recognized as valid mineral species (Burns and Burns, 1977a). This chapter presents the basis for determination of their mineralogy by infrared spectroscopy. It is a prerequisite to much of the mineralogical analyses of manganese oxide concentrations reported in subsequent chapters. The infrared spectra of many of the manganese oxides have been published (Gattow and Glemser, 1961a, 1961b; Glemser et al., 1961; Moenke, 1962; Valarelli et al., 1968; Agiorgitis, 1969; Kolta et al., 1971; van der Marel and Beutelspacher, 1976), but the quality of the data is generally too poor to show clear differences among the oxides. Using improved instrumentation and sample preparation techniques, I have found that the differences in the infrared spectra of the tetravalent manganese oxides are

sufficiently diagnostic to permit their identification in manganese oxide concentrations of the natural environment even when the oxides are highly disordered.

Chapter 2 also contains the results of research into some fundamental problems of tetravalent manganese oxide mineralogy. I have used infrared spectroscopy in conjunction with a variety of other techniques to investigate structural variations within the manganese oxides, to clarify understanding of the doubtful structures, to attempt to understand those structures which are as yet unknown, and to test the validity of synthetic materials as analogs of natural samples.

The presentation of these results follows the classification scheme of Burns and Burns (1975, 1977a, 1977b) for the tetravalent manganese oxides. This scheme is based on the nature of the polymerization of MnO_6 units, in which six oxygens surround a central manganese cation in approximately octahedral coordination. For each structure representative spectra are included with the text. Spectra of other samples are contained in Appendix B of this chapter as indicated in Table 1. Appendix figures are indicated by an "A" or "B" following the figure number. The intensities of infrared spectra may vary by a factor of 2 or 3 due to differences in sample particle size and dispersion in the pellet. For this reason I have presented the infrared spectra at concentrations such that all spectra have the same maximum intensity in the 1400 cm^{-1} to 200 cm^{-1} region. Each spectrum in the 4000 cm^{-1} to 1400 cm^{-1} region is presented at 4 times the concentration of its lower energy spectrum. The presentation

intensities listed in the figure captions allow the original intensity of the spectra to be calculated. The presentation intensity is 100 times the intensity in the figure divided by the intensity measured using the standard preparation techniques (Section 2).

2. EXPERIMENTAL DETAILS

Table 1 summarizes my data on the tetravalent manganese oxides. Determination of purity and mineralogy was done by X-ray powder diffraction using vanadium-filtered chromium radiation and a Debye-Scherrer camera. For some minerals the infrared spectrum is so distinctive that after an initial correlation was made between the X-ray diffraction pattern and the infrared spectrum, further X-ray work was not needed. When necessary, qualitative chemical analysis was used in addition to X-ray diffraction to determine mineralogy.

Infrared spectra were obtained with a Perkin-Elmer model 180 spectrophotometer on 2.0 mg of powdered sample dispersed in TlBr pellets for the 4000 cm^{-1} to 1400 cm^{-1} region and on 0.5 mg in TlBr and KBr pellets for the 1400 cm^{-1} to 200 cm^{-1} region. Pellets of 13 mm diameter were pressed for 1 minute at 19,000 psi. Since KBr is hygroscopic, it was not used in the 4000 cm^{-1} to 1400 cm^{-1} region, where water and hydroxide absorption occurs. TlBr is preferable to KBr since it is non-hygroscopic and, being a closer refractive index match to most manganese oxides, gives spectra of better quality. For this reason the figures presented are from TlBr pellets. Where the corresponding spectrum in KBr differs significantly, it is included in Appendix B. A vacuum dewar with KBr windows was used to obtain

Table 1: Sample information[1]

	sample #	locality	ident. #	ref. #	fig. #	purity x-ray	purity IR	chemistry
Pyrolusite MnO_2	1	Germany	CIT 2853		1B	pure	pure	
	2	Rossbach, Westphalia	CIT 4511		1B	pure	pure	
	3	Lake Valley, New Mexico	CIT 2402		1B	m,ram	pure	
	4	Nissan, Germany	HAV 93614		3,1B	pure	pure	58.3% Mn;(+3.96)
	5	Lake Valley, New Mexico	HAV 111929	2	2B	pure	pure	
	6	Sierra County, New Mexico	LCM 10995	2	3	pure	pure	59.5% Mn;(+3.94)
	7	Central New Mexico	CIT 2731		2B	pure	pure	
	8	Locality unknown	CIT 9430		2B	pure	pure	
	9	Synthetic	CIT 9431	3	3	pure	pure	60.0% Mn;(+3.92)
	10	Synthetic	CIT 9432	4	3	pure	pure	60.4% Mn;(+3.98)
	11	Synthetic	CIT 9433	5	3	pure	pure	61.8% Mn;(+3.99)
Nsutite $Mn(O,OH)_2 \cdot H_2O$	12	Nsuta, Ghana	CIT 9434		3B		pure	
	13	Salmchateau, Belgium	CIT 9196	6			m,cla	
	14	Hidalgo, Mexico	HWT M-23		4	pure	t,pyr	59.6% Mn;(+3.97)
	15	Oxen Claim, Utah	HWT UT-17	6			m,qtz	
	16	Synthetic	CIT 9435	7	5,3B	pure	pure	
	17	Synthetic	CIT 9436	8	4	pure	pure	58.4% Mn;(+3.63)
	18	Synthetic	CIT 9437	9	4,6,3B	pure	pure	59.5% Mn;(+3.89)
	19	Synthetic	CIT 0438	10	4	pure	pure	58.6% Mn;(+3.89)
Ramsdellite MnO_2	20	Chihuahua, Mexico	CIT 9439	11	7	pure	pure	
	21	Black Magic Mine, Calif.	CIT 9440		4B	t,hol	t,hol	
	22	Lake Valley, New Mexico	CIT 7486	12	4B	t,pyr	t,pyr	

Hollandite group								
Coronadite $PbMn_8O_{16}$	23	Broken Hill, N.S.W.	CIT 3523		5B		pure	*Mn,Pb,Si
	24	Bou Tazoutt, Morocco	HWT MOR-6	13,14	5B		pure	*Mn,Pb,v
	25	Inyo Co., Calif.	HAV 111927				M,qtz.	*Mn,Pb,Si
Crptomelane KMn_8O_{16}	26	Chihuahua, Mexico	CIT 9441	13	6B	t,tod	pure	*Mn,K,Ni,Fe
	27	Patagonia Mine, Arizona	HWT AR-22	13	9	pure	pure	*Mn,K
	28	Tiouine, Morocco	HWT MOR-1			t,qtz, brn	t,qtz	*Mn,K,Ba,Si,Al
	29	White Oak Mtn., Tenn.	HWT E-23		6B		pure	*Mn,K,Al,Si,Ba
	30	Synthetic	CIT 9442	15	6B	pure	pure	*Mn,K
Hollandite $BaMn_8O_{16}$	31	Soharis, Sweden	LCM 13875	14	7B		pure	*Mn,Ba,K,Ca,Fe,Al,Si
	32	Synthetic	CIT 9443	15	7B		pure	*Mn,Ba
Manjiroite $NaMn_8O_{16}$	33	Synthetic	CIT 9444	15	7B		pure	
Romanechite (Psilomelane) $(Ba,H_2O)_2Mn_5O_{10}$	34	Chihuahua, Mexico	CIT 9445	16	8B	pure	pure	
	35	Palos Verdes Hills, Calif.	CIT 9446	17	8B		t,brn	
	36	Mayfield Prospect, Texas	HWT, T-2		8B		pure	
	37	Pribble Mine, Virginia	HWT, E-48		10,8B		pure	
	38	Van Horne, Texas	HAV 97618	18	10	pure	pure	
Chalcophanite group								
Aurorite $(Mn,Ag,Ca)Mn_3O_7 \cdot 3H_2O$	39	Aurora Mine, Nevada	HST LU-21	19,20	9B		t,qtz	*Mn,Si,Ca,Cu,Ag,Zn,K,Ba
Chalcophanite $ZnMn_3O_7 \cdot 3H_2O$	40	Sterling Hill, New Jersey	CIT 406	13,21	12,9B	pure	pure	
	41	Sonora, Mexico	CIT 7134		9B		t,qtz	
Lithiophorite $(Al,Li)MnO_2(OH)_2$	42	Postmasburg, S.Africa	CIT 9447	22	13		pure	
	43	Sausalito, Calif.	CIT 7968		13,10B		pure	
	44	Greasy Cove, Alabama	HWT E-14	22	10B		pure	

Birnessite $(Na,Ca,K)Mn_7O_{14}\cdot 3H_2O$	45	Mt. St.Hilaire, Quebec	CIT 8509		11B	t,ser	m,ser	
	46	Boron, Calif.	CIT 9448	23		pure	t,sil	
	47	Cummington, Mass.	NMNH 115315	24	14	pure	t,cbn?	49.4% Mn;(+3.70)
	48	Synthetic, K	CIT 9449	25	11B	pure	pure	
	49	Synthetic, K	CIT 9450	26	14,11B	pure	pure	58.0% Mn;(+3.94);*Mn,K
	50	Synthetic, K	CIT 9451	27	14,11B	pure	pure	48.8% Mn;(+3.90)
	51	Synthetic, Mn	CIT 9452	28	14		pure	*Mn
	52	Synthetic, Na	CIT 9453	26	12B	pure	pure	*Mn,Na
	53	Synthetic, Ca	CIT 9454	26	12B	pure	pure	*Mn,Ca
	54	Synthetic, Na	CIT 9455	29	14	pure	pure	
Todorokite group								
Todorokite $(Mn,Ca,Mg)Mn_3O_7\cdot H_2O$	55	Palos Verdes Hills, Calif.	CIT 9456	17	15,13B		t,sil?	
	56	Chihuahua, Mexico	CIT 9457	11	13B		pure	
	57	Chihuahua, Mexico	CIT 9458	11	15		t,sil	
	58	Bombay, India	CIT 9459		15		pure	
	59	Miramati Mine, Japan	CIT 9460		13B		m,mgn	
	60	Charco Redondo, Cuba		30	15		pure	
	61	Unknown locality	HWT Mn-24	30	15		pure	
Woodruffite $(Zn,Mn)Mn_3O_7\cdot H_2O$	62	Sterling Hill, New Jersey	NMNH 114158	31	13B		pure	*Mn,Zn,Cu,Ca,Al
Rancieite $(Ca,Mn)Mn_4O_9\cdot 3H_2O$	63	Paxton's Cave, Virginia	NMNH 120601	32	17	pure	pure	
	64	Rancié Mtns., France	NMNH 128319	21, 32	17	t,tod	t,sil	
	65	Orienta Province, Cuba	HAV 110334	32	17,14B	m,brn	m,brn	
	66	Itia, Greece	CIT 9430	33	14B		pure	
Buserite $(Na,Mn)Mn_3O_7\cdot nH_2O$	67	Synthetic	CIT 9622	34	16	pure	pure	
	68	Synthetic, Co	CIT 9623	34	15B	pure	pure	
	69	Synthetic, Mn	CIT 9470	34	15B	m,bir, imp	pure	

Table 1 Footnotes

1. The following abbreviations are used for sample identification numbers: CIT = California Institute of Technology, HAV = Harvard University, LCM = Los Angeles County Museum of Natural History, HWT = The Hewett Collection in possession of the U.S. Geological Survey at Denver, Colorado, NMNH = National Museum of Natural History, The Smithsonian Institution; for X-ray and IR purity M indicates major impurities, m indicates minor impurities, t indicates trace impurites. I indicate a sample to be X-ray pure despite the presence of several weak lines which do not match other standard samples provided that these cannot be attributed to other phases. This was generally the case for the hollandite group and birnessite. The special case of pyrolusite is discussed in the text. For X-ray and Ir purity the following abbreviations are used: bir = birnessite, brn = braunite, cbn = carbonate, cla = clay minerals, hol = hollandite, imp = unidentified impurity, mgn = manganite, pyc = pyriochroite, pyr = pyrolusite, qtz = quartz, ser = serandite, sil = silicate, tod = todorokite. For chemistry the manganese oxidation state is enclosed in parentheses. Following *, elements detected by qualitative analysis are listed in approximate order of concentration; elements in trace quantity are underlined.
2. Mislabeled as ramsdellite in the collections.
3. Synthetic method: McKenzie, 1971.
4. Artificial δ-MnO_2; from National Carbon Company.
5. Manganese dioxide HP; from Diamond Shamrock Chemical Company; Baltimore, Maryland; 99.9% MnO_2, 0.005% Fe by their analysis.
6. Zwicker et al., 1962.
7. Synthetic method: preparation a for η'' - MnO_2 from Gattow and Glemser, 1961a.
8. Synthetic method: electrolytic preparation for η - MnO_2 from Gattow and Glemser, 1961a.
9. Synthetic method: Giovanoli et al., 1967.
10. Synthetic method: Giovanoli et al., 1967, 10.0 N HNO_3 was used in phace of 1.0 N HNO_3.
11. Finkelman et al., 1974.
12. Apparently a poor sample of Lake Valley ramsdellite since the ramsdellite structure was determined on material from Lake Valley.
13. Palanche et al., 1944.
14. Byström and Byström, 1950.

15. Synthetic method: preparation #1, McKenzie, 1971; Ba $(MnO_4)_2$ and $NaMnO_4$ were used in place of $KMnO_4$ for synthesis of hollandite and manjiroite[4] respectively.

16. The locality is described in Finkelman et al., 1974.

17. The locality is described in Mitchel and Corey, 1973.

18. Fleischer, 1960.

19. Radtke, et al., 1967.

20. Prior to analysis major calcite impurity was removed by 10 minute treatment with dilute acetic acid followed by washing with deionized water.

21. Wadsley, 1955.

22. Fleischer and Faust, 1963.

23. Brown et al., 1971.

24. Frondel et al., 1960a.

25. Synthetic method: The first preparation for δ-MnO_2 from Glemser et al., 1961.

26. Synthetic method: preparation #1, McKenzie, 1971; $Ca(MnO_4)_2$ and $NaMnO_4$ were used in place of $KMnO_4$ for synthesis of Ca and Na birnessites.

27. Synthesis method: as for preparation #8 (Buser et al., Table 4) but moles HCl = 0.125; from Buser et al., 1954.

28. Synthetic method: manganese(III) manganate(IV) was prepared according to Giovanoli et al., 1970b, and was dried 10 hours at room temperature under approximately 10^{-5} torr.

29. Synthetic method: Na manganese(II,III) manganate(IV) was prepared according to Giovanoli et al., 1970a, but was not dried. The solid from 0°C oxidation was washed by filtration and kept under deionized water.

30. Frondel et al., 1960b.

31. Frondel, 1953.

32. Richmond, 1969.

33. Bardossy and Brindley, 1978.

34. Synthetic method: buserite was prepared by the method of Giovanoli (1970a) for Na manganese(II,III) manganate(IV). The oxidation product was washed with deionized water and stored as an aqueous suspension. Co and Mn analogs were prepared by the method of McKenzie, 1971.

infrared spectra at liquid nitrogen temperature in the 4000 cm^{-1} to 1400 cm^{-1} region. Qualitative chemical analyses were done with an SEM equipped for energy dispersive X-ray analysis. Manganese oxidation state was determined by room temperature dissolution in excess 0.05 M Fe^{+2} in 0.5 M H_2SO_4 followed by back titration of excess Fe^{+2} with 0.002 M $KMnO_4$ and spectrophotometric determination of total Mn as MnO_4^-. This procedure is a modification of that by Moore (1950). Far-infrared spectra in the region 200 cm^{-1} to 35 cm^{-1} were obtained from a petroleum jelly mull of 10 mg of sample spread on a polyethylene plate.

3. THE CHAIN STRUCTURES: PYROLUSITE, NSUTITE, RAMSDELLITE

Structures

The chain structures of pyrolusite, nsutite, and ramsdellite are shown in Figure 1. In pyrolusite the octahedra share edges to form single chains along the c-axis. The chains are linked by shared vertices. In ramsdellite the chains are doubled by the sharing of edges between two adjacent single chains; these double chains are linked by shared vertices (Byström, 1949). Nsutite is thought (de Wolff, 1959; Laudy and de Wolff, 1963) to be a structural intergrowth of pyrolusite and ramsdellite in which layers of single and double chains alternate in random fashion. Thus, the possibility exists for a range of nsutites from a predominantly pyrolusite to a predominantly ramsdellite type.

Pyrolusite

Two structural forms of pyrolusite are thought to exist: the tetragonal form described above, which is characteristic of pyrolusite

Figure 1. Manganese oxide chain structures, looking approximately down c (Modified from Clark, 1972).

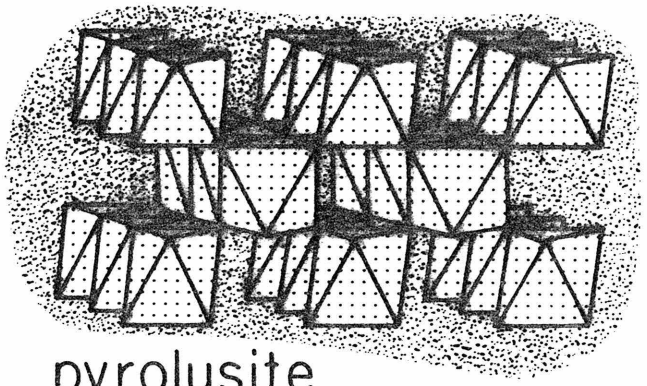

pyrolusite

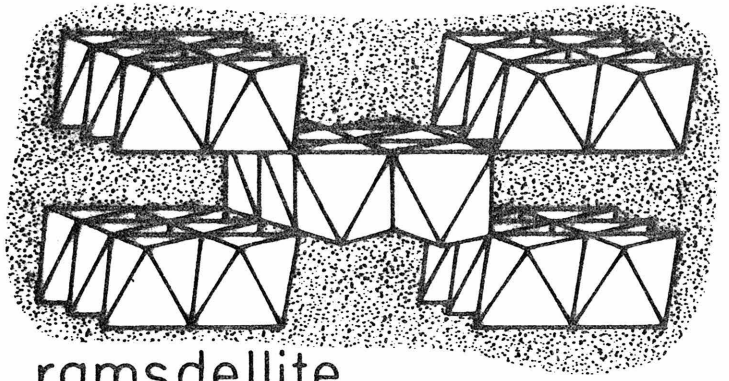

ramsdellite

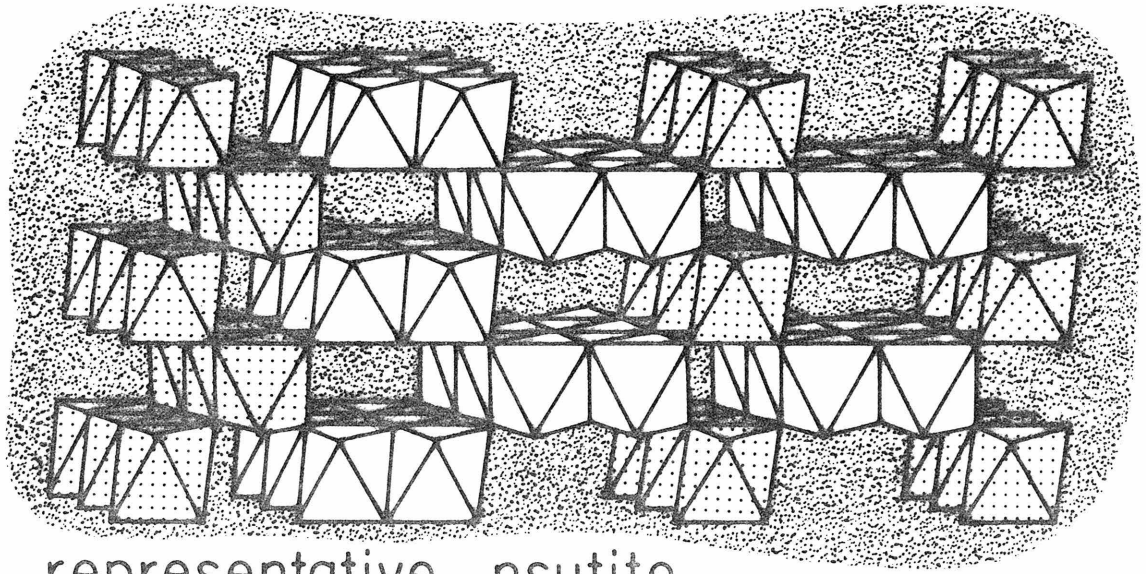

representative nsutite

pyrolusite

ramsdellite

of primary origin, and an orthorhombic modification characteristic of pyrolusite formed by alteration of manganite. No single crystal X-ray structural determination has yet been done for pyrolusite. The tetragonal structure is based on X-ray powder diffraction data, and the orthorhombic modification is postulated from broadening of several X-ray powder lines (de Wolff, 1959). Electron microscopy has revealed oriented lamellar pores in secondary pyrolusites which could be responsible for an orthorhombic distortion (Champness, 1971). Other possible causes are ramsdellite or manganite intergrowths.

The X-ray powder patterns of Figure 2 confirm the existence of an orthorhombic pyrolusite. The pyrolusite patterns are arranged in order of increasing broadness of the following lines (Miller indices in parenthesis): 2.20 Å (200), 1.97 Å (210), 1.62 Å (211), 1.391 Å (310), 1.305 Å (301), 1.203 Å (202). The 1.305 Å line is superimposed on line (112), which does not split. In pyrolusite #4 several of the lines are clearly resolved doublets and the overall pattern can be indexed to an orthorhombic cell bearing the following relation to the undistorted pyrolusite cell:

Tetragonal	orthorhombic
a = 4.42 Å	c = 4.44 Å
	a = 4.36 Å
c = 2.87 Å	b = 2.87 Å

The infrared spectra of this pyrolusite series support the conclusions of Champness (1971) regarding the origin of the orthorhombic distortion. The arrangement of these spectra (Figure 3) is based on that of the powder patterns. Although there is considerable variation, this variation bears no relation to the

Figure 2. X-ray powder diffraction patterns of the chain structure manganese oxides.

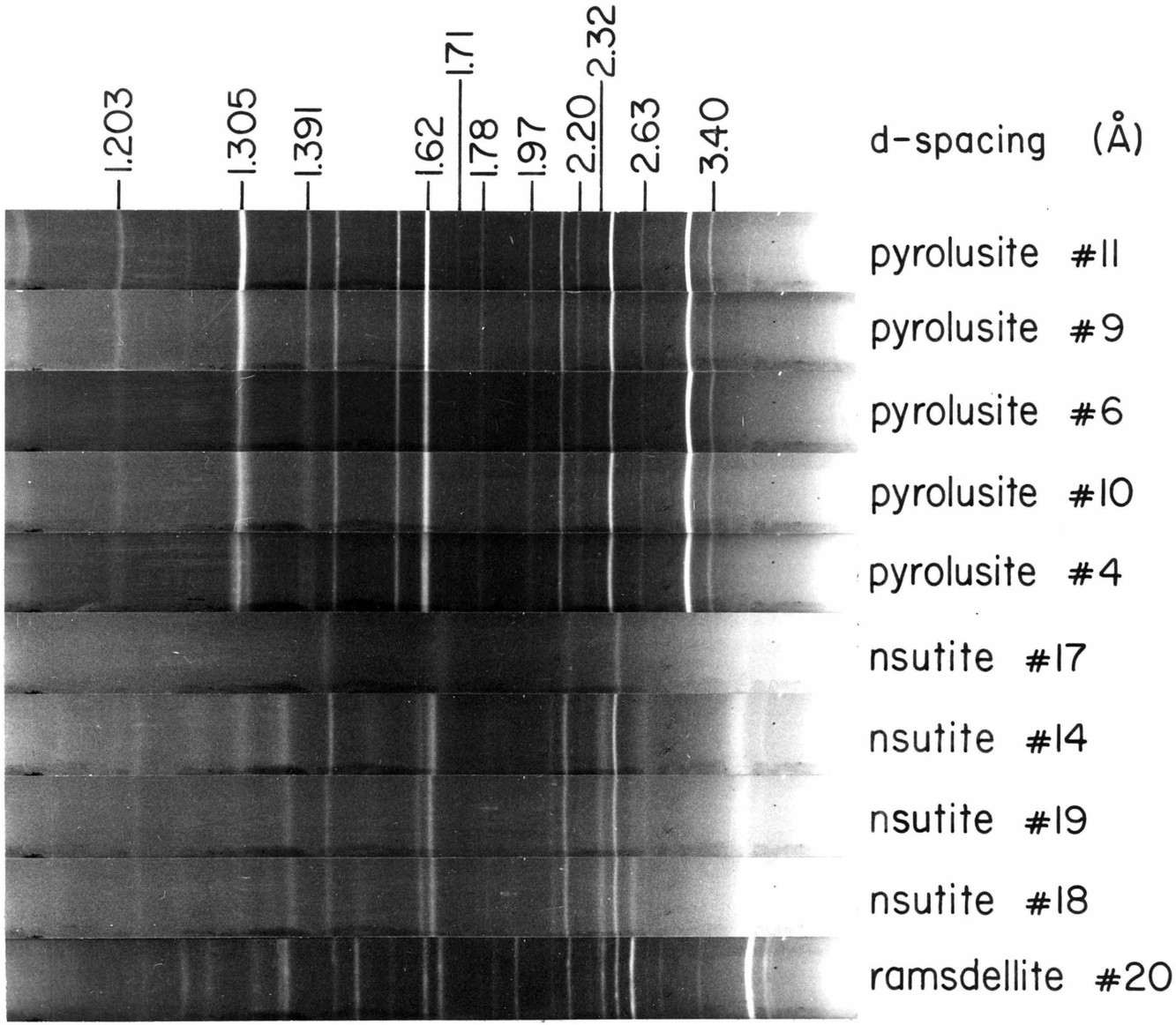
1.203
1.305
1.391
1.62
1.71
1.78
1.97
2.20
2.32
2.63
3.40
d-spacing (Å)
pyrolusite #11
pyrolusite #9
pyrolusite #6
pyrolusite #10
pyrolusite #4
nsutite #17
nsutite #14
nsutite #19
nsutite #18
ramsdellite #20

Figure 3. Infrared spectra of pyrolusites. Presentation intensities: #11, 161%; #9, 112%; #6, 143%; #10, 120%; #4, 127%.

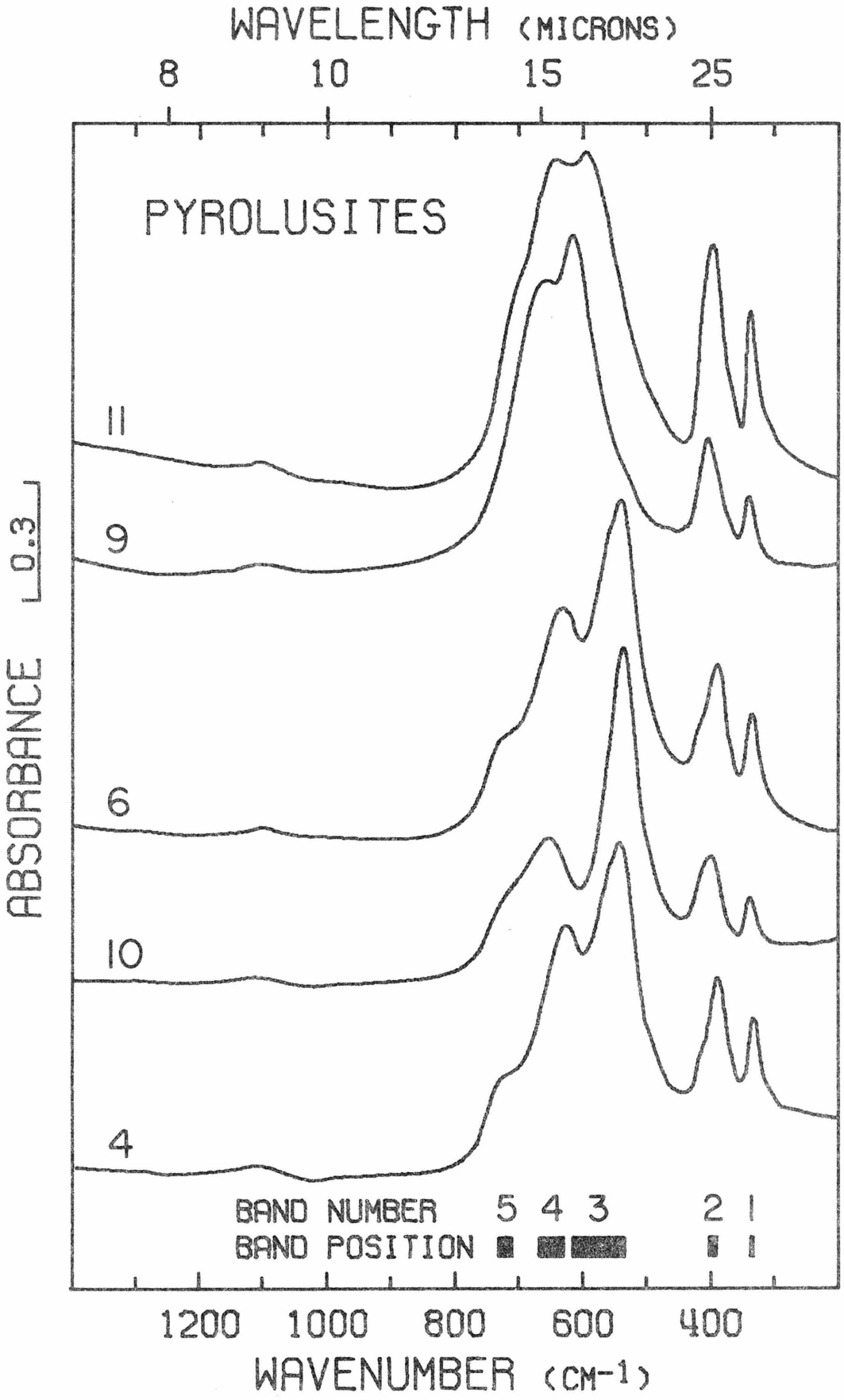
WAVELENGTH (MICRONS)
8
10
15
25
PYROLUSITES
11
9
6
10
4
0.3
ABSORBANCE
BAND NUMBER 5 4 3 2 1
BAND POSITION
1200
1000
800
600
400
WAVENUMBER (CM-1)

X-ray line broadening. This suggests that the structural basis for the orthorhombic distortion is one to which infrared spectroscopy is insensitive such as that suggested by Champness. The nsutite section will show that infrared spectroscopy is sensitive to changes in the concentration of ramsdellite double chains in a pyrolusite structure. Infrared spectroscopy is particularly sensitive to manganite due to its three sharp bands near 1100 cm^{-1} (Figure 4A). A weak band occurs in this region for all pyrolusite samples but its intensity bears no relation to orthorhombic distortion.

All the pyrolusite powder diffraction patterns contain lines at 3.40 Å, 2.63 Å, 2.32 Å, 1.78 Å, and 1.71 Å. These cannot be indexed on the tetragonal pyrolusite cell or on a superlattice of it. They can all be attributed to manganite, accounting for its four strongest lines. The weak infrared band near 1100 cm^{-1} present in all pyrolusites could be attributed to manganite or other hydroxide ion impurity or to an overtone of the intense absorption at lower energies. Even if attributed to manganite, it still limits the amount of manganite impurity to less than 5 percent for all the samples. The +3.99 manganese oxidation state found for pyrolusite #11 limits the amount of manganite to less than 1 percent although other pyrolusites could have as much as 8 percent based on their oxidation states. Their unindexed X-ray diffraction lines are not measurably stronger than those of pyrolusite #11. It appears that pyrolusites generally have some manganite impurity but that this does not cause the orthorhombic distortion.

The variation in the pyrolusite infrared spectra of Figure 3

is representative of pyrolusite samples in general and is a problem in its own right. Spectra are characterized by the following features:

Band 1: 335-340 cm^{-1}

Band 2: 390-400 cm^{-1}

Band 3: 535-615 cm^{-1}

Band 4: 630-670 cm^{-1}

Band 5: 705-735 cm^{-1}

Bands 1 and 2 show small variation in position and bear roughly the same intensity relationship to each other. Variation in the positions and relative intensities of bands 4 and 5 is somewhat greater, but the primary difference in the spectra is the position and relative intensity of band 3. Farmer (1974) has considered the effect particle shape would theoretically have on the infrared spectra of rutile, which is isostructural to pyrolusite and has a spectrum similar to it. He has suggested that this may be the cause of large variations in the infrared spectra of different powdered rutile samples. The major variation in going from a platy to a needle-like morphology is predicted to be a decrease in the band 3 position of several hundred wavenumbers, which is similar to the variations observed here for pyrolusite. Although scanning electron microcsopy did show variation in particle shape from needles to equant particles, this variation could be generated for a single sample by different grinding techniques with no effect on the position of band 3. It thus appears that particle shape is not responsible for the variation in pyrolusite infrared spectra.

Polarized reflectance spectra of pyrolusite #5 indicate that bands 1, 2, and 4 are polarized perpendicular to the c-axis and that band 3 is polarized parallel to the c-axis. Band 5 is not present in the reflectance spectra of pyrolusite #5, which is the only sample with single crystals large enough to yield reflectance spectra. These results are in complete agreement with the predictions of factor group analysis for the tetragonal pyrolusite structure. Band 3 is due to the displacement of the oxygen ions relative to the manganese ions along the direction of the octahedral chains (by analogy to isostructural rutile; Farmer, 1974). It is variation in the vibration frequency of this movement which is responsible for the major variation in the pyrolusite spectra, but it does not suggest any structural variation which may be its cause. The following section on nsutite will show that the presence of ramsdellite double chains is not responsible for the variation in the position of band 3, although it may be responsible for the presence of band 5 and the variation in the position of band 4. Manganese oxidation state (Table 1) is not correlated to the position of band 3.

In light of the unexplained variation in pyrolusite infrared spectra, the uncertainty regarding the unindexed X-ray lines, and the proven orthorhombic modification, detailed structural work on pyrolusite single crystals is warranted.

The positions and relative intensities of bands 1 and 2 uniquely and clearly distinguish pyrolusite from the other manganese oxides.

Nsutite

Natural and synthetic nsutites exhibit a range of X-ray diffraction patterns which have been interpreted as the result of variation in the number of pyrolusite single chains in a predominantly ramsdellite type double chain structure. The changes in X-ray line sharpness, number, and position in going from nsutite #18 to nsutite #17 in Figure 2 are in agreement with that expected in going from low to high "pyrolusite concentration" (de Wolff, 1959; Laudy and de Wolff, 1963). Heat treatment of nsutite produces a series of materials continuing this transition in X-ray pattern from that of nsutite to that of a disordered pyrolusite (Gattow and Glemser, 1961a; Brenet et al., 1958). Theoretical calculations (Laudy and de Wolff, 1963) have suggested that these represent increasing concentrations of pyrolusite single chains randomly distributed among the double chains rather than a physical mixture of pyrolusite and nsutite. This series is thus thought to represent a continuation of the structural series postulated for unheated samples.

Infrared spectroscopy has not shown the continuum expected if these series represent a continuous transition from ramsdellite to pyrolusite. The spectra presented in Figure 4 span the observed range of variation for unheated synthetic and natural samples. Their arrangement is based on that of their X-ray diffraction patterns in Figure 2. The spectra are characterized by the following features:

Band 1: 375-380 cm^{-1}

Band 2: 475 cm^{-1}

Band 3: 515-530 cm^{-1}

Band 4: 565-590 cm^{-1}

Band 5: 685-730 cm^{-1}

Although there is some variation in band position, particularly in the case of band 5, the differences in the nsutite spectra are primarily due to variation in band sharpness and relative intensity. The spectra show an increasing resemblance to that of ramsdellite (Figure 7) in accord with the X-ray data of Figure 2, but the nature of the trend is not continued for the heat-treated nsutites. I have progressively heated nsutite #19 and nsutite #16 and in each case obtained a series of X-ray powder patterns similar to that of Brenet et al. Both exhibit variations in infrared band position and intensity (Figures 5 and 6) which cannot be reproduced simply by addition of various proportions of pyrolusite and nsutite spectra. Figures 5 and 6 thus indicate the effect of varying "pyrolusite concentration." In each case with increasing "pyrolusite concentration" bands 2 and 5 (referring to Figure 4) shift smoothly to lower energies and band 2 shifts to higher energies. The other bands remain constant in position. The variation in Figure 4 is distinct from this. For example, heating nsutite #18 does not produce a material characterized by an infrared spectrum similar to nsutite #14 or #17. Instead each nsutite transforms toward a specific pyrolusite: nsutite #18 toward pyrolusite #10; nsutite #16 toward pyrolusite #9. Some property of the original nsutite thus "directs" it toward a specific pyrolusite on heating. It should be noted that pyrolusite band 3 has developed from different nsutite bands in Figures 5 and 6.

Figure 4. Infrared spectra of nsutites. Presentation intensities: #17, 145%; #14, 314%; #19, 78%; #18, 80%.

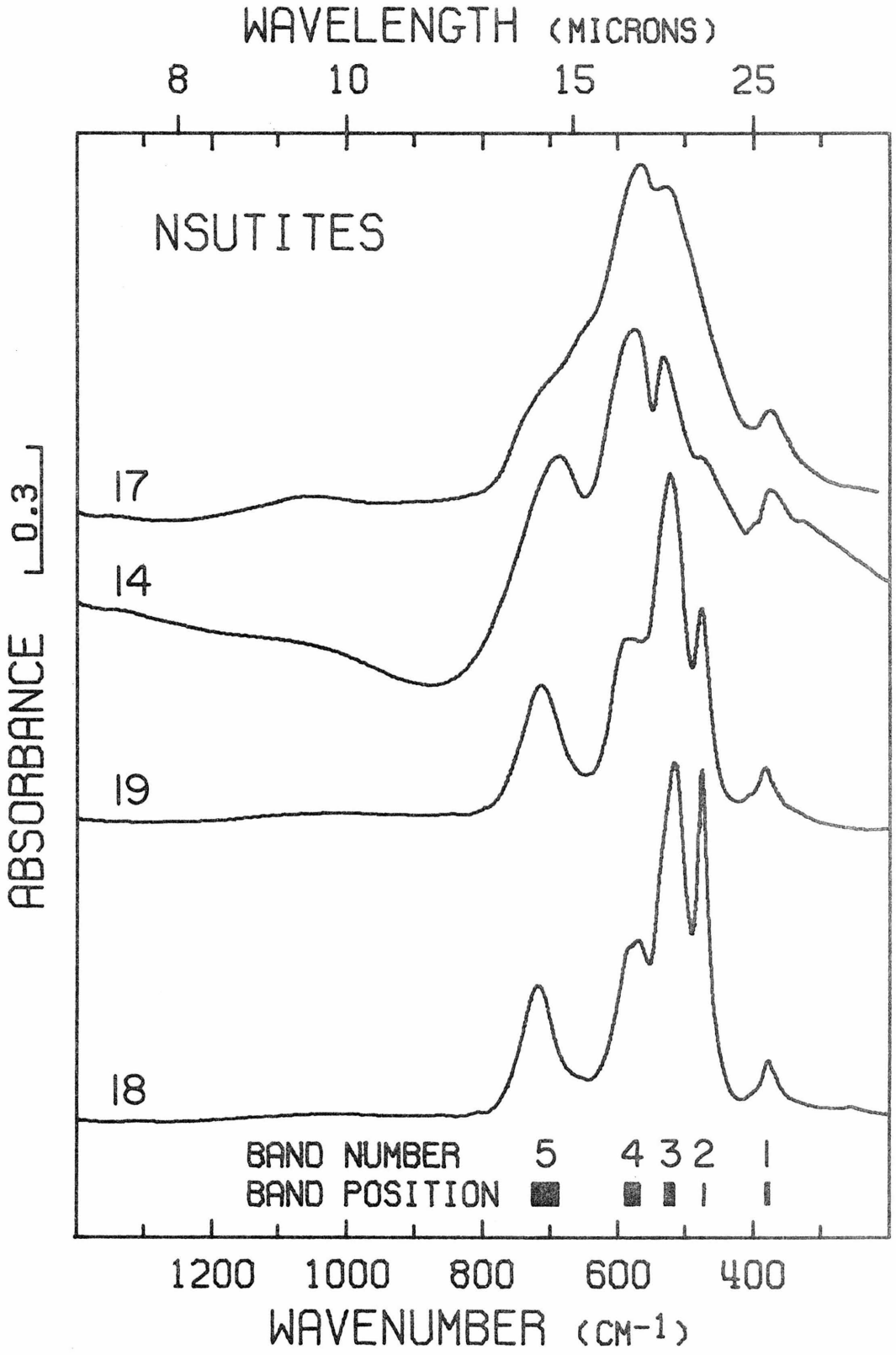
WAVELENGTH (MICRONS)
8
10
15
25
NSUTITES
17
14
19
18
0.3
ABSORBANCE
BAND NUMBER 5 4 3 2 1
BAND POSITION
1200
1000
800
600
400
WAVENUMBER (CM-1)

Figure 5. Infrared spectra of progressively heated nsutite #16. Presentation intensities: 480°C, 137%; 320°C, 120%; 270°C, 106%; 35°C, 105%.

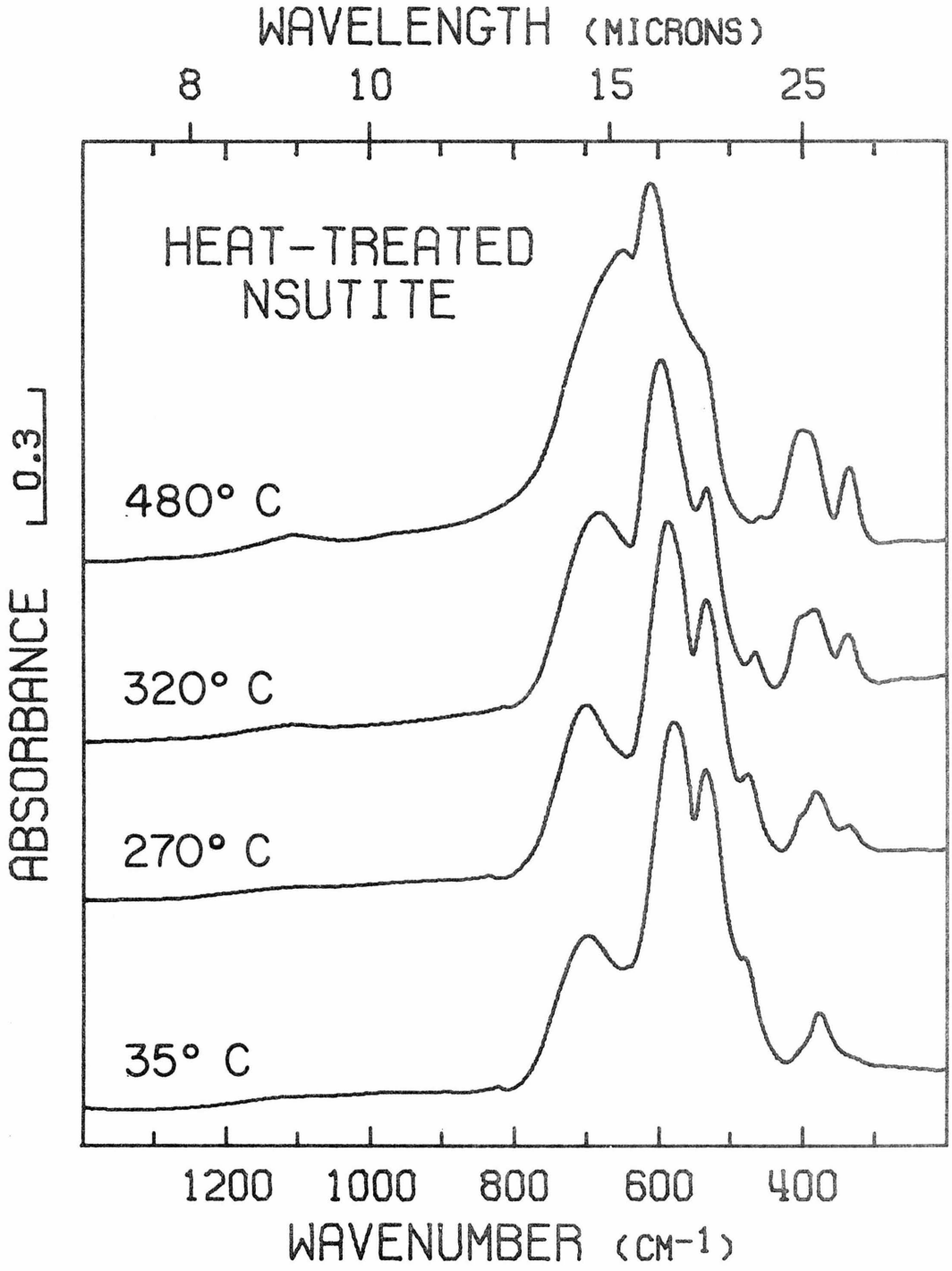
WAVELENGTH (MICRONS)
8
10
15
25
HEAT-TREATED
NSUTITE
480° C
320° C
270° C
35° C
ABSORBANCE
0.3
1200
1000
800
600
400
WAVENUMBER (CM-1)

Figure 6. Infrared spectra of progressively heated nsutite #18. Presentation intensities: 480°C, 62%; 320°C, 47%; 225°C, 66%; 35°C, 80%.

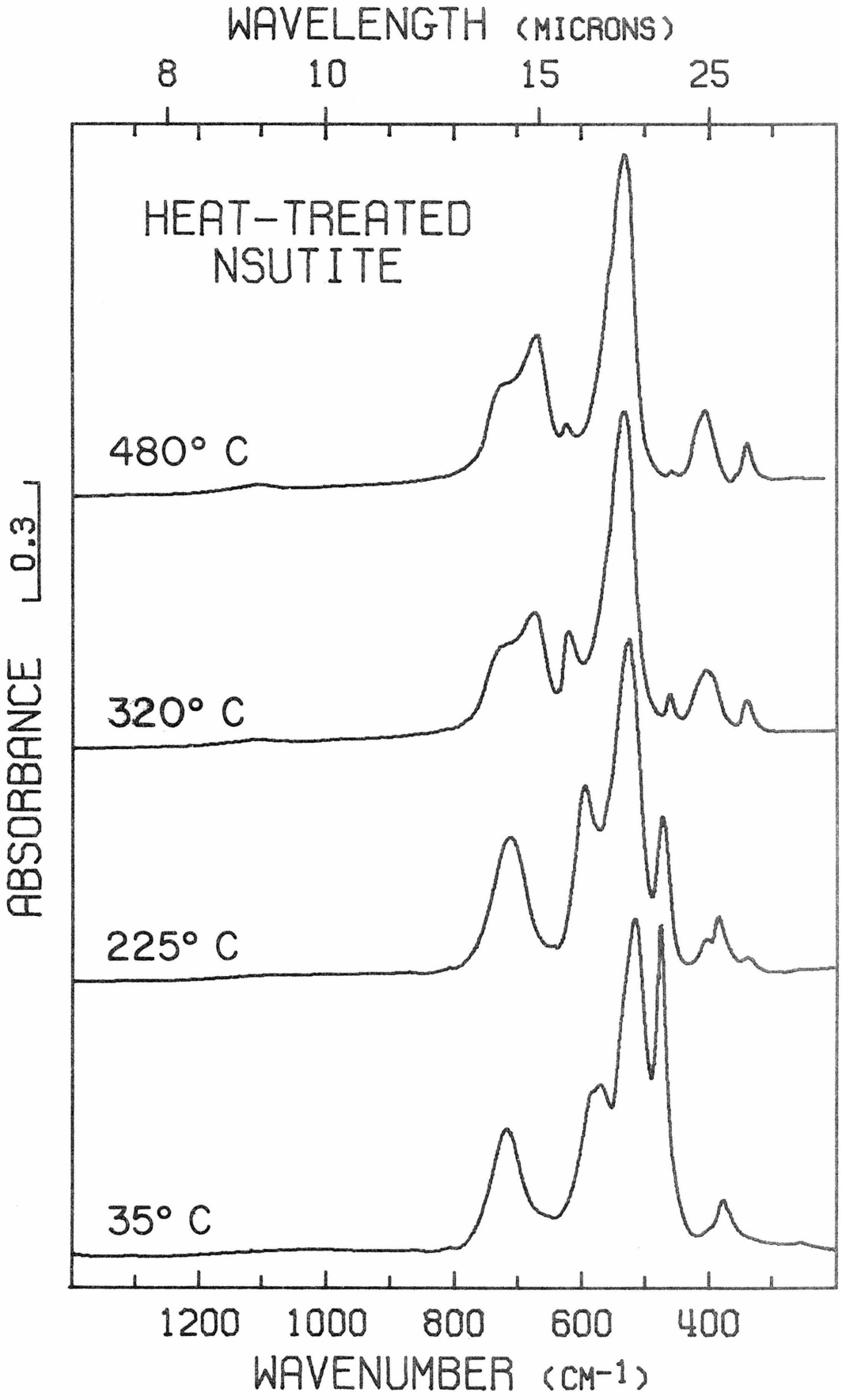
WAVELENGTH (MICRONS)
8
10
15
25
HEAT-TREATED
NSUTITE
480° C
320° C
225° C
35° C
ABSORBANCE
0.3
1200
1000
800
600
400
WAVENUMBER (CM-1)

Although the heat-treated nsutite series appears to be the result of variation in "pyrolusite concentration," the variation in the unheated series is primarily a reflection of the degree of crystalline order. In general, spectra of highly-ordered materials are characterized by sharp, well-defined absorption bands. As disorder increases, the bands become broader and less clearly resolved, but their wavenumber positions remain unchanged. Thus, Figure 4 exhibits an increasing degree of disorder from nsutite #18 to nsutite #17. This is reflected in the X-ray powder patterns as well. The decrease in sharpness and number of X-ray lines, which has commonly been interpreted as indicating a high "pyrolusite concentration" appears to be primarily indicative of disorder. Variation in manganese oxidation state (Table 1) bears no relation to the variation of Figure 4.

All nsutite spectra have a broad absorption in the region 3600 cm^{-1} to 3100 cm^{-1}. This is generally of low intensity but becomes more intense with decrease in crystalline order. It is attributable primarily to water in the more disordered cases, but may be either water or hydroxyl in those samples with a higher degree of order.

Nsutite #14 in Figure 4 is characteristic of the natural samples I have studied (Table 1). Natural processes at these localities apparently produce nsutites of similar crystalline order and "pyrolusite concentration."

The positions of band 1 and, in the lower energy part of its range of variation (Figure 4), band 5, distinguish natural nsutites

from the hollandite group, whose spectra are similar. Synthetic nsutites which have spectra close to that of ramsdellite can be distinguished from it by band 5, which is a single band in nsutite and split in ramsdellite and by the presence of the 3380 cm^{-1} band in ramsdellite. Infrared spectroscopy clearly distinguishes nsutite from other manganese oxides not discussed here.

Ramsdellite

The infrared spectrum of ramsdellite is shown in Figure 7. The X-ray powder pattern of this sample is shown at the bottom of Figure 2. Although I was able to obtain only one pure ramsdellite, spectra of three others were identical to Figure 7 in band number and position and with only minor variation in band intensity when absorption due to the impurities was subtracted.

The absorption at 3380 cm^{-1} and 1635 cm^{-1} occurs for all ramsdellite studied and is also present in pyrolusite #3, which contains ramsdellite impurity. The 1635 cm^{-1} band is due to an H_2O bending vibration. The intensity relationship of the two bands indicates that the major hydrous species is H_2O. The sharpness of the 3380 cm^{-1} band indicates that the water is in a well-defined crystallographic site. The ramsdellite structure was determined for a sample found to contain 1.3 percent water (Byström, 1949). This water was assumed to be an impurity. The presence of a crystallographically well-ordered water in all the ramsdellite samples argues strongly that it is an integral part of the ramsdellite structure. The intensities of the water bands are approximately the same intensity as those for the hydrous manganese oxide romanechite (Figure 10).

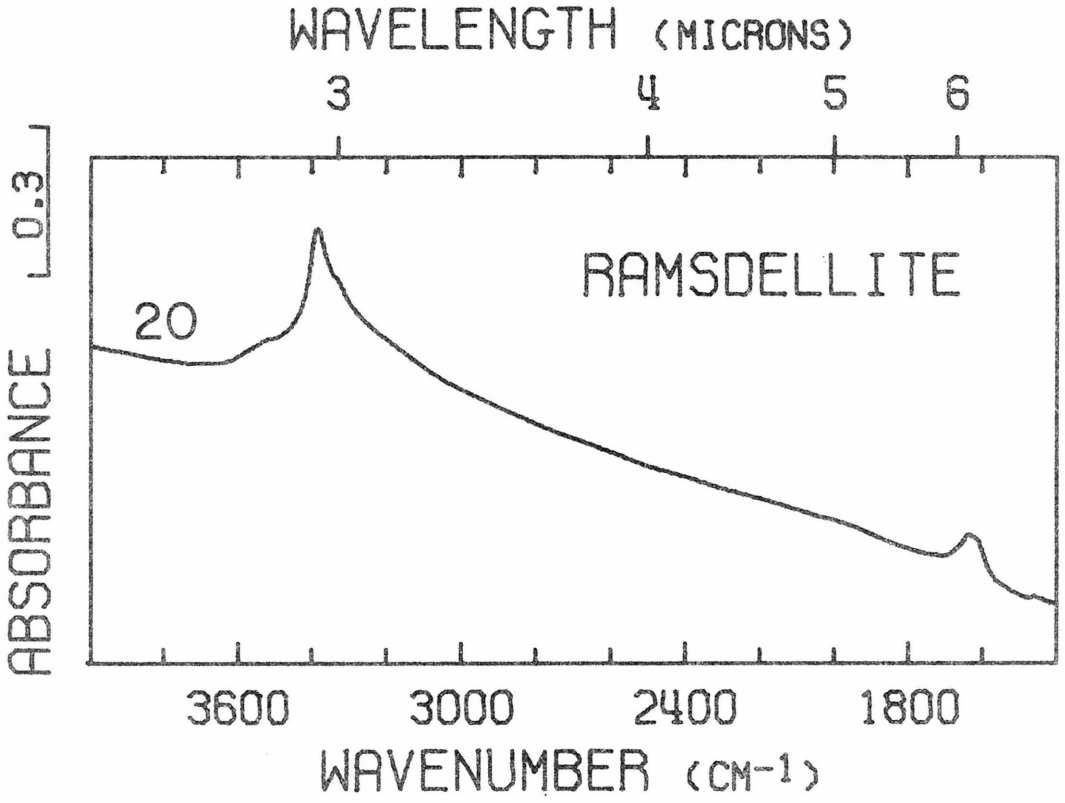

Figure 7. Infrared spectrum of ramsdellite. Presentation intensity: 137%. Figure continued on following page.

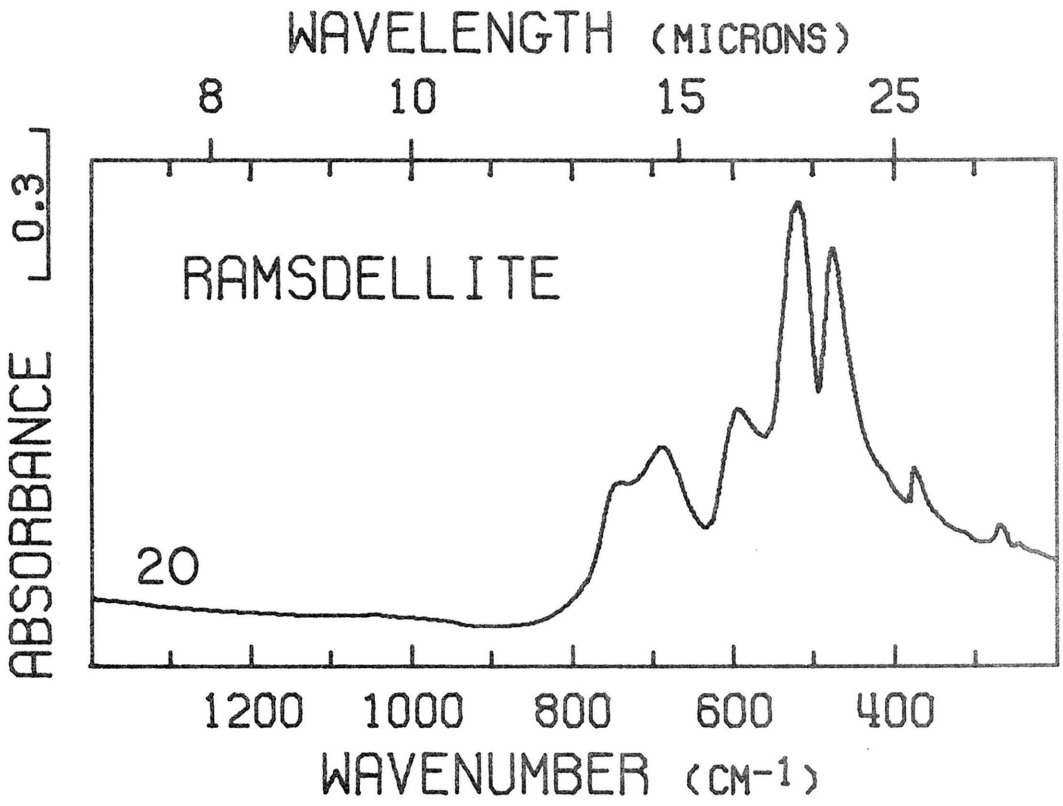

Figure 7. Continued from preceding page.

The overall character of the ramsdellite infrared spectrum clearly distinguishes it from all other manganese oxides except for the hollandite group and some synthetic nsutites. It is distinguished from the hollandite group by the 3380 cm^{-1} and 750 cm^{-1} bands and the position of the low intensity band at 375 cm^{-1}; from nsutite by the presence of the 3380 cm^{-1} and 750 cm^{-1} bands.

4. THE CHANNEL STRUCTURES: THE HOLLANDITE GROUP AND ROMANECHITE (PSILOMELANE)

Structures

The structure of the hollandite group minerals (Figure 8) consists of MnO_6 octahedra which share edges to form double chains as in ramsdellite (Byström and Byström, 1950, 1951). These double chains are linked by shared vertices forming channels. Ba, K, Pb, Na, and possibly water can be present in the channels and are coordinated to the oxygens of the double chains. The identity of the channel cations determines the mineral species.

There remains some question concerning the structure of romanechite. Wadsley (1953) determined the structure represented in Figure 8. It is similar to the hollandite structure except that the channels are broadened due to the presence of triple chains. He suggests that both water and barium are present in the channels in ordered fashion for any one channel but this order is not preserved among channels. The structure is monoclinic and has the chemical formula which is used here (Table 1) and which is supported by the work of Fleischer (1960). Mukherjee (1959, 1965), however, argued for an orthorhombic structure and a chemical formula with

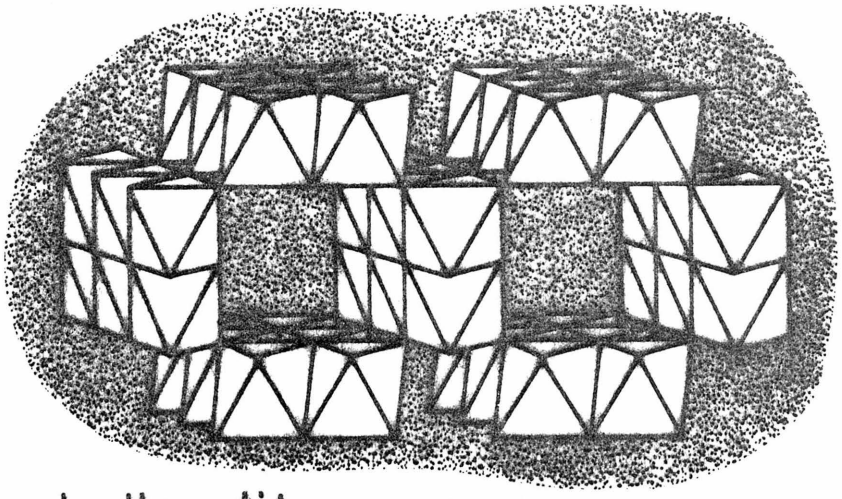

hollandite group

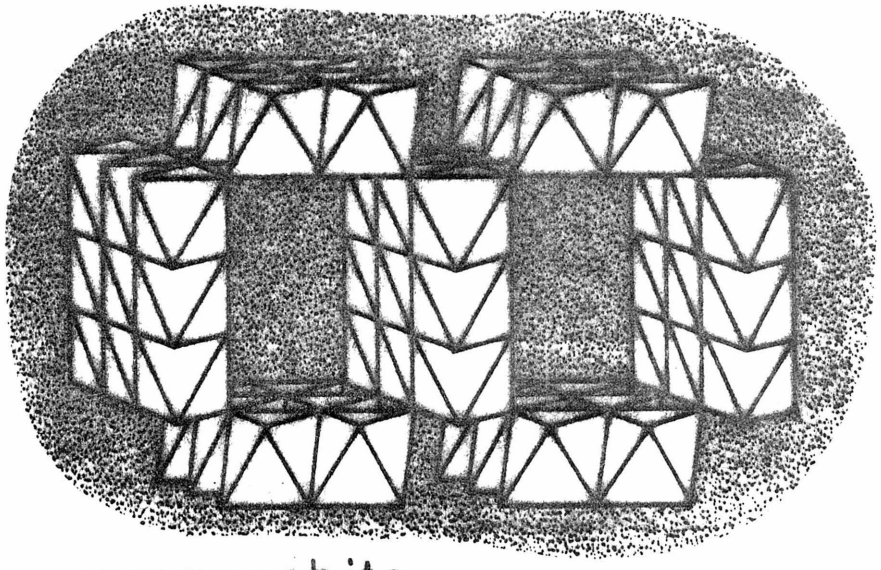

romanechite

Figure 8. Manganese oxide channel structures, looking approximately down the channels (modified from Clark, 1972).

hydrogen present as hydroxyl. He suggested that his differences from Wadsley are due primarily to the samples examined rather than the analyses and that Wadsley was working on an alteration product of true romanechite.

The Hollandite Group

Infrared spectroscopy in the 1400 cm^{-1} - 200 cm^{-1} region does not distinguish among the various minerals in the hollandite group; the spectrum in Figure 9 is representative of them all. The spectral features thus involve the vibrations of the octahedral framework shown in Figure 8 and do not include a significant contribution from the large cations in the channel. Far infrared spectra for synthetic hollandite and cryptomelane differ. Hollandite absorbs at 97 cm^{-1} and cryptomelane absorbs at 136 cm^{-1}. These absorptions might be associated with the channel constituents.

The only significant mid-infrared variation in the spectra of the hollandite group minerals listed in Table 1 is in band sharpness, which reflects variation in crystalline order. Variations in band position and relative intensity are minor when spectra are taken in TlBr. Spectra in KBr show significant differences in band intensity from the TlBr spectra and among each other (Figures 5B, 6B, and 7B) and, in one instance (Figure 6B, #26) there is a significant difference in band position. Hollandite #31 was shown to have monoclinic symmetry and cryptomelane #27 was shown to have tetragonal symmetry by Weissenberg single-crystal X-ray diffraction. No difference in the spectra of tetragonal versus monoclinic hollandite group minerals is apparent.

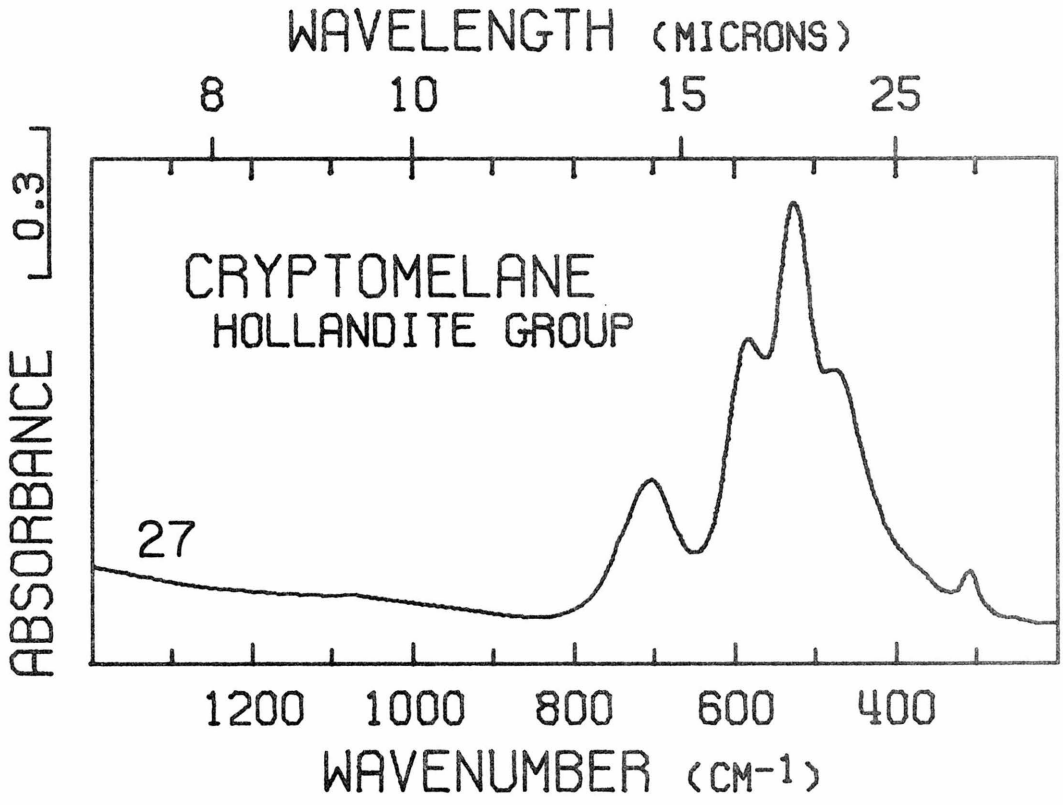

Figure 9. Infrared spectrum of cryptomelane, which is representative of the hollandite group. Presentation intensity: 133%.

Most hollandite group samples exhibit an extremely broad, low intensity absorption covering approximately the 3500 cm^{-1} to 2500 cm^{-1} region and a rather broad, low-intensity H_2O bending band near 1600 cm^{-1}. There must be some water in most samples; however, the broadness and weakness of the bands suggest that little is present and that it does not occupy well-defined crystallographic sites.

Hollandite group spectra are similar to those of ramsdellite, nsutite, and romanechite. Except for romanechite, these are all based structurally on the octahedral double-chain unit, but in hollandite these basic units are linked together to produce a different overall structure. In the 1400 cm^{-1} to 200 cm^{-1} region this difference is sometimes manifest in the infrared spectrum only below 400 cm^{-1} where the position of the band at 310 cm^{-1} is diagnostic of minerals of the hollandite group; however, the relative intensities of the three bands in the region 600 cm^{-1} to 450 cm^{-1} generally serve as an additional distinction from ramsdellite and natural nsutites. In the 4000 cm^{-1} to 1400 cm^{-1} region the 3380 cm^{-1} ramsdellite band distinguishes it from the hollandite group. Hollandite group minerals can be distinguished from romanechite by the additional romanechite bands, particularly those in the 4000 cm^{-1} to 1400 cm^{-1} region, and by the band near 600 cm^{-1}, which is generally prominent in the hollandite group spectra and only a weak shoulder in most romanechite spectra. Infrared spectroscopy clearly distinguishes hollandite group minerals from other manganese oxides not discussed here.

Romanechite (Psilomelane)

The infrared spectrum of romanechite resolves the uncertainty regarding the nature of its hydrous components. The three sharp bands in the 4000 cm^{-1} to 1400 cm^{-1} region of Figure 10 indicate a single, crystallographically-ordered type of water. They resemble, in intensity and position, the water found in channels of such minerals as beryl and cordierite (Goldman et al., 1977, 1978). The broad absorption near 3300 cm^{-1} may be due to a second, less ordered water, but is more likely an artifact due to the Christiansen effect (Prost, 1973), a result of refractive index mismatch between TlBr and the sample. The infrared spectrum shows no evidence for hydroxide ions. The intensity of the water bands varies from sample to sample, indicating a variable water content in accord with the chemical data of Fleischer (1960) for other romanechites. These results are completely in accord with the formula of Wadsley (1953), in which the hydrous component is water, and inconsistent with that of Mukherjee (1959, 1965), in which hydrogen is present as hydroxide ion. These water infrared features are characteristic of all the romanechites listed in Table 1 with the exception of #35, which has negligible absorption due to hydrous components. It thus appears that water rather than hydroxide ion is characteristic of romanechite as it commonly occurs. My evidence suggests that the samples I have examined are analogous to that of Mukherjee. Both samples which were X-rayed gave powder patterns whose line positions and relative intensities are in good agreement with Mukherjee's sample.

The 4000 cm^{-1} to 1400 cm^{-1} region of Figure 10 is

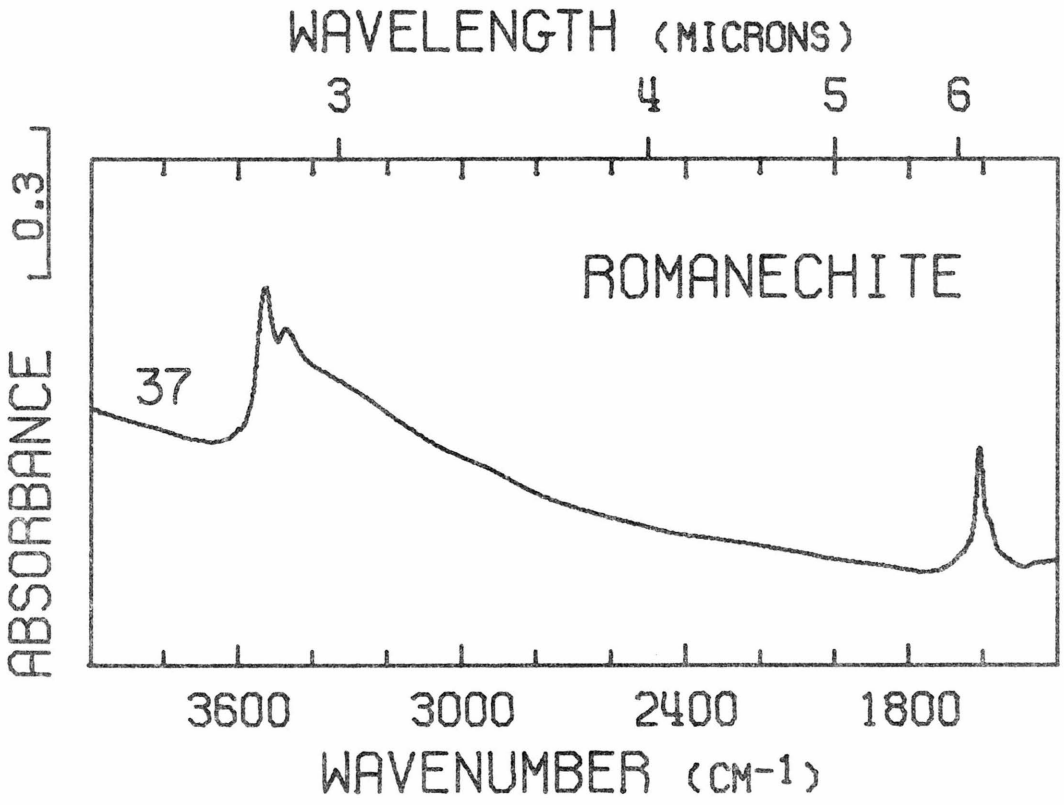

Figure 10. Infrared spectrum of romanechite (psilomelane). Different samples were chosen for each spectral region to best illustrate the infrared features. Presentation intensity: 251%. Figure continued on following page.

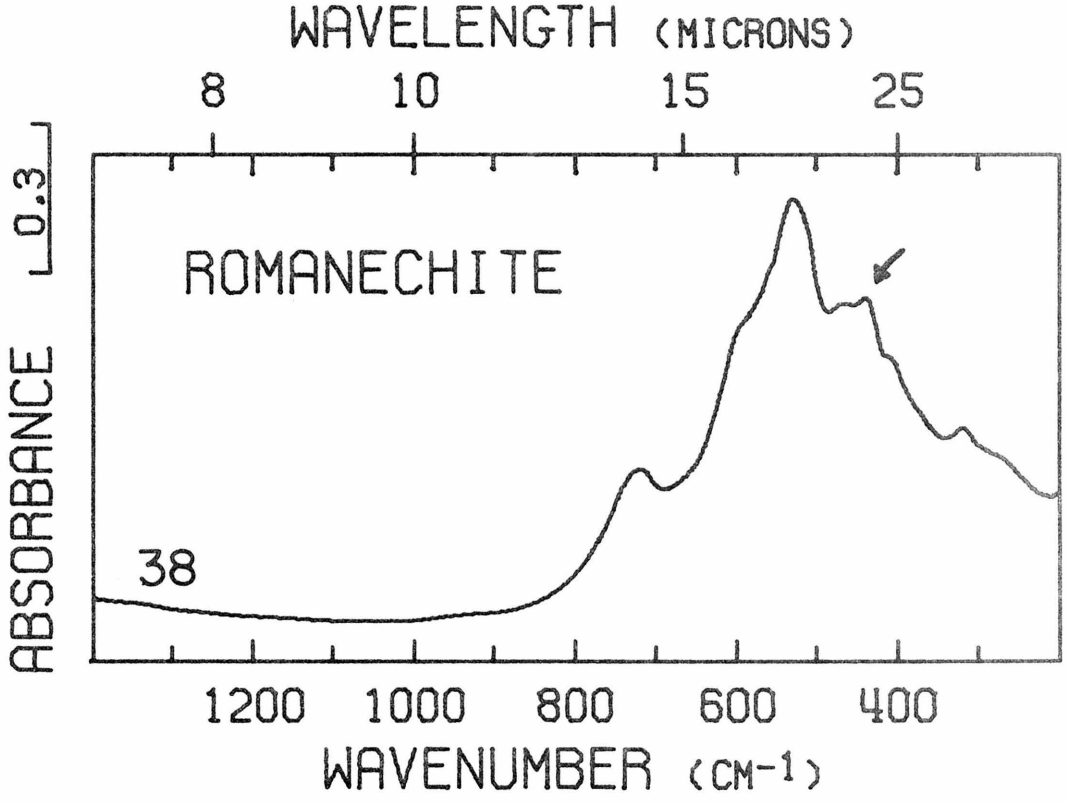

Figure 10. Continued from preceding page.

representative of the spectra of all the romanechites of Table 1. There is negligible variation in either band position or, with the exception of the band at 4400 cm^{-1} (arrow, Figure 10), in relative band intensity. Figure 10 shows the maximum relative intensity observed for the 440 cm^{-1} band. In some instances it is present only as a prominent shoulder of the 470 cm^{-1} band.

The same major bands are present in romanechite as in the nsutites, ramsdellite, and the hollandite group, but the relative intensities differ. The band near 600 cm^{-1} is invariably a weak shoulder, the band at 540 cm^{-1} is invariably the major band. In addition, two bands peculiar to romanechite occur at 440 cm^{-1}. Also diagnostic of romanechite are the weak bands at 320 cm^{-1} and 270 cm^{-1}, although the latter is so weak as to be missed in poorly crystalline samples. The positions and sharpness of water bands at 3530 cm^{-1}, 3470 cm^{-1}, and 1610 cm^{-1} are diagnostic of romanechite and are clearly recognizable in most samples. Infrared spectroscopy clearly distinguishes romanechite from other manganese oxides not discussed here.

5. THE LAYER STRUCTURES: THE CHALCOPHANITE GROUP AND LITHIOPHORITE

Structures

The chalcophanite structure (Wadsley, 1955) is based on layers of edge-shared MnO_6 octahedron (Figure 11). One out of seven octahedral sites in the MnO_6 layer is vacant. These layers alternate with layers of zinc and layers of water in the stacking sequence: Mn-O-Zn-H_2O-Zn-O-Mn. All waters are thought to be structurally

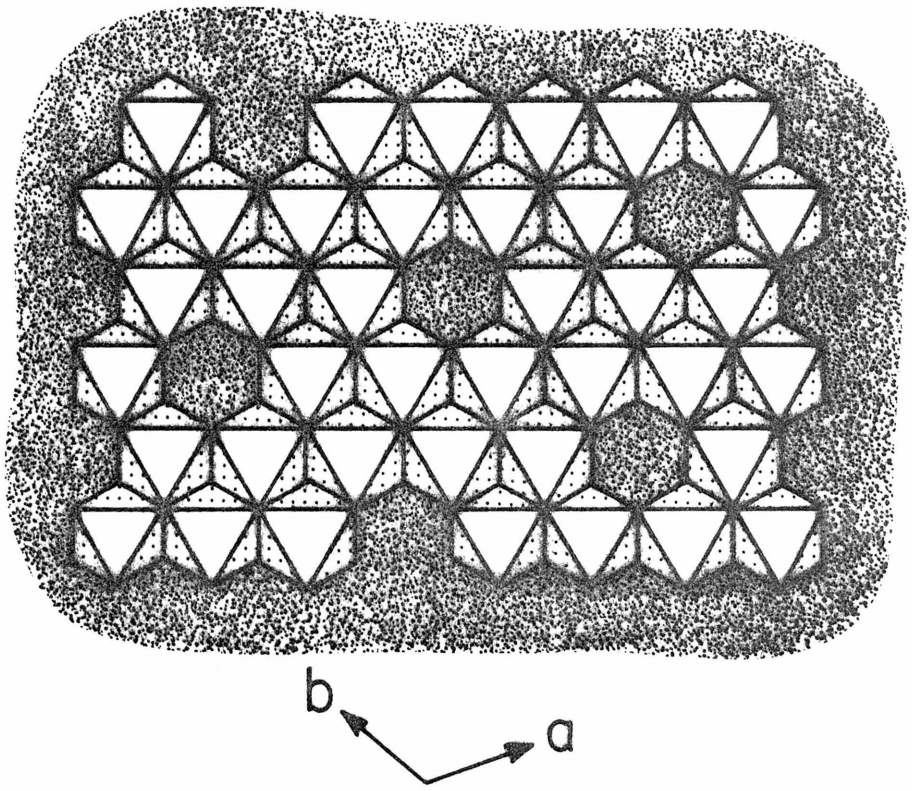

Figure 11. Chalcophanite MnO_6 layer structure, the ab plane.

equivalent, with weak hydrogen-bonding between water molecules. X-ray powder diffraction patterns suggest that aurorite has the chalcophanite structure (Radtke et al., 1967).

The structure of lithiophorite (Wadsley, 1952) consists of layers of edge-shared octahedra similar to those of chalcophanite but with all octahedral sites filled. These layers alternate with layers of $(Al,Li)(OH)_6$ octahedra. There is no ordering of the aluminum and lithium in these octahedral sites. Wadsley suggested that hydrogen bonding exists between layers and that the hydroxide ions are aligned perpendicular to the layers.

Chalcophanite and aurorite

The infrared spectrum of chalcophanite (Figure 12) matches exactly that from the other locality in Table 1 except for minor variation in relative band intensity. The 4000 cm^{-1} to 1400 cm^{-1} region of the spectrum has three sharp bands characteristic of water in a single, crystallographically-ordered site. The band position indicates approximately the same degree of hydrogen-bonding as in liquid water. These results support the suggestions of Wadsley that water is present in chalcophanite in a single structural position.

The infrared spectrum of aurorite (Figure 9B) indicates that it has the chalcophanite structure. The bands in its spectrum are identical in number and position to those of chalcophanite although there are some differences in relative intensity. The aurorite spectrum shows the effects of some crystalline disorder, which is not present in the chalcophanites.

The position and sharpness of the two water bands near

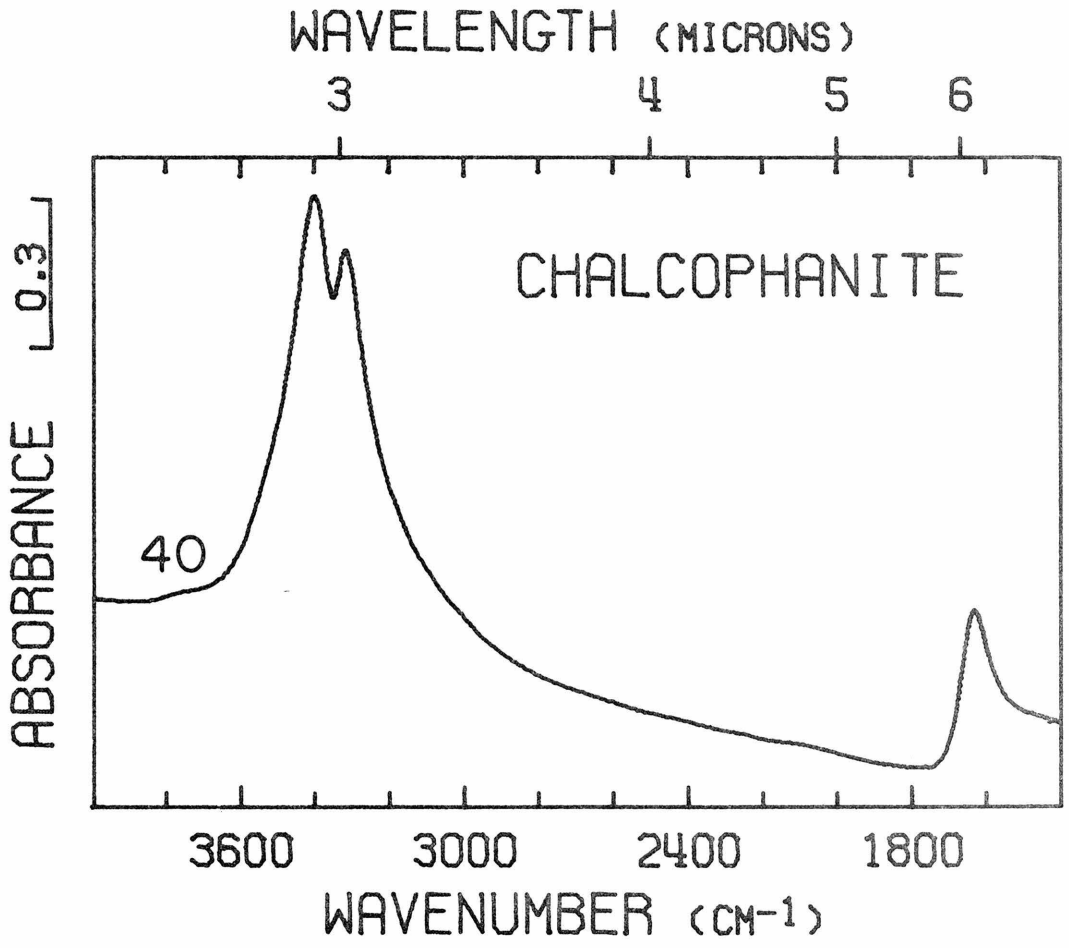

Figure 12. Infrared spectrum of chalcophanite. Presentation intensity: 161%. Figure continued on following page.

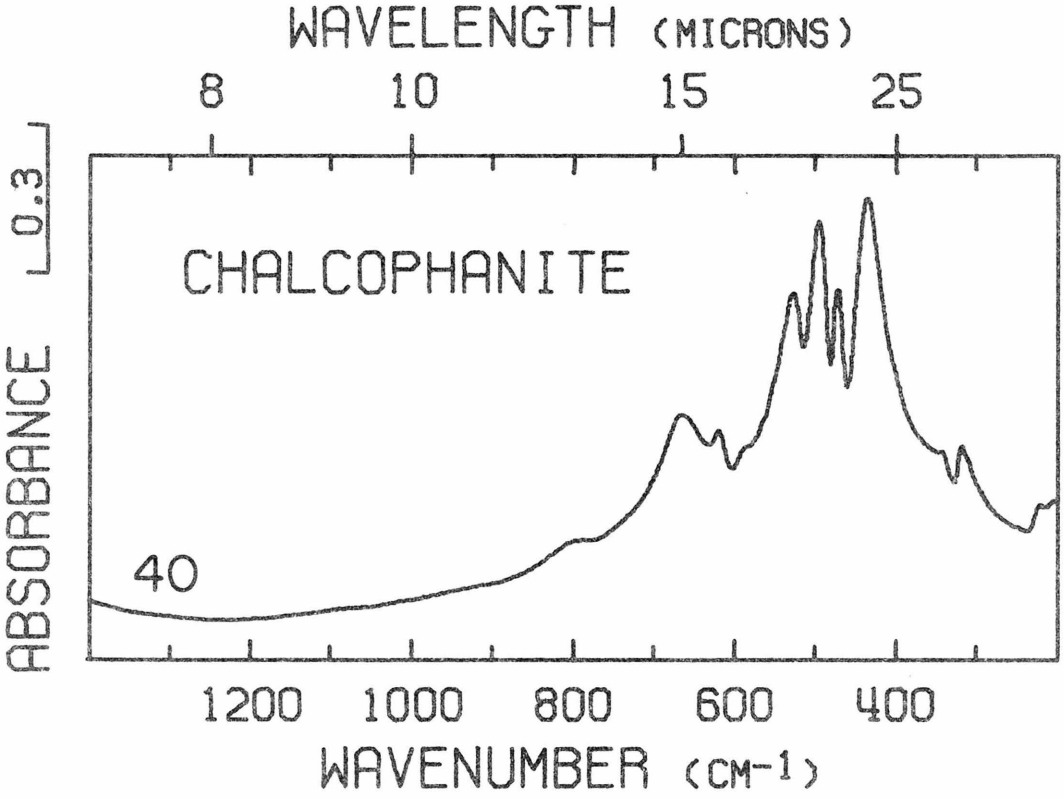

Figure 12. Continued from preceding page.

3400 cm^{-1} and the sequence of four bands in the 550 cm^{-1} to 400 cm^{-1} region distinguish chalcophanite and aurorite from all other manganese oxides.

Lithiophorite

Infrared spectra of lithiophorite are presented in Figure 13 for a well-crystallized sample (#42) and a poorly-crystallized one (#43). The spectrum of lithiophorite #44 is intermediate between these two. The single, sharp, intense absorption band near 3400 cm^{-1} together with the absence of the water bending mode near 1600 cm^{-1} indicates that a single type of hydroxide ion predominates. In addition, in the well-crystallized sample there are two weak shoulders on the low energy side of this band which are resolved at liquid nitrogen temperature. Single crystal, polarized infrared reflectance work shows that all three bands are polarized perpendicular to the basal cleavage. The hydroxide ions are thus aligned in this direction. These results confirm the suggestions of Wadsley (1952) regarding the crystallographic orientation of the hydroxide ions. The lower intensity bands may correspond to hydroxide in local environments created by statistically less probable populations of aluminum and lithium atoms in nearby octahedral sites.

Lithiophorite can be distinguished from all other manganese oxides by the intensity and position of the band near 3400 cm^{-1} and by the presence of the band near 1000 cm^{-1}. The positions of all the bands in the intensity relationship of Figure 13 are also diagnostic of lithiophorite.

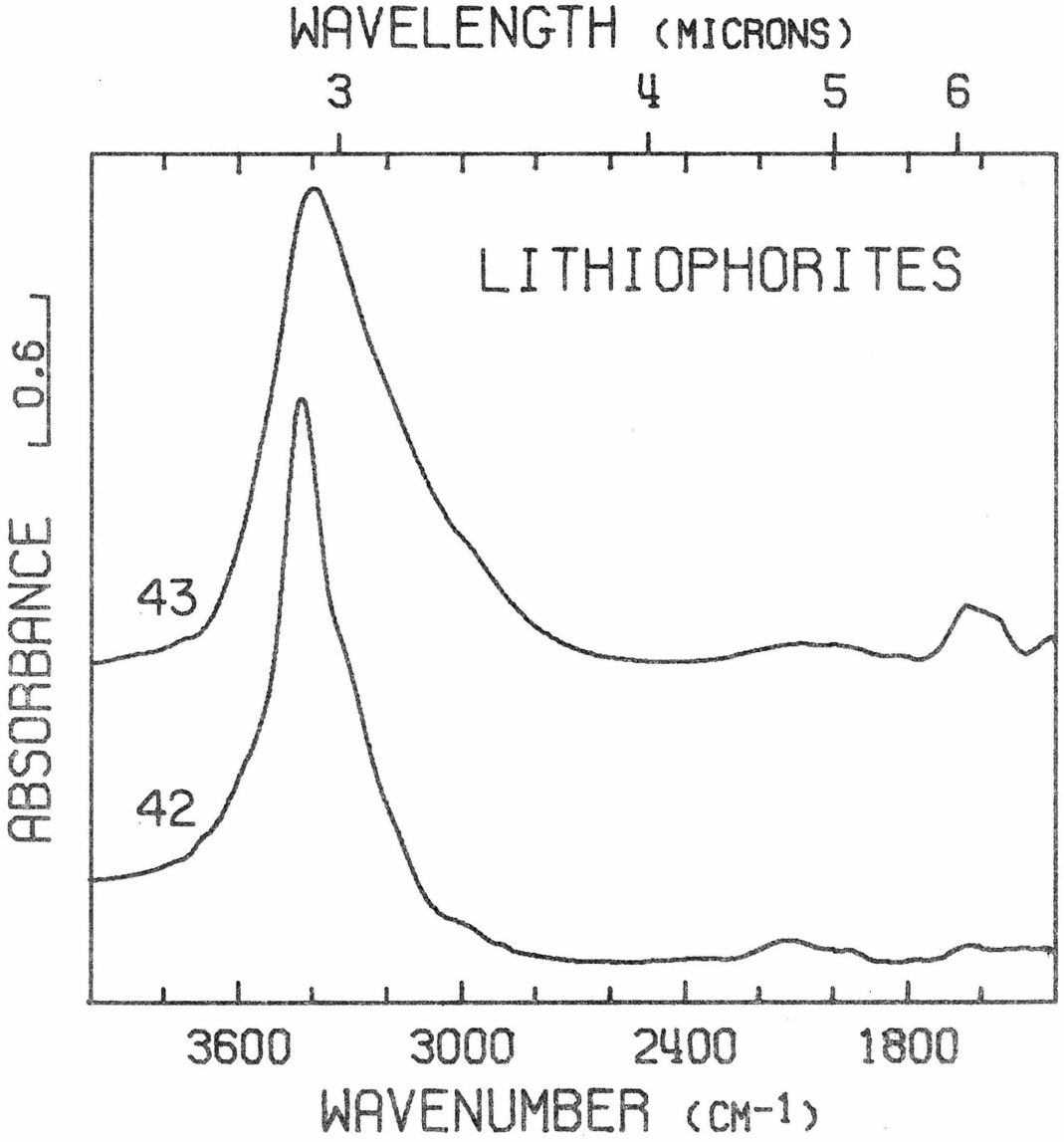

Figure 13. Infrared spectra of lithiophorites. Presentation intensities: #43, 172%; #42, 172%. Figure continued on following page.

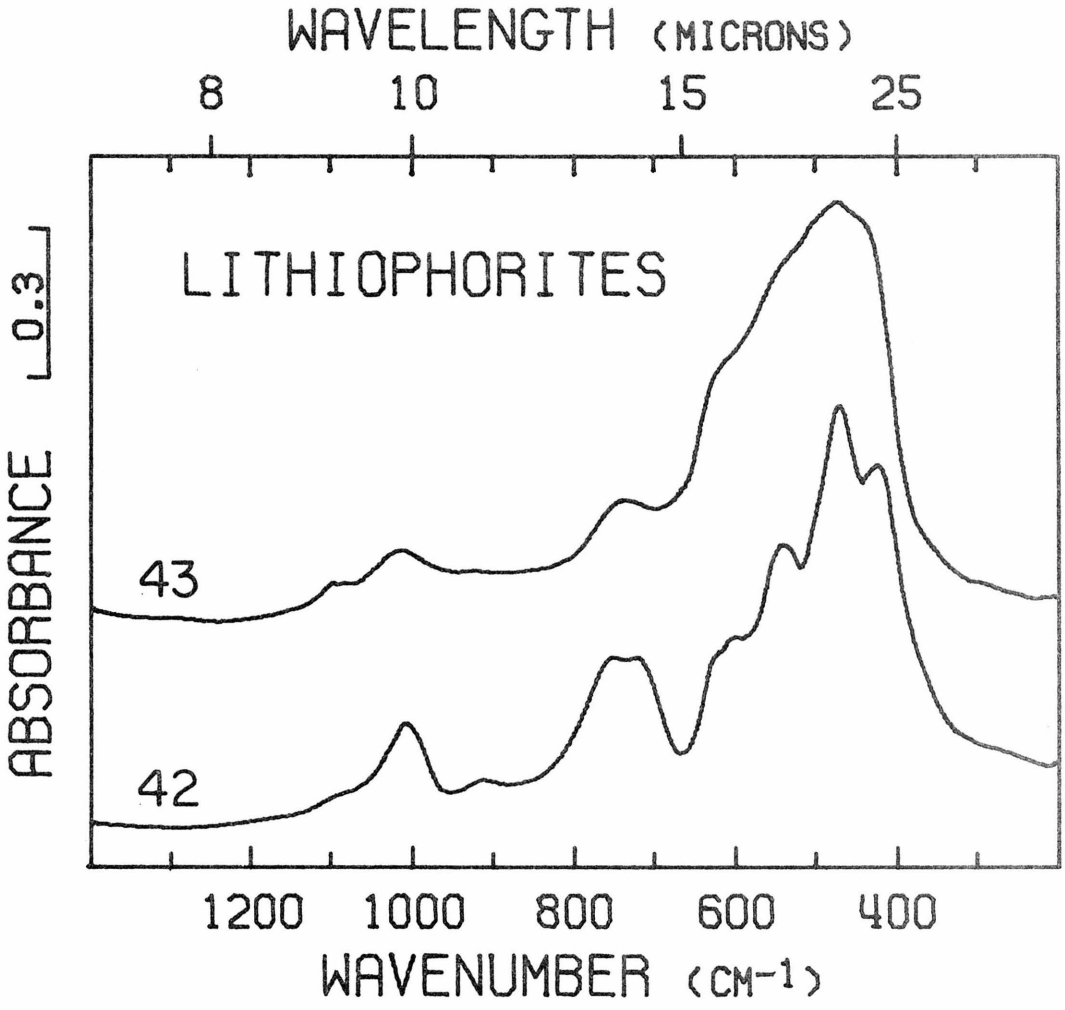

Figure 13. Continued from preceding page.

6. INCOMPLETELY CHARACTERIZED STRUCTURES: BIRNESSITE, THE TODOROKITE GROUP AND RANCIEITE

Structures

The structure of birnessite has been inferred from the postulated structures of presumed synthetic analogs (Giovanoli, et al., 1970a, 1970b). The proposed layered structure is similar to the chalcophanite structure. MnO_6 octahedral layers have a vacancy in one out of every six octahedral sites. These are separated by layers of lower valent cations and by layers of water and hydroxide ions.

The structure of todorokite is not known. On the basis of similarity in the X-ray powder diffraction patterns, lithiophorite has been suggested as a structural model, but the failure of attempts to synthesize Na^{+} and Mn^{3+}-substituted lithiophorites suggests that this is not the case (Giovanoli et al., 1973). Crystal morphology and cleavage suggest that todorokite has a channel structure similar to hollandite or romanechite (Burns and Burns, 1975, 1977a, 1977b).

The structure of rancieite is not known. On the basis of X-ray powder diffraction data Bardossy and Brindley (1978) have suggested that it has a layer structure with interlayer water. They suggest that rancieite and birnessite have the same structure, differing only in the identity of the interlayer cation, and raise the possibility that rancieite and birnessite should be considered minerals of the same group.

Birnessite

It is first necessary to address the question of the

relationship between synthetic and natural birnessites. X-ray powder diffraction does not establish beyond question that synthetic materials are truly analogous to natural birnessite. They are assumed to be the same on the basis of four or fewer X-ray lines which may vary in position by up to 0.5 Å (Burns and Burns, 1977a). The similarity in the infrared patterns of the synthetic preparations and natural birnessites confirms that most are structurally analogous (Figure 14). In the region 1400 cm^{-1} to 200 cm^{-1}, the spectra consist of the following features:

Band 1:	250 cm^{-1}	present in well-ordered samples
Band 2:	330-360 cm^{-1}	generally present; a weak feature
Band 3:	420-460 cm^{-1}	always present, generally a major feature
Band 4:	485-525 cm^{-1}	always a major feature; split in #54
Band 5:	555-575 cm^{-1}	generally present; a weak feature
Band 6:	620-660 cm^{-1}	always present; generally a weak feature
Band 7:	740-755 cm^{-1}	generally present; a weak feature

In the region 4000 cm^{-1} to 1400 cm^{-1}, the spectra consist of three bands centered near 3400 cm^{-1} and a fourth at 1640 cm^{-1}. Samples #45 and #46, the natural birnessites in Table 1 whose spectra are not included in Figure 14, resemble #50 and #47 respectively. Sodium manganese(II,III) manganate(IV) (#54) and manganese(III) manganate(IV) (#51), whose postulated structures are the basis for knowledge of the birnessite structure are both characterized by infrared spectra which are related to those of natural birnessite (#47). Manganese(III) manganate(IV) is the better analog. The positions, relative

Figure 14. (Following 2 pages) Infrared spectra of birnessites. Presentation intensities: #50, 106%; #47, 247%; #51, 99%; #49, 104%; #54, 53%.

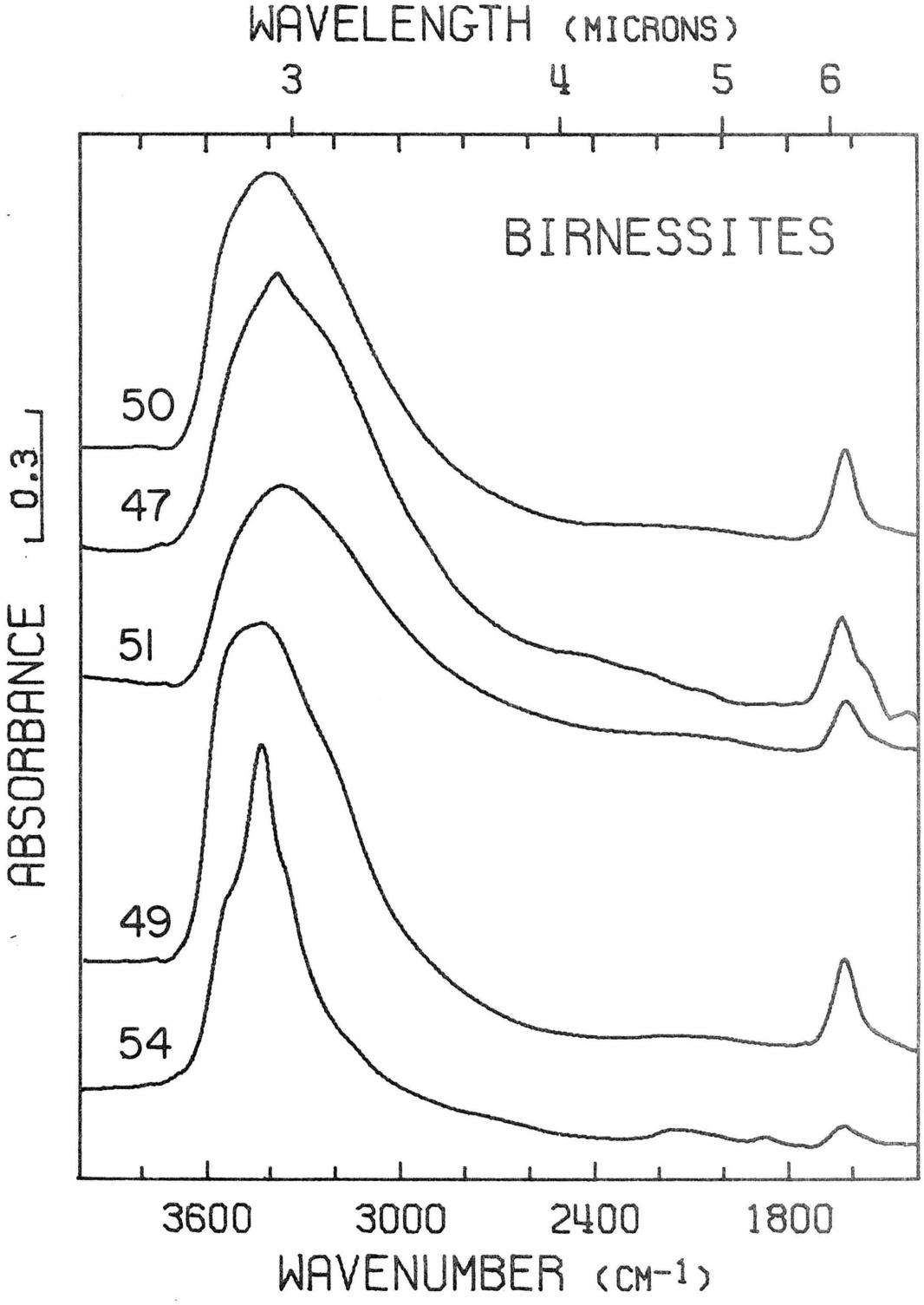
WAVELENGTH (MICRONS)
3
4
5
6
BIRNESSITES
50
47
51
49
54
0.3
ABSORBANCE
3600
3000
2400
1800
WAVENUMBER (CM-1)

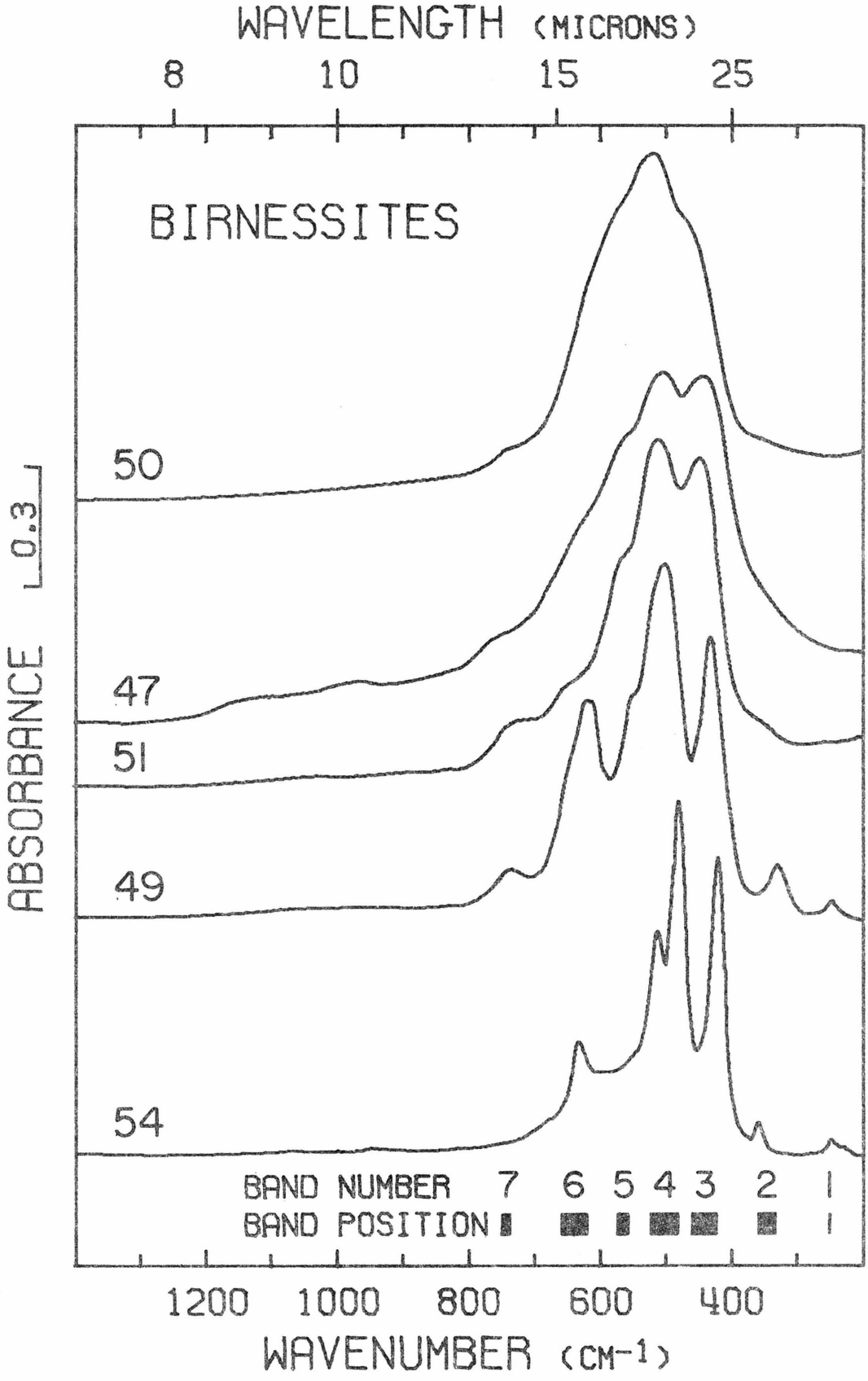
WAVELENGTH (MICRONS)
8
10
15
25
BIRNESSITES
50
47
51
49
54
0.3
ABSORBANCE
BAND NUMBER 7 6 5 4 3 2 1
BAND POSITION
1200
1000
800
600
400
WAVENUMBER (CM-1)

intensities and sharpness of its infrared features match closely those of the natural samples. There is some question of the validity of sodium manganese(II,III) manganate(IV) as a birnessite analog. If the bands do correlate with those of natural samples most are shifted by 20-40 cm^{-1}. It differs from all others in the position of band 2 and the absence of band 7. The sharpness of its bands indicates that it has a higher degree of order than the other samples. Structural changes relating to this ordering could be responsible for the band shifts. Other birnessite syntheses (Buser et al., 1954; Glemser et al., 1961; McKenzie, 1971) yield products which infrared spectroscopy confirms as birnessite. None have the high degree of order which characterizes sodium manganese(II,III) manganate(IV).

The spectra in Figure 14 span the range of variation for the birnessites in Table 1. The spectra are arranged top to bottom in order of increasing band sharpness, which reflects crystalline order. In general, X-ray powder patterns do not follow this trend in crystalline order. This may be due to the presence in some samples of a disordered component to which X-ray diffraction is insensitive. Sample #47 has the sharpest X-ray pattern. Most of the variation in Figure 14 is due to differences in crystalline order, but some variations must be related to other factors. A significant amount of the variation in band position is due to inclusion in the figure of the doubtful analog sodium manganese(II,III) manganate(IV). The variations are not due to manganese oxidation state or the identity of the large cation. Manganese oxidation state (Table 1) does not

correlate with any infrared features. Na, K, and Ca birnessites prepared by the same procedure differ in their band position and relative intensities less than different synthetic preparations of similarly substituted birnessite.

The birnessite spectra have several structural implications, which support its proposed structure. The position of the major bands in the 1400 cm^{-1} to 200 cm^{-1} region suggest that it has a layer structure (Section 7). The fact that the identity of the large cations does not influence these bands suggests that they are weakly bound to the MnO_6 octahedral layers. I interpret the 4000 cm^{-1} to 1400 cm^{-1} pattern as follows: a hydroxide ion in a specific crystallographic site produces the 3430 cm^{-1} band, and a less-ordered water produces the remaining features.

Natural birnessite is distinguished from most of the manganese oxides by the presence of bands 3 and 4 as two broad features. It can be distinguished from poorly-ordered chalcophanite and, generally, from todorokite by the features in the 4000 cm^{-1} to 1400 cm^{-1} region. It can be distinguished from rancieite by the position of band 7 near 750 cm^{-1}, by the absence of the band near 700 cm^{-1} in rancieite, and, generally, by the relative intensity and positions of the two major bands. Synthetic birnessite can be distinguished by these criteria and, for well-ordered material, by the general character of the spectrum. Some samples may be difficult to distinguish from highly disordered todorokite.

Todorokite

The variation in todorokite infrared spectra in Figure 15

Figure 15. (Following 2 pages) Infrared spectra of todorokites. Presentation intensities: #57, 91%; #61, 192%; #55, 198%; #58, 86%; #60, 106%.

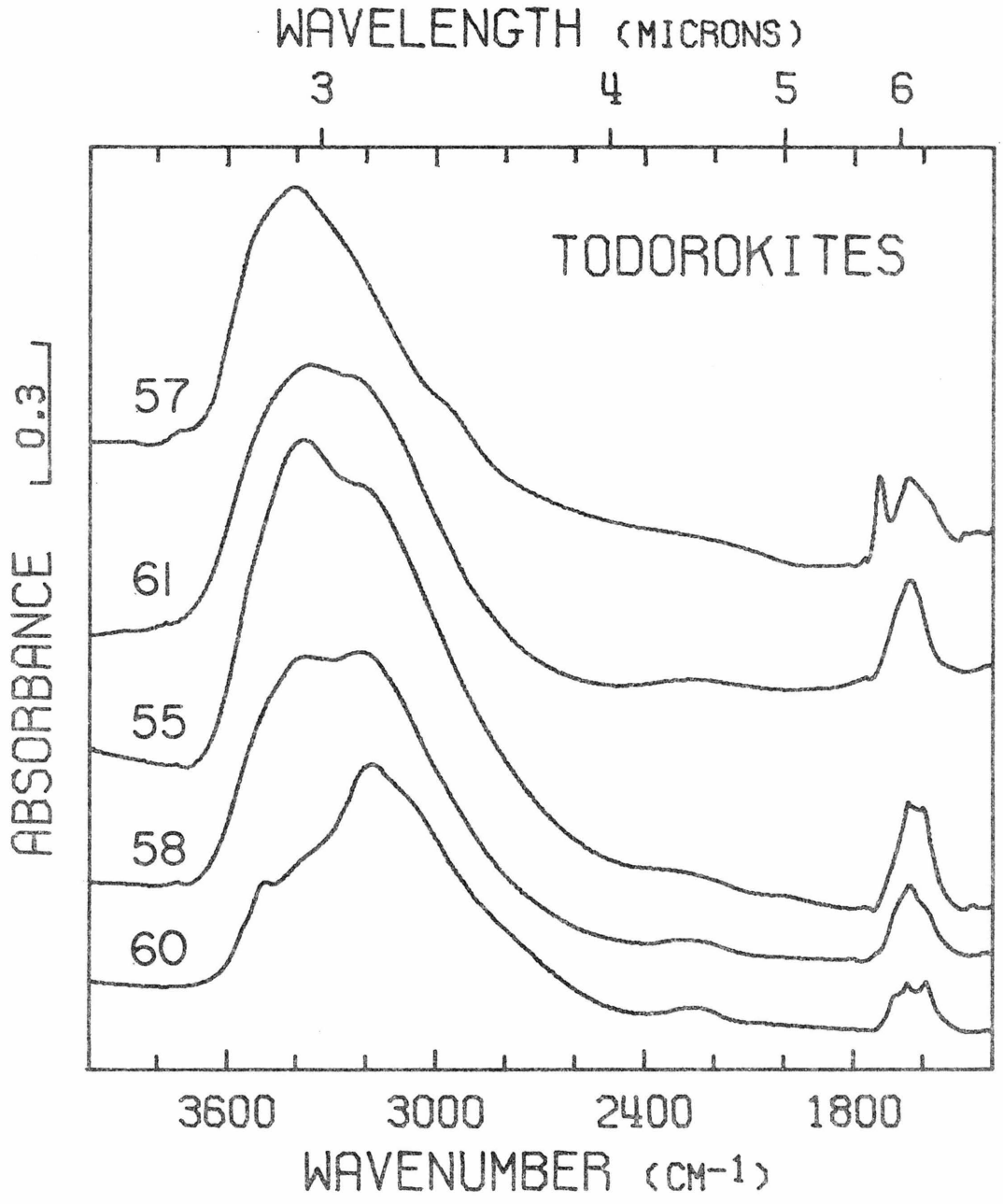
WAVELENGTH (MICRONS)
3
4
5
6
TODOROKITES
57
61
55
58
60
0.3
ABSORBANCE
3600
3000
2400
1800
WAVENUMBER (CM-1)

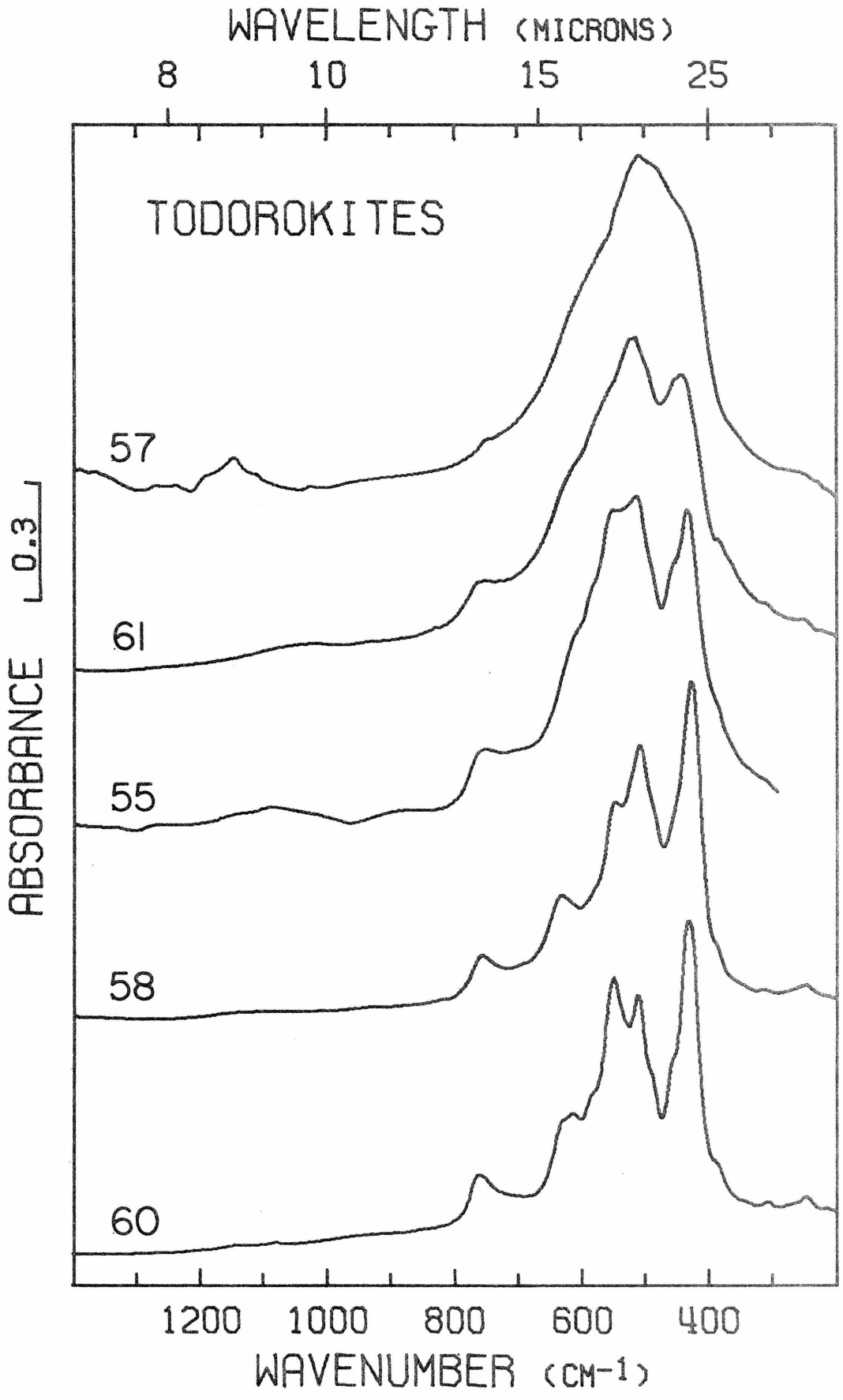
WAVELENGTH (MICRONS)
8
10
15
25
TODOROKITES
57
61
55
58
60
ABSORBANCE
0.3
1200
1000
800
600
400
WAVENUMBER (CM-1)

results primarily from differences in crystalline order and shows the effect of increasing order from top to bottom. The three todorokite spectra not presented in Figure 15 are similar to the spectra of samples #55 and #60. The low degree of order seen in the top spectrum is unusual. There is little variation in band position, and the spectrum of even the most disordered material retains indications of all but the most minor band of the well-crystallized material. There is significant variation in relative intensity of the three most intense bands (near 555 cm^{-1}, 510 cm^{-1}, and 435 cm^{-1}). The relative intensity of the 435 cm^{-1} band correlates with the degree of order suggested by band broadness; this is not true for the other two.

Todorokite absorption in the 4000 cm^{-1} to 1400 cm^{-1} region is more complex than that of the other manganese oxides. The three sharp features near 1600 cm^{-1} seen for the best-ordered material indicate multiple water environments in well-defined crystallographic sites. The band near 3500 cm^{-1} reflects a low degree of hydrogen bonding, but the position of the major band near 3200 cm^{-1} indicates that the dominant hydrogen-containing species is strongly hydrogen-bonded in the well-ordered samples. For todorokites of lower crystalline order the position of the major band near 3400 cm^{-1} suggests that the dominant species is disordered water with a lower degree of hydrogen-bonding. Assignment of the low intensity band near 2250 cm^{-1} is uncertain.

Todorokite presents three problems which can be resolved on the basis of infrared work: (1) the validity of lithiophorite as a structural model for todorokite is uncertain; (2) synthetic

todorokites have been prepared by cation exchange of the synthetic phase, buserite (McKenzie, 1971), which has an X-ray powder diffraction pattern resembling todorokite.[1] It has not been conclusively shown that these synthetic materials are analogous to natural todorokite; (3) the validity of todorokite as a single phase has been questioned (Giovanoli et al., 1971; Giovanoli and Bürki, 1975). They proposed that it is a mixture of buserite and the products of buserite's partial dehydration (birnessite) and reduction (manganite). I will present my work as it bears on these problems in the following order: (1) the structural relation of buserite to sodium manganese(II,III) manganate(IV); (2) the validity of synthetic todorokites and litiophorite as analogs of natural todorokite; (3) the validity of natural todorokite as a mineral species.

Buserite was prepared by the procedure of Giovanoli et al. (1970a). Its X-ray powder pattern in aqueous suspension matched that reported by Wadsley (1950a). The buserite infrared spectrum (Figure 16) was obtained from a TlBr pellet in which the wet solid was dispersed. Buserite was then partially dehydrated to form sodium manganese(II,III) manganate(IV) by heating 15 hours at 120°C under vacuum. X-ray powder diffraction showed the line near 7 Å characteristic of the partially dehydrated material with no trace of the 10 Å buserite

---

[1] Throughout this paper the term buserite will be used for the highly hydrated form of the synthetic material sodium manganese(II,III) manganate(IV), which is characterized by a strong X-ray line near 10 Å. The term sodium manganese(II,III) manganate(IV) will be used for the partially dehydrated compound with a strong X-ray line near 7 Å.

Figure 16. Infrared spectrum of buserite. Presentation intensity: 72%. Figure on following two pages.

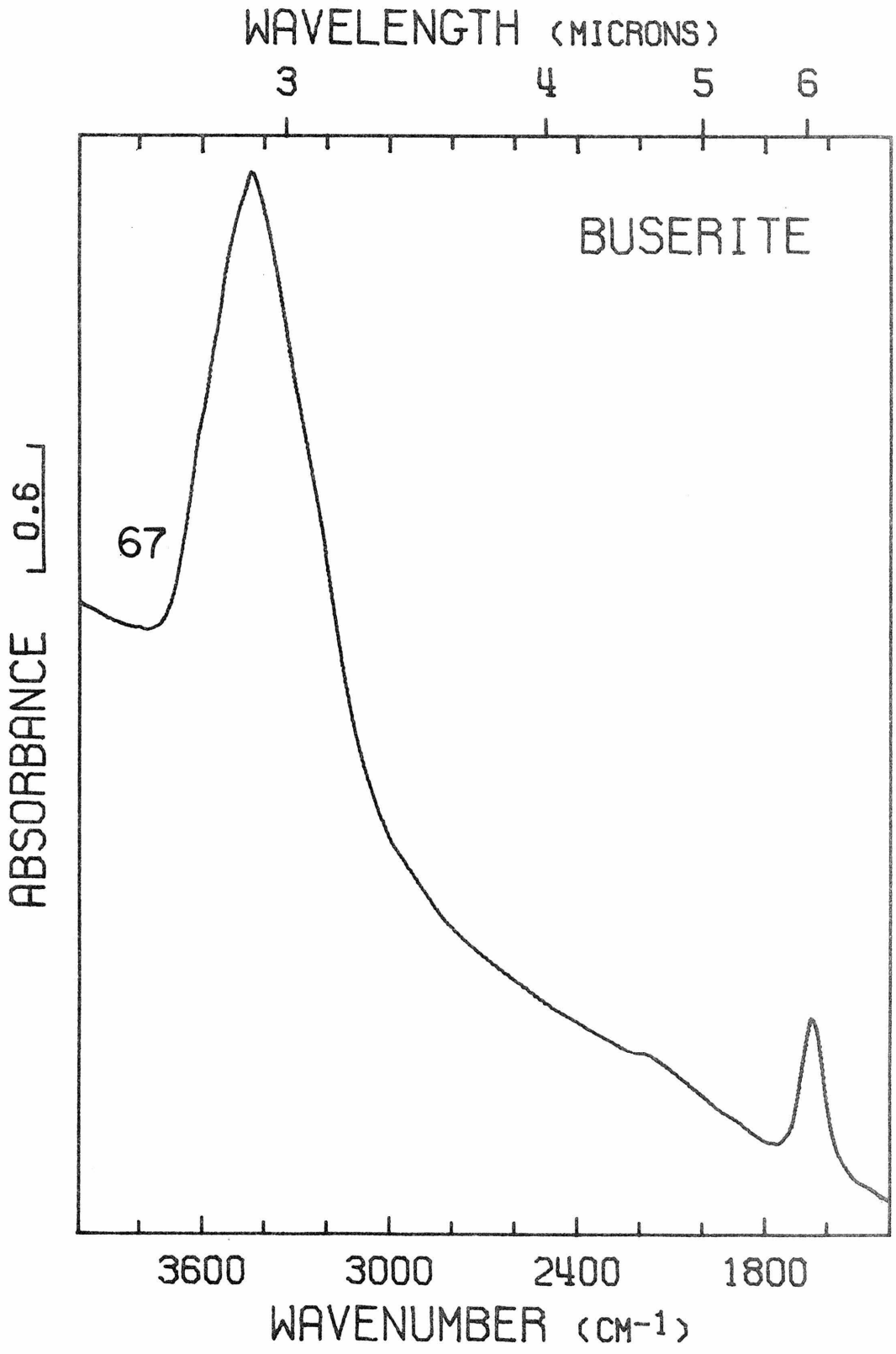
WAVELENGTH (MICRONS)
3
4
5
6
BUSERITE
67
ABSORBANCE
0.6
3600
3000
2400
1800
WAVENUMBER (CM-1)

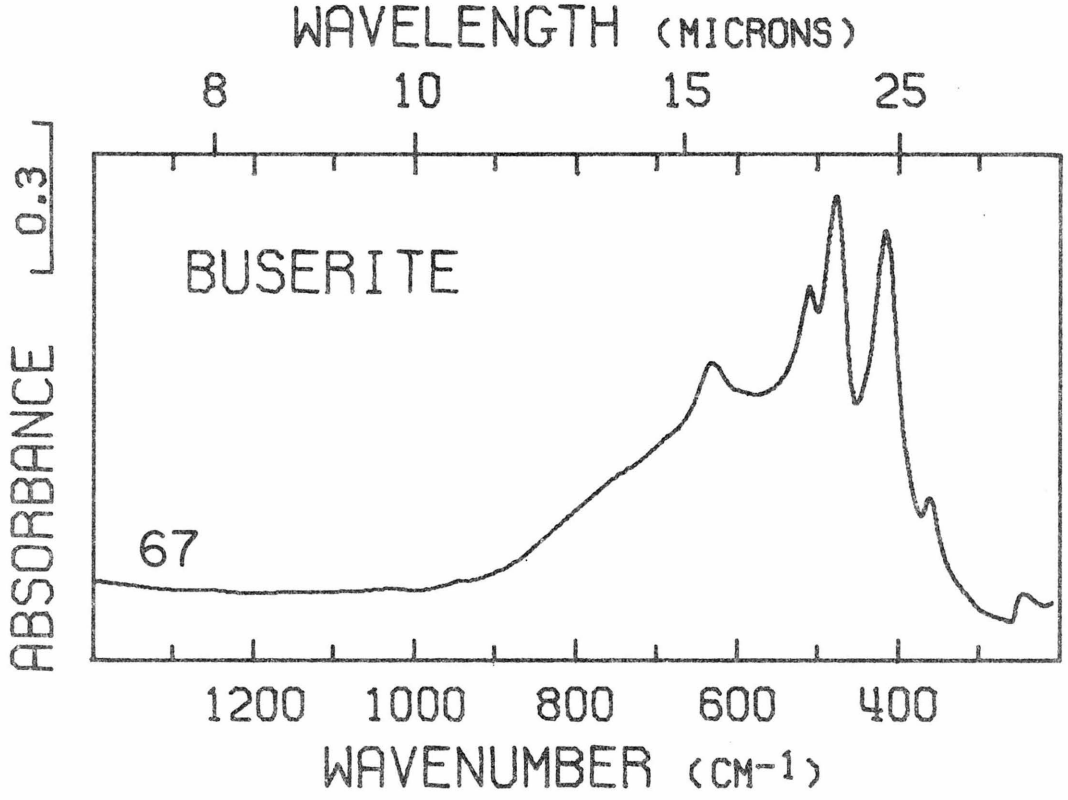
WAVELENGTH (MICRONS)
8
10
15
25
0.3
ABSORBANCE
BUSERITE
67
1200
1000
800
600
400
WAVENUMBER (CM-1)

line. The infrared spectrum of sodium manganese(II,III) manganate(IV) (Figure 14, #54) differs from buserite only in the lower magnitude of the water bands near 3400 cm^{-1} and 1650 cm^{-1} (partly due to the presence of liquid water in the buserite TlBr pellet) and in the absence of the broad band in the 700 cm^{-1} to 850 cm^{-1} region (which is probably due to librational motions of the liquid water in the buserite TlBr pellet). Buserite and sodium manganese(II,III) manganate(IV) are thus analogous structures. The shift from 10 Å to 7 Å spacing in these X-ray patterns is the result of water loss alone rather than a structural rearrangement of the manganese octahedral framework. In this way, these manganese oxides are analogous to some clay minerals which can undergo an irreversible collapse in basal spacing due to loss of water.

Comparison of the buserite and todorokite spectra show that buserite is not a todorokite analog. Significant differences in the structural arrangement of hydrous components is indicated by the dissimilarity of their spectra in the 4000 cm^{-1} to 200 cm^{-1} region. Band shifts of up to 40 cm^{-1} are required in order to correlate most bands in the 1400 cm^{-1} to 200 cm^{-1} region. Natural todorokites of varying crystalline order show no evidence for such large band shifts. The differences in the todorokite and buserite spectra in the 1400 cm^{-1}-200 cm^{-1} region indicate a different structural arrangement of the manganese octahedra. Cation-exchanged buserites, which have been reported as synthetic todorokites (McKenzie, 1971), have spectra identical in band position and relative intensity to the unexchanged buserite (Figure 15B). This indicates that they are not todorokite

analogs.

Lithiophorite is likewise not a structural model for todorokite. The lithiophorite hydroxide ion absorption is different from todorokites and its absorption bands in the 1400 cm^{-1} to 200 cm^{-1} region (Figure 13) do not coincide with todorokite features.

Infrared spectroscopy shows that todorokite cannot be a mixture of buserite, birnessite and manganite and strongly suggests that it is a valid mineral species. The todorokite spectrum cannot be produced by the addition of the spectra of buserite, birnessite, and manganite. Todorokites do not show evidence of manganite although as little as 5% could be recognized from the sharp metal-hydroxide bands near 1100 cm^{-1} and the hydroxide bands near 2700 cm^{-1} and 2100 cm^{-1} (Figure 4A). No combination of the bands of other manganese oxides can duplicate the water-hydroxide ion bands of the todorokite spectrum.

The spectrum of woodruffite (Figure 13B) shows it to be a structural analog of todorokite as has been assumed from the similarity of their X-ray powder patterns (Frondel, 1953).

Todorokite and woodruffite can generally be distinguished from all other manganese oxides by the presence of the band near 3200 cm^{-1}, the band near 760 cm^{-1}, and the three intense bands in the 600 cm^{-1} to 400 cm^{-1} region. Highly disordered samples may be difficult to distinguish from some birnessites.

Rancieite

Relatively little is known about the structure of rancieite and its relationship to other manganese oxides; no methods of synthesis are

available. My infrared work supports the conclusions of Bardossy and Brindley (1978) that rancieite has a layered structure closely related to birnessite. However, spectra of well-crystallized samples of each indicate that the structures differ significantly in the arrangement of the manganese octahedra.

The spectra of Figure 17 exhibit features due to rancieite although several samples contain impurities. X-ray powder diffraction shows no impurity in #63, minor todorokite and birnessite in #64, and minor braunite in #65. Braunite absorption in the spectrum of rancieite #65 has been removed from its spectrum in Figure 17.[2] Comparison of todorokite (Figure 15) and birnessite (Figure 14) spectra with the spectrum of rancieite #64 in Figure 17 indicates that these impurities do not contribute significantly to its spectrum.

Both X-ray diffraction and infrared spectroscopy indicate a close structural relation between rancieite and birnessite. The previously noted similarity in their X-ray powder patterns (Bardossy and Brindley, 1978) is documented in Table 2. Comparison of Figure 14, #47, and Figure 17, #65, indicate that spectra of poorly crystalline

---

[2] I used a difference technique to remove braunite absorption. An intense braunite infrared band occurs at 950 cm^{-1}, where there is no absorption by rancieite. The intensity of this band in the rancieite spectrum is a measure of the braunite contamination. This band was nulled in Figure 17, #65, by subtracting the spectrum of pure braunite (Figure 1A) at 7.2 percent of its measured intensity, thereby removing braunite absorption in the entire 1400 cm^{-1} to 200 cm^{-1} range.

Table 2. X-ray powder diffraction data on birnessite and rancieite

Birnessite			Rancieite		
d-spacing (Å)	relative strength	# samples with line	d-spacing (Å)	relative strength	# samples with line
7.06-7.40	S	9	7.50-7.57	S	7
4.69	W	1	4.4	W	2
3.55-3.72	MS-W	9	3.72-3.77	M	7
3.32	M	1			
3.27	M	1			
2.40-2.47	MS-W	9	2.46-2.47	M-W	7
2.33-2.37	M	2	2.31-2.35	M	7
2.03-2.09	M	2	2.03-2.06	W	7
1.78	W	1	1.75-1.76	M-W	6
1.71	M	1			
1.44-1.45	W	1			
1.41-1.43	MS-W	9	1.42-1.43	M-W	7
1.40	W	1	1.38-1.40	W	4
1.32	W	1			
1.23	W	1	1.22-1.28	W	2
1.22	W	1			
1.18	W	1			
1.17	W	1			
1.10	W	1			
1.01	W	1			

S = strong, M = medium, W = weak; data from: Burns and Burns (1977a), Richmond et al. (1969), Glover (1977), and this work.

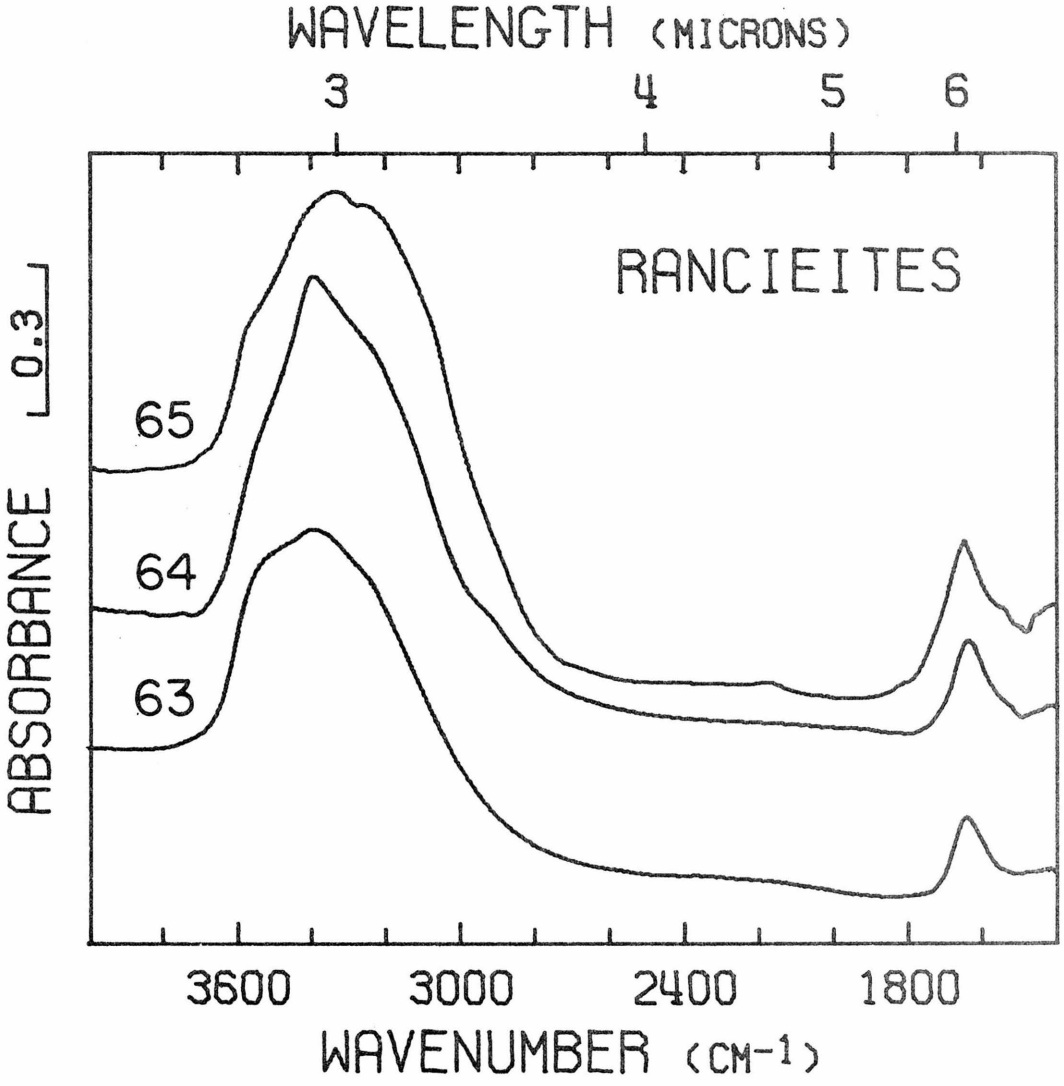

Figure 17. Infrared spectra of rancieites. Presentation intensities: #65, 478%; #64, 115%; #63, 62%. Absorption of braunite impurity removed from the spectrum of #65 (text footnote 2).

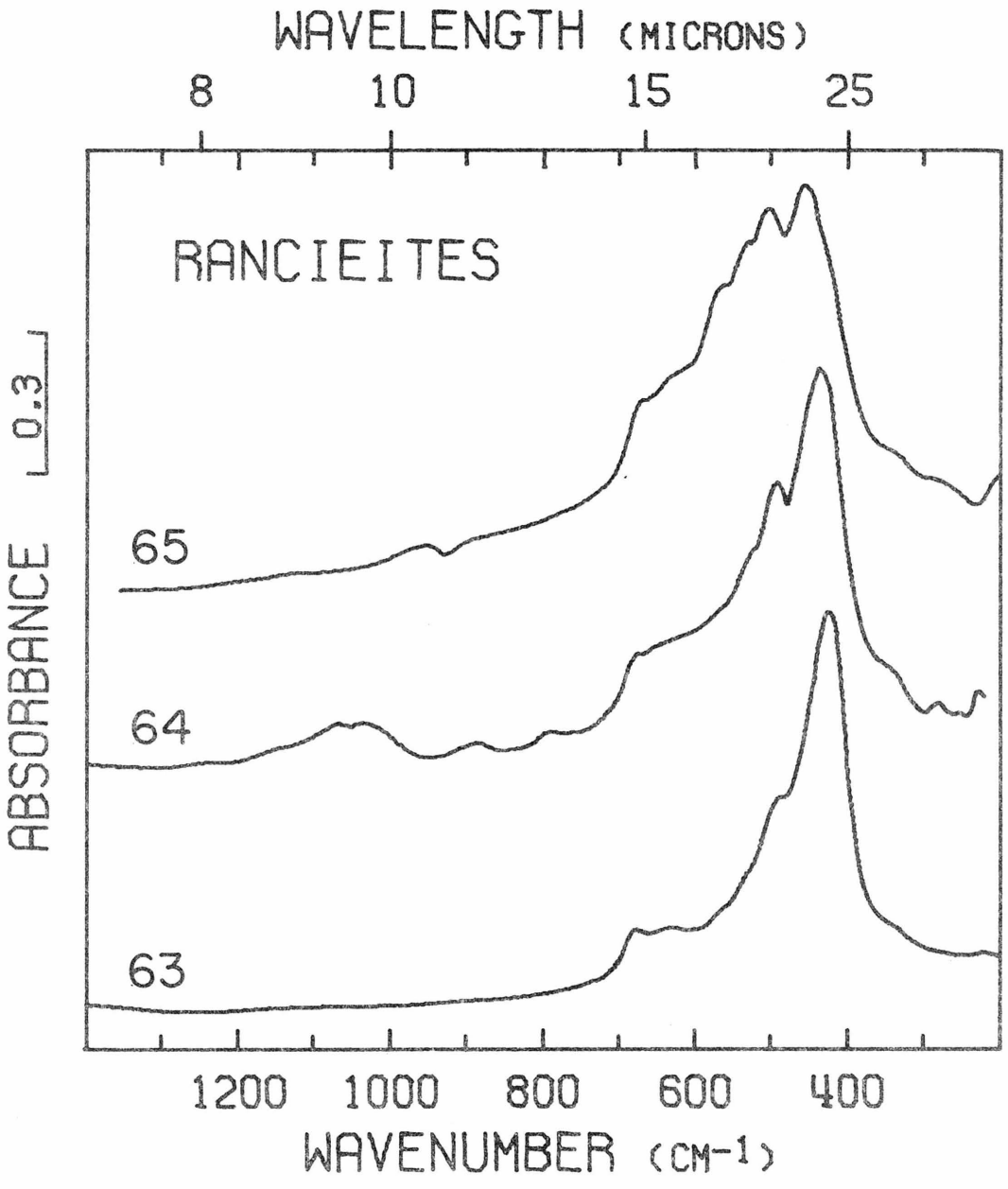

Figure 17. Continued from preceding page.

samples of the two minerals may be nearly indistinguishable in the 1400 cm^{-1} to 200 cm^{-1} region. In the 4000 cm^{-1} to 1400 cm^{-1} region all rancieites are indistinguishable from birnessite. This suggests that rancieite has a layer structure similar to that of birnessite and that the structural arrangement of the hydrous components is analogous. Spectra of the samples of greater crystalline order, however, are different in the 1400 cm^{-1} to 200 cm^{-1} region (Figure 14, #49 and #54; Figure 17, #63). Thus, while rancieite and birnessite have related structures, the structures are different. I will consider the structural implications of rancieite spectra more fully in Section 7.

Most rancieite samples can be distinguished from all other manganese oxides by the high relative intensity of the band at 425 cm^{-1}. Some samples can easily be confused with disordered todorokite or birnessite; however, the weak absorption at 680 cm^{-1} distinguishes rancieite from these other two, which absorb at 760 cm^{-1} and 750 cm^{-1} respectively.

7. GENERAL RELATIONS OF INFRARED SPECTRA TO STRUCTURE

The infrared spectra of the manganese oxides are dependent only on the MnO_6 octahedral framework with the exception of lithiophorite. If bands in the spectra are the result of vibrations in which the large cations participate significantly, then changes in the mass of these cations should be reflected in the spectra. However, substitution in the hollandite group and the birnessites leaves the spectra in the mid-infrared region unchanged. Neither could the effect of cation substitution be seen for chalcophanite

and aurorite and for todorokite and woodruffite although the extent of the change is less since it involves incomplete substitution involving elements of relatively similar mass. Therefore, I conclude that the large cations are not involved in the bands in this region of the spectra. Only for lithiophorite, where light atoms other than manganese form a major part of the crystal structure are bands in the 1400 cm^{-1} to 200 cm^{-1} region clearly attributable to other cations. Lithiophorite bands near 1000 cm^{-1} and 900 cm^{-1} are probably due to (Al,Li)-OH. The reason for this insensitivity to large cations may be that the bonds are relatively weak and therefore absorb at lower energies. Hollandite and cryptomelane spectra differ in the 200 cm^{-1} to 30 cm^{-1} region, and the difference may be due to the identity of the channel cations. An alternative explanation is that the large cations are of too low a concentration in the structures to give observable bands.

Infrared spectroscopy provides some indication of the polymerization by edge-sharing of the MnO_6 octahedra in manganese oxides. In Figure 18 the positions of the major bands of those minerals with known structure are plotted versus their average MnO_6 octahedral polymerization. A trend is observed showing a general decrease in band energy with increasing octahedral polymerization. The point for manganosite (Figure 5A) is included as well.[3] This

[3]Manganosite, MnO, has the NaCl structure. Being a Mn^{+2} mineral it is not strictly applicable to a trend involving predominantly Mn^{+4} minerals; however, the similarity in the positions of the low energy bands of ramsdellite and groutite (Figure 7, Figure 2A) which have

Figure 18. Correlation of octahedral polymerization with major infrared band positions. Dot size approximately proportional to band intensity. Intense absorption band positions define a trend which relates to octahedral edge-sharing.

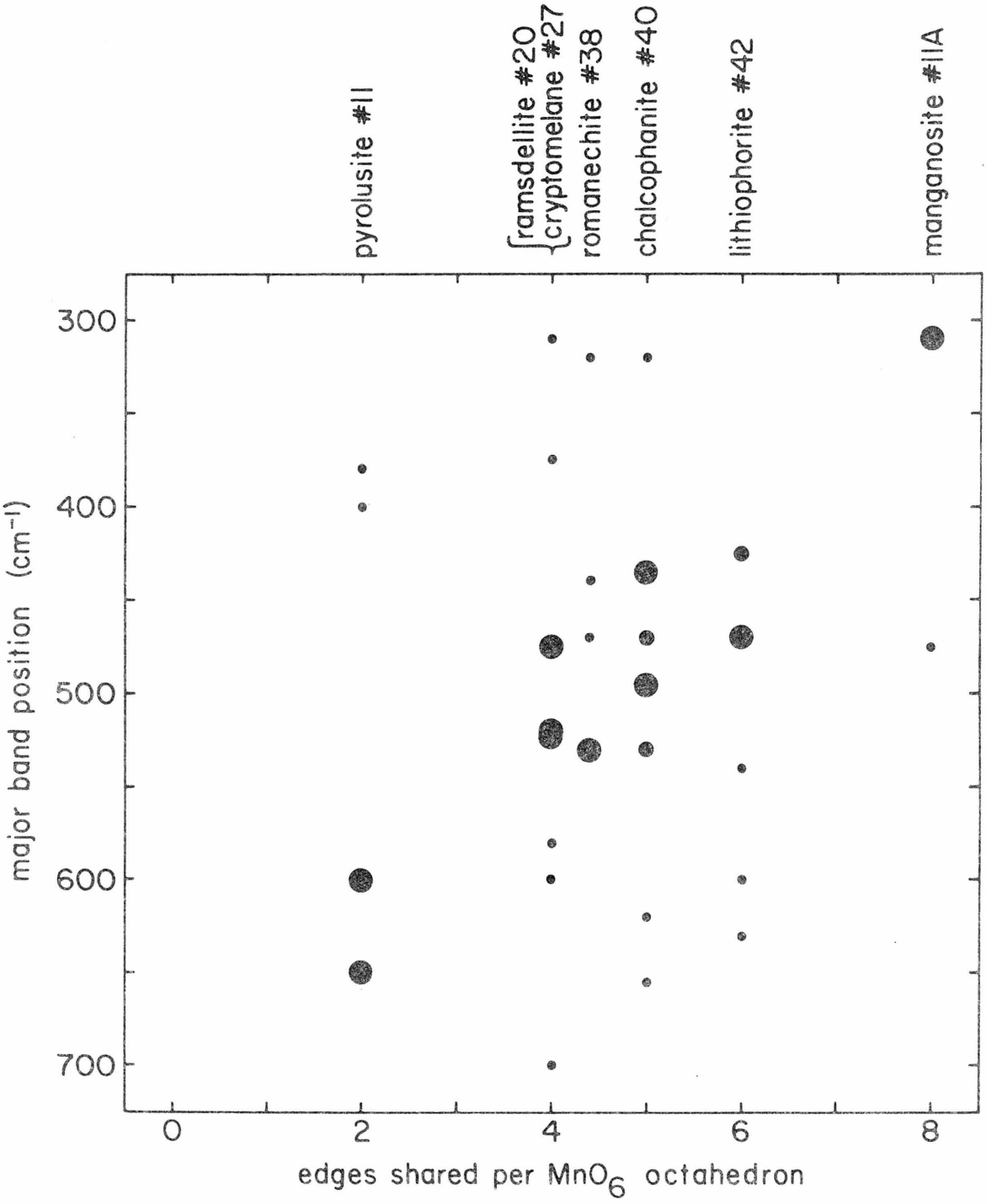
pyrolusite #11
ramsdellite #20
cryptomelane #27
romanechite #38
chalcophanite #40
lithiophorite #42
manganosite #11A
major band position (cm⁻¹)
300
400
500
600
700
0
2
4
6
8
edges shared per MnO6 octahedron

trend can be used in conjunction with a direct comparison of infrared patterns to infer unknown structures. The position of the low-energy bands of birnessite support its proposed layer structure (Giovanoli et al., 1970a,b), which places it at 4.8 shared edges per octahedron.

The spectra of todorokite suggest that its structure is based on MnO_6 octahedral layers. The positions and intensities of the major bands of todorokite samples with the highest crystalline order suggest a polymerization near 5 shared edges per octahedron. This is consistent with a highly polymerized chain or channel structure and with a layer structure containing some vacancies. In order to attain a polymerization of 5 shared edges per octahedron in a chain or channel structure it is necessary to build the structure from units whose average polymerization is 5. This corresponds to quadruple chains. No chain or channel manganese oxides composed of such large units are known to exist. It appears that for highly polymerized structures a layer structure is preferred. Direct comparison of todorokite spectra to those of other manganese oxides supports this. All known layer structures have a strong band in the 400 cm^{-1} to 450 cm^{-1} region which is analogous to the 430 cm^{-1} band of todorokite. Strong absorption in this region does not occur for the chain and channel structures. These suggestions disagree with

---

analogous structures (Byström, 1949; Dent Glasser and Ingram, 1968) and differ in oxidation state suggests that structure rather than oxidation state is the dominant factor in determining band position.

previous work suggesting that todorokite has a channel structure (Burns and Burns, 1977). This was based on the needle-like morphology of todorokite and the presence of two perfect cleavage planes seen under the electron microscope. I have found that todorokite occurs in other morphologies as well. Todorokite #58 has a platy morphology reminiscent of birnessite. Weissenburg single crystal X-ray diffraction indicates that the sample is ordered in the same plane as the plates but disordered in planes perpendicular to them. This suggests that it consists of a random superposition of single crystal todorokite plates and eliminates the possibility that it is a mass of needles that appear morphologically as a plate.

The spectra of rancieite suggest a polymerization near 6 shared edges per octahedron, which corresponds to a filled octahedral layer. Spectra of samples of birnessite, todorokite, and rancieite of poor crystalline order are similar in the 1400 cm^{-1} to 200 cm^{-1} region. As the order in the samples of the three minerals increases their spectra become more distinct from one another. This suggests that birnessite, todorokite, and rancieite are built of fundamentally similar units and that it is the ordering of these units which makes the minerals distinct from one another.

8. THE LOWER VALENT MANGANESE OXIDES

Appendix A contains spectra of well-characterized samples of the lower valent manganese oxides. In some cases these are necessary for the interpretation of the earlier sections of the paper. Others

are included so that the papers may serve as a compilation of the spectra of all manganese oxides commonly encountered in nature. They illustrate the ability of infrared spectroscopy to produce patterns diagnostic for each mineral phase for the whole range of naturally occurring manganese oxides. It extends the usefulness of this paper as a data base for further structural work on the manganese oxides.

9. CONCLUSIONS

Infrared spectroscopy has proven to be a useful tool for the mineralogical identification of the tetravalent manganese oxides. Different oxides can be distinguished by absorption patterns due to vibrations of the MnO_6 octahedral framework in the 1400 cm^{-1} to 200 cm^{-1} region. The 4000 cm^{-1} to 1400 cm^{-1} region is often diagnostic due to absorption associated with the hydrous components of the oxides.

Because of its sensitivity to short range order, infrared spectroscopy gives more reliable information than X-ray diffraction when applied to disordered and finely particulate samples. With X-ray diffraction a small amount of well-crystallized material in a disordered or finely particulate matrix can give the impression that the whole sample is well-crystallized. The lack of correspondence between the degree of order indicated by these two techniques for the birnessite samples is a manifestation of this effect. X-ray diffraction data alone could lead to an error in mineralogical identification of a disordered material if a well-crystallized minor component of different mineralogy is present. For minerals

which have only a few characteristic X-ray diffraction lines, such as birnessite, todorokite, and rancieite, infrared spectroscopy has shown that X-ray diffraction alone may be an insufficient test for the validity of synthetic analogs.

Infrared spectroscopy can also contribute to the determination of the structures and structural relationships among the tetravalent manganese oxides. I have been able to suggest features of the unknown oxide structures based on their infrared spectra and the relation of these spectra to those of manganese oxides with known structure. I have applied infrared spectroscopy to the role of water and hydroxide ion, whose presence and structural orientations can only be infrared from X-ray and chemical data.

Now that infrared spectra of well-characterized manganese oxide samples are available to serve as standards, this technique should find wider application for mineralogical identification of manganese oxides in the terrestrial and aquatic environments.

CHAPTER 2 APPENDIX A

My work on the lower-valent manganese oxides is summarized in this appendix. Table 1A contains information on sample locality and purity. Figures 1A-8A, which are included in this appendix, are representative of the various manganese oxides listed in Table 1A. They were all obtained on TlBr pellets under the same conditions as the figures presented in the text. Where the corresponding spectrum in KBr differs significantly it is included in Appendix B. Spectra of samples in Table 1A not included in this appendix are contained in Appendix B as indicated in Table 1A.

Table 1A. Sample information[1]

	sample #	locality	ident. #	ref. #	fig. #	purity x-ray	purity IR
Braunite Mn_7SiO_{12}	70	Palos Verdes Hills, Calif.	CIT 9461	2	1A	pure	pure
Groutite MnO(OH)	71	Cuyuna Range, Minnesota	NMNH 105004	3	2A,16B	pure	pure
	72	Talcville, New York	NMNH 113969	4	16B		pure
	73	Anadia, Portugal	NMNH 133850		16B		t,qtz
Hausmannite Mn_3O_4	74	Langban, Sweden	CIT 9462		17B		pure
	75	Synthetic	CIT 9463	5	3A,17B	pure	pure
	76	Synthetic	CIT 9618	6	17B		pure
Manganite MnO(OH)	77	Sagamore Mine, Minnesota	CIT 6048		18B	t,imp	pure
	78	Synthetic	CIT 9619	7	4A	pure	pure
Manganosite MnO	79	Langban, Sweden	CIT 2400		19B	t,pyc	t,pyc
	80	Synthetic	CIT 9620	8	5A,19B		pure
Marokite $CaMn_2O_4$	81	Tachgagalt, Morocco	LCM 13888		6A	pure	pure
Partridgeite Mn_2O_3	82	Postmasburg, S. Africa	HAV 110400		20B		pure
	83	Synthetic	CIT 9621	9	7A	t,pyr	t,pyr?
Quenselite $PbMnO_2(OH)$	84	Langban, Sweden	CIT 3097		8A	pure	pure

Table 1A Footnotes

1. The abbreviations and the criteria for X-ray purity are the same as for Table 1.
2. Mitchell and Corey, 1973.
3. Gruner, 1947.
4. Segeler, 1959.
5. Synthetic method: Giovanoli et al., 1967.
6. Manganous manganic oxide from Diamond Shamrock Chemical Company; Baltimore, Maryland.
7. Synthetic method: The synthetic method of Wadsley (1950b) for psilomelane produced a pure manganite. It was subsequently found that the manganous manganate used was contaminated with hausmannite.
8. Manganous oxide from Diamond Shamrock Chemical Company; Baltimore, Maryland; 0.01% Fe, 0.5% MnO_2 by their analysis.
9. Manganese sesquioxide HPX from Diamond Shamrock Chemical Company; Baltimore, Maryland.

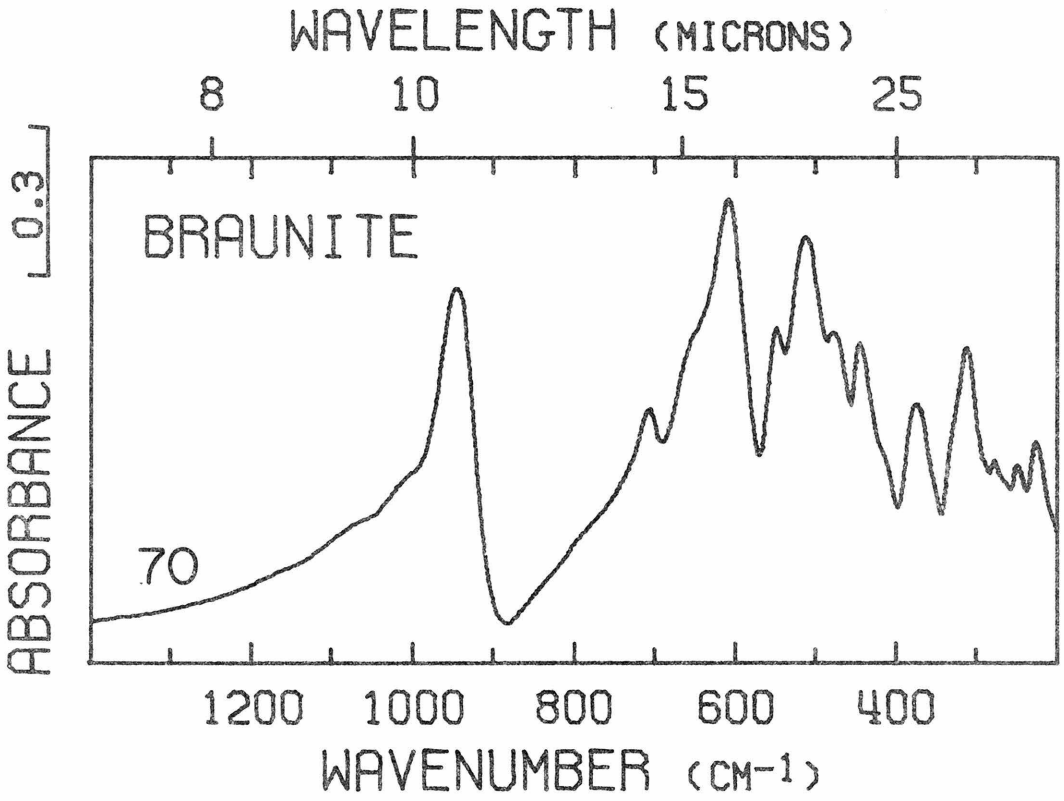

Figure 1A. Infrared spectrum of braunite. Presentation intensity: 344%.

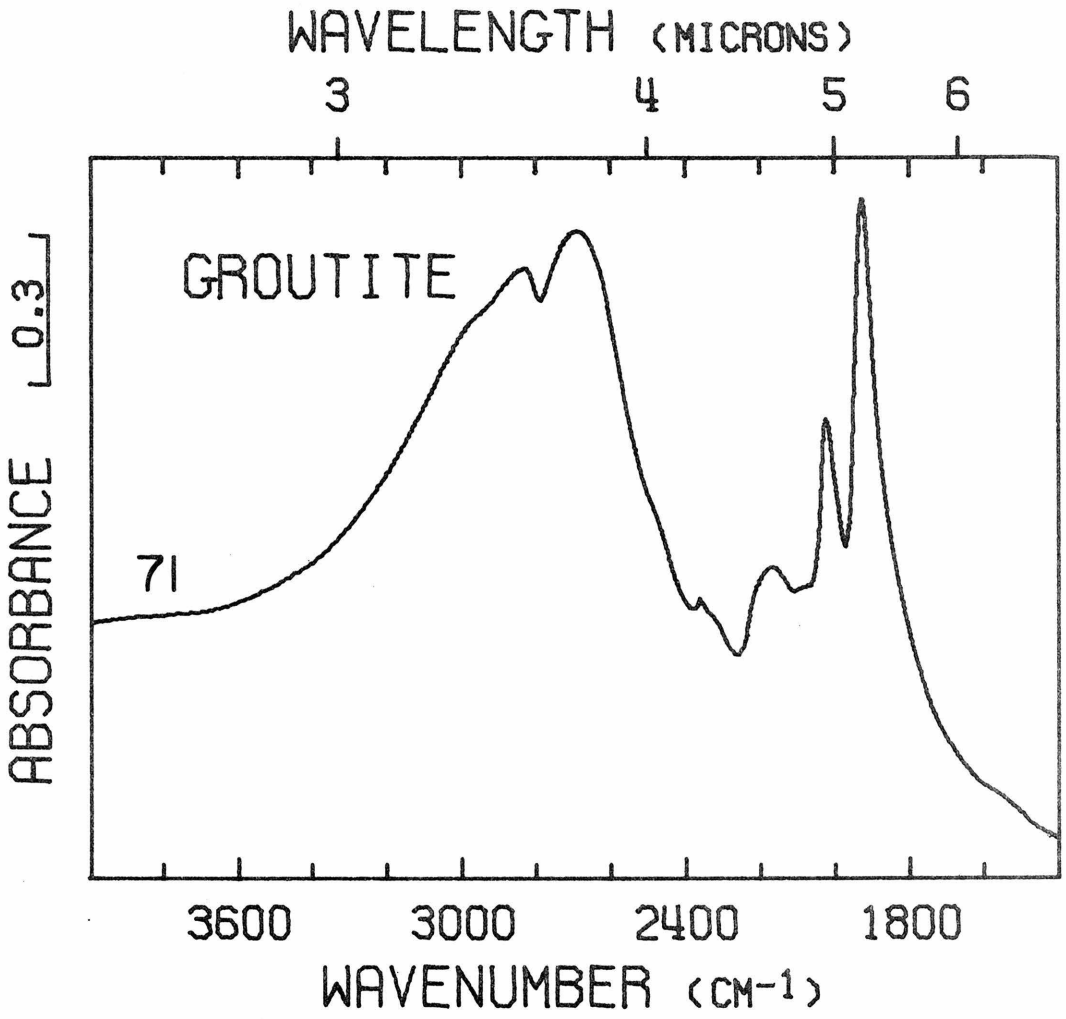

Figure 2A. Infrared spectrum of groutite. Presentation intensity: 268%. Figure continued on following page.

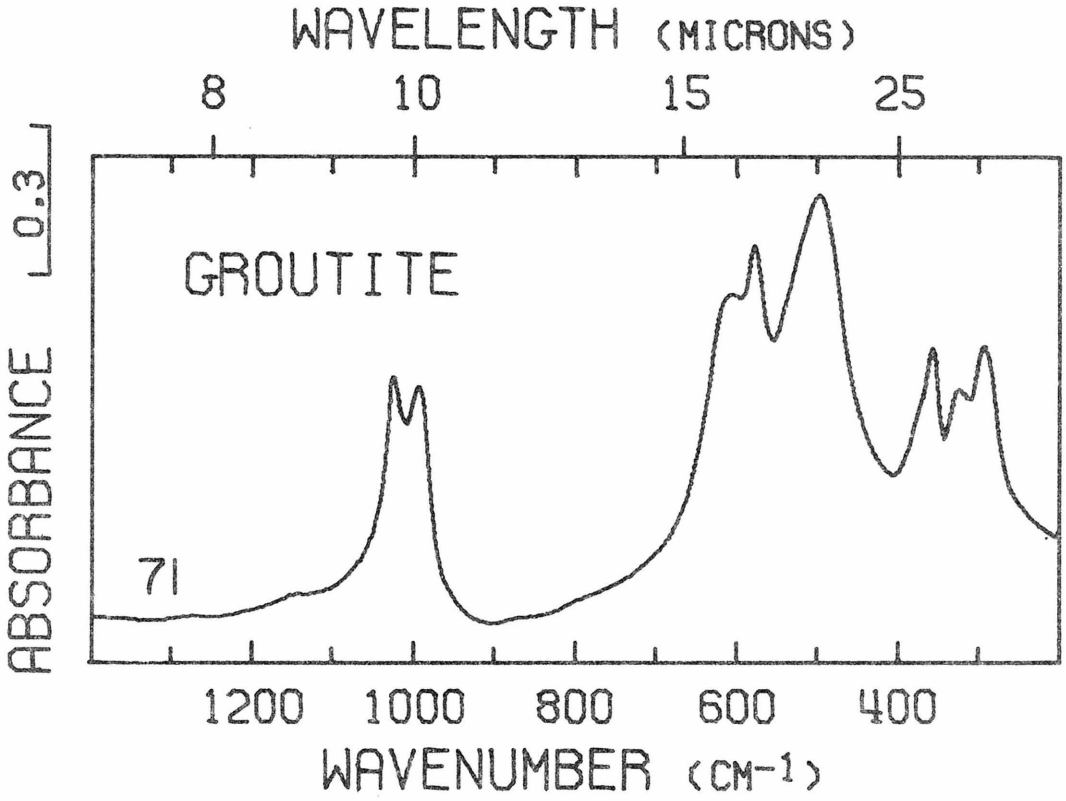

Figure 2A. Continued from preceding page.

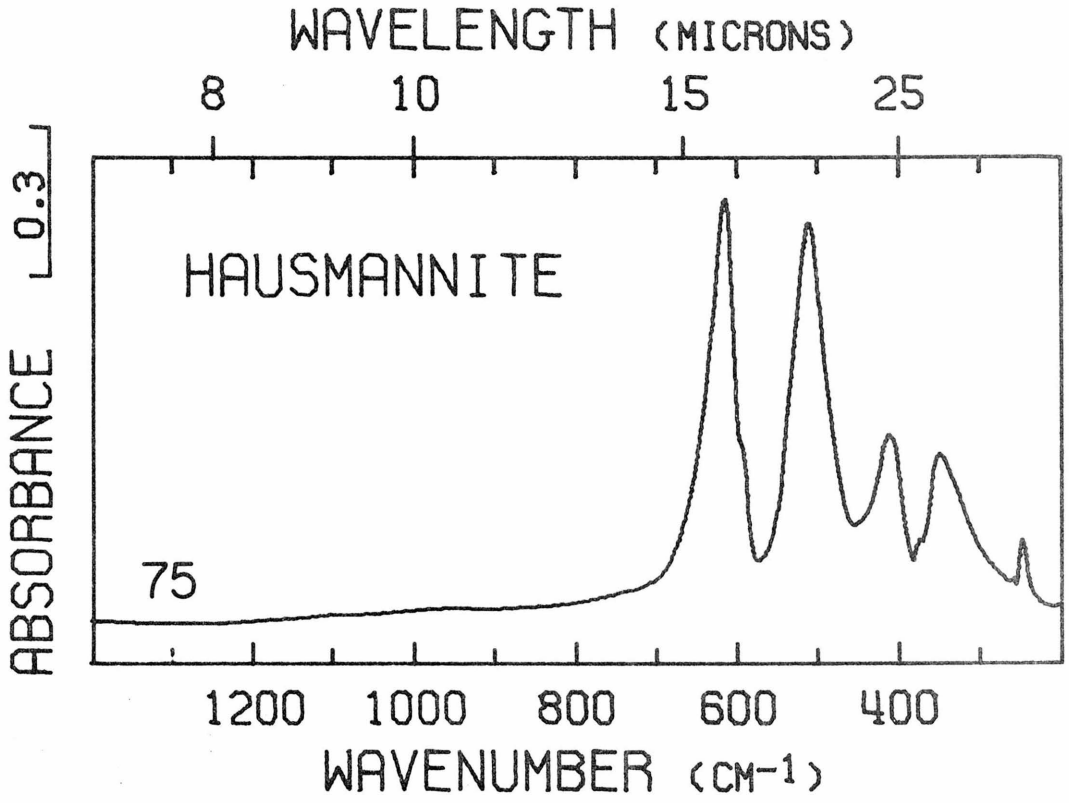

Figure 3A. Infrared spectrum of hausmannite. Presentation intensity: 182%.

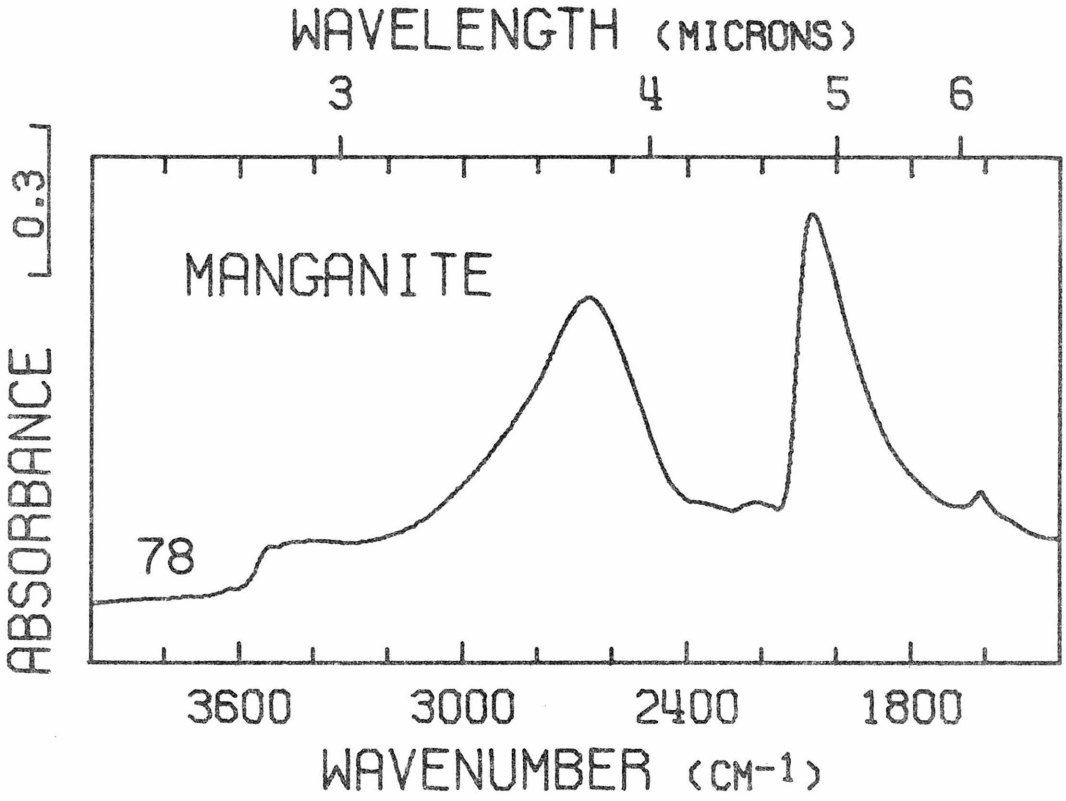

Figure 4A. Infrared spectrum of manganite. Presentation intensity: 81%. Figure continued on following page.

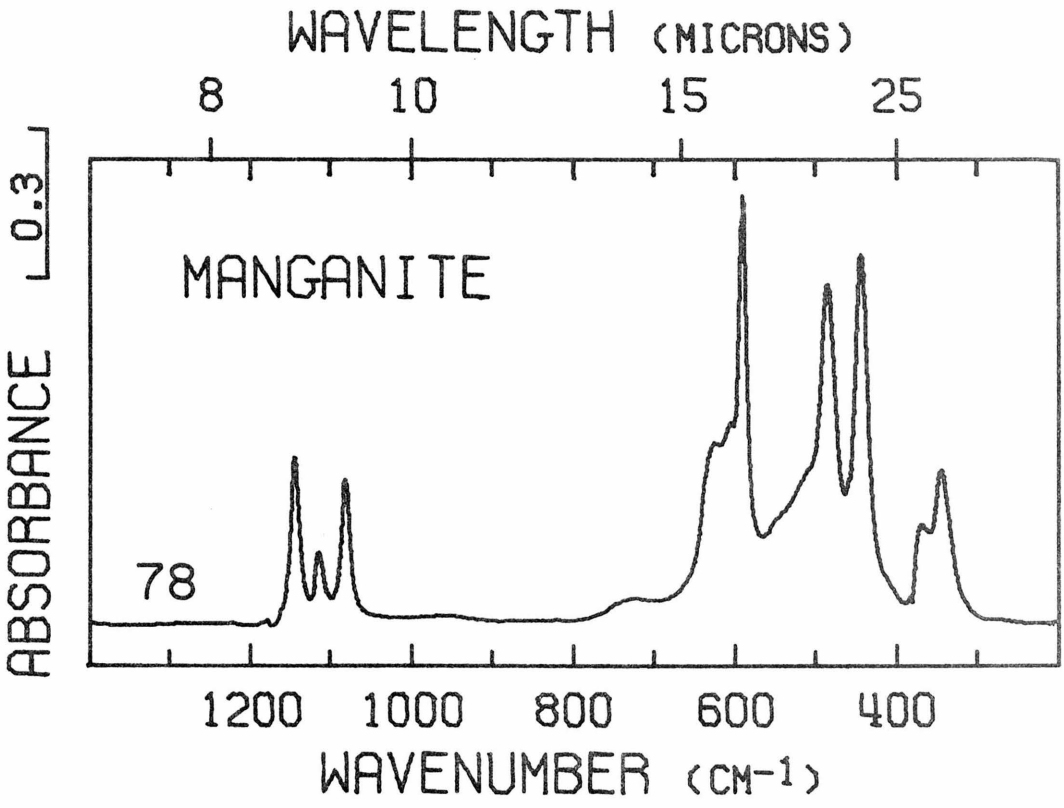

Figure 4A. Continued from preceding page.

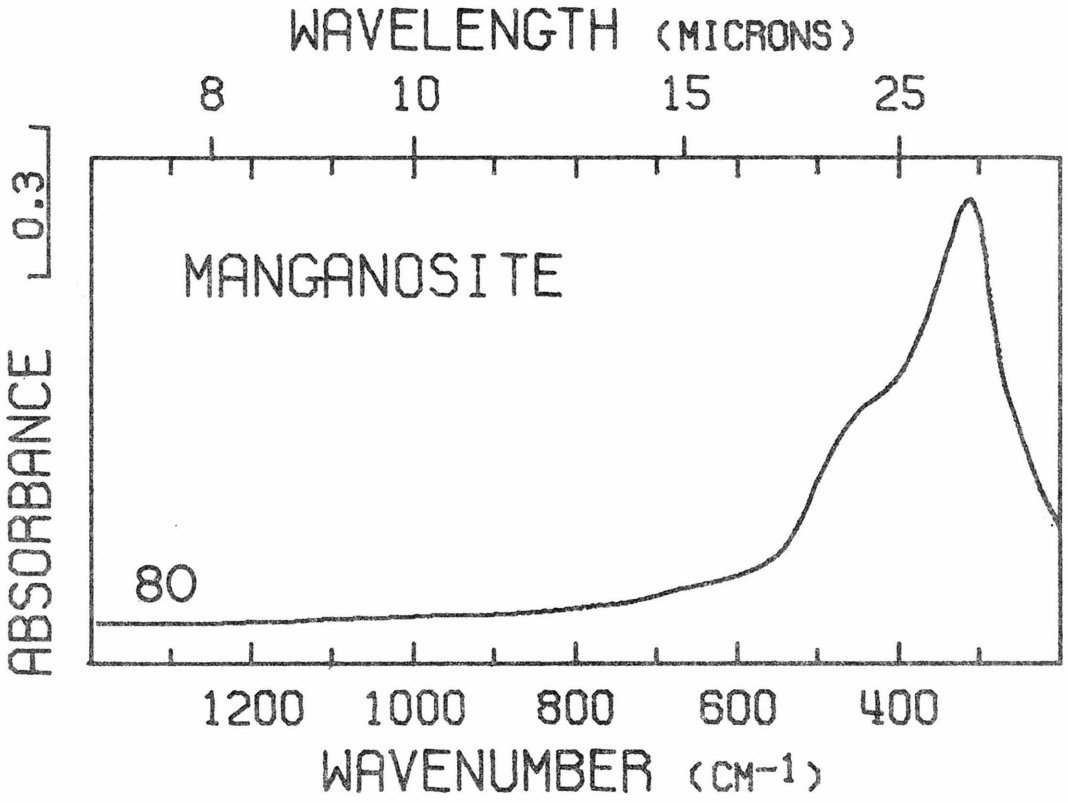

Figure 5A. Infrared spectrum of manganosite. Presentation intensity: 244%.

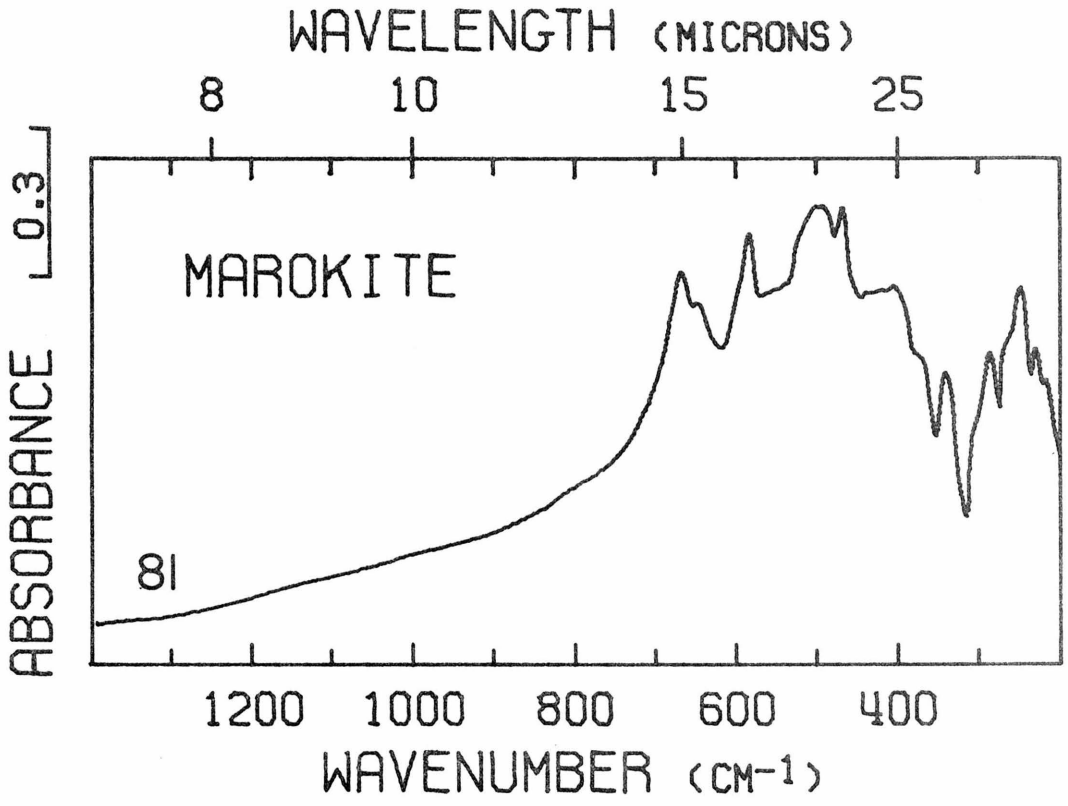

Figure 6A. Infrared spectrum of marokite. Presentation intensity: 414%.

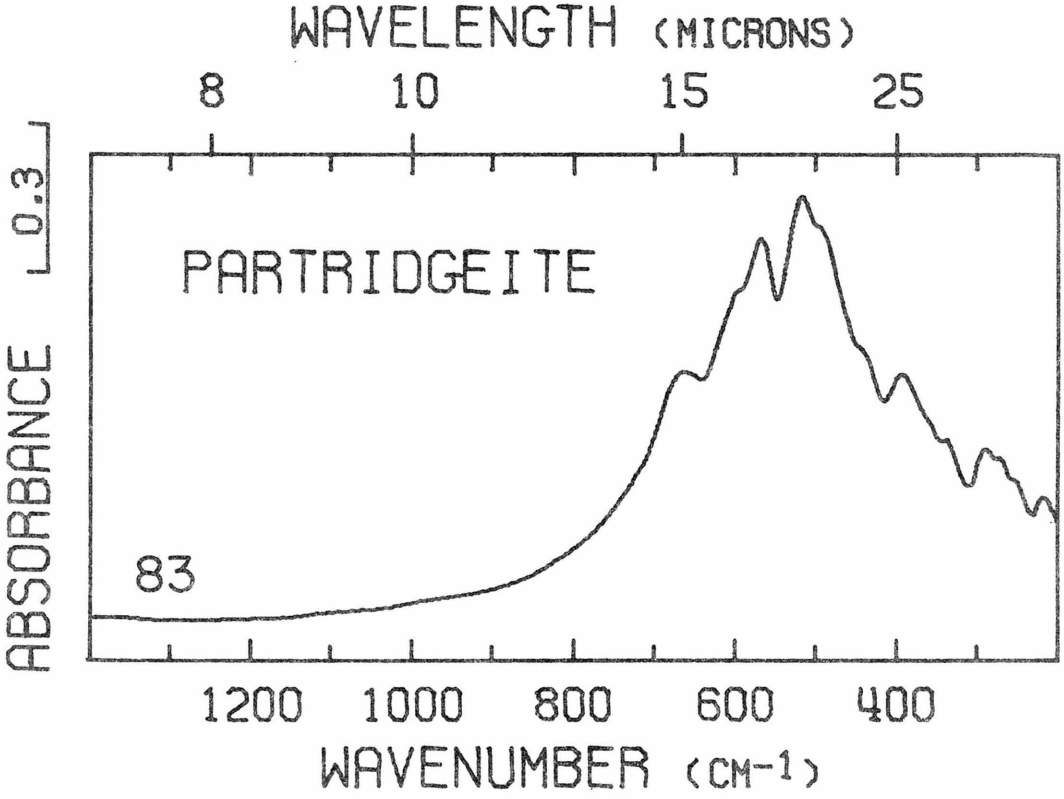

Figure 7A. Infrared spectrum of partridgeite. Presentation intensity: 248%.

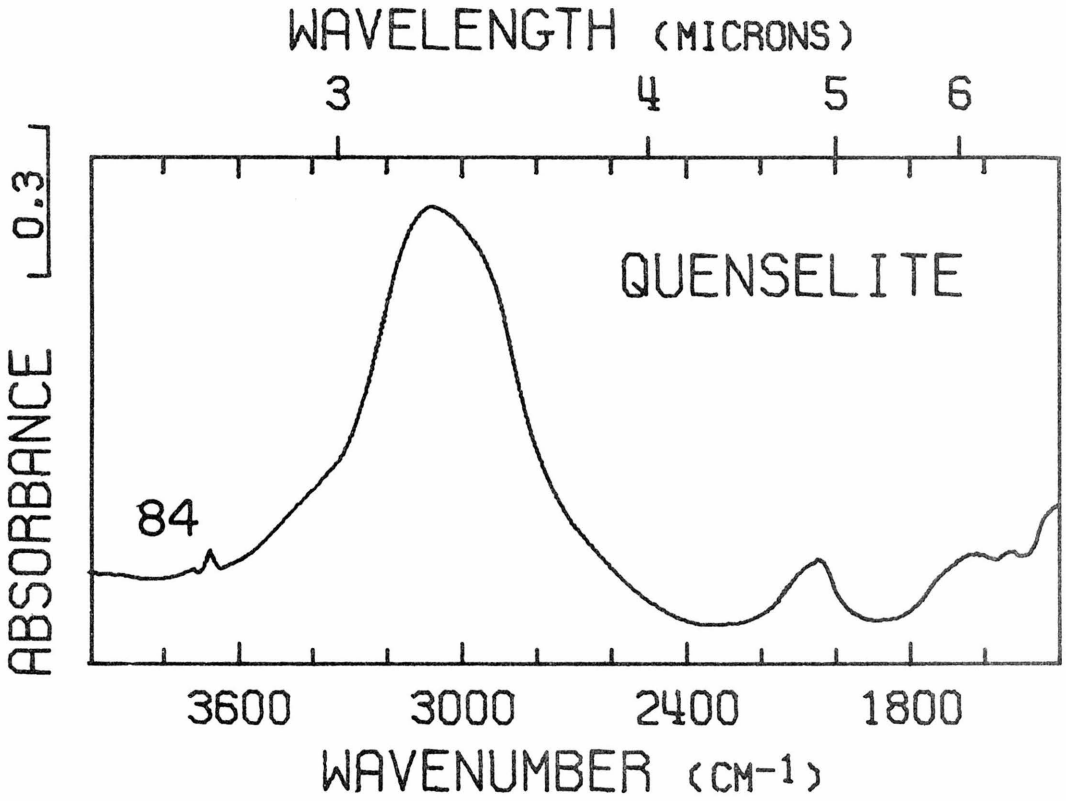

Figure 8A. Infrared spectrum of quenselite. Presentation intensity: 404%. Figure continued on following page.

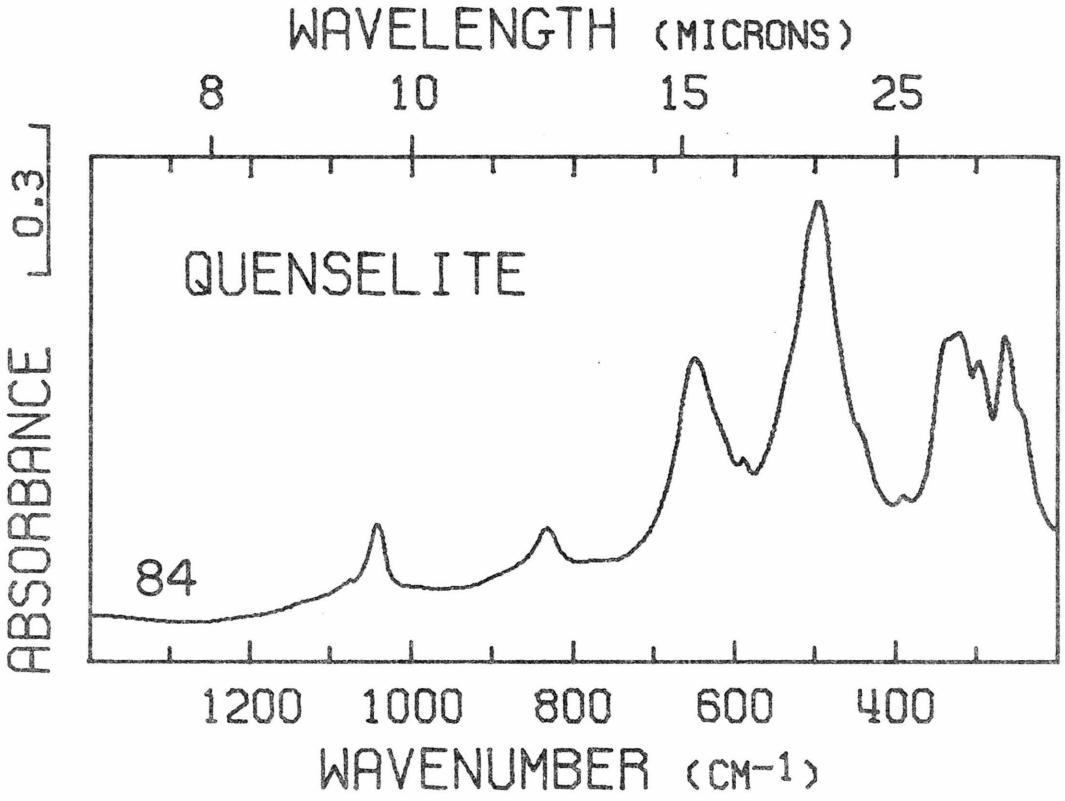

Figure 8A. Continued from preceding page.

CHAPTER 2 APPENDIX B

This appendix contains infrared spectra of samples listed in Table 1 and Table 1A, which are not contained elsewhere in this chapter. Some are included here because they are helpful but not necessary to the discussions in the text of Chapter 2; others, because they show significant differences due to the use of KBr rather than TlBr. At least one spectrum of each of the nearly pure samples in Table 1 and Table 1A are also included here to give a fuller picture of the variation present in infrared spectra of the manganese oxides.

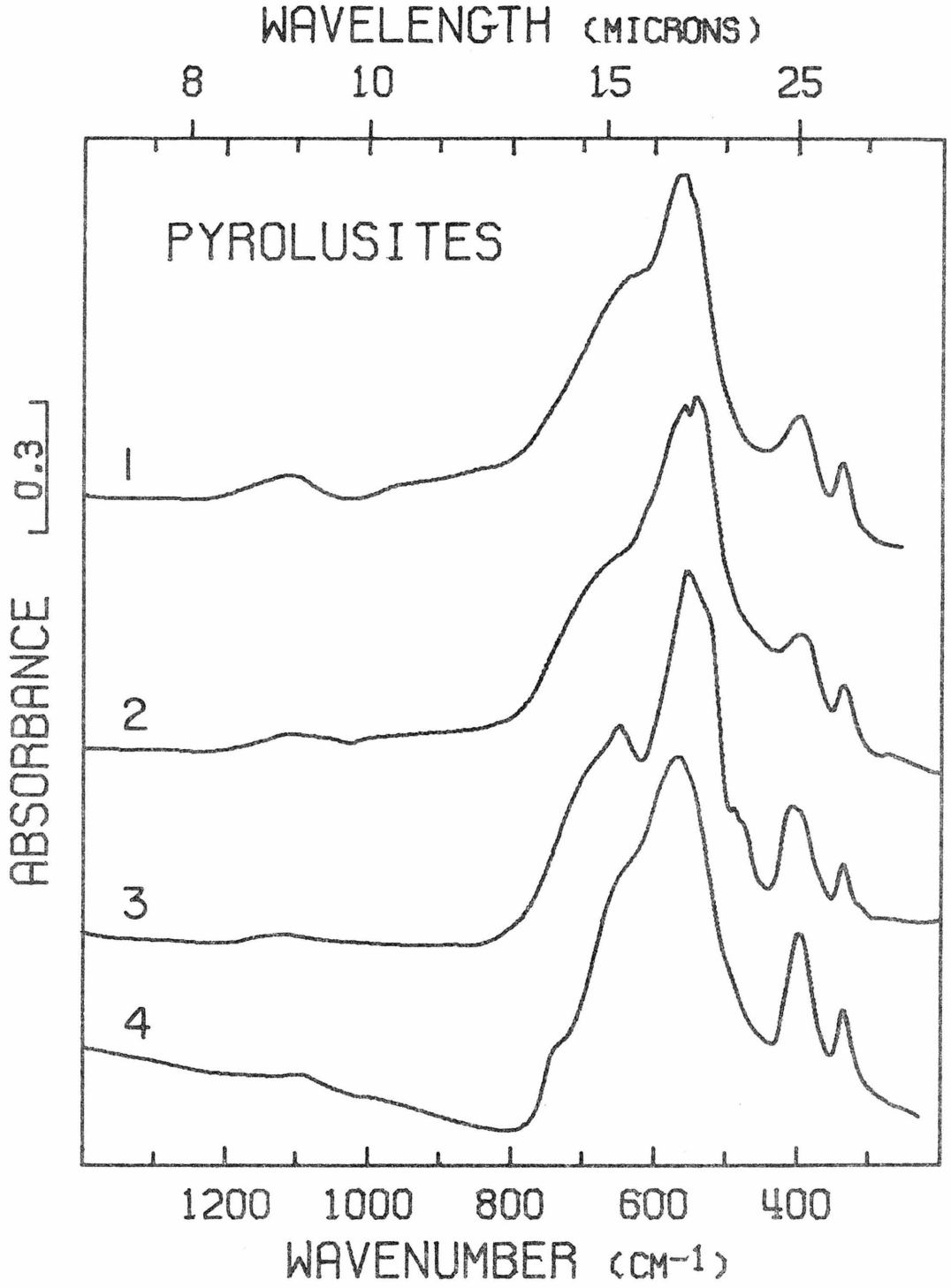

Figure 1B. Infrared spectra of pyrolusites. Presentation intensities and pellet types: #1, 230%, TlBr; #2, 223%, TlBr; #3, 142%, TlBr; #4, 148%, KBr.

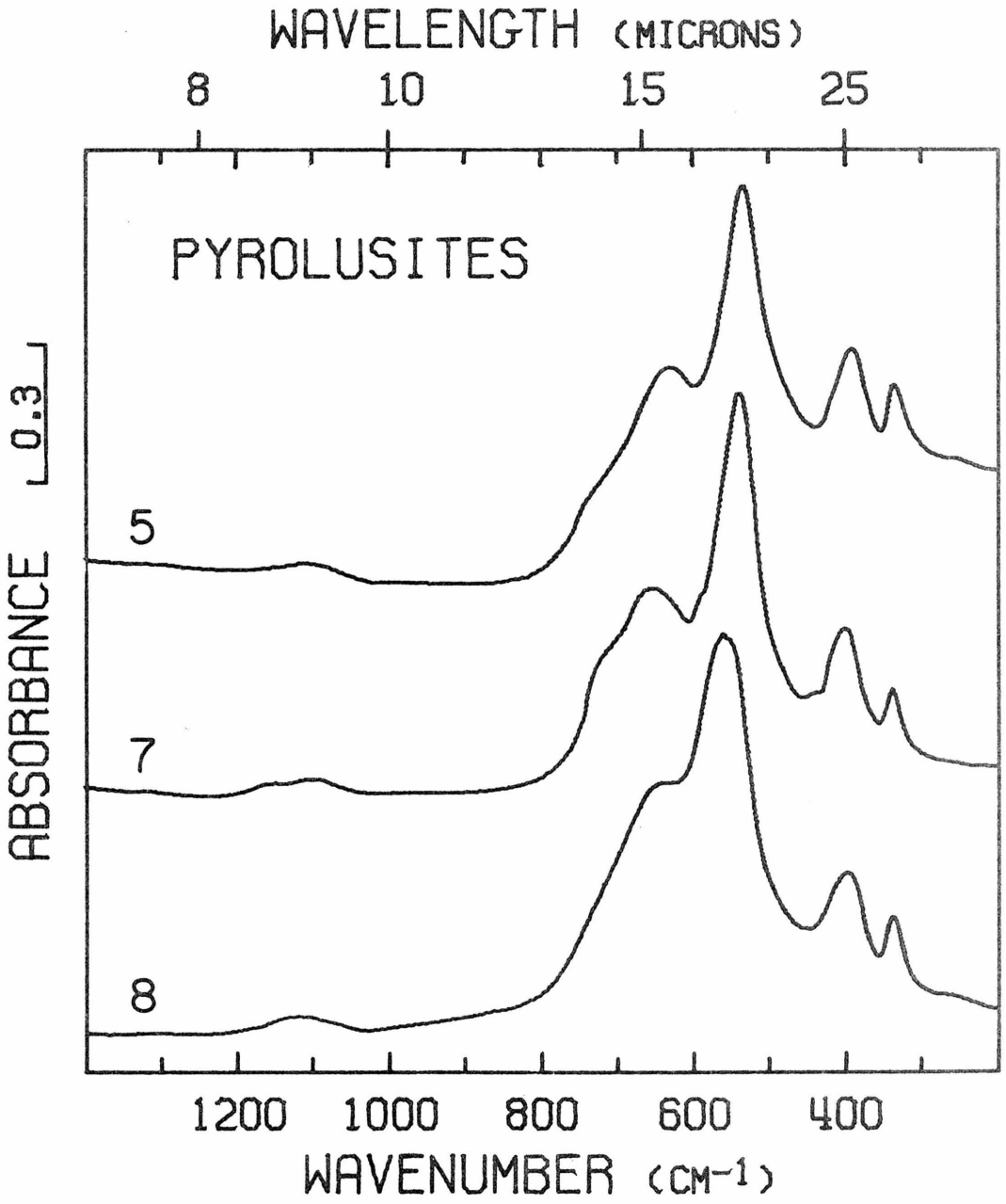

Figure 2B. Infrared spectra of pyrolusites, continued. Presentation intensities and pellet types: #5, 264%, TlBr; #7, 101%, TlBr; #8, 177%, TlBr.

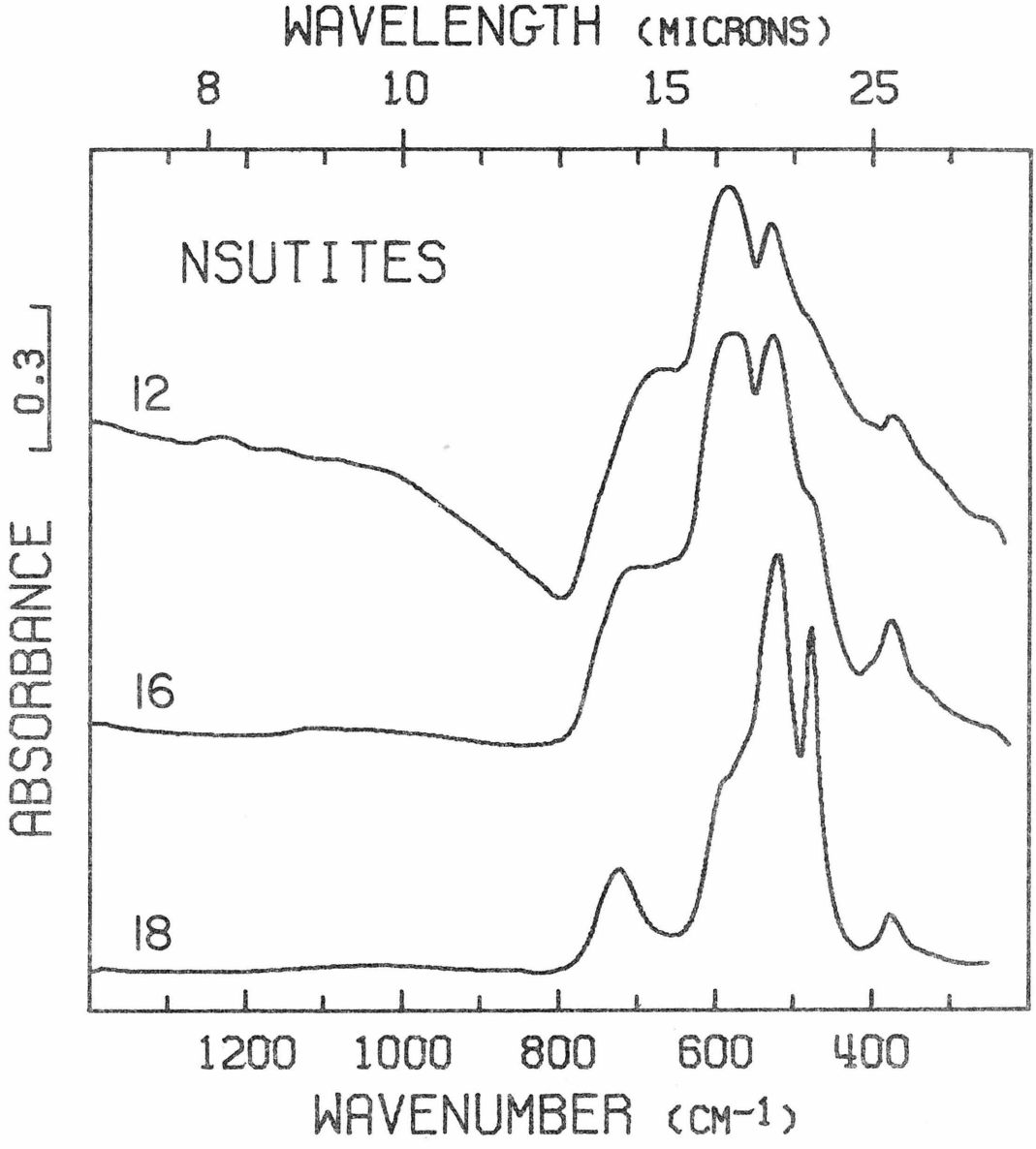

Figure 3B. Infrared spectra of nsutites. Presentation intensities and pellet types: #12, 280%, KBr; #16, 147%, KBr; #18, 79%, KBr.

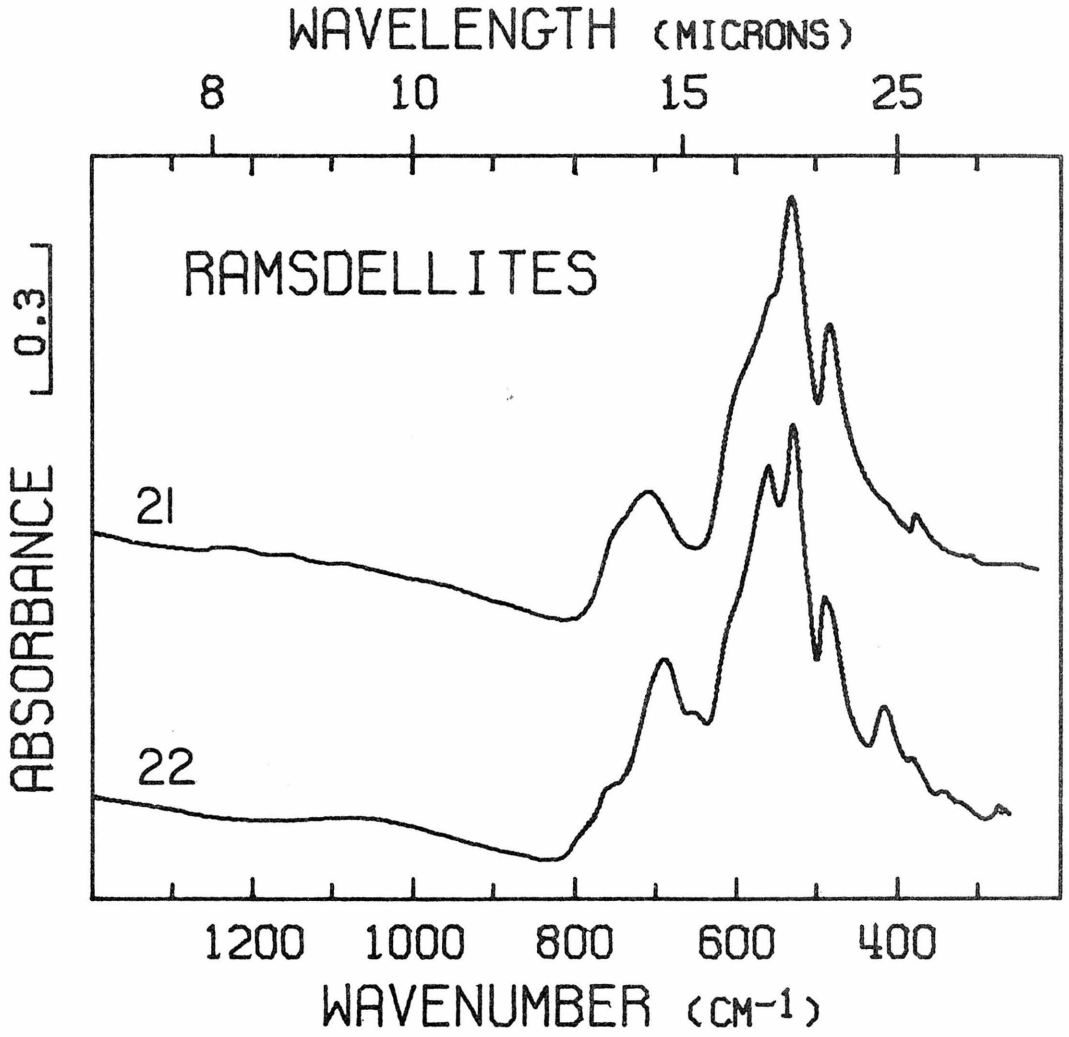

Figure 4B. Infrared spectra of ramsdellites. Presentation intensities and pellet types: #21, 161%, KBr; #22, 161%, KBr.

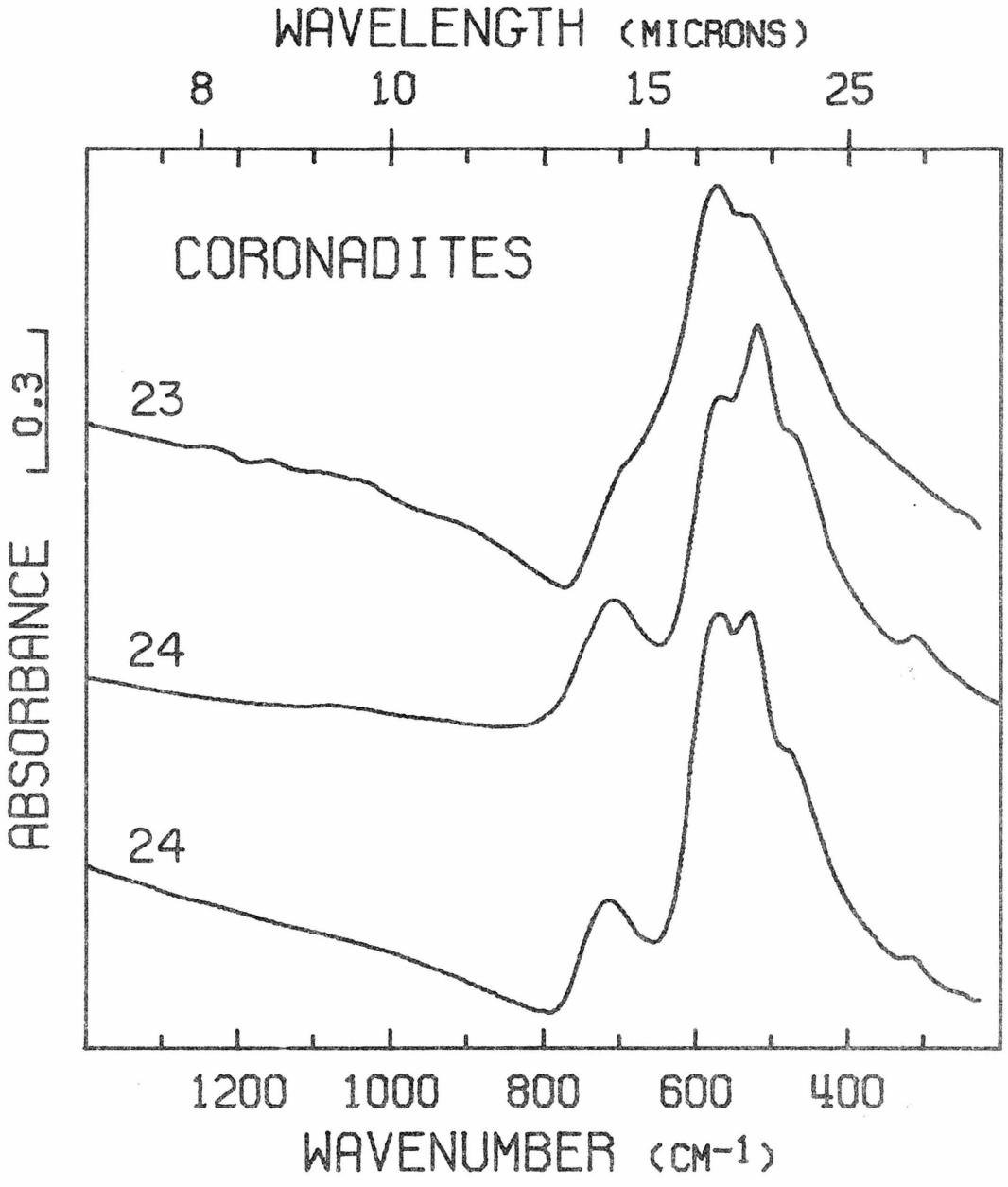

Figure 5B. Infrared spectra of coronadites. Presentation intensities and pellet types: #23, 404%, KBr; #24, 256%, TlBr; #24, 294%, KBr.

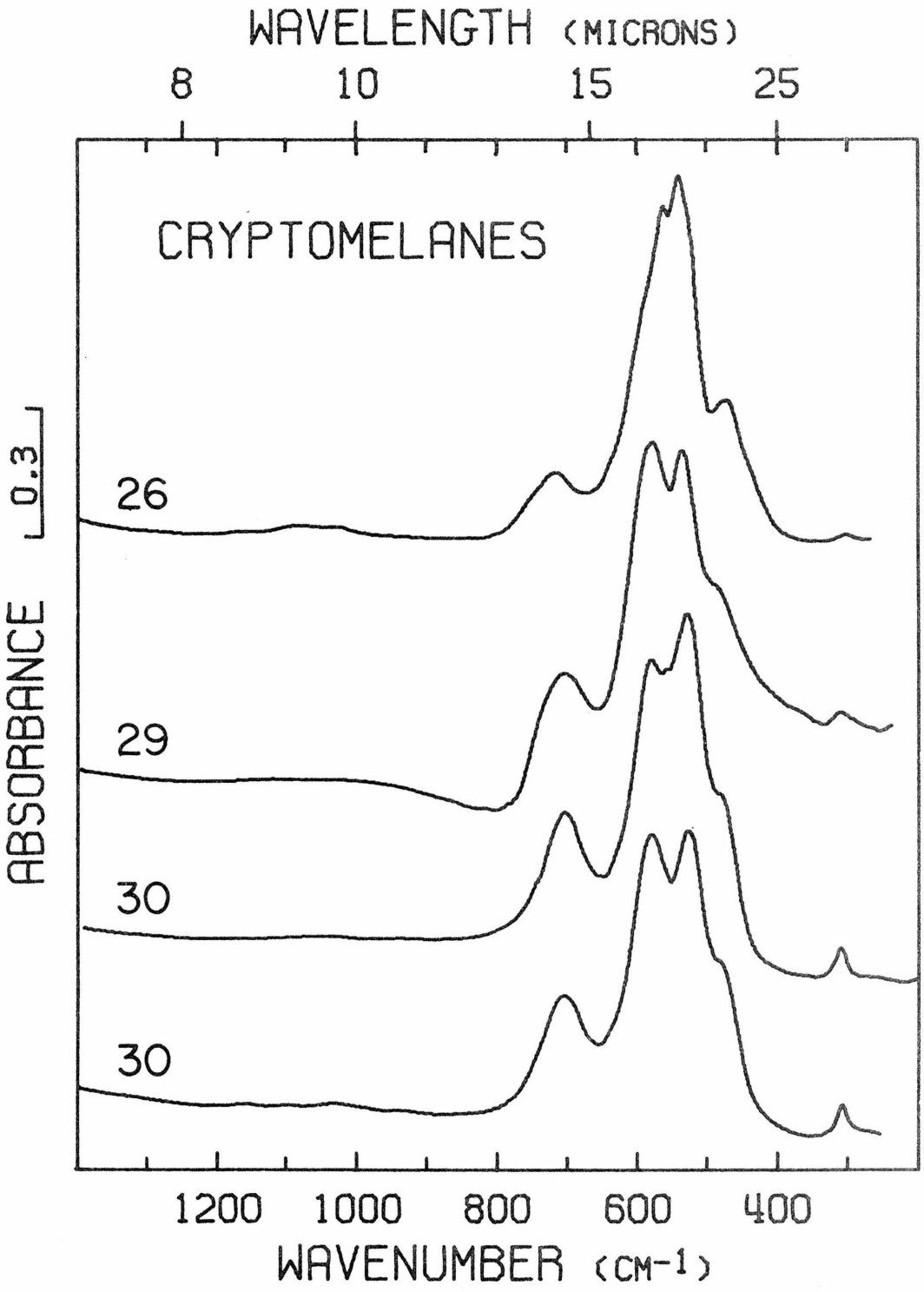

Figure 6B. Infrared spectra of cryptomelanes. Presentation intensities and pellet types: #26, 87%, KBr; #29, 243%, KBr; #30, 124%, TlBr; #30, 183%, KBr.

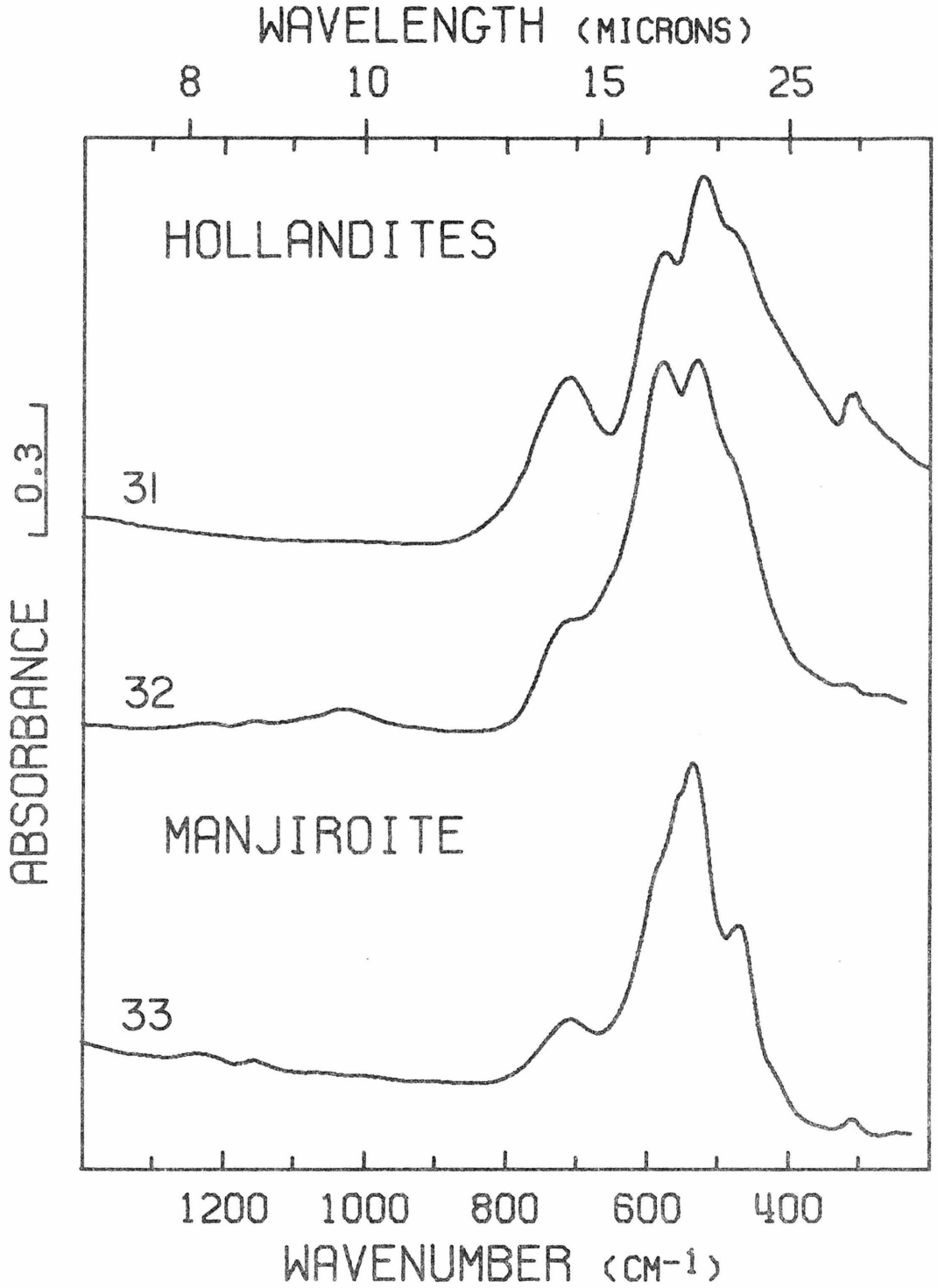

Figure 7B. Infrared spectra of hollandites and manjiroite. Presentation intensities and pellet types: #31, 252%, TlBr; #32, 186%, KBr; #33, 118%, KBr.

Figure 8B. Infrared spectra of romanechites. Presentation intensities and pellet types: #34, 102%, KBr; #35, 207%, KBr; #36, 280%, KBr; #37, 138%, TlBr; #37, 180%, KBr.

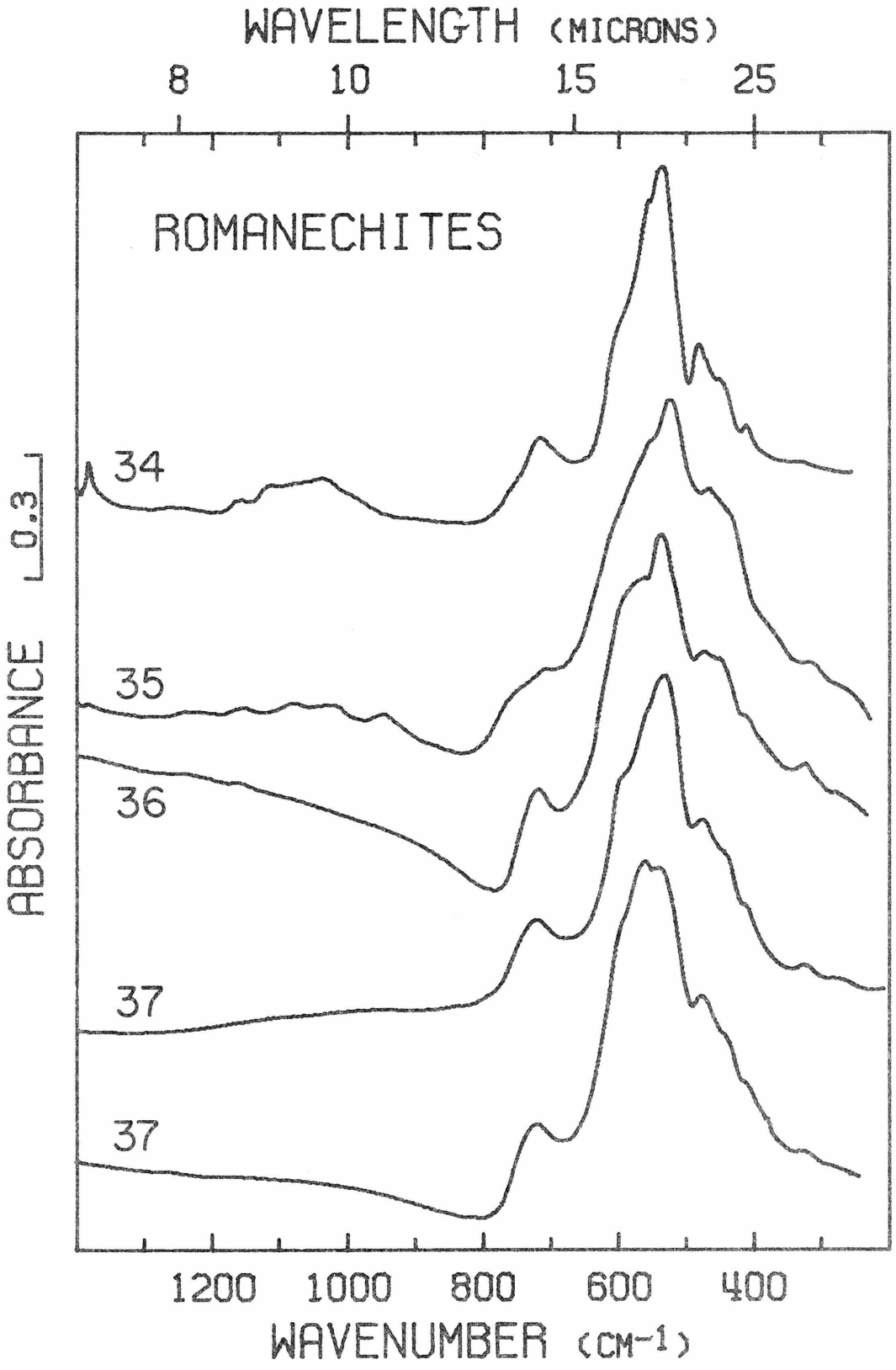
WAVELENGTH (MICRONS)
8
10
15
25
ROMANECHITES
34
35
36
37
37
0.3
ABSORBANCE
1200
1000
800
600
400
WAVENUMBER (CM-1)

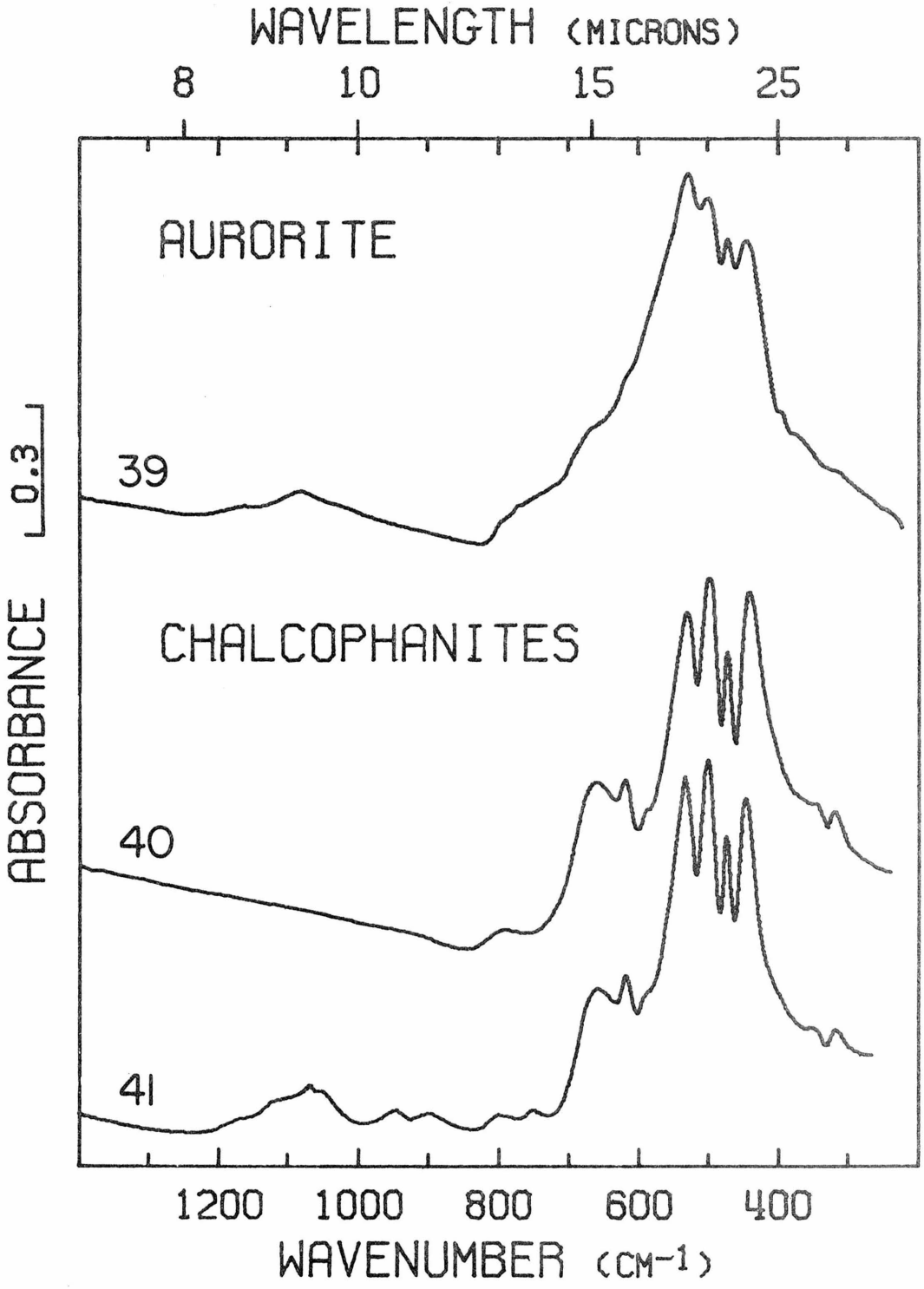

Figure 9B. Infrared spectra of aurorite and chalcophanites. Presentation intensities and pellet types: #39, 256%, KBr; #40, 164%, KBr; #41, uncertain, KBr.

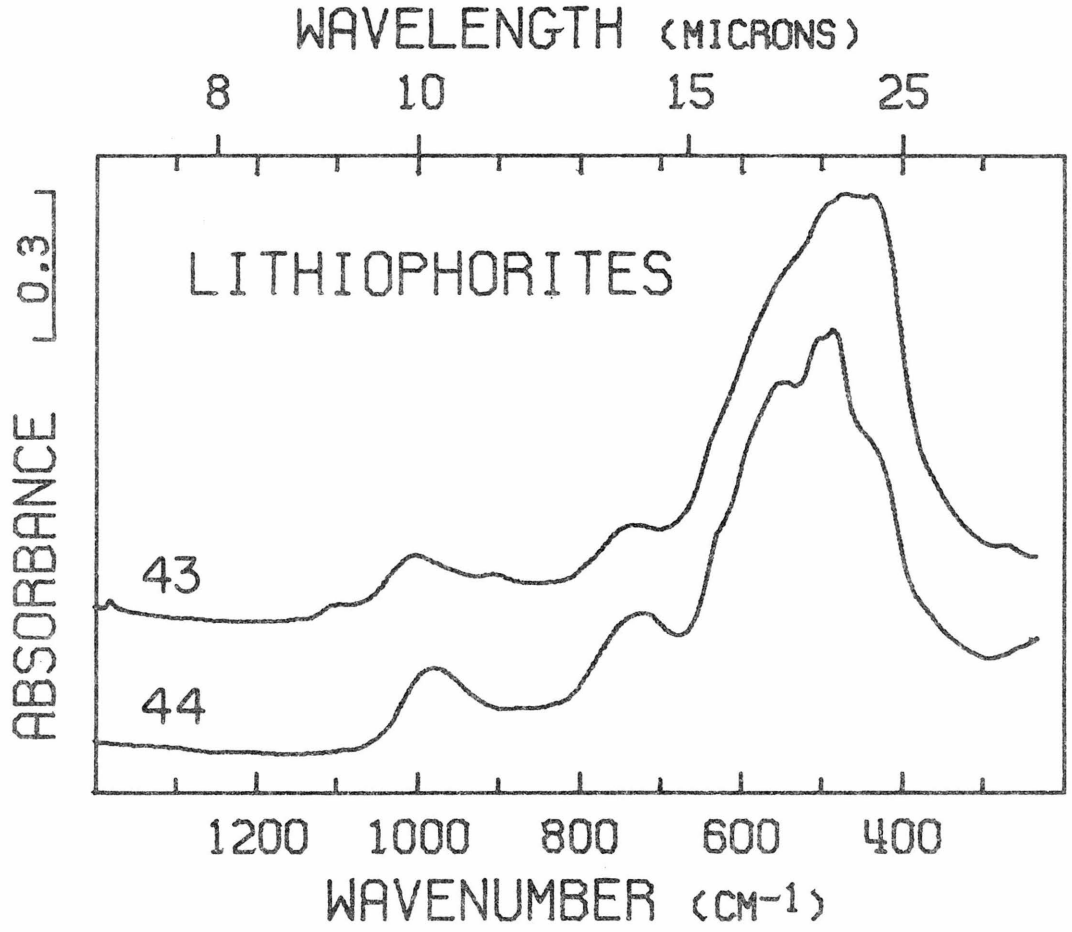

Figure 10B. Infrared spectra of lithiophorites. Presentation intensities and pellet types: #43, 151%, KBr; #44, 167%, KBr.

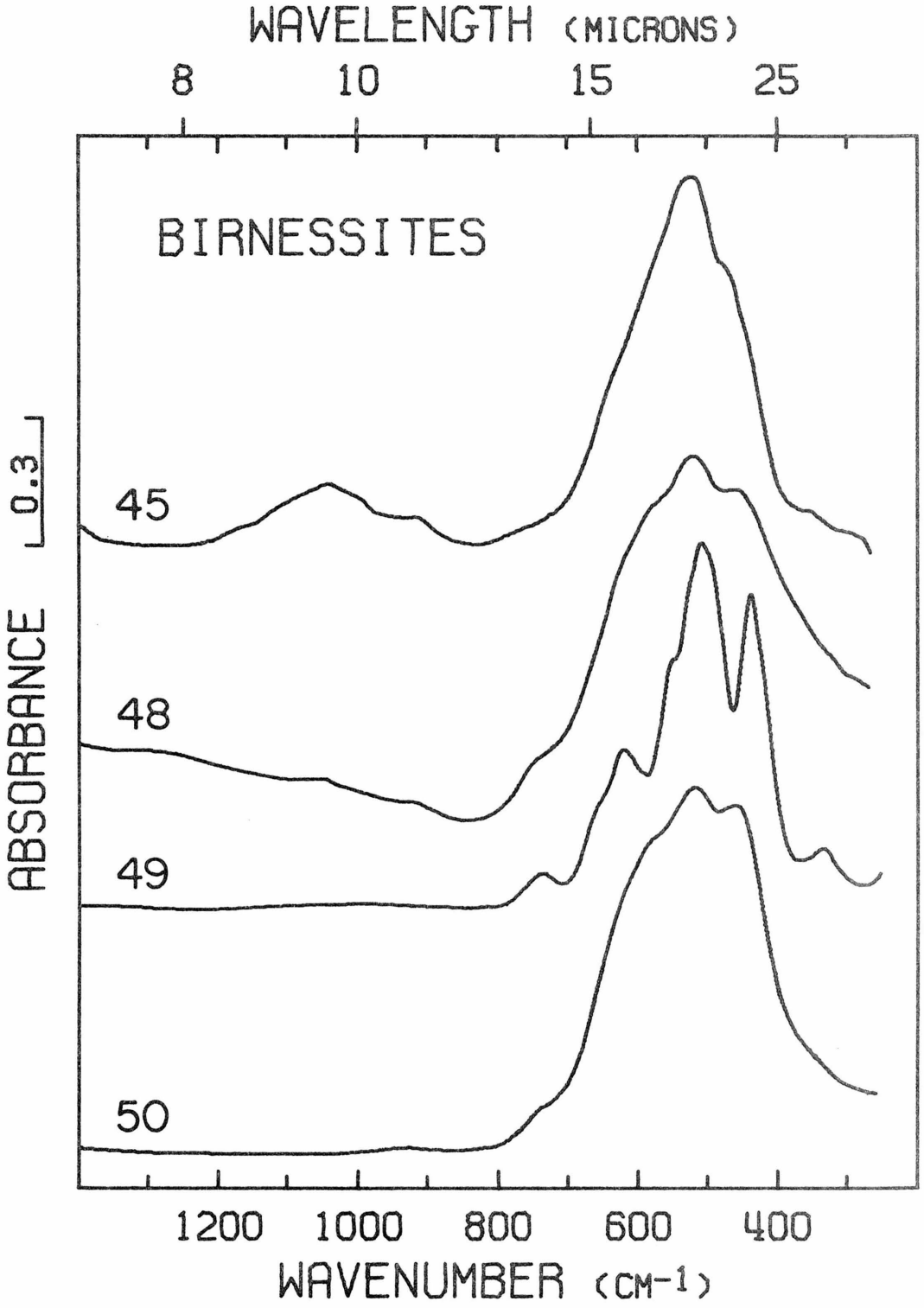

Figure 11B. Infrared spectra of birnessites. Presentation intensities and pellet types: #45, uncertain, KBr; #48, 350%, KBr; #49, 101%, KBr; #50, 163%, KBr.

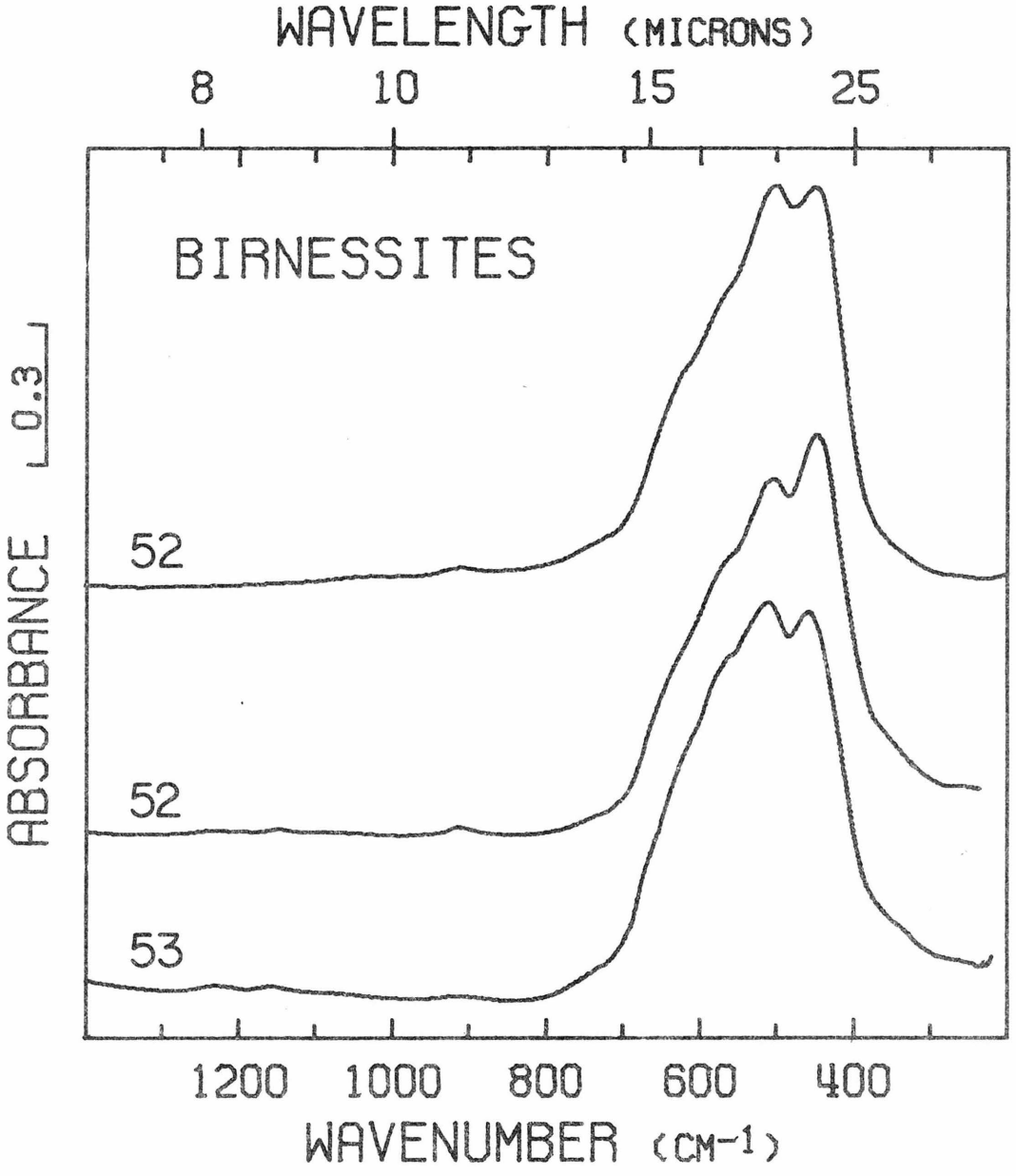

Figure 12B. Infrared spectra of birnessites, continued. Presentation intensities and pellet types: #52, 114%, TlBr; #52, 114%, KBr; #53, 140%, KBr.

Figure 13B. Infrared spectra of todorokites and woodruffite. Presentation intensities and pellet types: #55, 155%, KBr; #56, 198%, KBr; #59, 172%, KBr; #62, 175%, KBr.

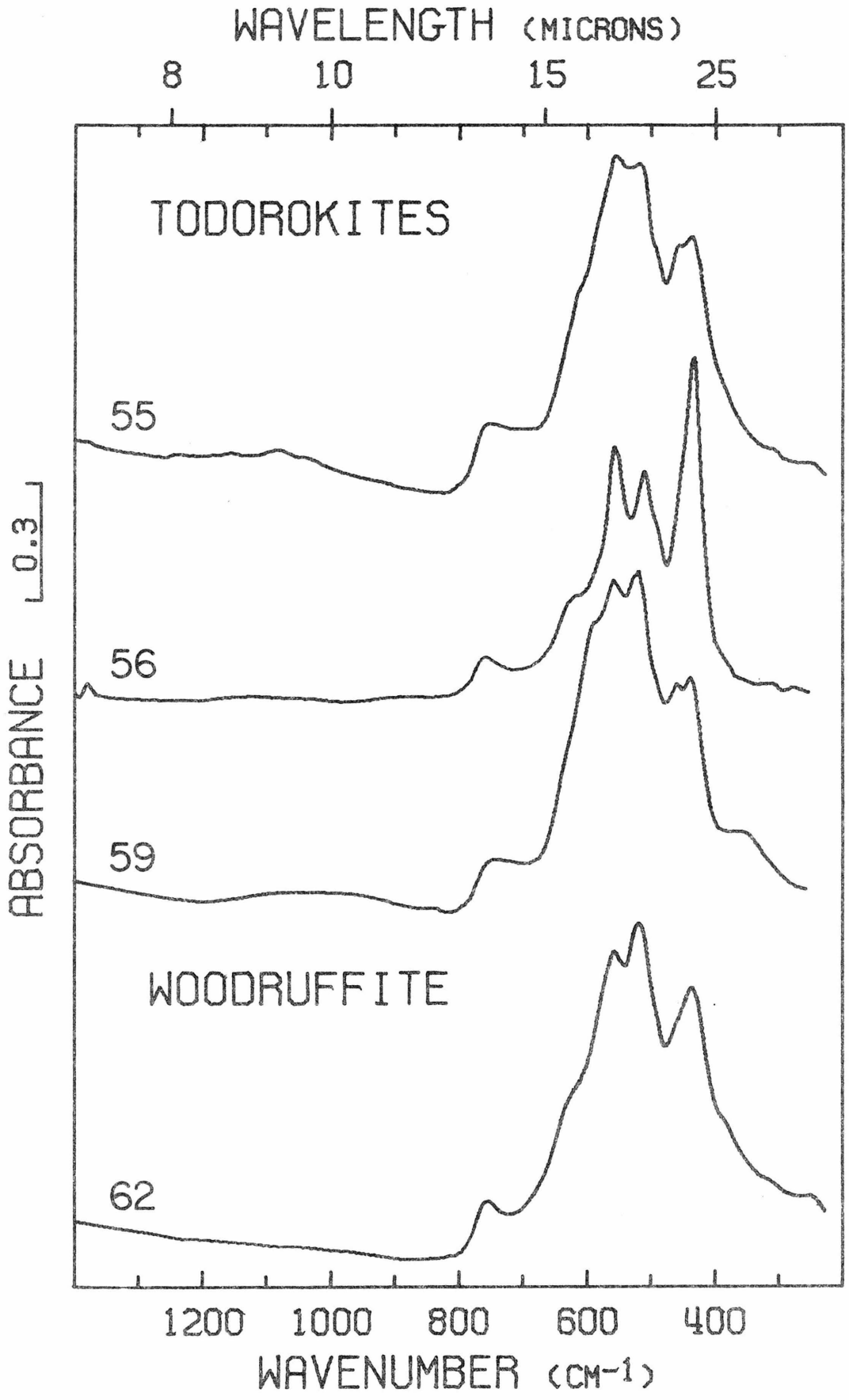
WAVELENGTH (MICRONS)
8
10
15
25
TODOROKITES
55
56
59
WOODRUFFITE
62
0.3
ABSORBANCE
1200
1000
800
600
400
WAVENUMBER (CM-1)

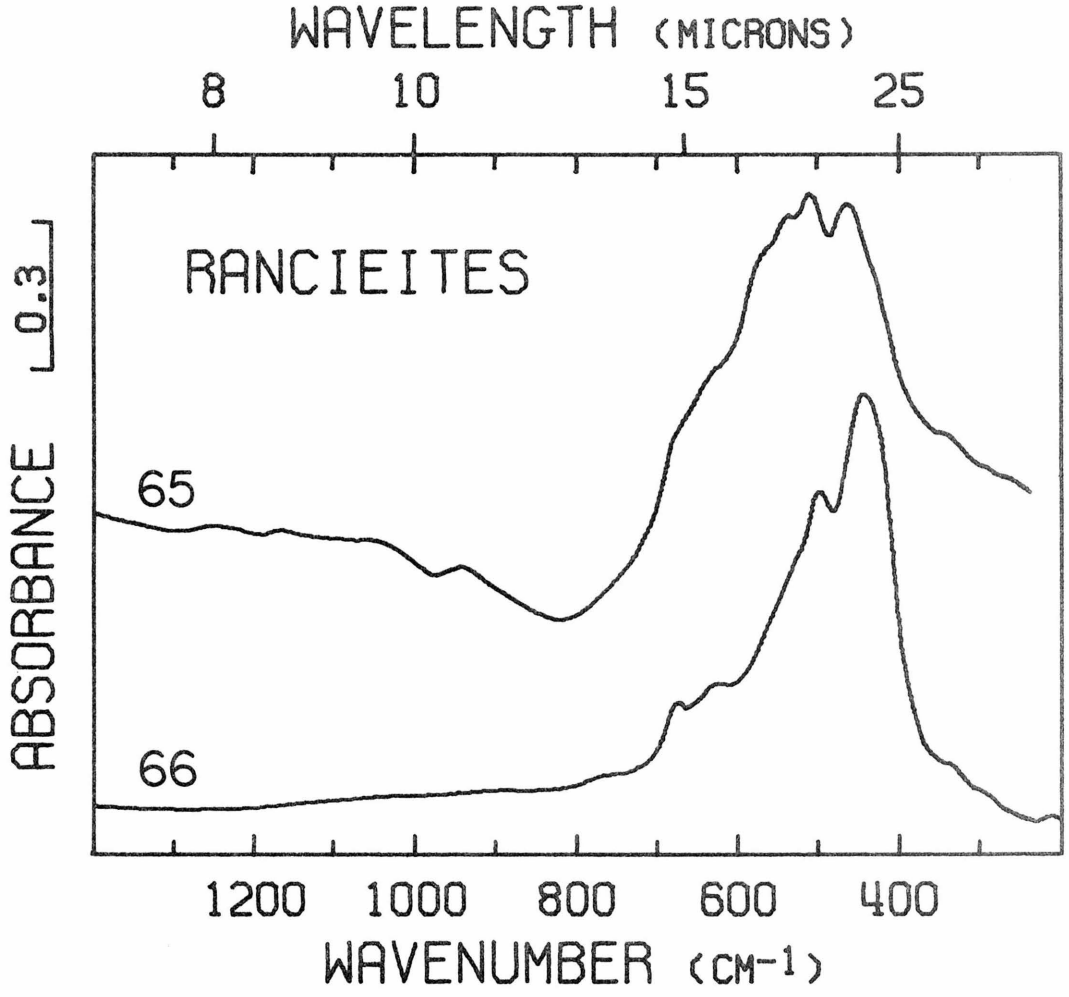

Figure 14B. Infrared spectra of rancieites. Presentation intensities and pellet types: #65, 412%, KBr; #66, 112%, TlBr. Absorption of braunite impurity removed from the spectrum of #65 (see text footnote 2).

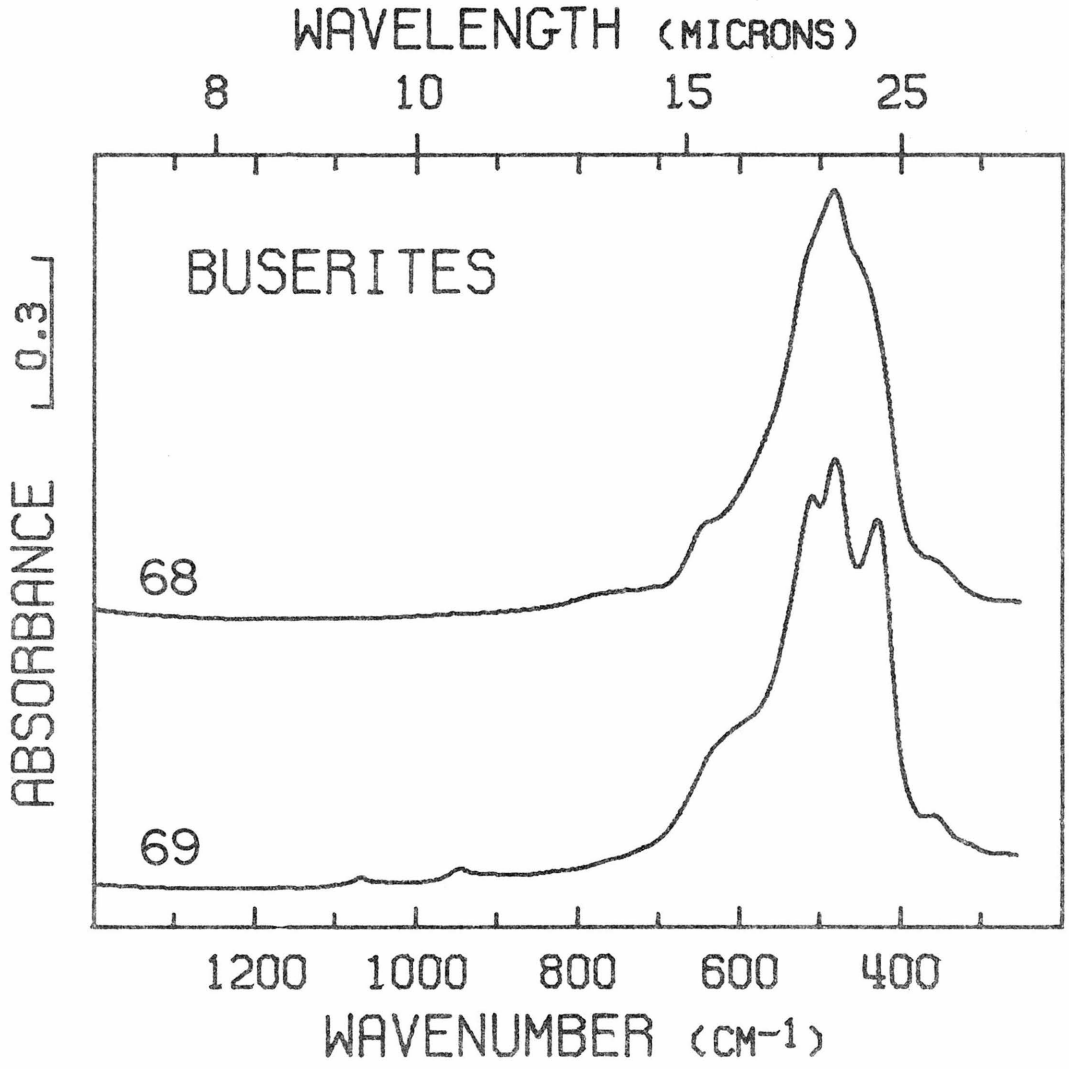

Figure 15B. Infrared spectra of buserites. Presentation intensities and pellet types: #68, 120%, KBr; #69, 97%, KBr.

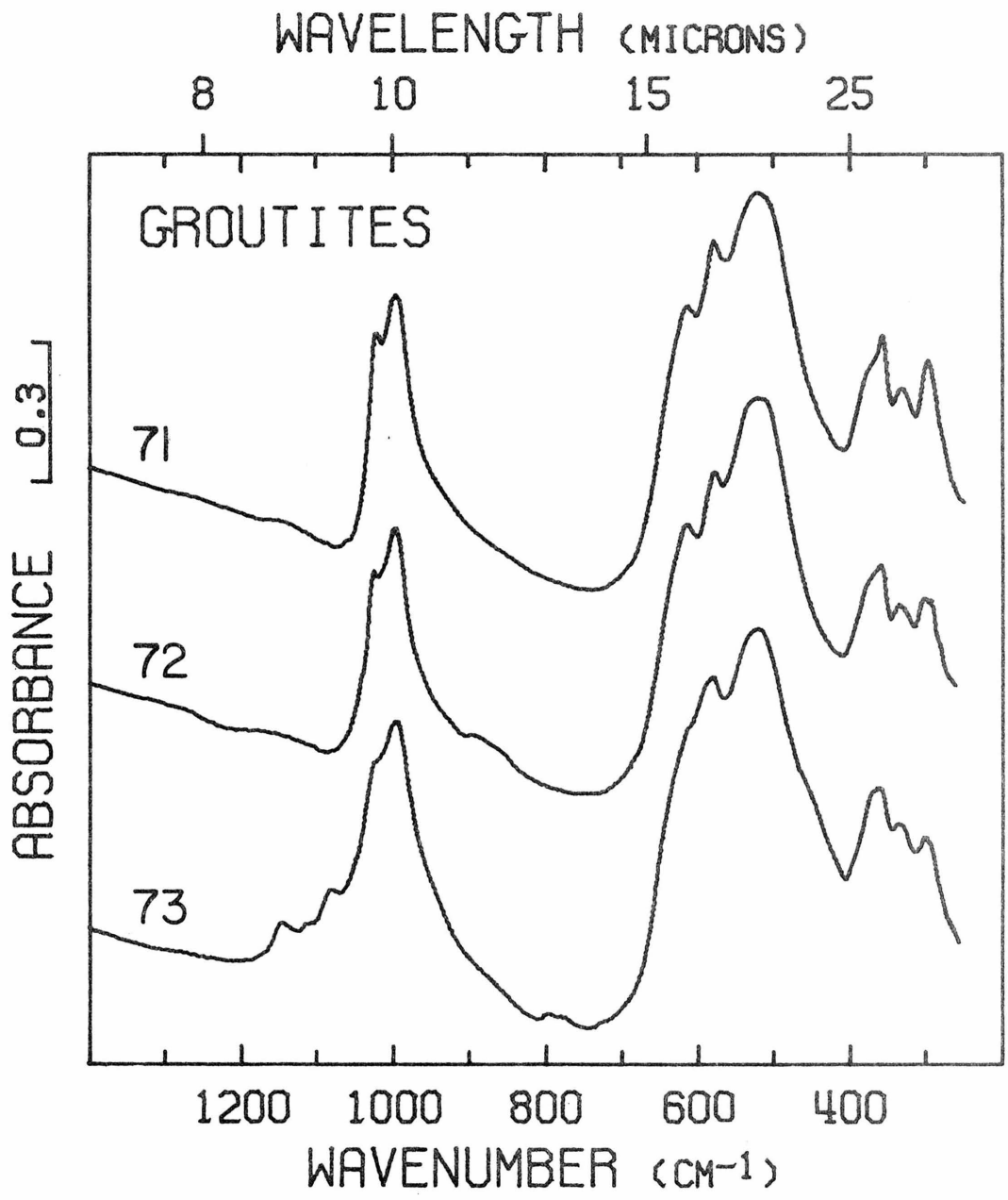

Figure 16B. Infrared spectra of groutites. Presentation intensities and pellet types: #71, 244%, KBr; #72, 256%, KBr; #73, 296%, KBr.

Figure 17B. Infrared spectra of hausmannites. Presentation intensities and pellet types: #74, 316%, KBr; #75, 188%, KBr; #76, 276%, KBr.

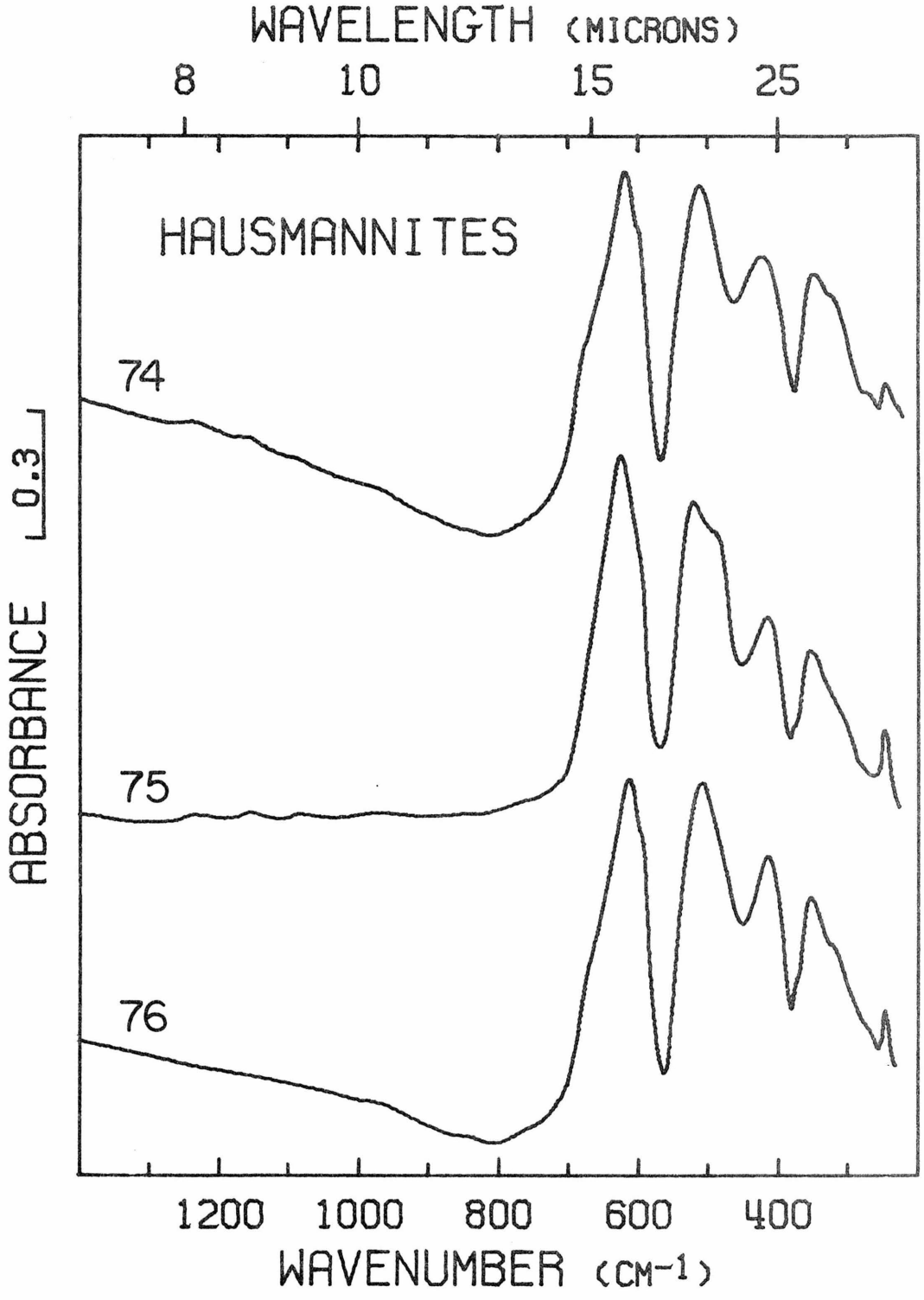
WAVELENGTH (MICRONS)
8
10
15
25
HAUSMANNITES
74
75
76
0.3
ABSORBANCE
1200
1000
800
600
400
WAVENUMBER (CM-1)

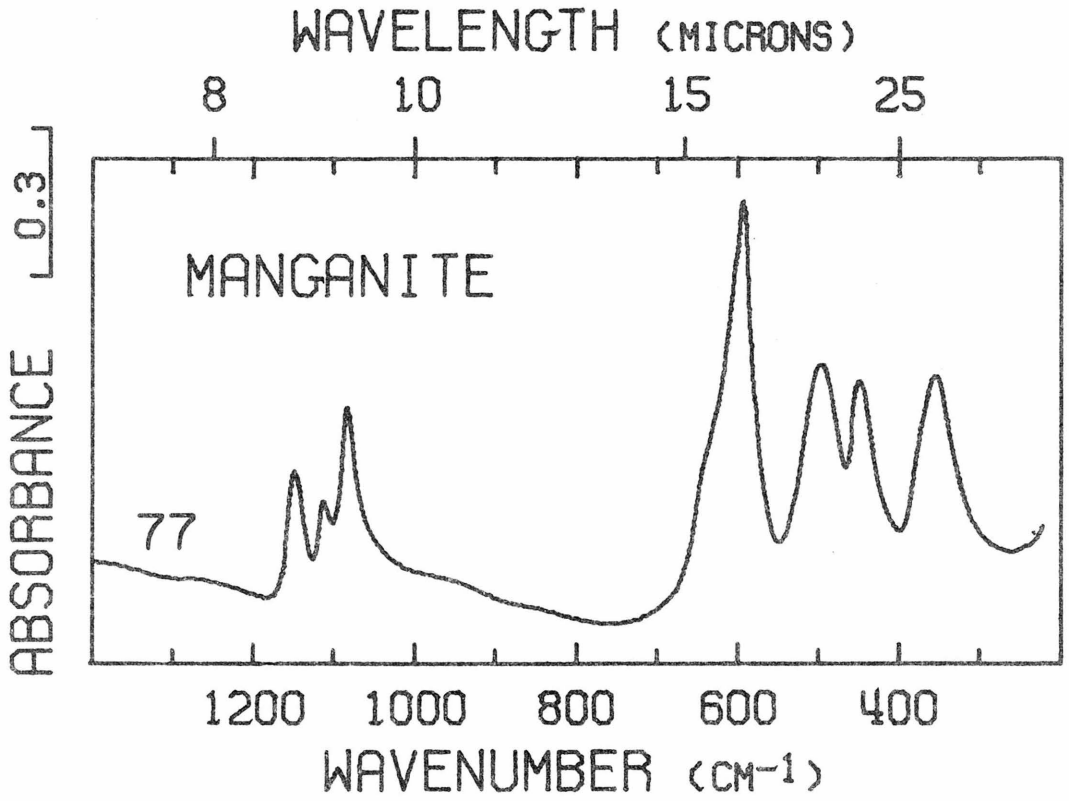

Figure 18B. Infrared spectrum of manganite. Presentation intensity and pellet type: 149%, KBr.

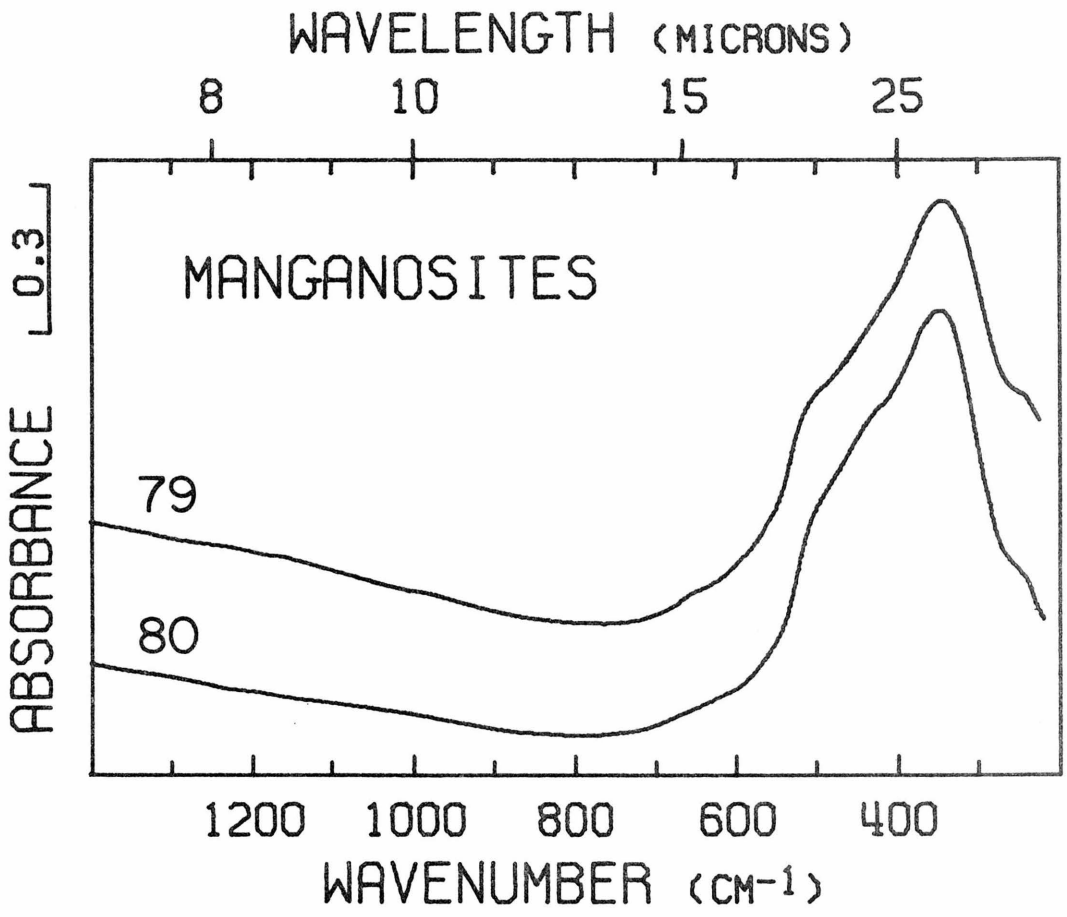

Figure 19B. Infrared spectra of manganosites. Presentation intensities and pellet types: #79, 260%, KBr; #80, 242%, KBr.

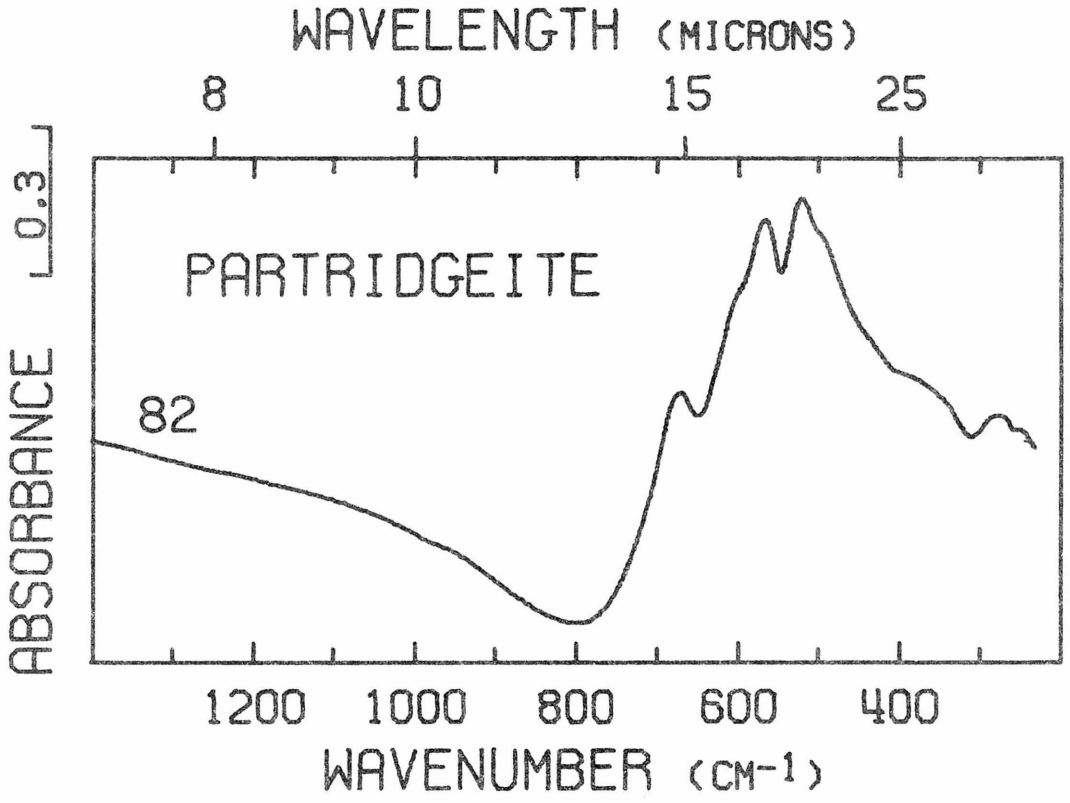

Figure 20B. Infrared spectrum of partridgeite. Presentation intensity and pellet type: 294%, KBr.

REFERENCES

Agiorgitis, G. (1969) Über differential-thermoanalytische und infrarotspektroscopische Untersuchungen von Mangan-Mineralien. Tschermaks Miner. u. Petrogr. M.H. 13, 273-283.

Bardossy, G., and Brindley, G.W. (1978) Rancieite associated with a karstic bauxite deposit. Am. Miner. 63, 762-767.

Brenet, J.P., Gabano, J.P., and Seigneurin, M. (1958) Transformations thermiques d'oxydes de manganese. In: Papers presented to the section on Inorganic Chemistry (16th International Congress of Pure and Applied Chemistry, Paris, 1957). London: Butterworth Scientific Publications, 69-80.

Brown, F.H., Pabst, A., and Sawyer, D.L. (1971) Birnessite on colemanite at Boron, California. Am. Miner. 56, 1057-1064.

Burns, R.G., and Burns, V.M. (1975) Structural relationships between the manganese(IV) oxides. In: Manganese Dioxide Symposium Vol. 1, Kozawa, A. and Brodd, R.J. (eds.). Cleveland: The Electrochemical Society, 306-327.

Burns, R.G.,and Burns, V.M. (1977a) Chapter 7, Mineralogy. In: Marine Manganese Deposits, Glasby, G.P. (ed.). Amsterdam: Elsevier, 185-248.

Burns, R.G., and Burns, V.M. (1977b) The mineralogy and crystal chemistry of deep-sea manganese nodules, a polymetallic resource of the twenty-first century. Phil. Trans. R. Soc. Lond. A. 286, 283-301.

Buser, W., Graf, P., and Feitknecht, W. (1954) Beitrag zur Kenntnis der

Mangan(II) manganite und des δ-MnO_2. Helv. Chim. Acta 37, 2322-2333.

Byström, A.M. (1949) The crystal structure of ramsdellite, an orthorhombic modification of MnO_2. Acta Chim. Scand. 3, 163-173.

Byström, A., and Byström, A.M. (1950) The crystal structure of hollandite, the related manganese oxide minerals, and α-MnO_2. Acta Crystallogr. 3, 146-154.

Byström, A., and Byström, A.M. (1951) The positions of the barium atoms in hollandite. Acta Crystallogr. 4, 469.

Champness, P.E. (1971) The transformation manganite → pyrolusite. Mineralogical Magazine 38, 245-248.

Clark, G.M. (1972) The Structures of Non-molecular Solids: A Coordinated Polyhedron Approach. London: Applied Science Publishers.

deWolff, P.M. (1959) Interpretation of some δ-MnO_2 diffraction patterns. Acta Crystallogr., 12, 341-345.

Dent Glasser, L.S., and Ingram, L. (1968) Refinement of the crystal structure of groutite, α-MnOOH. Acta Crystallogr., 24, 1233-1236.

Farmer, V.C. (ed.) (1974) The Infrared Spectra of Minerals. Mineral Society of London, London.

Finkelman, R.B., Evans, Jr., H.T., and Matzko, J.J. (1974) Manganese minerals in geodes from Chihuahua, Mexico. Mineralogical Magazine 39, 549-558.

Fleischer, M. (1960) Studies of the manganese oxide minerals. III. Psilomelane. Am. Miner. 45, 176-187.

Fleischer, M., and Faust, G.T. (1963) Studies on manganese oxide

minerals VII. Lithiophorite. Schweiz. Mineral. Petrogr. Mitt. 43, 197-216.

Frondel, C. (1953) New manganese oxides: hydrohausmannite and woodruffite. Am. Miner. 38, 761-769.

Frondel, C., Marvin, U.B., and Ito, J. (1960a) New data on birnessite and hollandite. Am. Miner. 45, 871-875.

Frondel, C., Marvin, U.B., and Ito, J. (1960b) New occurences of todorokite. Am. Miner. 45, 1167-1173.

Gattow, G., and Glemser, O. (1961a) Darstellung und Eigenshaften von Braunsteinen. II (Die γ- und η-Gruppe der Braunsteine). Z. Anorg. Allg. Chem. 309, 20-36.

Gattow, G., and Glemser, O. (1961b) Darstellung und Eigenshaften von Braunsteinen. III (Die ε-, β, und α-Gruppe der Braunsteine, über Ramsdellite und über Umwandlung der Braunsteine). Z. Anorg. Allg. Chem. 309, 121-232.

Giovanoli, R., Maurer, R., and Feitknecht, W. (1967) Zur Struktur des γ-MnO_2. Helv. Chem. Acta., 50, 1073-1080.

Giovanoli, R., Stähli, E., and Feitknecht, W (1970a) Über Oxidhydroxide des vierwertigen Mangans mit Schichtengitter 1. Mitteilung: Natriummangan (II,III) manganat (IV). Helv. Chim. Acta, 53, 209-220.

Giovanoli, R., Stähli, E., and Feitknecht, W. (1970b) Über Oxidhydroxide des vierwertigen Mangans mit Schiechtengitter 2. Mitteilung: Mangan (III) - manganat (IV). Helv. Chim. Acta 53, 453-464.

Giovanoli, R., Feitknecht, W., and Fischer, F. (1971) Reduktion von Mangan (III) - manganat (IV) mit Zimtalkohol. Helv Chim. Acta 54, 1112-1124.

Giovanoli, R., Bühler, H., and Sokolowska, K. (1973) Synthetic lithiophorite: electron microscopy and x-ray diffraction. J. Microsc., Paris 18, 271-284.

Giovanoli, R., and Bürki, P. (1975) Comparison of x-ray evidence of marine manganese nodules and nonmarine manganese ore deposits. Chimia 29, 266-269.

Glemser, O., Gattow, G., and Meisiek, H. (1961) Darstellung und Eigenschaften von Braunsteinen. I (Die δ-Gruppe der Braunsteine). Z. Anorg. Allg. Chem. 309, 1-19.

Glover, E.D. (1977) Characterization of a marine birnessite. Am. Miner. 62, 278-285.

Goldman, D.S., Rossman, G.R., and Dollase, W.A. (1977) Channel constituents in cordierite. Am. Miner 62, 1144-1157.

Goldman, D.S., Rossman, G.R., and Parkin, K.M. (1978) Channel constituents in beryl. Phys. Chem. Miner, in press.

Gruner, J.W. (1947) Groutite, $HMnO_2$, a new mineral of the diaspore-goethite group. Am. Miner. 32, 654-659.

Kolta, G.A., Kerim, F.M.A., Azim, A.A.A. (1971) Infrared absorption spectra of some manganese dioxide modifications and their thermal products. Z. Anorg. Allg. Chem. 384, 260-266.

Laudy, J.H.A., and de Wolff, P.M. (1963) X-ray investigation of the γ-β transformation of MnO_2. Appl. Sci. Res. Sect. B 10, 157-168.

McKenzie, R.M. (1971) The synthesis of birnessite, cryptomelane, and some other oxides and hydroxides of manganese. Mineralogical Magazine 38, 493-502.

Mitchell, R.S., and Corey, A.S. (1973) Braunite and sursassite from

Los Angeles County, California. Mineralogical Record 4, 290-293.

Moenke, H. (1962) Mineral spectren. Akademie-Verlag, Berlin.

Moore, T.E., Ellis, M., and Selwood, P.W. (1950) Solid oxides and hydroxides of manganese. J. Am. Chem. Soc. 72, 856-872.

Mukherjee, B. (1959) X-Ray study of psilomelane and cryptomelane. Mineralogical Magazine 32, 166-171.

Mukherjee, B. (1965) Crystallography of psilomelane, $A_3X_6Mn_8O_{16}$. Mineralogical Magazine 35, 643-655.

Palanche, C., Berman, H., and Frondel, C. (1944) Dana's System of Mineralogy, Volume I. John Wiley and Sons, Inc., New York.

Prost, R. (1973) The influence of the Christiansen effect on I.R. spectra of powders. Clays Clay. Miner. 21, 363-368.

Radtke, A.S., Taylor, C.M., and Hewett, D.F. (1967) Aurorite, argentian todorokite and hydrous silver-bearing lead manganese oxide. Econ. Geol. 62, 186-206.

Richmond, W.E., Fleischer, M., and Mrose, M.E. (1969) Studies on manganese oxide minerals. IX rancieite. Bull. Soc. Fr. Mineral. Cristallogr. 92, 191-195.

Segeler, C.G. (1959) Notes on a second occurrence of groutite. Am. Miner. 44, 877-878.

Valarelli, J.V., Perrier, M., and Vicentini, G. (1968) Infrared spectra of some manganese minerals. An. Acad. brasil. Ciênc. 40, 289-296.

van der Marel, H.W., and Beutelspacher, H. (1976) Atlas of Infrared

Spectra of Clay Minerals and their Admixtures. Elsevier, Amsterdam.

Vaux, G., and Bennet, H. (1937) X-ray studies on pyrolusite (including polianite) and psilomelane. Mineralogical Magazine 24, 521-526.

Wadsley, A.D. (1950a) A hydrous manganese oxide with exchange properties. J. Am. Chem. Soc. 72, 1782-1784.

Wadsley, A.D. (1950b) Synthesis of some hydrated manganese minerals. Am. Miner. 35, 485-499.

Wadsley, A.D. (1952) The structure of lithiophorite, $(Al,Li)MnO_2(OH)_2$. Acta. Crystallogr. 5, 676-680.

Wadsley, A.D. (1953) The crystal structure of psilomelane, $(Ba,H_2O)_2Mn_5O_{10}$. Acta. Crystallogr. 6, 433-438.

Wadsley, A.D. (1955) The crystal structure of chalcophanite, $ZnMn_3O_7 \cdot 3H_2O$. Acta Crystallogr. 8, 165-172.

Zwicker, W.K., Groeneveld Meijer, W.O.J., and Jaffe, H.W. (1962) Nsutite - a widespread manganese oxide mineral. Am. Miner. 47, 246-266.

CHAPTER 3

THE CHEMICAL, MINERALOGICAL, AND STRUCTURAL CHARACTERIZATION OF DESERT VARNISH[1]

1. INTRODUCTION

Desert varnish is a dark coating up to 500 micrometers thick which occurs on rock surfaces exposed in arid and semi-arid regions throughout the world. It is most frequently dull brown, but when well-developed, varnish forms a shiny black surface, from which its name derives. Frequently associated with this dark coat is an orange coat which is best-developed in contact with the soil on the bottom of desert pavement stones but occurs to some degree on the bottom of varnished stones generally. I will consider both phenomena as desert varnish since their characterization in this chapter shows them to be closely related. The physical description of varnish has been presented in detail for occurrences in the Mojave Desert, California (Engel and Sharp, 1958).

It has been estimated that 75 percent of the coherent bedrock exposures of the southern California deserts is varnished to a degree that is recognizable (Engel and Sharp, 1958). In addition, most desert pavements and many colluvial and alluvial desert deposits have well-developed varnish. Vertical stripes of desert varnish,

---

[1]Most of the work presented in this chapter has been published in Science and Chemical Geology: Potter, R.M., and Rossman, G.R. (1977) Desert varnish: the importance of clay minerals, Science, 196, 1446-1448. Potter, R.M., and Rossman, G.R. (1979) The manganese and iron oxide mineralogy of desert varnish. Chemical Geology, in press.

manganese veils, are a distinctive feature of cliff faces throughout the Colorado Plateau. It is thus not surprising that desert varnish has attracted comment and speculation on its origin for well over 100 years (Blake, 1857, 1905; Merrill, 1898; White, 1924; Laudermilk, 1931; Blackwelder, 1948).

More recently, attention has been focused on desert varnish for three additional reasons. (1) It is similar in chemistry (and, as I will show, mineralogy and structure) to other manganese oxide concentrations of the low temperature environment, notably marine manganese nodules (Bauman, 1976). This suggests that the formation mechanisms may be related and that the study of desert varnish may lead to a greater understanding of the genesis of the other manganese concentrations. (2) Desert varnish has potential for the relative age-dating of petroglyphs and other artifacts of early man (Goodwin, 1960; Hayden, 1976; Bard et al., 1978). For geologists as well, desert varnish may be a useful age-dating tool; volcanic flows in arid regions of the western United States frequently have well-developed varnish coatings which are presumably related to their ages. A greater understanding of the nature of desert varnish and its formation are necessary in the evaluation and possible development of these applications. (3) The trace element chemistry of desert varnish may be useful in geochemical prospecting. Since variations in the mineralogy and formation mechanism of desert varnish could cause significant variations in its trace element chemistry, it is important that both be understood in order to reliably interpret the trace element data. Despite the field study and extensive laboratory

examination which these considerations stimulated, the nature of desert varnish remained a matter of debate (Hunt, 1954, 1961; Engel and Sharp, 1958; Marshall, 1962; Lakin et al., 1963; Scheffer et al., 1963; Hunt and Mabey, 1966; Hooke et al., 1969; Krumbein, 1971; Hayden, 1976). This was partly due to a lack of mineralogical and structural information. On the basis of X-ray diffraction varnish was thought to be amorphous; no work was directed toward an understanding of the overall structural organization of the coating.

This chapter presents the results of a detailed chemical, mineralogical, and structural characterization of desert varnish using infrared spectroscopy in conjunction with a variety of electron optic, chemical and other techniques. From it has emerged an accurate knowledge of the varnish coating itself which has significantly altered our conception of it. This characterization suggests several features of the varnish formation mechanism and indicates the most fruitful directions for further research into the formation problem. It has important consequences for the use of desert varnish for age-dating and geochemical prospecting.

2. SAMPLE LOCALITIES AND PREPARATION

I collected samples of desert varnish for detailed study from three localities in the Mojave Desert, California, which provide well-developed varnish on a wide range of lithologies. Samples of desert varnish for more limited study were collected in order to ascertain the generality of my results. These came from eleven localities throughout the southwestern United States and from one locality in Israel (Table 1 of Chapter 4). Mineralogical information on these

samples is presented in Chapter 4 (Table 1), which deals with manganese oxide concentrations in general. My analysis of these samples is discussed in this chapter as it bears on the generality of my detailed analysis of the three localities. Engel and Sharp (1958) have studied these three localities in detail and present complete lithologic and environmental descriptions. Since it seems likely that these localities will become type localities for desert varnish (with the probable exception of the Stoddard Wells locality which is being destroyed by off-road vehicles), exact geographical descriptions of my sample sites are given here.

Four Buttes: Several small buttes capped by andesite are located approximately 300 meters south of the southwest corner of section 32, T.15 N., R.11 E., Halloran Springs Quadrangle, California. Thick black varnish occurs on andesite boulders in several boulder fields. Samples were taken from several fields on the north side of the buttes at an altitude of approximately 3480 feet. This locality has particularly good examples of shiny and dull varnish.

Salt Spring: California State Highway 127 passes just northeast of an outlier of the Avawatz Mountains in the northeast corner of section 32, T.15 N, R.7 E., Avawatz Pass Quadrangle, California. The closest approach of the mountains to the highway is by a small knob connected by a saddle to the main mass of the mountains. On the saddle, located approximately 300 meters southwest of the highway, varnish is well-developed on outcrops and desert pavement of argillaceous quartzite. Pavement stones have well-developed orange coat, and samples were collected at an altitude of approximately

720 feet. On the slope immediately to the west approximately 500 meters from the road black varnish is locally very well-developed on outcropping quartzite. Samples were collected from one outcrop at an altitude of approximately 760 feet.

Stoddard Wells: Desert pavement stones having well-developed varnish with both black and orange coats were collected slightly northeast of the center of section 22, T.8 N., R.2 W., Barstow Quadrangle, California. This locality is approximately 1 kilometer west of the Stoddard Well Road and at an elevation of approximately 2900 feet.

For in situ examination of varnish, mm-sized chips broken from the field samples were washed with deionized water, dried and examined under 40 X magnification to insure an undisturbed surface. Powered samples were prepared as follows: Milligram quantities of varnish were scraped from the rock surface with a tungsten needle under 20 X magnification. The resultant flakes were examined under 40 X magnification, contaminating pieces of rock were mechanically removed and the material was ground to a fine powder. The degree of contamination from underlying rock was measured by infrared spectroscopy. Comparison of the height of the quartz bands near 800 cm^{-1} for the Salt Spring and Stoddard Wells localities indicated a minimum purity of 93% for both samples. This is a lower limit of purity since some quartz is a normal constituent of varnish. No rock impurity could be detected in the Four Buttes samples based on the plagioclase band near 600 cm^{-1}.

3. EXPERIMENTAL DETAILS

Manganese oxidation state was determined by dissolution in excess 0.05 M Fe^{+2} in 0.5 M H_2SO_4 followed by back titration of Fe^{+2} with 0.002 M $KMnO_4$, and colorimetric determination of manganese. Several chemical extraction techniques were used to remove or isolate various components of desert varnish. Manganese oxides were isolated by treatment with 48% HF for 1 minute followed by centrifugation and washing with deionized water. Clays were isolated by dithionite/citrate extraction (Mehra and Jackson, 1960) followed by washing with 1.0 M $SrCl_2$ to saturate the exchange positions with Sr^{+2}. Dissolution for 1 hour with 0.05 M Fe^{+2} in 0.5 M H_2SO_4 was used to isolate iron oxides and clays. Although this procedure removes nearly half of the iron, it is preferable to acidic H_2O_2 or the hydroxylamine procedure (Chao, 1972), both of which leave sufficient manganese to interfere with the near infrared spectrum of iron oxide. No attempt was made to optimize either the HF or the Fe^{+2}/H_2SO_4 extractions.

Major element chemistry was determined by an election microprobe technique similar to that of Brown (1977). Ten milligrams of powdered material were fused in air on an iridium filament at about 1600°C and then quenched to a glass by a blast of air. The resulting beads were mechanically removed from the filament, mounted in epoxy, polished, and carbon coated. Their chemical composition was analyzed on a MAC-5-SA3 electron microprobe employing the Bence-Albee corrections (Bence and Albee, 1968, Albee and Ray, 1970). Samples rich in manganese sometimes contained areas of very fine, dark crystals 1 micron or less in size, but appeared homogeneous to the 20

micrometer electron beam of the probe. Analyses of areas rich in crystals did not differ from those without crystals. Thermogravimetric analyses of powered samples were obtained with a Mettler thermoanalyzer. X-ray power diffraction data are on samples oriented by sedimentation from water suspension onto a glass microscope slide. Near infrared spectra were obtained with a Cary 17I spectrophotometer on samples dispersed in TlCl; infrared spectra were obtained with a Perkin-Elmer Model 180 spectrophotometer on 0.50 mg of powdered sample dispersed in 200 mg KBr and dried overnight at 120°C under vacuum to remove water adsorbed on the KBr. This treatment affected only those infrared features due to adsorbed water. Qualitative chemical analyses of selected morphologies was done with an SEM equipped for energy dispersive X-ray analysis. Thin sections of desert varnish were made on samples vacuum impregnated with epoxy and polished to a thickness of about 10 micrometers.

4. CHEMISTRY

Most previous chemical analyses of desert varnish have been done on chemical extracts, which may not reflect the overall varnish composition, or on material with a large but unknown degree of contamination from the underlying rock. Hooke et al. (1969) have avoided these problems by use of the electron microprobe for in situ analyses, but this has introduced uncertainties due to the highly hydrous nature of varnish and is not well suited to determination of the average chemical composition. The microprobe analyses of fused beads reported in Table 1 are the first analyses to be free of these uncertainties. I made no attempt to control oxidation state when

Table 1. Chemical composition of desert varnish black, orange, and dithionite-extracted black coats[a]

	Four Buttes		Salt Spring			Stoddard Wells		
	black[b] coat	extracted[c] coat	black coat	orange coat	extracted[c] coat	black coat	orange coat	extracted[c] coat
	Oxide weight percent[d]		Oxide weight percent[d]			Oxide weight percent[d]		
K_2O	1.36	2.41	1.82	3.57	2.89	1.89	2.91	2.95
Na_2O	0.12	0.37	0.12	0.19	0.38	0.23	0.27	0.92
CaO	0.72	0.45	0.73	0.99	0.52	1.28	0.97	0.48
SrO[e]	0.00	6.70	0.00	0.00	3.90	0.00	0.00	3.75
MgO	2.22	3.90	2.86	4.27	4.00	2.43	3.26	2.74
MnO	16.69	0.08	13.52	0.14	0.12	22.63	0.10	0.07
FeO	21.40	7.15	16.78	8.91	6.29	10.96	10.47	5.01
TiO_2	1.07	1.66	0.92	0.79	1.52	0.78	0.82	0.93
Al_2O_3	21.20	23.28	21.28	27.09	23.21	20.01	26.38	23.75
SiO_2	30.00	54.54	36.35	53.10	56.74	34.35	53.71	60.06
P_2O_5	2.46	0.33	1.86	0.10	0.17	1.10	0.14	0.09
BaO	0.76	0.16	0.60	0.18	0.05	1.22	0.02	0.06
Total	98.00	101.03	96.84	99.33	99.79	96.88	99.05	100.81
n[f]	5	4	5	3	4	4	3	3
H_2O[g]	14.2	N.D.	14.5	13.5	N.D.	11.0	5.5	N.D.
Mn Oxid. St.	+3.93	N.D.	+3.76	N.D.	N.D.	+3.91	N.D.	N.D.
	cation percent		cation percent			cation percent		
K	1.81	2.95	2.35	4.32	3.53	2.50	3.56	3.59
Na	0.25	0.70	0.25	0.34	0.69	0.44	0.52	1.71
Ca	0.81	0.46	0.80	1.02	0.52	1.44	0.98	0.46
Sr[e]	0.00	3.76	0.00	0.00	2.20	0.00	0.00	2.05
Mg	3.43	5.62	4.40	6.03	5.72	3.95	4.66	3.87
Mn^{2+}	0.51	0.00[h]	1.42	0.00[h]	0.00[h]	0.90	0.00[h]	0.00[h]
Mn^{4+}	14.16	0.06	10.35	0.11	0.12	19.06	0.06	0.06
Fe[i]	18.60	5.79	14.50	7.05	5.09	9.51	8.40	3.99
Ti	0.81	1.22	0.74	0.57	1.10	0.62	0.58	0.68
Al	25.97	26.48	25.84	30.19	26.32	24.54	29.73	26.55
Si	31.16	52.61	37.49	50.25	54.59	35.80	51.40	56.98
P	2.18	0.29	1.61	0.06	0.12	0.94	0.11	0.06
Ba	0.31	0.06	0.25	0.06	0.00	0.50	0.00	0.00

[a] All analyses except H_2O and Mn oxidation state are by electron microprobe. N.D. = not determined. The following elements were looked for but not found in wavelength scan: F, S, Cl, V, Cr, Co, Ni, Cu, Zn, Br, Y, Zr, Nb, Mo, Rh, Pd, Ag, Cd, Sn, La, Ce, Nd, Hf, Ta, W, Re, Ir, Pt, Au, Pb, Th, U, Ca, As, Ge.

[b] A mixture of shiny and dull varnish.

[c] The associated black coat whose analysis is reported here is the material extracted.

[d] Standard deviations for oxides present in greater than 1 weight percent are generally below 2% of the oxide weight percent. Standard deviations for oxides present in less than 1 weight percent are generally below 20% of the oxide weight percent.

[e] Dithionite extracted coats were washed with 1 M $SrCl_2$ to saturate the exchange positions with Sr^{+2}.

[f] n = number of replicate analyses.

[g] Determined by weight loss on heating to 1000 °C.

[h] All Mn reported as Mn^{+4}.

[i] Fe must be predominately in the +3 oxidation state based on mineralogy and absence of spectroscopic features due to Fe^{+2} near 1000 nm.

fusing the samples. The low totals for the black coat analyses are probably the result of incomplete reduction of manganese and iron to the +2 valence state. Recalculation of MnO as MnO_2 and FeO as Fe_2O_3 always results in totals greater than 100 by several percent.

Infrared spectroscopy indicates that only traces of carbonate, organic material, and nitrogen (as ammonium ion and nitrate) occur in varnish. The water content can thus be determined from the weight loss on heating and is reported in Table 1. Negligible organic carbon has been found in desert varnish by mass spectrometry (R.N. Rogers, Los Alamos Scientific Laboratory, personal communication, 1975).

The chemical composition of the oxide phases can be calculated from the data in Table 1. The mineralogy section will show that nearly all Si is in phases which are unaffected by the dithionite extraction procedure. Thus, if the silicon content from the analysis of an untreated coat is nulled by subtraction of a percentage of the analysis of its associated extracted coat, the difference is the chemical composition of the oxide phases (Table 2). The chemical differences between black and orange coats are included in Table 2 for use in conjunction with infrared data.

Table 2 shows that manganese, iron, and aluminum are the principal non-silicate constituents of the black coat and that iron and aluminum are the principal non-silicate constituents of the orange coat. Barium is associated with manganese. Phosphorous also appears to be associated with manganese. It is not present in the orange coat, which has been found to differ significantly from the

Table 2. Chemical differences between varnish coats calculated from Table 1 by nulling the Si content of different coats

	Four Buttes cation percent	Salt Spring cation percent			Stoddard Wells cation percent		
	black-extracted	black-extracted	orange-extracted	black-orange	black-extracted	orange-extracted	black-orange
K	0.1	-0.1	1.1	-0.9	0.2	0.3	0.0
Na	-0.2	-0.2	-0.3	0.0	-0.6	-1.0	0.1
Ca	0.5	0.4	0.5	0.0	1.2	0.6	0.8
Sr	-2.2	-1.5	-2.0	0.0	-1.3	-1.8	0.0
Mg	0.1	0.5	0.8	-0.1	1.3	1.2	0.5
Mn	14.6	11.7	0.0	11.7	19.9	0.0	19.9
Fe	15.2	11.0	2.4	9.2	7.0	4.8	3.7
Ti	0.1	0.0	-0.4	0.3	0.2	0.0	0.2
Al	10.3	7.8	6.0	3.3	7.9	5.8	3.8
Si	0.0	0.0	0.0	0.0	0.0	0.0	0.0
P	2.0	1.5	0.0	1.6	0.9	0.1	0.9
Ba	0.3	0.2	0.1	0.2	0.5	0.0	0.5
K+Na+Ca+Sr[a]	-1.8	-1.4	-0.7	-0.9	-0.5	-1.9	0.9

[a]The negative total for these cations is due to chemical differences in the exchangeable cations of clay minerals which comprise the silicate phase. It may also reflect differences in the clay mineralogy of the two materials compared.

black coat only in its manganese content.

5. MINERALOGY

Silicate Phases

The silicate phases in desert varnish have been identified by the combined application of infrared spectroscopy and X-ray diffraction. Desert varnish has a characteristic infrared spectrum which bears no relation to that of underlying rock and is dominated by the absorption of sheet silicates. The spectra of Stoddard Wells desert varnish (Figure 1) are representative of black and orange coat spectra from all localities. In each instance the infrared spectrum of the rock immediately underlying the varnish differs significantly from that of its varnish coating. This eliminates the possibility that the underlying rock itself is a significant component of the varnish. The major infrared bands occurring near 3620 cm^{-1}, 1030 cm^{-1}, 530 cm^{-1}, and 470 cm^{-1} are diagnostic for illite, montmorillonite, and mixed-layer illite-montmorillonite clay minerals (Stubičan and Roy, 1961; Farmer and Russell, 1964; Oinuma and Hayashi, 1965; Heller-Kallai, 1975). The identification of this type of clay mineral as the major phase in desert varnish becomes more obvious when the manganese and iron oxides are removed by extraction with sodium dithionite (Mehra and Jackson, 1960). The spectrum of the extracted black coat from Stoddard Wells (Figure 2) is representative of spectra of extracted black and orange coats from all three localities. The extracted coat spectra show greater resolution of band structure in the 800 cm^{-1} to 400 cm^{-1} region due to the absence of manganese and iron oxides, which absorb in this

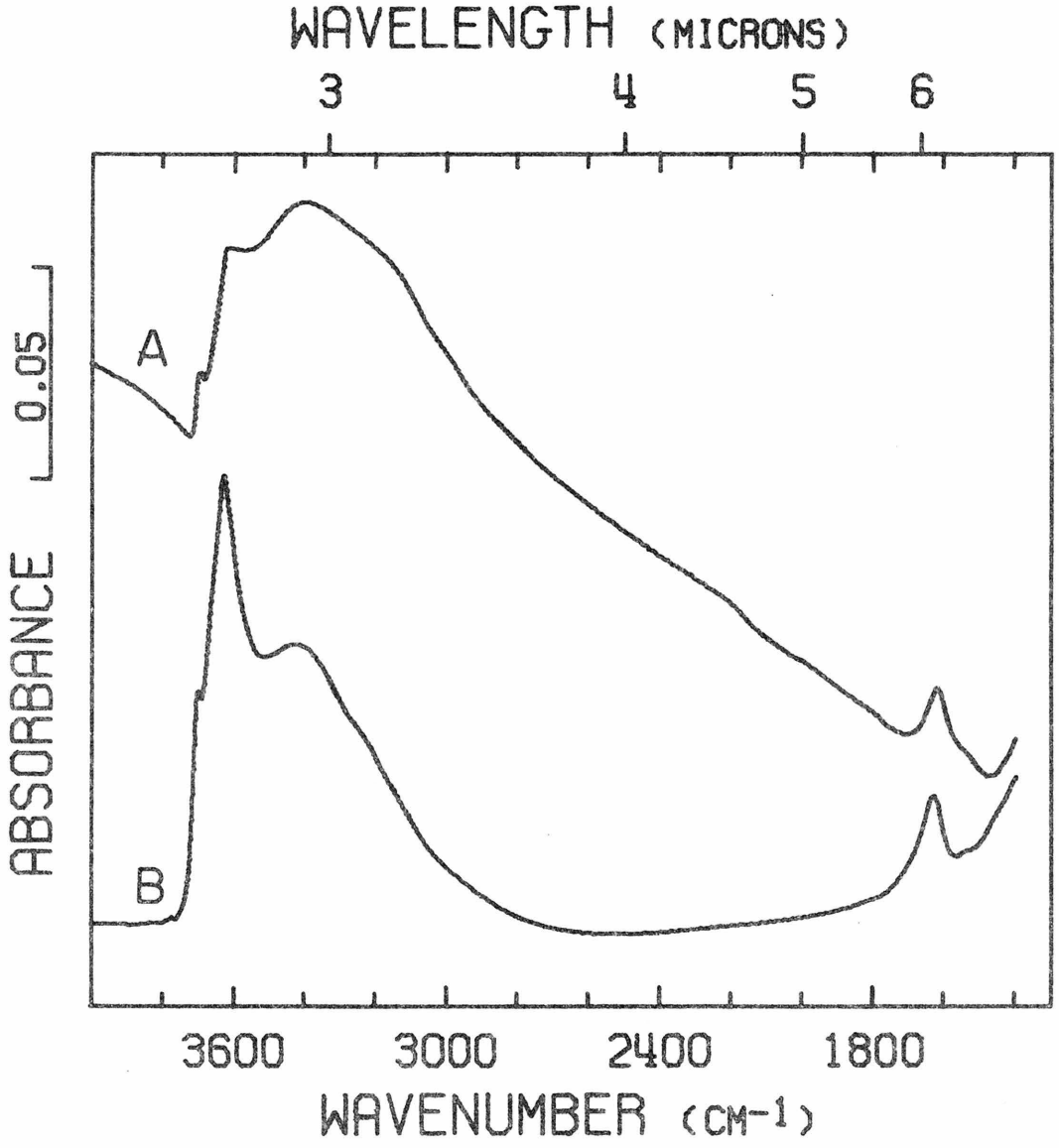

Figure 1. Infrared spectra of desert varnish from Stoddard Wells: A. Black coat; B. Orange coat. Figure continued on following page.

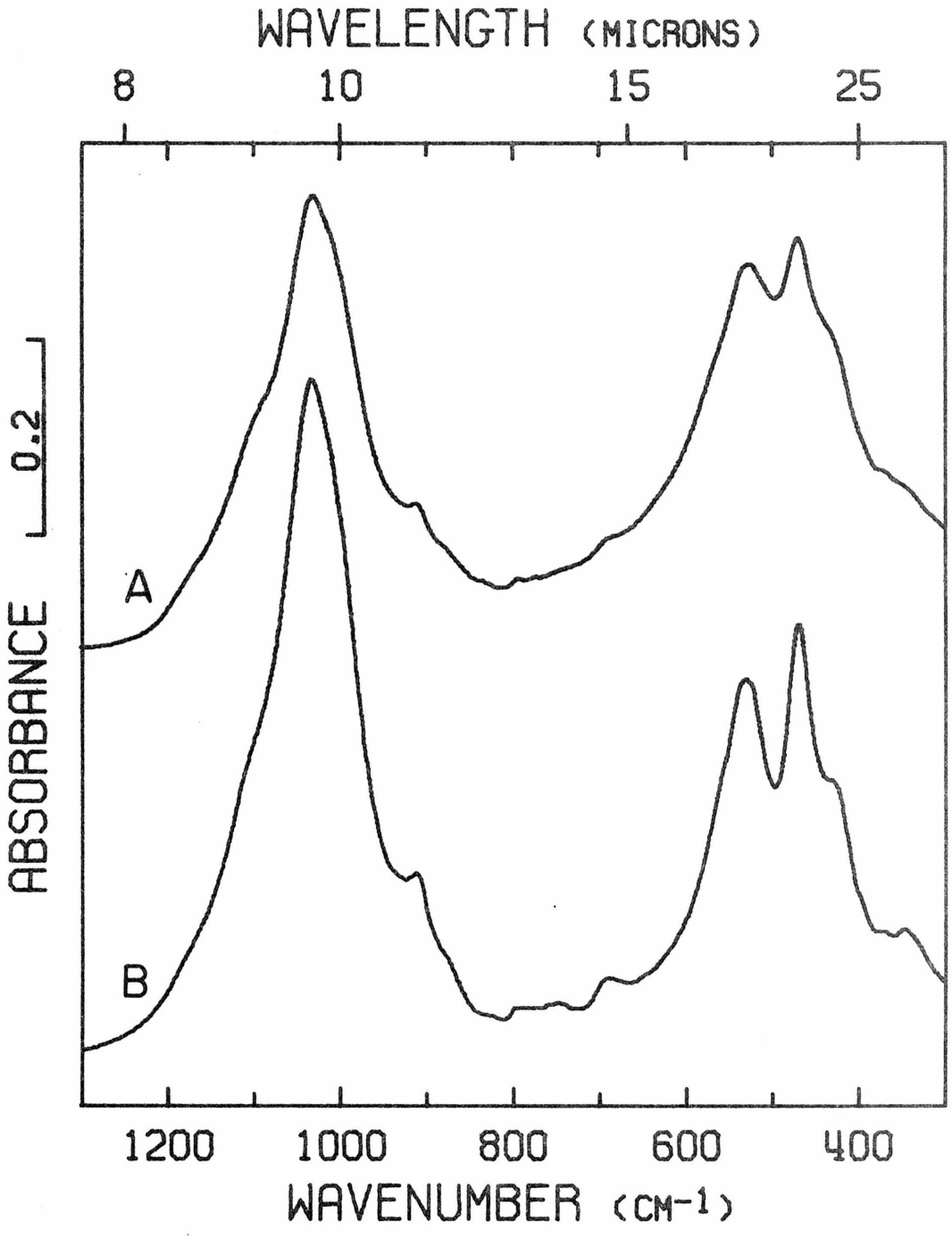

Figure 1. Continued from preceding page

Figure 2. Infrared spectrum of desert varnish extracted black coat from Stoddard Wells compared to various clay minerals. In order to aid comparison, each standard clay spectrum is presented at a concentration which makes its major absorption band equal in intensity to that of the varnish spectrum. This removes differences due to particle size and dispersion of the sample in the KBr pellet.

A. Extracted coat

B. Illite (Morris, Illinois, Kerr et al., 1949)

C. Mixed-layer illite-montmorillonite, 20% montmorillonite (Hower et al., 1976)

D. Mixed-layer illite-montmorillonite, 80-85% montmorillonite (Hower et al., 1976)

E. Montmorillonite (Upton, Wyoming, Kerr et al., 1949)

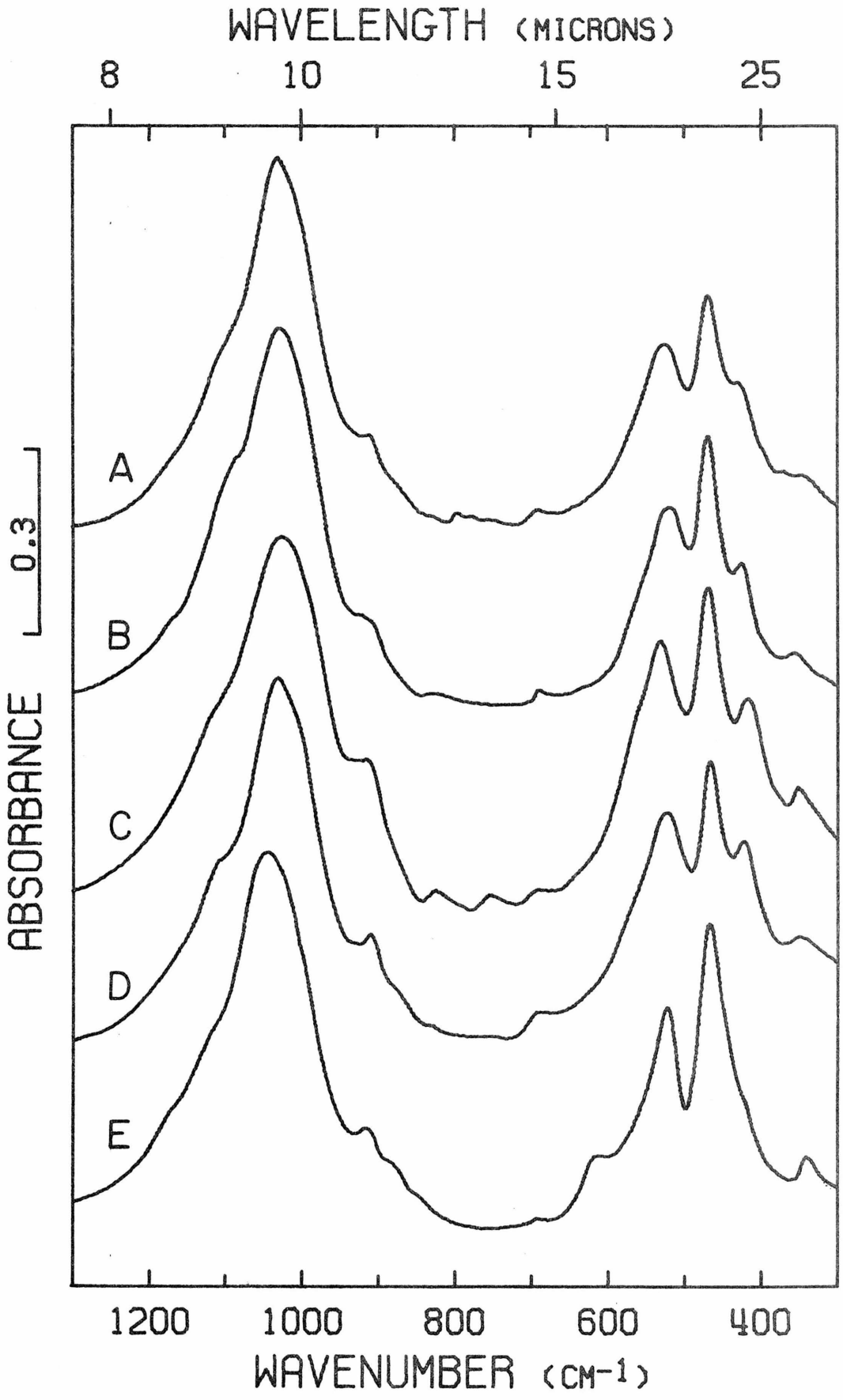
WAVELENGTH (MICRONS)
8
10
15
25
A
B
C
D
E
0.3
ABSORBANCE
1200
1000
800
600
400
WAVENUMBER (CM-1)

region. Comparison with spectra of reference clay minerals characterized by X-ray diffraction (Figure 2) indicates that the dominant component in desert varnish is either illite, mixed-layer illite-montmorillonite, or both. Through infrared studies of reference clays[2] and their mixtures I have been able to place an upper limit of 20 percent on the amount of discrete octahedrally-substituted montmorillonite present in the varnish clays; however, I have found infrared spectroscopy insensitive to the illite-montmorillonite ratio in mixed-layer clays (for example, Figure 2). Peaks in varnish spectra which are not due to these clay minerals are attributable to minor amounts of water (3400 cm^{-1} and 1625 cm^{-1}), quartz (795 cm^{-1}, 775 cm^{-1}, 400 cm^{-1}, and 370 cm^{-1}), and kaolinite (3700 cm^{-1}).

X-ray diffraction on oriented samples of dithionite-extracted desert varnish confirms the results from infrared spectroscopy. X-ray patterns from the Four Buttes locality (Figure 3) is representative of those from all three localities. Unextracted

---

[2]The following reference clays were used in this study: Illites from Fithian, Illinois; Morris, Illinois; and Beavers Bend, Okalahoma. Montmorillonites from Upton, Wyoming; Chambers, Arizona; and Otay, California. All but the Beavers Bend illite are API reference clays (Kerr et al., 1949). Mixed-layer illite-montmorillonite reference clays are from Oligicene-Miocene sediments of the Gulf Coast of the United States. Analytical data on them appear in Hower et al. (1976). Samples spanned the range 20 to 85 percent montmorillonite.

Figure 3. X-ray powder diffraction data for varnish from Four Buttes

A. Dithionite-extracted black coat

B. Dithionite-extracted black coat; treated with ethylene glycol at 60°C for 24 hours

C. Untreated black coat

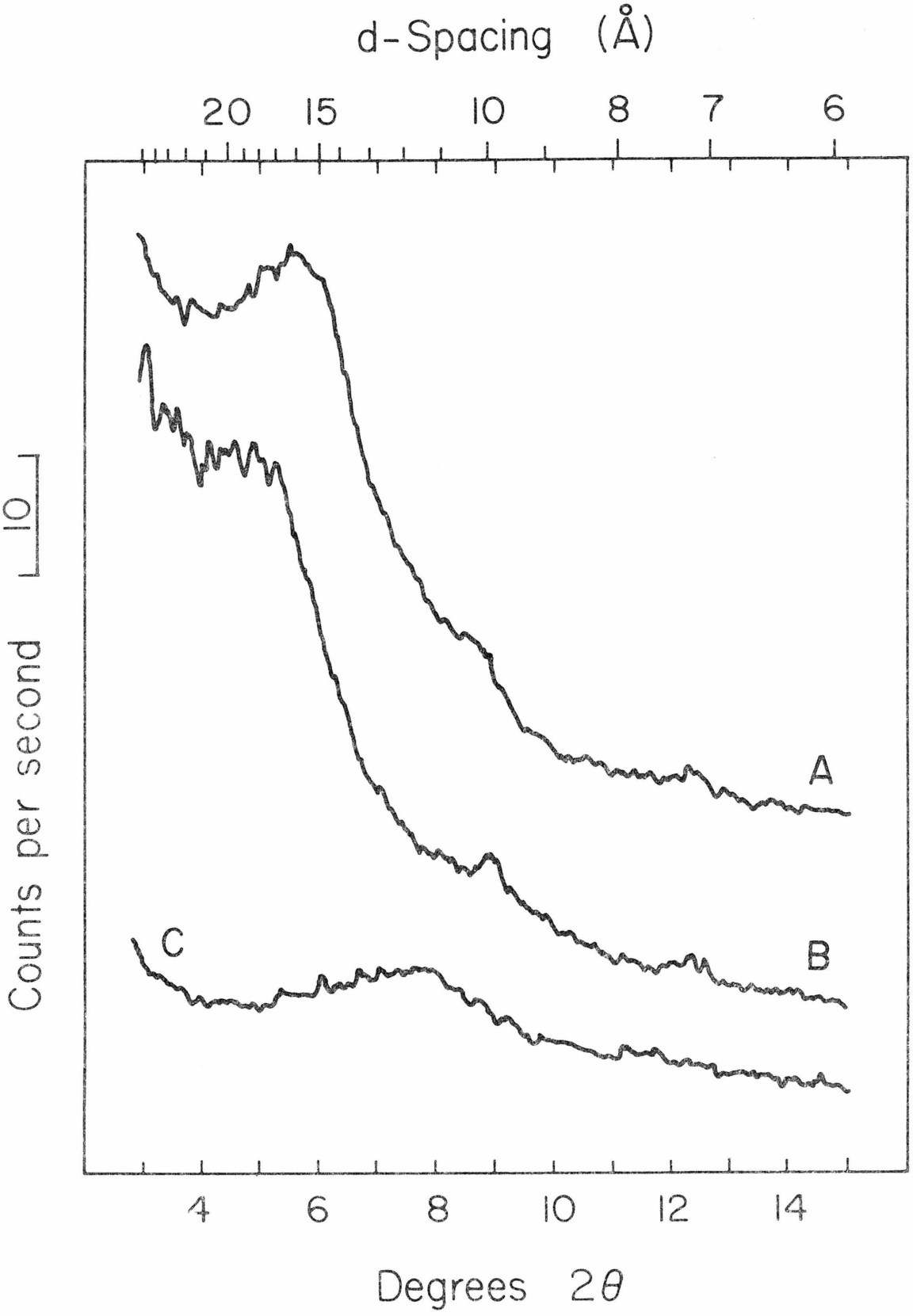
d-Spacing (Å)
20
15
10
8
7
6
Counts per second
10
A
B
C
4
6
8
10
12
14
Degrees 2θ

Table 3. Exchange capacity of desert varnish clays calculated from the extracted coat analyses of Table 1.[a]

	Four Buttes	Salt Spring	Stoddard Wells
non-exchangeable positions K + Ca + partial Na milliequivalents/100 g clay	49	76	83
exchangeable positions Sr + partial Na milliequivalents/100 g clay	70	44	54
percent montmorillonite in mixed-layer clay	60	45	45

[a]It is assumed that Na in an extracted coat in excess of that necessary to null the Na in the associated black coat is exchangeable.

samples yield patterns with a single, broad peak (Figure 3C) characteristic of unoriented clays and easily confused with broad peaks observed for poorly-ordered or amorphous materials. This lack of orientation in the untreated samples accounts for previous reports that varnish is X-ray amorphous (Engel and Sharp, 1958; Scheffer et al., 1963). Extracted varnish samples yield X-ray diffraction patterns characteristic of clay minerals (Figure 3A). The nature of the expansion in d-spacing which occurs after the sample has been treated with ethylene glycol (Figure 3B) identifies the major component as a mixed-layer illite-montmorillonite clay (Hower and Mowatt, 1966; Reynolds and Hower, 1970; Thorez, 1975). X-ray diffraction patterns also indicate small amounts of quartz, discrete illite, and possibly chlorite in some samples and are consistent with a small amount of kaolinite in most.

The exchange capacities of desert varnish clays (Table 3) can be calculated from the data of Table 2 and are consistent with that expected from illite-montmorillonite mixed layer clays (Weaver and Pollard, 1973). The percent montmorillonite (Table 3) is calculated from the exchange capacity using the calibration of Ormsby and Sand (1954) and is in agreement with the X-ray data. Because varnish contains small amounts of kaolinite and possibly chlorite and discrete illite, the calculated percent montmorillonite in the mixed-layer clay is a lower limit.

The clay mineralogy reported here for the three localities studied in detail was found to be characteristic of varnish from most of the other localities examined; however, several had a

dominantly kaolinitic clay mineralogy with only minor illite-montmorillonite type clays (Table 1 of Chapter 4).

Infrared spectroscopy indicates a trace of quartz in all varnishes studied. The amount found in varnish from the Four Buttes locality, where the underlying rock contains no quartz, is approximately two percent. This is representative of varnishes from the other localities.

Manganese Oxide Phase

No manganese oxide minerals have previously been identified in desert varnish. X-ray diffraction data for varnish from the Four Buttes locality (Figure 3C) is similar to that from the other localities I have studied in detail. No peaks attributable to manganese oxides are present. Infrared spectra of desert varnish (Figure 1) indicate the presence of hydrous oxides absorbing near 3400 cm^{-1} and in the 800 cm^{-1} to 400 cm^{-1} region, but mineralogical identification is not possible directly owing to the strong absorption of the clay minerals. I have obtained infrared spectra of the oxides by computer generation of difference spectra (Figure 4). Silicate absorption in the spectra of samples containing oxides is removed by subtracting some fraction of the spectra of the associated extracted coat. This fraction is determined by the relative heights of the band near 1000 cm^{-1}, which is due wholly to silicate absorption.

The low intensity of the features near 1000 cm^{-1} in the difference spectrum (Figure 4C) indicate that there are only minor differences between the crystallinity and mineralogy of the silicates

Figure 4. Infrared difference spectra procedure illustrated for varnish from Stoddard Wells

A. Black coat

B. Dithionite-extracted black coat

C. Difference spectrum (A-0.70B) showing four features (labeled) due to manganese and iron oxide absorption

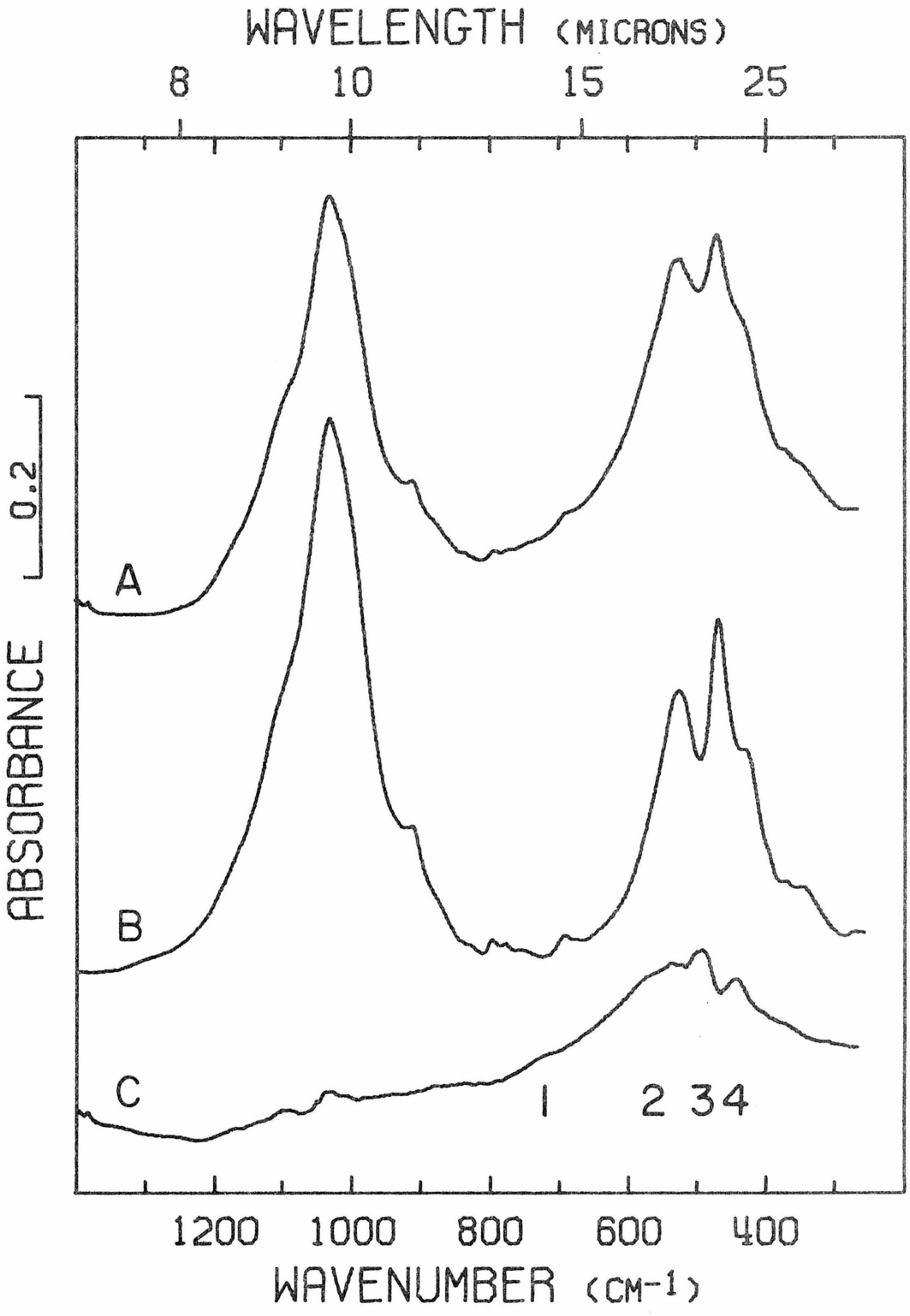
WAVELENGTH (MICRONS)
8
10
15
25
ABSORBANCE
0.2
A
B
C
1
2
3
4
1200
1000
800
600
400
WAVENUMBER (CM-1)

in the extracted and unextracted varnish. The other features of the spectrum are numbered in Figure 4 and all occur in the region in which oxides commonly absorb. This eliminates the possibility that manganese and (most) iron are present in phases other than the oxides.

In order to test the validity of this difference procedure, it was applied to 7:3 mixtures of Stoddard Wells soil clays with each of the manganese oxides nsutite and todorokite, which have sharp infrared features and provide a rigorous test of the procedure. The manganese oxide spectra were reproduced without artifacts (Figures 5 and 6). In particular, bands 3 and 4 are not artifacts of the procedure due to oversubtraction of the two sharp clay features near 500 cm^{-1}.

Figure 7 contains the difference spectra for the black coats from all three localities. Difference spectra from other localities are similar (Chapter 4, Figure 1A). These spectra are of a mixture of manganese, iron, and aluminum oxides (Table 2). Correlation of spectral features with variations in chemistry make it possible to assign features 1, 3, and 4 to manganese oxide and feature 2 to iron oxide. Figure 7E is a spectrum of purer manganese oxide than is Figure 7D since, for the former, the orange coat rather than the extracted coat was used to null silicate absorption (Table 2). Comparison of the two figures shows the effect of iron and aluminum removal. Loss in absorption intensity occurs only in the 550 cm^{-1} region. For all three localities, the iron and aluminum content in the black coats can be correlated with the magnitude of the

Figure 5. Infrared spectra illustrating the validity of the difference procedure using nsutite (#18, Chapter 2)

A. Dithionite-extracted mixture

B. 7:3 mixture; Stoddard Wells soil clay: nsutite

C. Difference spectrum

D. Nsutite at the concentration expected for the difference spectrum

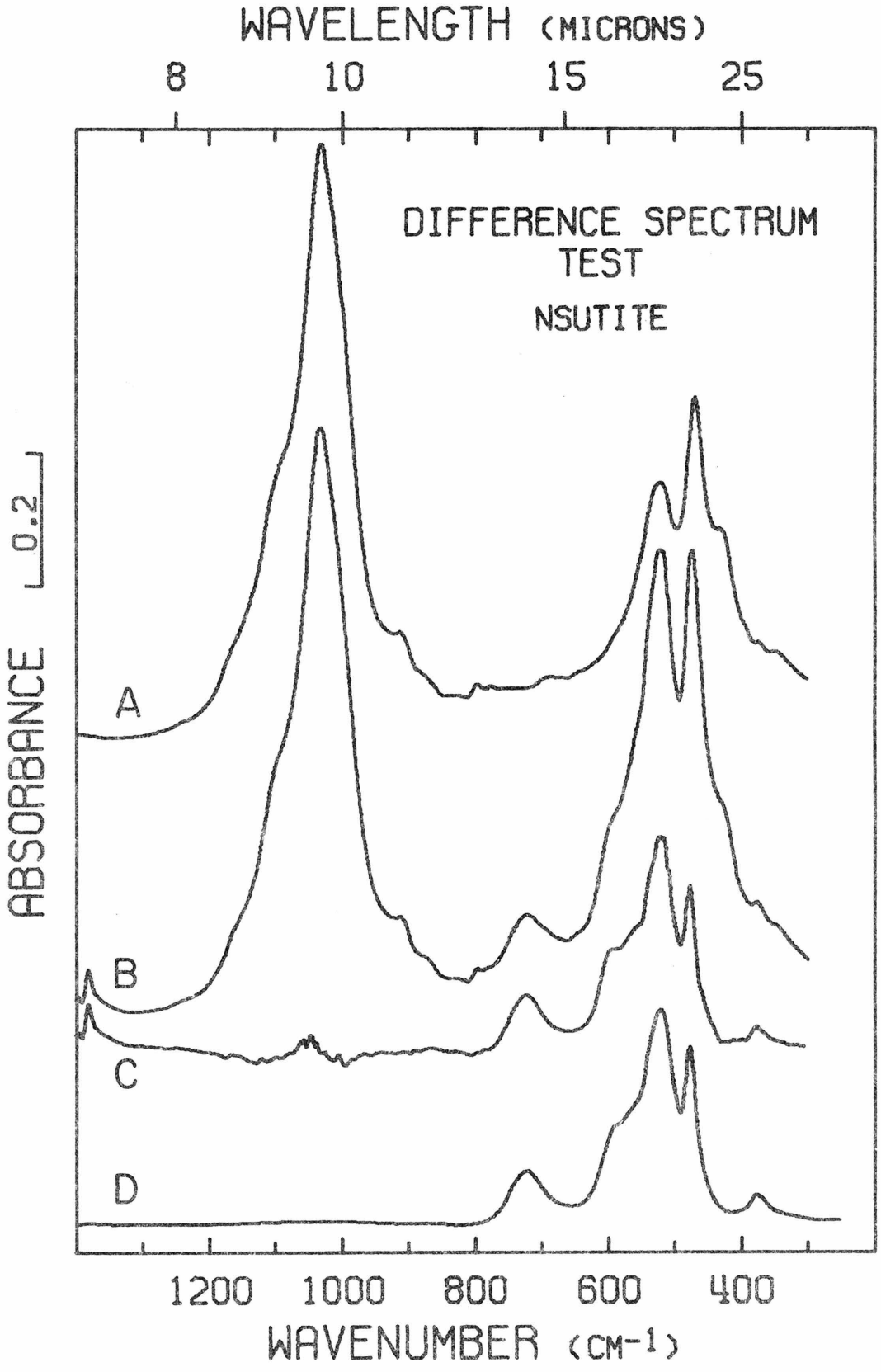
WAVELENGTH (MICRONS)
8
10
15
25
DIFFERENCE SPECTRUM
TEST
NSUTITE
ABSORBANCE
0.2
A
B
C
D
1200
1000
800
600
400
WAVENUMBER (CM-1)

Figure 6. Infrared spectra illustrating the validity of the difference procedure using todorokite (#60, Chapter 2)

A. Dithionite-extracted mixture

B. 7:3 mixture; Stoddard Wells soil clay: todorokite

C. Difference spectrum

D. Todorokite at the concentration expected for the difference spectrum

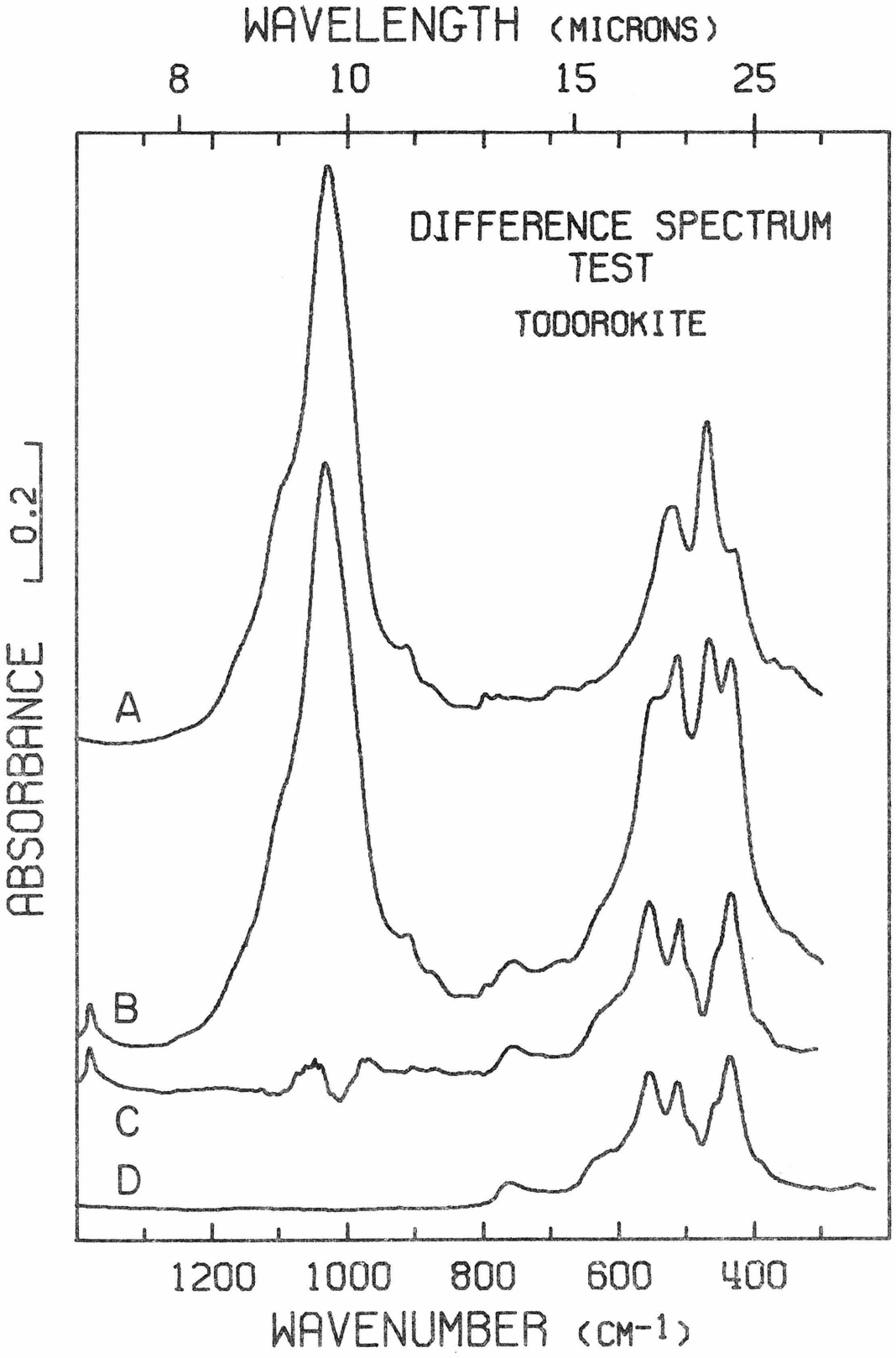
WAVELENGTH (MICRONS)
8
10
15
25
DIFFERENCE SPECTRUM
TEST
TODOROKITE
ABSORBANCE
0.2
A
B
C
D
1200
1000
800
600
400
WAVENUMBER (cm-1)

Figure 7. Infrared difference spectra of black coats compared to infrared spectra of birnessites

A. Four Buttes: shiny black coat - dithionite-extracted black coat

B. Four Buttes: dull black coat - dithionite-extracted black coat

C. Salt Spring: black coat - dithionite-extracted black coat

D. Stoddard Wells: black coat - dithionite-extracted black coat

E. Stoddard Wells: black coat - orange coat

F. Natural poorly-ordered birnessite (#47, Chapter 2) at an equivalent concentration to manganese oxide in spectra D and E

G. Synthetic well-ordered birnessite (#49, Chapter 2) at an equivalent concentration to manganese oxide in spectra D and E

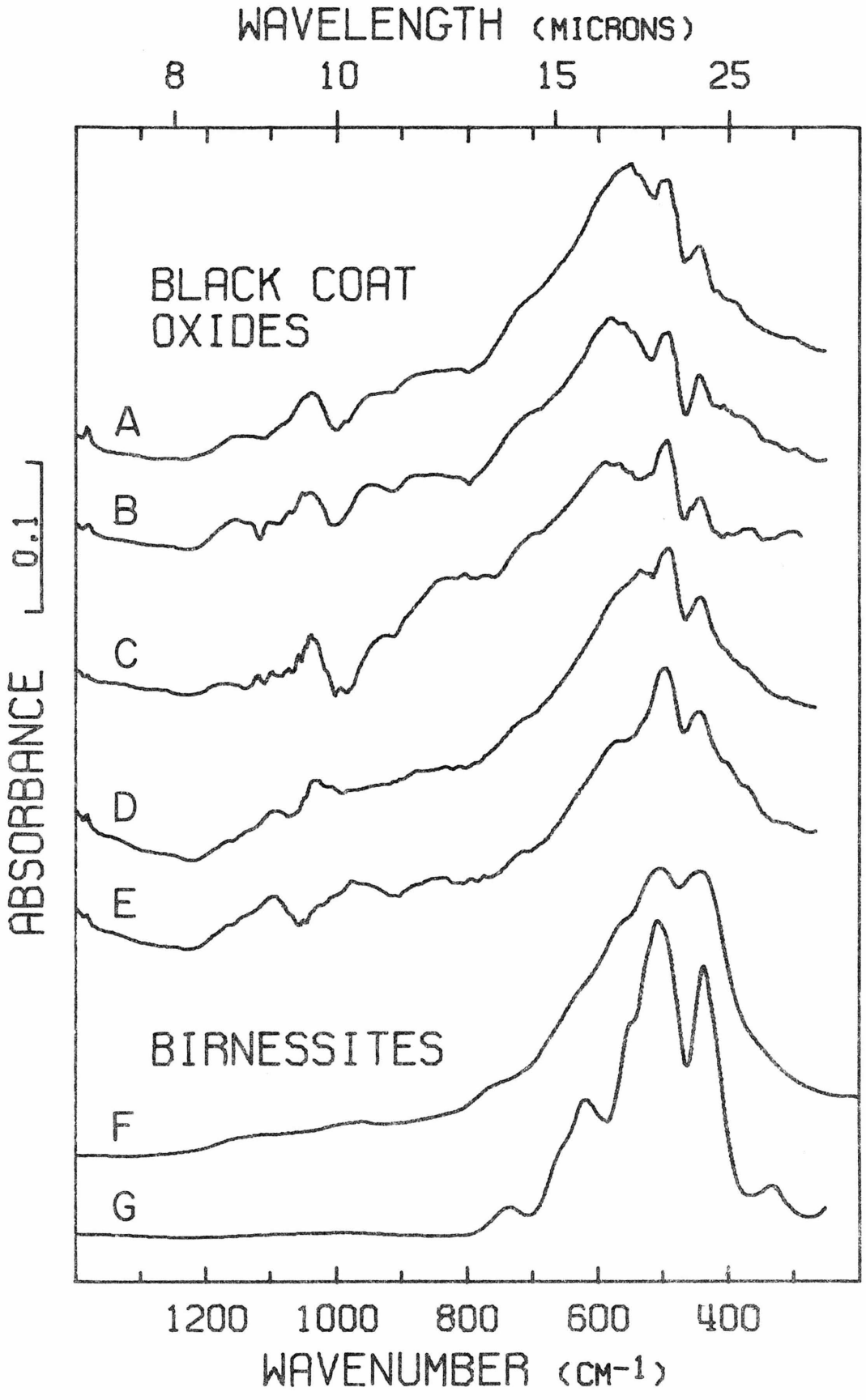
WAVELENGTH (MICRONS)
8
10
15
25
BLACK COAT
OXIDES
A
B
C
D
E
BIRNESSITES
F
G
0.1
ABSORBANCE
1200
1000
800
600
400
WAVENUMBER (CM-1)

absorption in the 550-600 cm^{-1} region (Table 2, Figure 7).

Comparison of these difference plots to spectra of well-characterized manganese oxides (Chapter 2) identifies features 3 and 4 as due to birnessite, $(Na,Ca,K)Mn_7O_{14}\cdot 3H_2O$ (Figure 7.) The oxidation state of manganese in the black coat is consistent with this identification. The data in Table 2 were used to calculate the amount of birnessite expected if all manganese in varnish is present in that mineral. The reference spectra (Figures 7F and 7G) are presented at a concentration equivalent to that in the Stoddard Wells black coat (Figure 7D). Feature 1 can be attributed to birnessite, but not unambiguously. Romanechite (psilomelane), $(Ba,H_2O)_2Mn_5O_{10}$ and the hollandite series, $(Ba,K,Pb,Na)M_8O_{16}$, both have a band near 720 cm^{-1} in addition to stronger bands near 550 cm^{-1} (Chapter 2), which could be responsible for some of the absorption of varnish oxides in that region.

The birnessite in desert varnish appears to be characterized by a high degree of order and small particle size. The difference between the two birnessite reference spectra (Figures 7F and 7G) is essentially one of crystalline order. As material becomes well ordered at the level of several unit cells, its infrared bands become more sharply defined. The sharpness of features 3 and 4 in the varnish birnessite spectra require that it be well ordered. The absence of X-ray lines for a well-ordered material can only be explained by a particle size below 0.1 μm.

Infrared spectra of hydrofluoric acid-extracted desert varnish confirms the predominantly birnessite manganese mineralogy.

The spectrum of the residue of varnish after HF extraction (Figure 8C) is altered from that obtained by the difference technique (Figure 7A). Features 1 and 2 are absent and features 3 and 4 are less sharp. Loss of feature 2 is expected due to removal of iron and aluminum by the extraction procedure. The other effects are what is expected if the material has been disordered, and are observed for HF extraction of the well-ordered standard birnessite (previous to extraction, Figure 7G; after extraction, Figures 8A and 8B).[3] The small particle size of the desert varnish birnessite is probably responsible for the greater degree of disorder produced in it by the extraction. Longer treatment of the standard birnessite produces a closer match to the varnish extract. Samples of todorokite, nsutite, and cryptomelane, tetravalent manganese oxides commonly occurring in poorly crystalline form in the weathering environment, were each treated with HF and the infrared spectra of the residues compared to the unextracted material. There was no evidence of alteration or dissolution of these minerals. Thus, the spectrum of HF extracted varnish and its alteration from that obtained by the difference technique are both evidence for a birnessite mineralogy.

Iron Oxide Phase

The absorption by iron oxide in the near infrared, where the varnish silicates do not absorb light, was used to identify hematite as the major iron oxide phase in desert varnish. The spectrum of orange coat from Stoddard Wells has a single band at approximately

---

[3] HF extraction reduced the average manganese oxidation state from +3.94 to +3.71, which may be associated with the disordering process.

Figure 8. Comparison of the infrared spectra of HF-extracted black coat and HF-extracted birnessite

A. Synthetic birnessite (#49, Chapter 2, Figure 7G) treated with HF for 1 minute

B. Synthetic birnessite (#49, Chapter 2, Figure 7G) treated with HF for 60 minutes

C. Shiny black coat from Four Buttes treated with HF for 1 minute

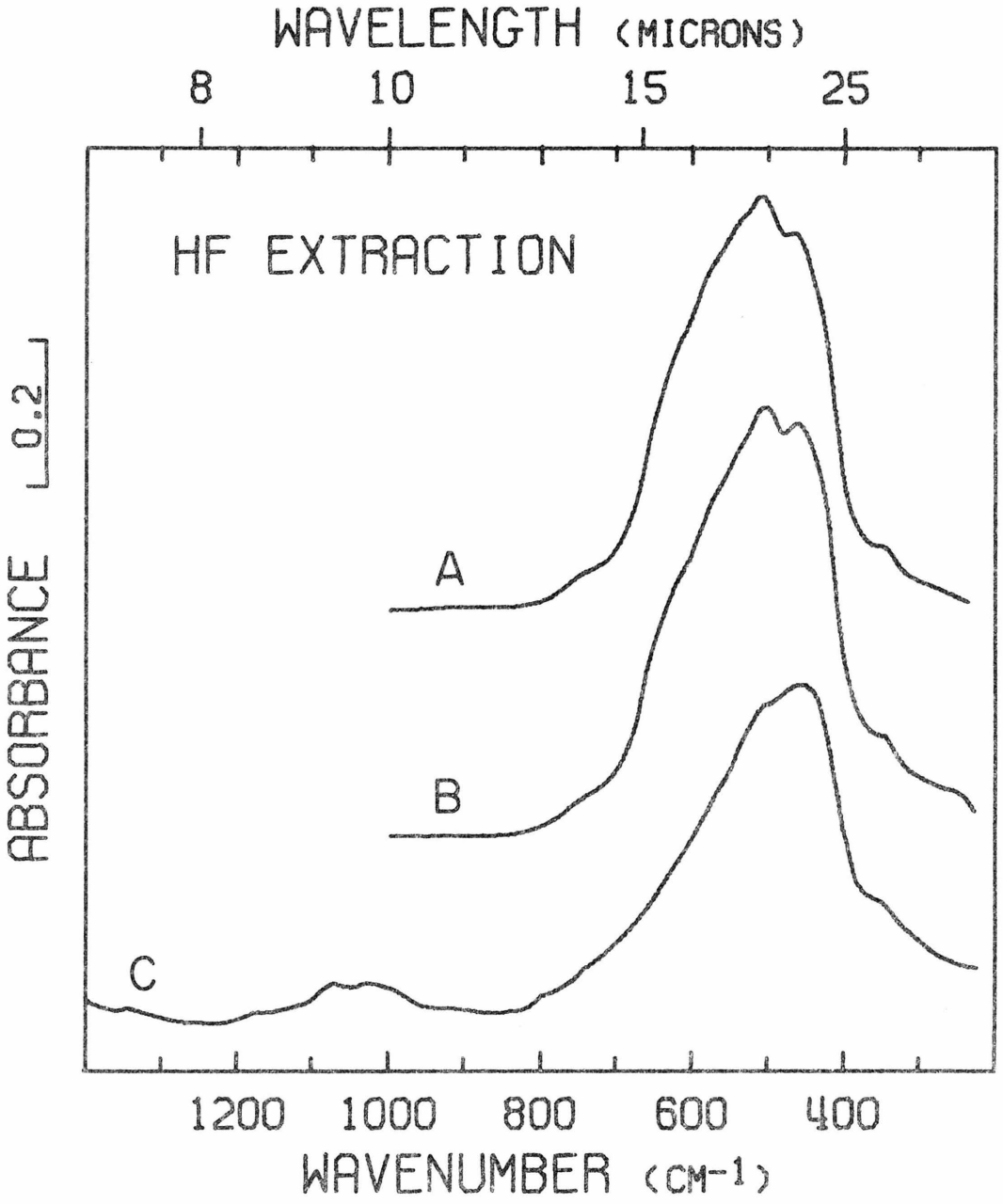
WAVELENGTH (MICRONS)
8
10
15
25
HF EXTRACTION
ABSORBANCE
0.2
A
B
C
1200
1000
800
600
400
WAVENUMBER (CM-1)

855 nm (Figure 9). The position of this band is diagnostic for hematite. All other iron oxides both crystalline and amorphous have this absorption maximum at greater than 890 nm (Webb and Gray, 1974).[4] The weak hematite band near 660 nm is masked in the orange coat due to scattering of light by clay minerals. The hematite reference spectrum is presented at an iron concentration equal to that in the orange coat presented.

Band maxima for other localities may be shifted to longer wavelengths by up to 20 nm. Spectra of iron oxide mixtures indicate that hematite must comprise at least 90% of the iron oxides in these varnishes. Because manganese oxides absorb strongly throughout the near infrared region, spectra of iron in the black coat cannot be obtained directly. The spectra of black coats from which the manganese oxides have been extracted by Fe^{+2}/H_2SO_4 have band maxima at the same position as their associated orange coats. This suggests that the iron oxide mineralogy is unaffected by the extraction procedure and that it is representative of all the iron oxide present in the unextracted black coat. The mid-infrared data are consistent with the identification of hematite in the orange coats although the noise of the difference procedure is large (Figure 10).

Other Phases

No spectroscopic or X-ray diffraction evidence exists for any other phase in desert varnish. Chemical data (Table 2) suggest the presence of a high aluminum phase. This is supported by energy

[4] Iron oxide spectra not included in this reference were obtained from synthetic samples characterized by X-ray diffraction and transmission electron microscopy.

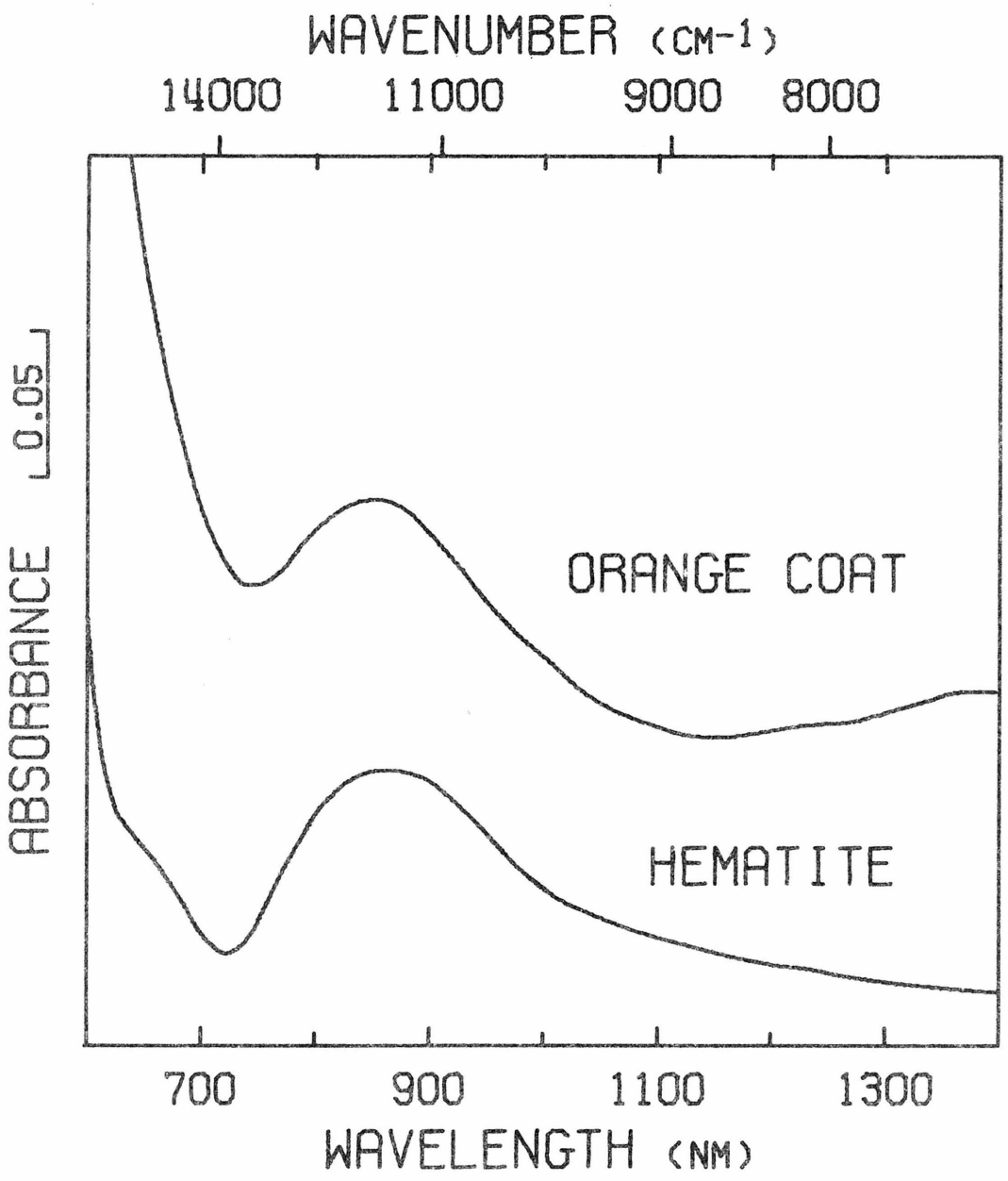

Figure 9. Near infrared spectra of desert varnish orange coat from Stoddard Wells compared to the near infrared spectrum of hematite.

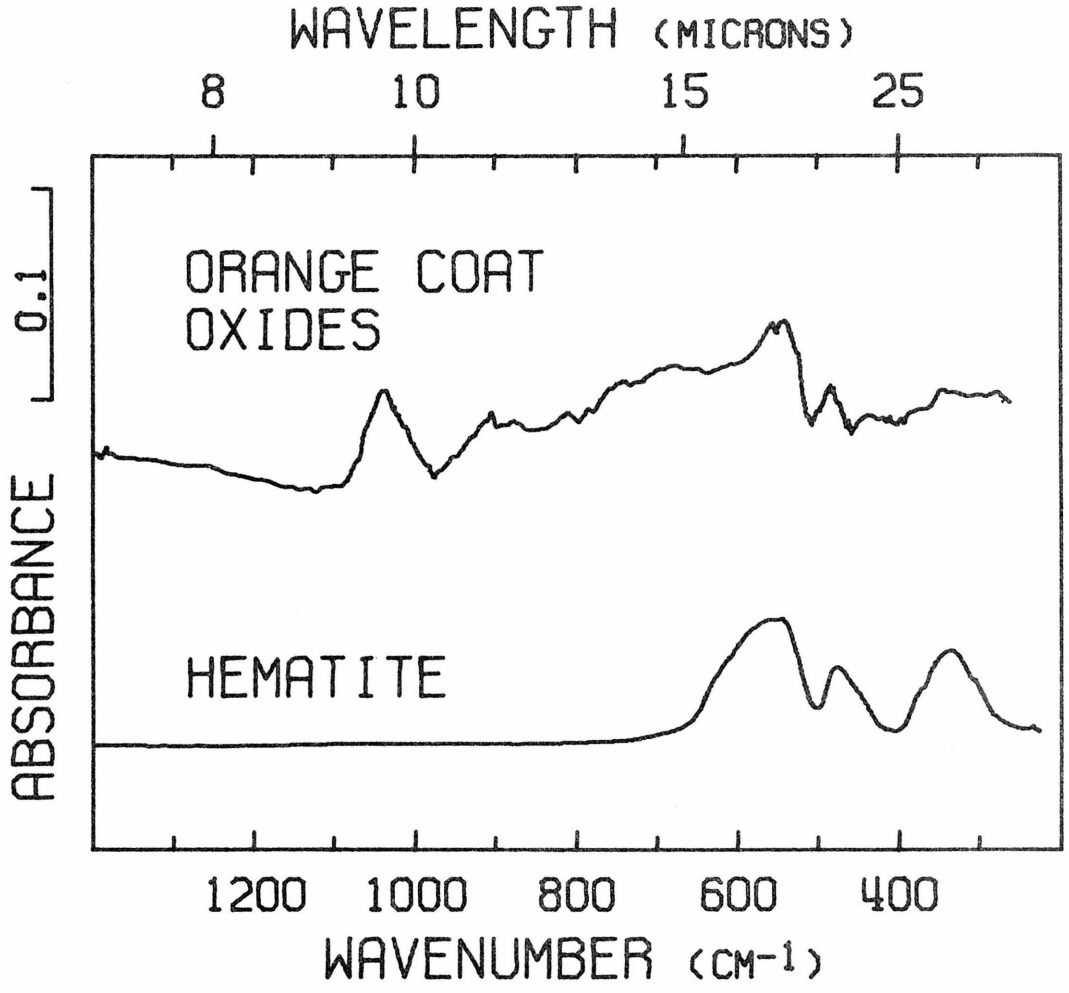

Figure 10. Infrared difference spectra of orange coat from Stoddard Wells compared to the infrared spectra of hematite at an equivalent concentration.

dispersive X-ray analysis of the varnish surface, which shows that aluminum is the major component in some areas of at least a few micrometers in diameter.

6. STRUCTURE

Scanning electron microscopy of the varnish surface shows no morphologies which are characteristic of manganese and iron oxides and could therefore be the basis for a second, independent identification of mineralogy. The surface views shown in Figures 11 and 12 are representative of the variation seen for varnish surface morphology. This variation in micromorphology is responsible for the difference in varnish sheen. The distinction between shiny and dull varnish is particularly well-developed at the Four Buttes locality. Both coats have the same mineralogy but the smooth surface of the shiny varnish (Figure 11A) reflects light more coherently than the rough surface of the dull varnish (Figure 11B). This difference may be the result of mechanical polish or differences in pathways of water movement at the varnish site. The ridges making the λ pattern in Figure 11B are the surface expression of irregular joints which penetrate into the varnish coating as shown by the arrows in Figure 11C and in Figure 13A. Water movement along these joints may cause the ridges by increased deposition.

Scanning electron micrographs of fracture surfaces approximately perpendicular to the varnished rock surface (transverse views; Figures 11C, 11D, and 12C) show that varnish is a distinct morphological entity having an abrupt boundary with the underlying rock. This coating is the varnish itself, not a weathering feature in

Figure 11. Desert varnish morphology as seen by SEM

A. Surface view of Four Buttes shiny black coat; bar = 30 micrometers

B. Surface view of Four Buttes dull black coat; bar = 30 micrometers

C. Transverse view of Salt Spring black coat; bar = 100 micrometers

D. Transverse view of Four Buttes dull black coat; bar = 100 micrometers

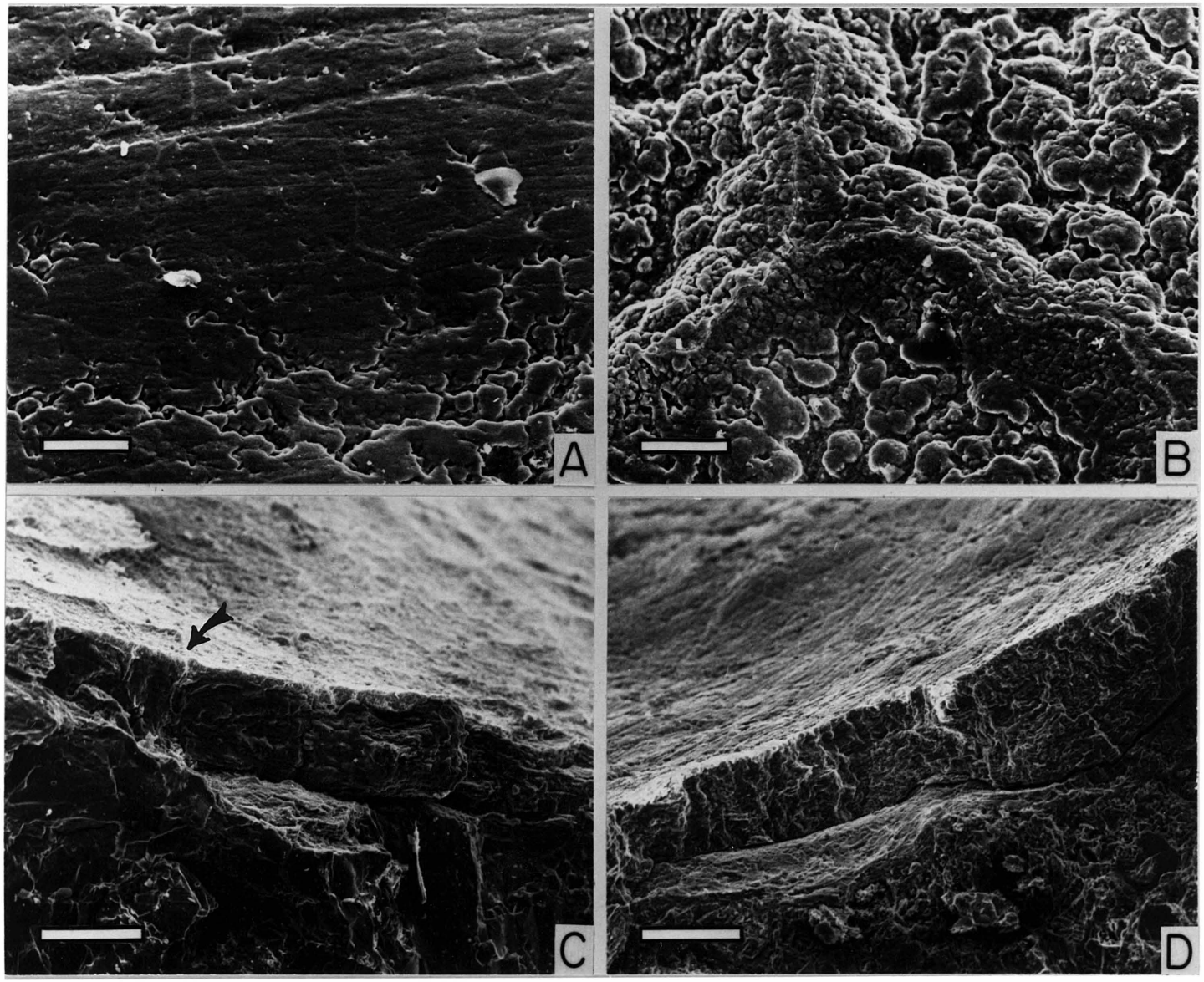
A
B
C
D

Figure 12. SEM comparison of the morphologies of untreated and dithionite-extracted varnish from Stoddard Wells

A. Surface view of untreated black coat; bar = 100 micrometers

B. Surface view of dithionite-extracted black coat; bar = 100 micrometers

C. Transverse view of untreated orange coat; bar = 10 micrometers

D. Transverse view of dithionite-extracted orange coat; bar = 10 micrometers

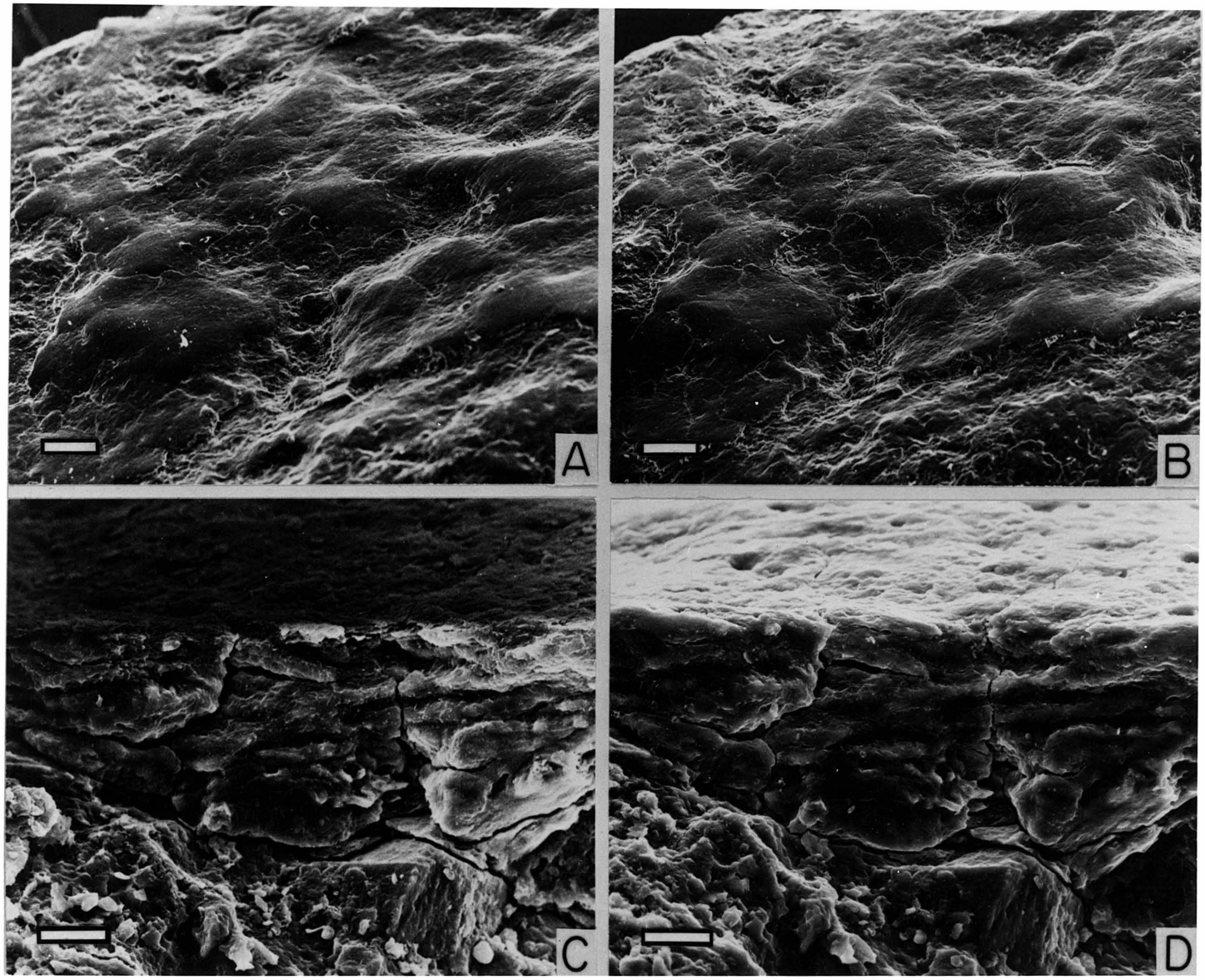
A
B
C
D

which varnish is found. It is correlated with the presence of stain as seen in the light microscope, and in those areas where the stain is absent, the coating is absent as well. Under the SEM varnish occasionally shows organized internal structure in transverse view. Thin section photomicrographs of desert varnish in both reflected and transmitted light (Figure 13) show the abrupt morphological boundary between varnish and rock which is seen with the SEM. Oxide stain is confined entirely to the surficial clay layer and does not appear to be derived from mafic minerals in the underlying rock. The internal structure of the varnish coating was first noted by Perry and Adams (1978), who have analyzed compositional differences among the layers. These internal structures are clearly depositional features, not relict rock structures.

Scanning electron micrographs of varnish before and after removal of the oxides by dithionite extraction (Figures 12A and 12B for black coat and Figures 12C and 12D for orange coat) indicate that desert varnish is an intimate mixture of clays and oxides to the sub-micrometer level.[5] No significant changes in morphology can be seen as a result of removal of the oxides. Increased magnification shows no significant morphological differences larger than sub-micrometer dimensions. Although thin sections clearly show oxide

---

[5]Chemical analysis of the upper surface of the Four Buttes black coat by ESCA (electron spectroscopy for chemical analysis), a surface analytical technique, supports this. The analysis indicates major silicon, aluminum, manganese, and iron. Thus, even at the varnish surface, where the highest oxide concentration is expected, the clays still appear to be present.

Figure 13. Photomicrographs of Four Buttes black coat in 10 micrometer thin section.

A. Transmission; bar = 100 micrometers; taken in monochromatic orange light to enchance contrast within the varnish

B. Transmission cross-polarized light; bar = 100 micrometers

C. Reflection; bar = 100 micrometers

D. Transmission, increased magnification of the lower left area of Figure 13A; bar = 30 micrometers; taken in monochromatic orange light to enhance contrast within the varnish

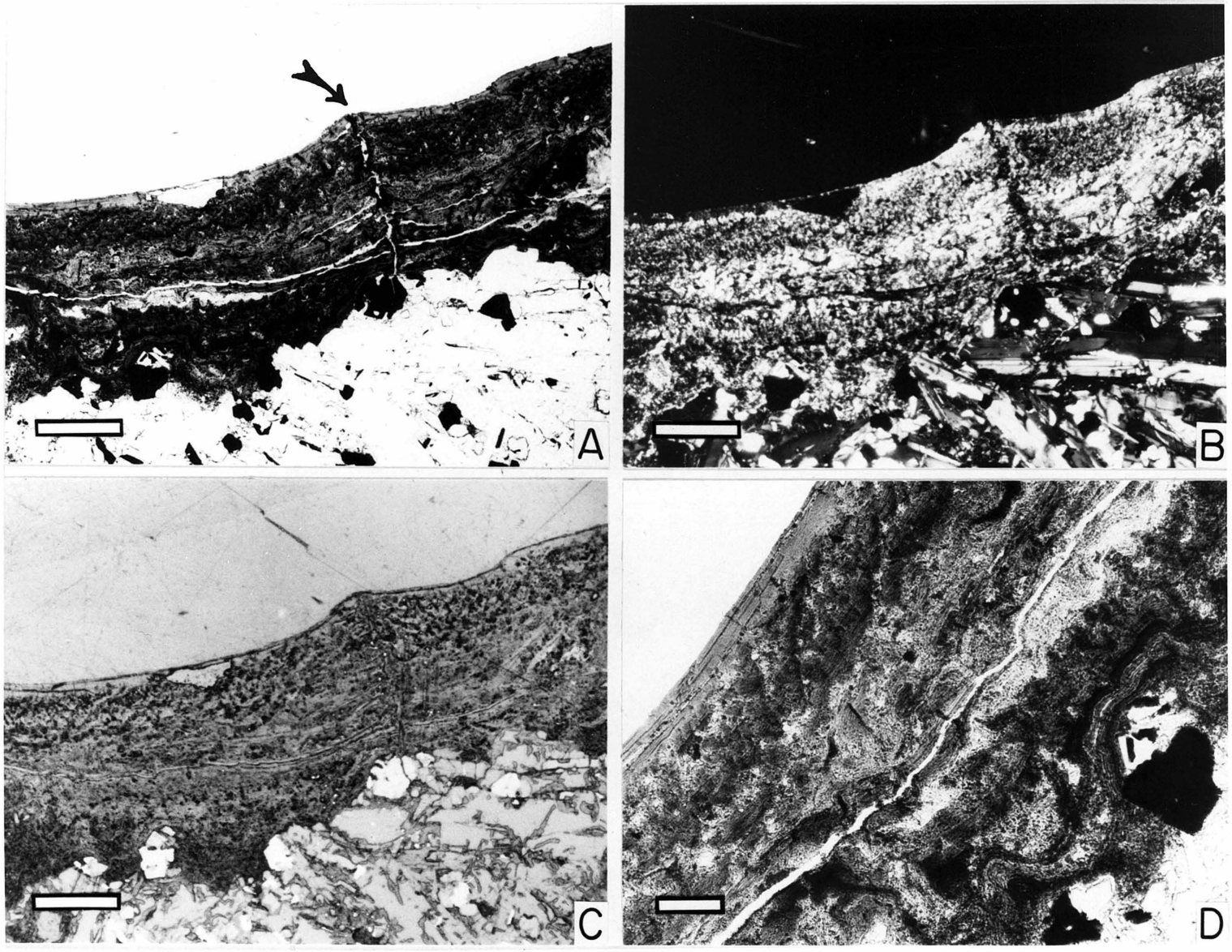
A
B
C
D

concentration gradients, removal of varnish oxides leaves no holes corresponding to areas of locally high oxide concentration. After extraction of the oxides the surface retains its sheen. Thus, shine is not the result of smoothing a rough clay surface by oxide deposition. During and after oxide removal care must be taken to keep the clays floculated, otherwise they go into suspension and the coating is destroyed. This suggests that the oxides cement the clay particles together. Cementation of several particles in random orientation is probably responsible for the X-ray diffraction pattern of untreated black coat (Figure 3), which is typical of unoriented clays.

Thin sections of the Four Buttes black coat reveal a 15 micrometer thick surface layer which lacks the fine structure apparent in the rest of the varnish coating (Figure 13D; upper left). This layer is characterized throughout its extent by coherent extinction directions under crossed-polarizers and by coherent pleochroism (dark brown for light polarized parallel to the layers; light brown for light polarized perpendicular to the layers). Perry and Adams (University of Washington, personal communication, 1978) have found this to be a general feature of desert varnish. This is further evidence for the intimate association of clays and oxides and suggests a topotactic relationship between them. The uniform color and coherent pleochroism of the layer indicates that birnessite, which is responsible for the color, is uniformly distributed and in a single orientation throughout the layer. Under the SEM some desert varnish shows a coherent fabric due to clay minerals oriented roughly parallel

to the rock surface. Epitaxial growth of birnessite on these oriented clays would result in the pleochroism observed in thin section. Sheet structure manganese oxides absorb light polarized parallel to their layers more strongly than that polarized perpendicularly because of the greater interaction among the manganese ions within the layers.

7. GENETIC IMPLICATIONS OF THE CHARACTERIZATION

None of the minerals identified in desert varnish are primary minerals of the substrate except for quartz. The material in varnish is thus derived from the rock by weathering or is transported from external sources to the surface. The clays are of external origin. The abrupt demarcation of varnish from the underlying rock and the depositional features revealed in thin section are inconsistent with their formation in place by weathering processes. For varnish on quartz both the clays and the oxides must be of external origin. My work supports the suggestions of Engel and Sharp (1958) and Hooke et al. (1969) that the oxides have been mobilized in varnish formation and suggests that their source is largely external to the rock. They are found in intimate mixture with clays which are themselves of external origin, and they bear no spatial relation to obvious sources in the underlying rock. The three localities I have studied here show no relation between manganese content in the rock and in the varnish. Nor is such a trend observable in the data of other workers (Engel and Sharp, 1958; Lakin et al., 1963; Hooke et al., 1969). Although my data show a correlation between iron content in the rock and in the varnish, this correlation is not

observable in the data of these other workers.

Wind is a likely transport mechanism for varnish material. It operates throughout the desert and is known to transport clays. After dust storms rock surfaces are covered with a fine layer of clay which is not easily removed (D.E. Martin, personal communication, 1977). It seems likely that part of this material is stabilized and incorporated into varnish. For extensive bedrock exposures without a higher source of alluvium wind is the most likely transport mechanism for the clays. For other types of varnish localities, however, clays may be carried in suspension by water or splashed to the surface by rain. The morphology of varnish on desert pavement stones suggests the association with water movement (Engel and Sharp, 1958; Hooke et al., 1969). Transport of manganese and iron must depend on water because their concentration in varnish and the Mn/Fe ratio far exceeds those of any likely source material.

Both clays and oxides are always found in varnish whereas adjacent unvarnished areas usually have neither. Physically distinct ferromanganese deposits such as manganese dendrites occur in the same environment as desert varnish and frequently have little or no clay (Chapter 4). Thus, clay is more than a passive contaminant in varnish. In some instances it may serve as a medium for capillary movement of varnishing solutions. Deposition of the manganese and iron oxides within the clay matrix might then cement the clay layer. The clay may aid in the deposition. Illite is known to fix manganese under the pH and Eh conditions at which varnish forms (Reddy and Perkins, 1976). In this way the clay and oxide phases may be

mutually dependent: the clay depending on the oxides for resistance to erosion; the oxides depending on the clay for transport and deposition. This would explain why neither pure clay nor pure ferromanganese oxide coatings are associated with desert varnish. In addition to adsorption of manganese and iron from solution the clays may directly influence the manganese oxide mineralogy. The hexagonal arrangement of the oxygens in either the tetrahedral or the octahedral layers of the clay minerals could form a suitable template for crystallization of the layered structures of birnessite. The average O-O distance of the tetrahedral layer is 3.00 Å in illite-montmorillonite mixed-layered clays, which differs only 3.4 percent from the 2.90 Å distance of the hexagonally close-packed oxygens in birnessite. The nature of the pleochroism of desert varnish in thin section suggests that this epitaxial relation is a common characteristic of desert varnish.

CONCLUDING STATEMENTS

Summary of results

Desert varnish is a distinct entity which shows little mineralogical variation among all the localities examined. The black coat consists predominantly of illite-montmorillonite mixed-layer clays, birnessite, and hematite. The orange coat is identical to the black coat except that it lacks birnessite. The relative amounts of these phases in a varnish coating do not vary greatly with locality. Desert varnish is an intimate physical mixture of these phases and is distinguished from the underlying rock by an abrupt change in chemistry, mineralogy, and morphology.

The origin of the material in varnish appears to be external to the rock on which it forms. The clays are transported in particulate form, probably by wind and water. The form in which the iron and manganese reach the varnish surface remain undetermined, but water is certainly involved in their transport.

The processes of oxide concentration and deposition at the varnish site are not yet fully understood. Clay minerals appear to be necessary for the formation of an oxide stain and I have suggested that this involves the influence of the clays on oxide deposition and transport. Other factors may be involved such as the catalytic oxidation of manganous ion by tetravalent manganese oxides or the topotactic growth of manganese oxides on iron oxides suggested for manganese nodules (Burns and Burns, 1977).

The role of biological processes in varnish formation

In light of the widely-held view that biological processes are important in desert varnish formation (Scheffer, et al., 1963; Krumbein, 1971; Bauman, 1976), the relation of my results to possible biological roles merits specific discussion. Manganese oxidizing bacteria have been cultured from small black fungal bodies which are frequently associated with desert varnish but occur on unvarnished rock surfaces as well (R. Perry and J. Adams, University of Washington, personal communication, 1976). Although clays and iron oxides are intimately associated with these bodies, they contain no manganese, and it seems likely that they bear little relation to varnish development. The appearance of desert varnish in thin section (Figures 13A and 13D) bears some similarity to that of stromatolites, which are formed by

accretion of material on blue-green algae; no other evidence of biological activity has been found in the varnish itself.

My work places constraints on the role of biological processes in desert varnish formation but does not rule it out. The absence of organic matter in desert varnish requires that either the coating be reworked inorganically to remove chemical evidence of biological activity or that the biological activity operate at a distance from the varnish site, perhaps through modification of water chemistry or mobilization of manganese and iron. It seems unlikely that biological activity is involved in the transport and deposition of clay minerals, one of the major processes in varnish formation. Since the oxide mineralogy of desert varnish is now known, research into the mineralogy of manganese and iron oxides precipitated by such organism as bacteria and blue-green algae may aid in the evaluation of their role in varnish formation.

Implications for age-dating

It has long been known that variations in the degree of desert varnish development on surfaces in similar environments often reflect differences in their ages (Blackwelder, 1948; Hunt, 1954, 1961; Hunt and Mabey, 1966). Under favorable circumstances, varnish has been used in conjunction with archeological artifacts to infer the relative ages of adjacent surfaces (Clements and Clements, 1953; Hayden, 1976), but it is not yet possible to use varnish for quantitative age determination. In general, varnish cannot be used with confidence for even the relative age-dating of surfaces. Bard et al. (1978) are presently attempting to develop a reliable dating method based on the

overall chemistry of desert varnish.

The results of my characterization of desert varnish bear directly on its use for age-dating. The common mineralogy and structure of desert varnish from the locations studied here imply a common formation mechanism. Attempts to develop a dating method are thus dealing with a single entity rather than a range of phenomena and their results should be widely applicable. On the basis of my characterization studies several potential approaches have been eliminated:

(1) Paleomagnetic dating of desert varnish based on the magnitude or orientation of the magnetic vector of its iron oxides does not appear to be a viable approach. Measurement of the magnetization of small wafers of rock coated on one side with desert varnish showed that both the black and orange coats are magnetically weak. Even on quartzite, the signal was dominated by that of the rock.

(2) Although the varnish thickness can be measured, it is too variable to be used quantitatively as a dating technique.

(3) Layer counting as in tree ring dating is not possible. Although there is some layering, it is highly irregular and discontinuous. Varnish frequently appears to grow laterally rather than vertically.

(4) Attempts to date by chemical means cannot rely on elements in the clays, since they are not authigenic.

(5) Since there is negligible carbon in desert varnish, carbon-14 dating is not possible.

The best possibility for quantitatively determining the age

of a desert varnish coating lies with the chemistry of its manganese and iron oxide phases. These appear to be authigenic and at the time of their formation may incorporate unstable elements which would allow radiometric dating. Subsequent leaching or remobilization of the oxides are likely to present problems but they have not yet been shown to be insurmountable. Since airborne dust is probably a major source of varnish material, varnish chemistry is likely to reflect significant changes in the chemistry of airborne material. Recent examples are the injection of transuranium elements from atomic weapon testing and aerosol lead from the use of leaded gasoline in automobiles. The influence of events such as these on varnish isotopic or chemical composition might allow different age groups of varnish to be distinguished if the events occurred sufficiently long ago.

Implications for geochemical prospecting

Initial work on the use of desert varnish for geochemical prospecting found several correlations between varnish trace element chemistry and mineralization (Lakin et al., 1963). The work was not continued, however, because variation in abundance of many trace elements appeared to be dependent on the manganese concentration. My characterization of varnish indicates that the trace element contents of its manganese and iron oxides have great promise for use in geochemical prospecting. Manganese and iron are probably brought to the varnish site in solution. It is likely that these solutions reflect the trace element chemistry of the local environment and control the trace element chemistry of the oxides that are formed.

Variations in oxide mineralogy which might cause anomalous differences in trace element chemistry are absent. In light of this, the potential of desert varnish for geochemical prospecting should be reevaluated utilizing the relation of trace element abundance to manganese and iron content.

REFERENCES

Albee, A.L., and Ray, L. (1970) Correction factors for electron microanalysis of silicates, oxides, carbonates, phosphates, and sulfates. Anal. Chem., 42, 1409-1414.

Bard, J.C., Asaro, F., and Heizer, R.F. (1978) Perspectives on dating of prehistoric Great Basin petroglyphs by neutron activation analysis. Archeometry, 20, 85-88.

Bauman, A.J. (1976) Desert varnish and marine ferromanganese oxide nodules: congeneric phenomena. Nature, 259, 387-388.

Bence, A.E., and Albee, A.L. (1968) Empirical correction factors for the electron microanalysis of silicates and oxides. J. Geol., 76, 382-403.

Blackwelder, E. (1948) Historical significance of desert laquer (abstr.). Geol. Soc. Am. Bull., 59, 1367.

Blake, W.P. (1857) Geological report in Explorations and surveys for a railroad route from the Mississippi River to the Pacific Ocean. 33rd Congr. Senate Ex. Doc. 78, 5, pt. 2, 370 pp.

Blake, W.P. (1905) Superficial blackening and discoloration of rocks especially in desert regions. Am. Inst. Mining Engineers Trans., 35, 371-375.

Brown, R.W. (1977) A sample fusion technique for whole rock analysis with the electron microprobe. Geochim. et Cosmochim. Acta, 41, 435-438.

Burns, R.G., and Burns, V.M. (1977a) Chapter 7, Mineralogy. In: Marine Manganese Deposits, Glasby, G.P. (ed.) Amsterdam: Elsevier, 185-248.

Chao, T.T. (1972) Selective dissolution of manganese oxides from soils and sediments with acidified hydroxylamine hydrochloride. Proc. Soil. Sci. Soc. Am., 36, 764-768.

Clements, T., and Clements, L. (1953) Evidence of Pleistocene man in Death Valley, California. Geol. Soc. Am. Bull., 64, 1189-1204.

Engel, C.G., and Sharp, R.P. (1958) Chemical data on desert varnish. Bull. Geol. Soc. Am., 69, 487-518.

Farmer, V.C., and Russell, J.D. (1964) The infrared spectra of layer silicates. Spectrochim. Acta, 20, 1149-1173.

Goodwin, A.J.H. (1960) Chemical alteration (Patination) of stone. In R.F. Heizer and S.F. Cook, Eds. The Application of Quantitative Methods in Archeology, p. 300-324. Quadrangle Books, Chicago.

Hayden, J.D. (1976) Pre-altithermal archeology in the Sierra Pinacate, Sonora, Mexico. Am. Antiquity, 41, 274-288.

Heller-Kallai, L. (1975) Interaction of montmorillonite with alkali halides. In. S.W. Bailey, Ed. Proceedings of the International Clay Conference, 361-372. Applied Publishing, Wilmette, Illinois.

Hooke, R. LeB., Yang, H., and Weiblen, P.W. (1969) Desert varnish: an electron probe study. J. Geol., 77, 275-288.

Hower, J., and Mowatt, T.C. (1966) The mineralogy of illites and mixed-layer illite/montmorillonites. Am. Miner., 51, 825-854.

Hower, J., Eslinger, E.V., Hower, M.E., and Perry, E.A. (1976) Mechanism of burial metamorphism of argillaceous sediments 1. Mineralogical and chemical evidence. Geol. Soc. Am. Bull., 87, 725-737.

Hunt, C.B. (1954) Desert varnish. Science, 120, 183-184.

Hunt, C.B., and Mabey, D.R. (1966) General geology of Death Valley, California. United States Geol. Surv. Prof. Pap. 494A. 90-92.

Hunt, C.B. (1961) Stratigraphy of desert varnish. United States Geol. Surv. Prof. Pap. 424B, 194-195.

Kerr, P.F. et al. (1949) American Petroleum Institute Research Project 49, Preliminary Reports 1 to 8. American Petroleum Institute, New York.

Krumbein, W.E. (1971) Biologische Entstehung von Wüstenlack. Umschau in Wissenschaft und Technik, 7, 240-241.

Lakin, H.W., Hunt, C.B., Davidson, D.F., and Oda, U. (1963) Variation in minor-element content of desert varnish. United States Geol. Surv. Prof. Pap. 475B, 28-31.

Laudermilk, J.D. (1931) On the origin of desert varnish. Am. J. Sci., 21, 51-66.

Marshall, R.R. (1962) Natural radioactivity and the origin of desert varnish. Am. Geophys. Union Trans., 43, 446.

Mehra, O.P., and Jackson, M.L. (1960) Iron oxide removal from soils and clays by a dithionite-citrate system buffered with sodium bicarbonate. In: A Swineford, Ed., Proceedings of the Seventh National Conference on Clays and Clay Minerals, p. 317-327. Pergamon, Oxford.

Merrill, G.P. (1898) Desert varnish. United States Geol. Surv. Bull., 150, 389-391.

Ormsby, W.C., and Sand, L.B. (1954) Base-exchange: an analytical tool for mixed-layer aggregates. In: A. Swineford, Ed., Proceedings

of the Second National Conference on Clays and Clay Minerals, p. 254-261. Pergamon, Oxford.

Oinuma, K., and Hayashi, H. (1965) Infrared study of mixed-layer clay minerals. Am. Miner., 50, 1213-1227.

Perry, R.S., and Adams, J.B. (1978). Growth zones in desert varnish (abstr.) Geol. Soc. Am. Abstracts with Programs, 10, 141-142.

Reddy, M.R., and Perkins, H.F. (1976) Fixation of manganese by clay minerals. Soil Sci., 121, 21-24.

Reynolds, Jr., R.C., and Hower, J. (1970) The nature of interlayering in mixed-layer illite-montmorillonites. Clays and Clay Min., 18, 25-36.

Scheffer, F., Meyer, B., and Kalk, E. (1963) Biologische Ursachen der Wüstenlackbildung. Z. für Geomorphologie N.F., 7, 112-119.

Stubičan, V., and Roy, R. (1961) Isomorphous substitution and infrared spectra of the layer lattice silicates. Am. Miner., 46, 32-51.

Thorez, J. (1975) Phyllosilicates and Clay Minerals. Lelotte, Dison, Belgium.

Weaver, C.E., and Pollard, L.D. (1973) The Chemistry of Clay Minerals. Elsevier, Amsterdam.

Webb, J., and Gray, H.B. (1974) Structural studies of the ferritin core and related iron(III) polymers. Biochim. et Biophys. Acta, 351, 224-229.

White, C.H. (1924) Desert varnish. Am. J. Sci., 7, 413-420.

CHAPTER 4

THE MINERALOGY OF MANGANESE OXIDE CONCENTRATIONS OF THE TERRESTRIAL WEATHERING ENVIRONMENT

This chapter is divided into two parts. Part 1 is a general survey of the mineralogy of manganese oxide concentrations from the surface or near-surface environment. Part 2 is a mineralogical study of manganese concretions from late-Cenezoic rocks in Baja California, Mexico, and is presented as a separate entity since the manganese concretions from Baja California are not necessarily the product of near-surface processes operating on the time-scale of even thousands of years.

PART 1

INTRODUCTION

Manganese oxide concentrations are a common product of terrestrial weathering processes. Concentrations with variable morphology, chemistry, and physical properties occur in diverse environments throughout the world: desert varnish in arid and semi-arid regions, manganese dendrites within and on the surfaces of rocks, deposits within cracks in rocks, and associated with rivers, caves, and glaciers.

Determination of manganese oxide mineralogy of these phenomena by X-ray diffraction has been difficult or impossible owing to the finely particulate and disordered nature of the manganese oxides and the presence of silicate phases as major components of the deposits. For this reason the structural and genetic relations among them are

poorly understood.

Infrared spectroscopy is particularly useful for mineralogical analyses of these manganese oxide concentrations. It eliminates ambiguity frequently caused by silicate components (such as the confusion of kaolinite and birnessite). Because it is sensitive to short range order, it provides mineralogical information on even the most disordered and finely-particulate phases.

This part of Chapter 4 presents the results of a mineralogical study of a wide range of manganese oxide concentrations of the terrestrial weathering environment. Infrared spectroscopy indicates distinct differences in mineralogy which can be correlated with the morphology of the deposit and its depositional environment.

Identification of manganese oxide mineralogy is by direct comparison to spectra of well-characterized manganese oxide samples (Chapter 2). For each type of manganese oxide concentration, infrared spectra representative of those on which manganese oxide mineralogy is based are included in the text. Spectra of other samples listed in Table 1 are included in Appendix A.

EXPERIMENTAL DETAILS

I prepared powdered samples as follows: Milligram quantities of the manganese oxide concentrations were removed from their substrates by scraping with a tungsten needle under 20 X magnification. The resultant material was examined under 40 X, light-colored contaminants removed, and the material ground under toluene to a fine powder in a boron carbide mortar and pestle. When carbonate was present in the sample, it was removed by treatment with 1.0 M acetic acid for

5 minutes prior to any further analysis. Manganese and iron oxides were extracted from the samples by the sodium dithionite procedure (Mehra and Jackson, 1960), which was shortened to a single 5-minute extraction to minimize the effect on the silicates. Infrared spectra of the samples, their dithionite-extracted residues, and the manganese oxide standards were obtained with a Perkin-Elmer Model 180 spectrophotometer on 0.50 mg of powdered sample dispersed in 200 mg KBr and dried overnight at 120°C under vacuum to remove water adsorbed on the KBr. This treatment affected only those infrared features due to adsorbed water. In the figures I have presented spectra at various percentages of their true intensities to facilitate comparison. The intensity for any sample may vary by a factor of 2 or 3 due to differences in its particle size and degree of dispersion in the KBr. I obtained infrared spectra of the manganese oxides in samples by computer generation of difference spectra (for example, Figure 1). Absorption due to silicates was removed from a spectrum (Figure 1C) by subtracting from it that fraction of the extracted residue spectrum necessary to null the absorption near 1000 cm^{-1} (Figure 1D), which is due wholly to silicates. The resulting difference spectrum (Figure 1B) is that of the manganese and iron oxides in the sample. For desert varnish samples, where manganese and iron are present in comparable concentrations, features attributable to both manganese and iron oxide are present. The other deposits studied here are either free of iron or have it present in sufficiently lower concentration than manganese that it does not interfere with the determination of manganese oxide

mineralogy. I used a scanning electron microscope equipped with an energy-dispersive X-ray analyzer for semi-quantitative chemical analyses. X-ray powder diffraction was done with a Debye-Scherrer camera using vanadium-filtered chromium radiation.

RESULTS

Desert Varnish

The results of a detailed study of samples 1-3 (Table 1) have been reported in Chapter 3. The additional samples listed in Table 1 confirm the generality of those results. Desert varnish invariably consists of the manganese oxide birnessite in intimate mixture with hematite and large amounts of clay minerals. The clays are generally of the illite-montmorillonite type with minor kaolinite, but in several samples this concentration ratio is reversed.

Manganese Dendrites

I define manganese dendrites as those manganese oxide concentrations which exhibit a dendritic pattern. They may be within the rock matrix (internal), along fractures surfaces in the rock or on its surface.

Ring (channel) structure manganese oxide minerals (Burns and Burns, 1977) are characteristic of all three types of manganese dendrites. With a single exception (#18) the manganese mineral present in the dendrites has been found to be romanechite $(Ba,H_2O)_2Mn_5O_{10}$ or one of the following hollandite group minerals: hollandite, $BaMn_8O_{16}$; cryptomelane, KMn_8O_{16}; coronadite, $PbMn_8O_{16}$. Figures 1 and 2 are representative of the spectral data on which mineralogical identification is based, although generation of difference spectra was

Table 1. Sample information*

Deposit type	#	Locality	Mn mineralogy Accessory mineralogy	Chemistry	Description
desert varnish	1	Four Buttes,Ca.	birnessite I-M/Hem,Kao//Qtz	-	coating on andesite boulders
	2	Salt Spring,Ca.	birnessite I-M/Hem,Kao//Qtz	-	coating on small quartzite outcrop
	3	Stoddard Wells,Ca.	birnessite I-M/Hem,Kao//Qtz	-	coating on desert pavement rhyolite and quartz cobbles
	4	Little Colorado Cyn.,Az.	birnessite Kao/I-M//Qtz†	-	streaked "stain" coating quartz conglomerate canyon walls
	5	Biklabito,N.M.	birnessite** I-M/Hem,Kao//Qtz	-	coating on small sandstone outcrop and desert pavement dacite porphyry cobbles
	6	Petroglyph Park,N.M.	birnessite** I-M/Kao//†	-	coating on basalt outcrop
	7	Thunderbird Park,Az.	birnessite I-M/Hem,Kao//Qtz	-	coating on desert pavement basalt cobbles
	8	Funeral Peak,Ca.	birnessite** I-M/Kao,Qtz//†	-	coating on colluvial gneiss and hornfels cobbles
	9	Olo Cyn.,Az.	birnessite** I-M/Kao//Qtz†	-	coating on alluvial limestone cobbles
	10	Cady Mtns.,Ca.	birnessite I-M/Kao//Qtz†	-	coating on desert pavement volcanic rock cobbles
	11	Lake Pleasant,Az.	birnessite I-M/Kao//†	-	coating on small banded iron formation outcrop
	12	Eetza Mtn.,Nev.	birnessite** I-M/Kao//†	-	coating on basalt boulders
	13	Negev Desert,Israel	birnessite Kao/Hem,I-M//Qtz	-	coating on chert artifact in desert pavement
	14	Fort Davis,Tx.	birnessite** I-M/Kao,Qtz//†	-	coating on basalt cobble
manganese dendrites	15	Soda Mtns.,Ca.	coronadite none	Mn,Pb/Ca//Zn,Cu,Al,Si,Fe	surficial dendrites up to 1 mm thick on alluvial sandstone cobble
	16	Southwestern United States	cryptomelane Kao//Cbn,Qtz	Mn/K,Ca//Si,Al,Fe	internal dendrites < 100 μm thick in felsite
	17	South Dakota	romanechite I-M/Kao,Qtz,Fld//	Mn,Si,Ba/Al,Ca//Mg,Pb,Fe,Na	fracture surface and internal dendrites < 100 μm thick on pegmatitic feldspar

	18	Pala,Ca.	todorokite /Kao//	Mn,Si,Al/Ca,Ti//Fe,K,Pb	surficial and internal dendrites up to 1 mm thick on pegmatite
	19	Barstow,Ca.	romanechite Cla/Cal,Qtz//	Ca,Mn,Si/Ba//K,Mg,Al	fracture surface dendrites up to 1 mm thick on siltstone outcrop
	20	Argus Peak,Ca.	hollandite Qtz//Kao	Mn,Si,Ba/K//Ca,Al,Pb	internal dendritic stain in siltstone outcrop
	21	Afton Canyon,Ca.	hollandite Cbn,Ser//	Mn,Si,Mg/Al,Ba//Ca	internal dendritic stain in calcareous claystone alluvial boulder
	22	Cady Mtns.,Ca.	romanechite //Qtz	Mn,Ba//Si,Ca,K	surficial dendrites up to 1 mm thick on alluvial volcanic rock
	23	Beechworth,Australia	cryptomelane Kao//Qtz	Mn/K//Ba,Si,Al,Mg	surficial dendrites up to 1 mm thick on granite
	24	Oro Preto,Brazil	hollandite I-M//	Mn/Ba/K,Al,Si//Ca	internal dendrites < 100 µm thick in micaceous lamellae of quartz mica schist
cave deposits	25	Southeastern United States	birnessite //Qtz,Cla	Mn,Fe,Ca/Si//K,Ba	veins of purer material in concretions of oxide and clay from a dry streambed
	26	Southeastern United States	birnessite /Kao,I-M,Qtz//	Mn,Si,Fe,Ca/Cl,Al//Mg,Na	coating on pebbles of varied lithology from a dry streambed
stream deposits	27	Ladysmith,Wis.(Flambeau R.)	birnessite /Cla,organics//	Si,Mn,Fe,Al/Ca,Mg//	coating < 100 µm thick on streambed quartzite cobbles
	28	Athens,Ga.(Turkey Cr.)	birnessite /Kao//organics	Mn,Fe/Ca//Al,Si,Ni,Ba	coating < 100 µm thick on streambed gneiss cobbles
	29	Pilar,N.M.(Rio Grande R.)	birnessite I-M/Kao,Nit//	Si,Al,Mn,Ca,Fe//Ti,K,Mg	coating < 100 µm thick on basalt cobbles in splash zone
	30	Long Pond Quad.,Me.(Pyrite Cr.)	nsutite none	Mn//Al,Ba,Si,Ca,K,Fe	concretions in stream alluvium
	31	The Forks Quad.,Me.(Shawn Cr.)	birnessite /I-M,Qtz//	Mn,Si,Al,Fe/Ca//K,Zn	concretions in stream alluvium
	32	Montezuma,Col.(Deer Cr.)	birnessite /Kao//	Mn/Si,K//Al	mountainside deposit probably associated with a spring
miscellaneous samples subglacial deposit	33	Jackson Glacier,Mont.	birnessite or todorokite Qtz//Chl	Si,Al,Mn,Fe,Mg/Ca,K//	coating < 100 µm on siltstone outcrop surface under glacier
	34	Khumbu Region,Nepal	birnessite or todorokite** none	Si,Al,Fe,Mn/K,Ti,Ca//Mg	coating < 100 µm on gneiss outcrop surface under glacier
crack deposit	35	Sierra Natl.Forest,Ca.	romanechite + ? Kao/Qtz//	Mn,Si,Al//K,Ca,Mg,Fe	coating up to 1 mm thick on granite outcrop near a water seep
	36	Cady Mtns.,Ca.	hollandite + romanechite /Qtz//	Mn,Ba/Si,Al,Mg//K	coating up to 1 mm thick on volcanic rock outcrop

counterfeit Mn deposits	37	Sierra Natl.Forest,Ca.	none organic//	-	coating up to 1 mm thick on granite outcrop in a water seep
	38	Rock Creek,Ca.	none organic//	-	coating up to 1 mm thick on granite boulders in stream splash zone
	39	Summit Meadow Lk.,Ca.	none iron oxide//	Fe/Al,Mn,Si//	coating up to 1 mm thick on granite in lake outlet streambed
	40	Meteor Crater,Az.	none organic//	-	dendritic growth on shocked sandstone
	41	Antarctic	none polished surface	-	polished surface of hornfels which has the appearance of desert varnish

*The following abbreviations are used: I-M = illite-montmorillonite mixed-layer clay, illite, or muscovite, which are nearly indistinguishable by infrared spectroscopy; Kao = kaolinite; Hem = hematite; Qtz = quartz; Cbn = carbonate; Fld = feldspar; Cla = unidentified clay mineral; Ser = serpentine; Nit = nitrate; Chl = chlorite. The symbols / and // are used to indicate roughly the relative amounts of accessory minerals and of chemical elements. Accessory minerals listed to the left of a single slash are present in such high concentration that they dominate the infrared spectrum. Accessory minerals to the left of a double slash are in sufficient concentration that they significantly affect the spectrum. Accessory minerals to the right of the double slash are detected by infrared spectroscopy but are present in too low a concentration to significantly alter the spectrum. Chemical elements to the left of a single slash are the dominant constituents; those between single and double slashes are minor constituents; those to the right of a double slash are trace constituents. This is based roughly on peak height from the energy dispersive X-ray detector without any quantitative corrections. More detailed information concerning sample locality and description is found in Appendix B.

**Noise introduced by the generation of difference spectra is too large to allow determination of manganese mineralogy. Instead, it is inferred from direct comparison to other spectra of the same phenomenon with similar accessory minerals.

+An iron oxide phase is present. I have not determined its mineralogy but presume it to be hemetite on the basis of color.

Figure 1. Infrared spectra identifying romanechite in manganese dendrite #17:

A. Romanechite standard #34, 41% intensity.
   In this and subsequent figures the standard number for manganese oxide samples refers to Table 1 in Chapter 2.

B. Difference spectrum of C and D, 100% intensity

C. Unextracted dendrite, 100% intensity

D. Extracted dendrite, 51% intensity

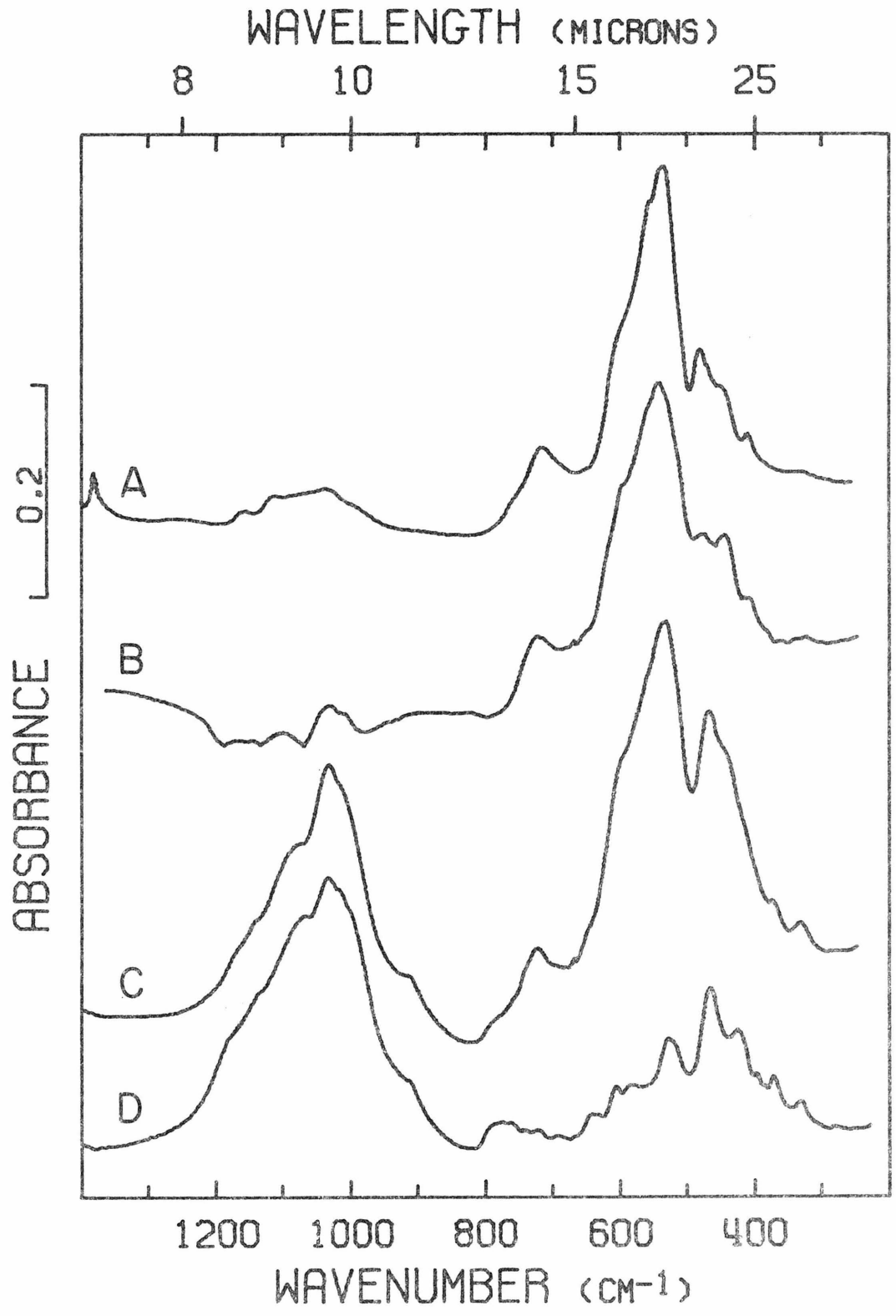
WAVELENGTH (MICRONS)
8
10
15
25
0.2
ABSORBANCE
A
B
C
D
1200
1000
800
600
400
WAVENUMBER (CM-1)

Figure 2. Infrared spectra identifying hollandite group mineral in manganese dendrite #24

A. Cryptomelane standard #28, 28% intensity

B. Difference spectrum of C and D, 100% intensity

C. Unextracted dendrite, 100% intensity

D. Extracted dendrite, 75% intensity

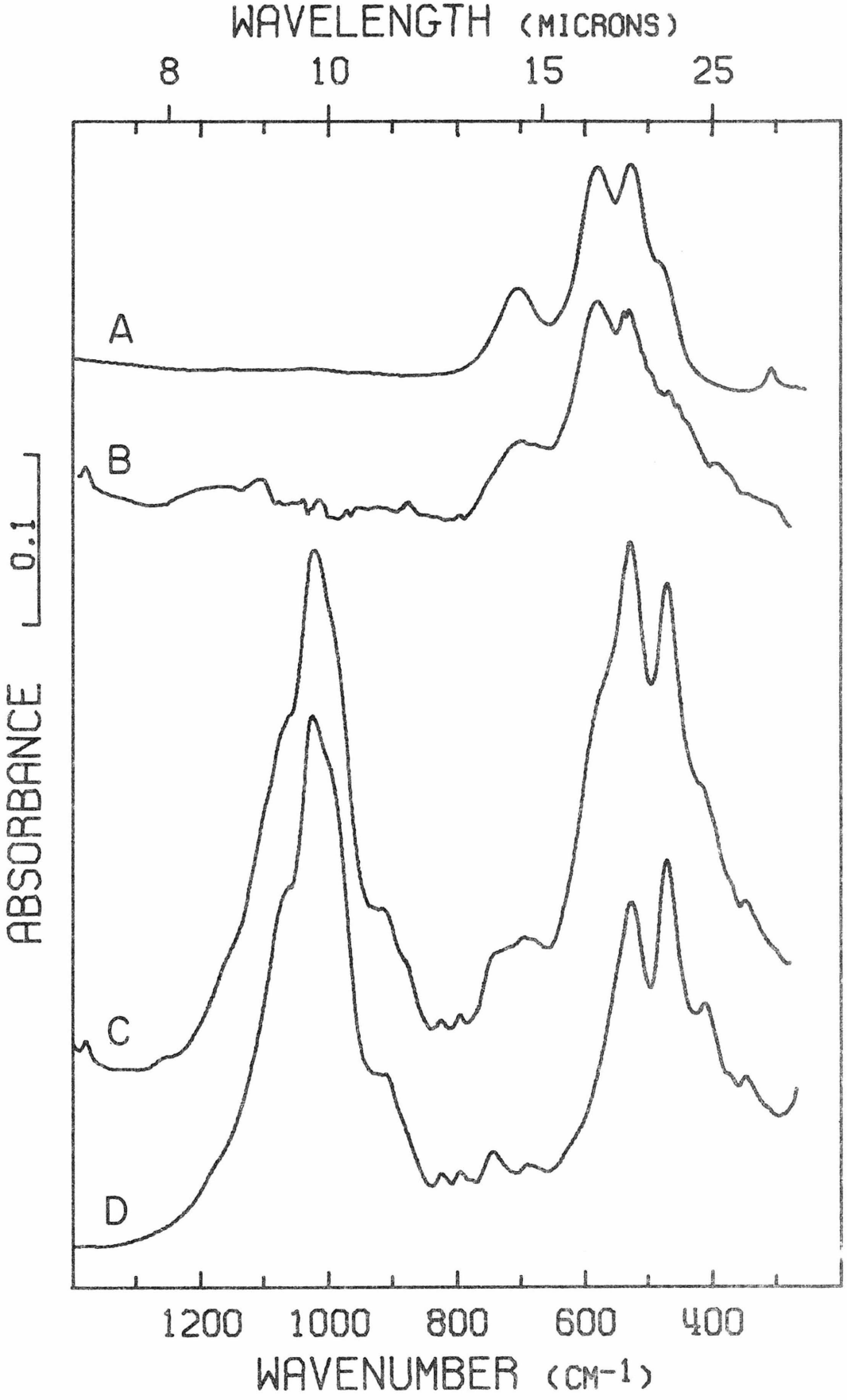
WAVELENGTH (MICRONS)
8
10
15
25
A
B
0.1
ABSORBANCE
C
D
1200
1000
800
600
400
WAVENUMBER (CM-1)

not necessary in all cases. I used chemical analysis to distinguish different hollandite group minerals because their infrared spectra are identical in the 4000 cm^{-1} to 200 cm^{-1} region. Distinguishing features between the romanechite of Figure 1 and the hollandite of Figure 2 are the position of the band near 700 cm^{-1}, the intensity of the band near 600 cm^{-1} (which is a prominent band in the hollandite group minerals and only a shoulder in romanechite), and the presence of the weak band near 450 cm^{-1} for romanechite. In addition, romanechite has H_2O absorption bands at 3520 cm^{-1}, 3470 cm^{-1}, and 1605 cm^{-1} (Figure 7), which distinguish it from all other manganese oxides. My chemical data (Table 1) show high Ba concentrations in those samples with romanechite mineralogy and thereby support the infrared results. The single example of a non-channel structure manganese oxide, #18, was unambiguously identified as todorokite, $(Mn,Ca,Mg)Mn_3O_7 \cdot H_2O$ (Figure 3). I have found no dendrites with pyrolusite mineralogy. The term "pyrolusite dendrite" is a misnomer and should be discontinued.

Manganese dendrites have no characteristic accessory mineralogy such as the high concentration of clay minerals present in desert varnish. Some dendrites are nearly pure manganese oxide. In others the manganese oxide is mixed with various carbonate or silicate minerals characteristic of the weathering environment. These accessory minerals are not necessarily involved in the dendrite formation process. The fracture surface dendrites of sample #17 appear to be a local staining of clay minerals which are present throughout the fractures. Accessory minerals of the internal dendrites are in many cases simply

Figure 3. Infrared spectra identifying todorokite in manganese dendrite #18

A. Todorokite standard #55, 136% intensity

B. Unextracted dendrite, 100% intensity

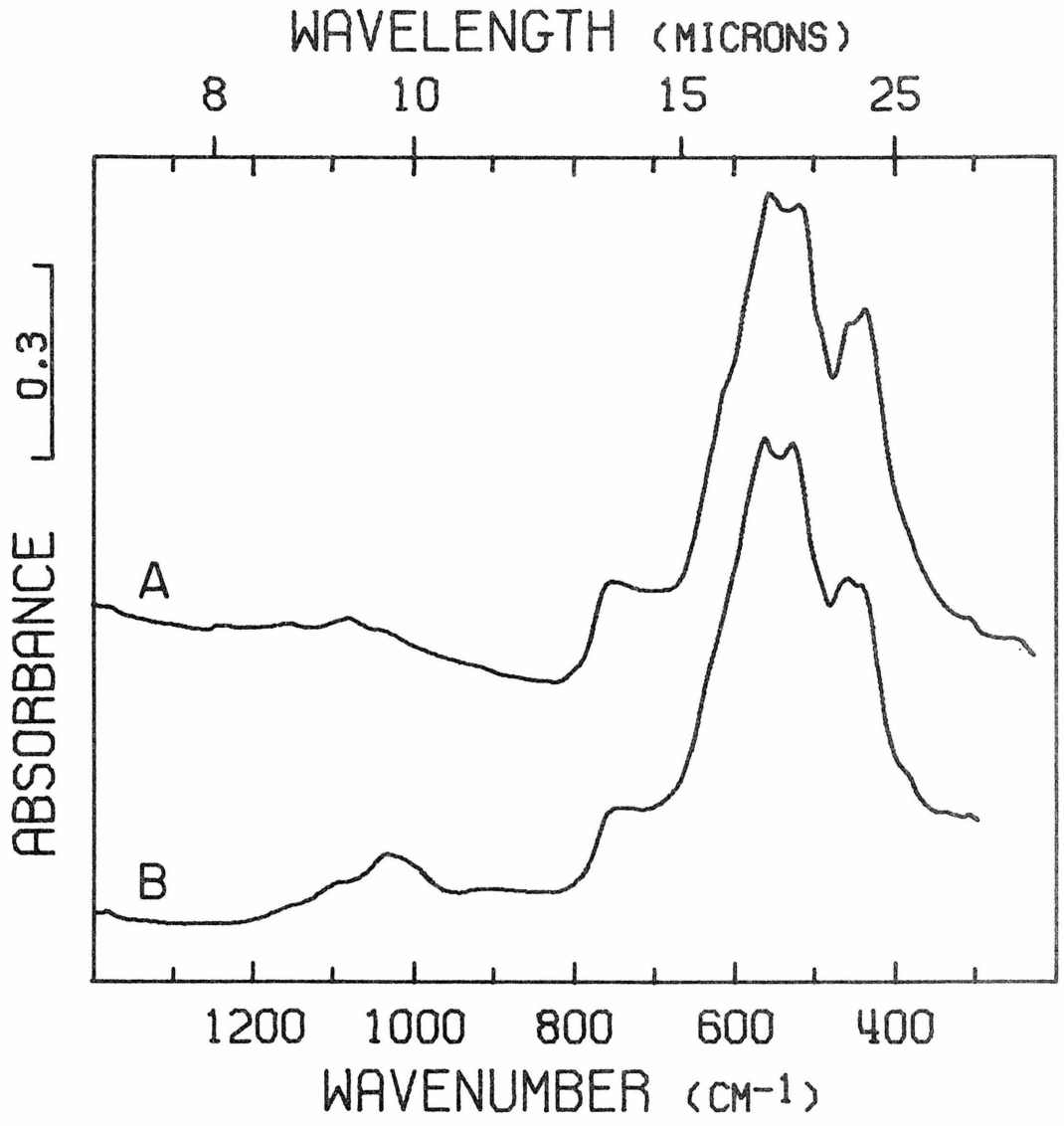
WAVELENGTH (MICRONS)
8
10
15
25
ABSORBANCE
0.3
A
B
1200
1000
800
600
400
WAVENUMBER (CM-1)

the minerals of the rock matrix in which the dendrites have formed.

Manganese dendrites do not generally have a high degree of chemical homogeneity. The manganese concentration varies greatly throughout the stained area in those dendrites which are not pure oxide. In most dendrites areas tens of microns in size can be found which are predominantly manganese oxide. The chemical analyses in Table 1 are from these areas. In other areas the dendrite chemistry is dominated by the accessory minerals. Manganese dendrites appear to be manganese oxide coatings on a substrate composed of the accessory minerals. I have found only trace quantities of iron in manganese dendrites. This distinguishes them from other manganese concentrations which generally contain iron as one of the major constituents.

Stream Deposits

The stream deposit samples include coatings on stones from both the streambed and the splash zone and concretions from stream alluvium. The dominant manganese mineralogy of these samples is birnessite, $(Na,Ca,K)Mn_7O_{14}\cdot 3H_2O$. Figure 4 is representative of the spectral data on which this mineralogical identification is based. The two intense, poorly resolved bands near 500 cm^{-1} are characteristic of birnessite and distinguish it from all other manganese oxides (Chapter 2), although it is easily confused with some todorokite samples. Most todorokites have spectra distinct from that of Figure 4C (Figure 3A, for example), but the spectrum of highly disordered todorokite (Figure 4A) is similar. The nearly equal intensity of the two major absorption bands of Figure 4C and the positions of the weak

Figure 4. Infrared spectra identifying birnessite in stream deposit #31

A. Disordered todorokite standard #57, 120% intensity

B. Birnessite standard #47, 100% intensity

C. Difference spectrum of D and E, 100% intensity

D. Unextracted deposit, 100% intensity

E. Extracted deposit, 14% intensity

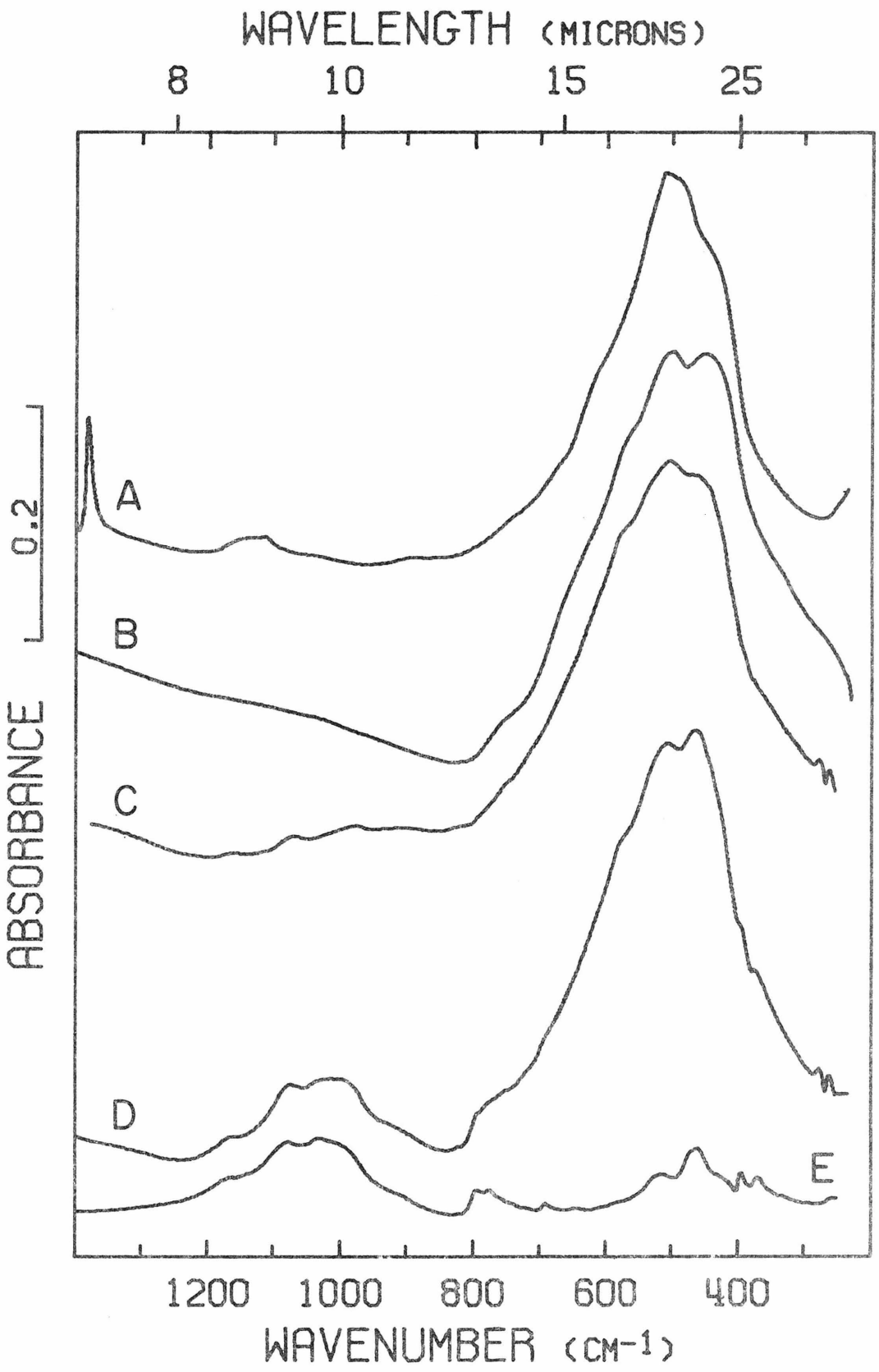
WAVELENGTH (MICRONS)
8
10
15
25
ABSORBANCE
0.2
A
B
C
D
E
1200
1000
800
600
400
WAVENUMBER (CM-1)

Figure 5. Infrared spectra identifying nsutite in river deposit #30

A. Cryptomelane standard #28, 110% intensity

B. Nsutite standard #16, 88% intensity

C. Unextracted river deposit, 100% intensity

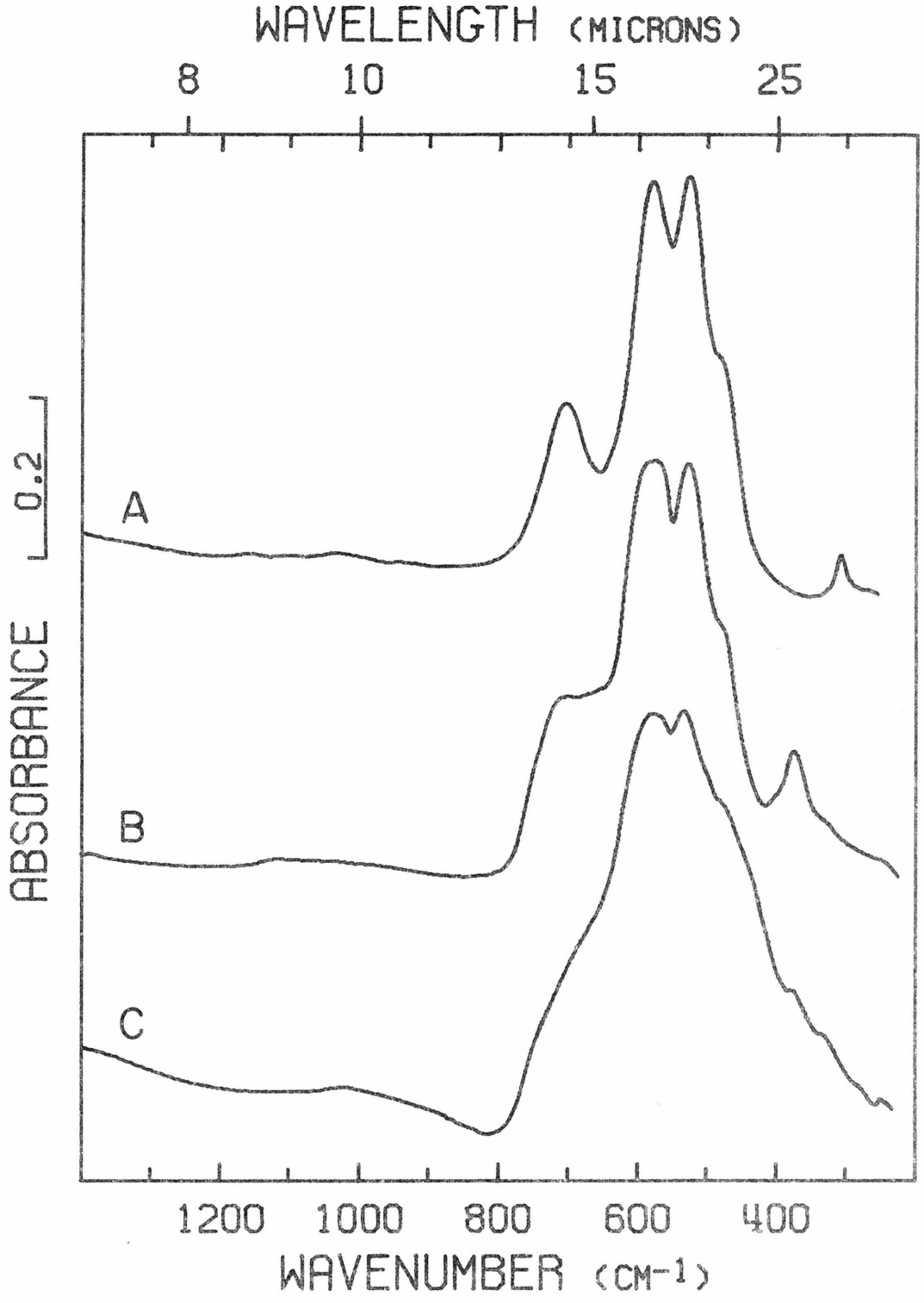
WAVELENGTH (MICRONS)
8
10
15
25
0.2
ABSORBANCE
A
B
C
1200
1000
800
600
400
WAVENUMBER (CM-1)

shoulders at higher wavenumber indicate a birnessite rather than a todorokite mineralogy. Qualitative chemical analyses of the river deposits support a birnessite mineralogy. Invariably Ca and/or K are present in minor amounts. Nowlan (1976) has found birnessite in one stream in Maine and noted that many samples from his other Maine localities (samples #30 and #31, Table 1) have the two broad X-ray lines characteristic of δ-MnO_2, which has been shown to be a disordered birnessite (Buser et al., 1954).

I have identified sample #31 as nsutite, $Mn(O,OH)_2 \cdot H_2O$ on the basis of its infrared spectrum (Figure 5) and chemistry. The spectrum of sample #31 is characteristic of nsutite in the broadness of its band near 580 cm^{-1} and in the positions of the weak bands at energies lower than 400 cm^{-1}. However, the reliability of identification on this basis alone is questionable because of the strong similarity between the infrared spectra of sample #31 and the hollandite group minerals. Qualitative chemical analysis, which indicates only traces of cations other than manganese, confirms the nsutite mineralogy. Because of differences in cation absorption properties, this mineralogical difference may have profound effects on the use of manganese oxides trace elements for geochemical exploration.

Stream deposits do not, in general, exhibit the high degree of separation of manganese from iron seen for the manganese dendrites. I found iron to be a major constituent of many samples. More extensive chemical analyses (Carpenter et al., 1975; Nowlan, 1976) indicate that this is generally true for Turkey Creek and Pyrite Creek (Table 1). Nowlan's report of nearly equal amounts of manganese and iron in Pyrite

Creek deposits represents the average composition; my analyses are of the manganese rich areas.

Cave Deposits

The two cave deposits I have examined are both predominantly birnessite and resemble the river deposits in all respects, which is not surprising since they came from dry streambeds in caves. Birnessite and romanechite have previously been reported from caves (Moore and Nicholas, 1964), where they form coatings on stream cobbles and soot-like layers on walls and other cave surfaces.

Miscellaneous

Subglacial manganese deposits: I have examined samples from two areas where a receding glacier has exposed bedrock surfaces stained with manganese oxides. The infrared spectrum of the manganese oxide is attributable to either a disordered birnessite or a disordered todorokite (Figure 6). The latter is a better match although the intensity of the lower energy birnessite band is variable (Chapter 2). I have suggested (Chapter 2) that birnessite and todorokite disorder to the same structural entity. If this suggestion is correct, a continuum exists between the two structures, and as disorder increases the distinction between the two minerals becomes meaningless. Except for a slight increase in the amount of chlorite, the bulk of the stained material does not differ from the rock matrix, which is predominantly quartz. In both samples iron, probably as iron oxide, is a major constituent. It appears that the oxides are deposited on the rock in relatively pure form, although a correlation of stain with the presence of a clay source has been noted

Figure 6. Infrared spectra identifying birnessite in subglacial deposit #33

A. Disordered todorokite standard #57, 75% intensity

B. Birnessite standard #47, 60% intensity

C. Difference spectrum of D and E, 100% intensity

D. Unextracted subglacial deposit, 100% intensity

E. Extracted subglacial deposit, 53% intensity

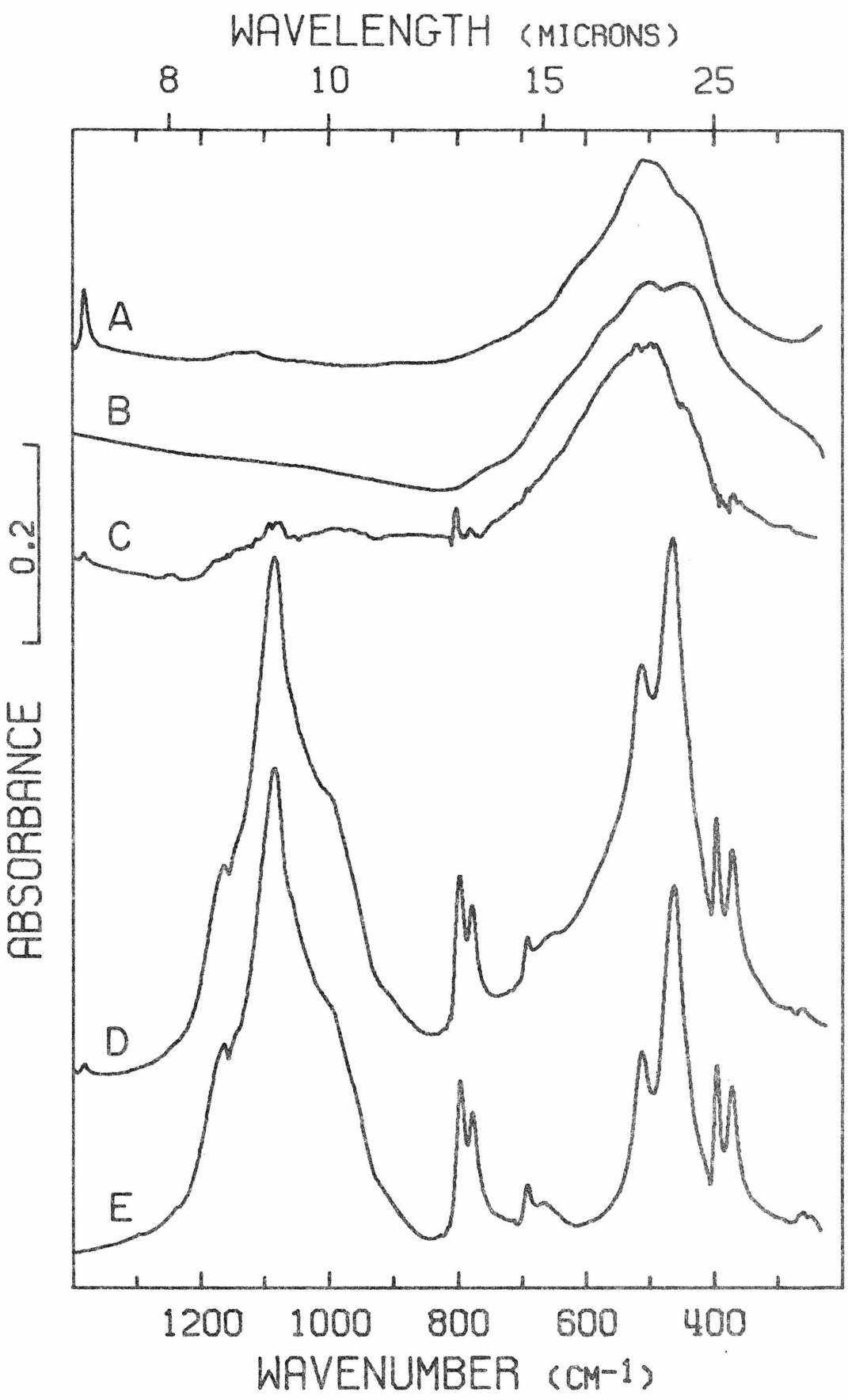
WAVELENGTH (MICRONS)
8
10
15
25
A
B
C
D
E
0.2
ABSORBANCE
1200
1000
800
600
400
WAVENUMBER (CM-1)

(B. Kamb, California Institute of Technology, personal communication, 1978).

Crack deposits: The two manganese crack deposits I have examined resemble manganese dendrites in manganese mineralogy, accessory mineralogy, and iron content. I have too few samples to generalize from these results. These crack deposits formed at unknown depth within the rock and should be distinguished from more surficial crack deposits which have formed within the upper few centimeters of the crack in association with desert varnish at the surface and iron oxide-clay deposits deeper in the crack. The appearance and association of these surficial crack deposits suggests that they resemble desert varnish in mineralogy and composition.

Counterfeit manganese deposits: Polished surfaces, organic matter, and iron oxide with traces of manganese oxide can each give the appearance of a manganese oxide stain. Although careful field examination can generally distinguish these phenomena from manganese concentrations it is sometimes necessary to ascertain the presence of manganese oxide by laboratory tests. Several examples are listed in Table 1.

CONCLUSIONS

My results indicate that distinctions between manganese oxide concentrations based on their morphologic relations in the terrestrial weathering environment have a sound basis in terms of the mineralogy of the manganese oxides and their accessory minerals. Desert varnish, manganese dendrites, and stream deposits each have a characteristic mineralogy which reflects their different morphologies and

environments. Desert varnish is composed predominantly of illite-montmorillonite and kaolinite clay minerals with lesser and somewhat variable amounts of hematite and birnessite. In manganese dendrites, the manganese is generally present as romanechite or a hollandite group mineral and is sometimes the major constituent of the dendrites. The accessory silicate mineralogy is variable, and iron oxide is present in only trace amounts. Manganese oxide of a birnessite mineralogy is the dominant phase in manganese stream deposits, but minor iron oxide and clay minerals are generally present. The diverse mineralogy previous workers have reported for manganese soil concretions (Taylor et al., 1964; Gallaher et al., 1973; Ross et al., 1976) contrasts with desert varnish, manganese dendrites, and stream deposits. This reflects the wide range of environmental conditions possible in soils. Data on several subglacial deposits and crack deposits (Table 1) suggests that the former resemble river deposits and the latter, manganese dendrites. This is reasonable in terms of the environmental conditions.

The characteristic differences I have discussed may reflect differences in the formation mechanisms of the manganese deposits and are therefore useful in further understanding these mechanisms. The variable mineralogy and quantity of manganese dendrite accessory minerals and their frequent similarity to minerals of the rock matrix argue strongly that they are simply passive contaminants. I can rule out several of the possible factors which might control a romanechite vs hollandite group mineralogy in manganese dendrites. The presence of Ba does not direct the mineralogy to romanechite as evidenced by the

presence of hollandite in three dendrites. Rock lithology shows no correlation with mineral species, nor does the relation of the dendrite to the rock (internal, fracture surface, or surficial). Romanechite is stable to conversion to hollandite up to at least 400°C (Fleischer, 1960) so that thermal history, except as it may influence primary mineralogy, is probably not an important factor in this regard. The relation between romanechite and hollandite is a closer one than distinct mineral names might suggest. Turner and Buseck (1979) have shown that intergrowth occurs between the two minerals at the level of the unit cell and have explained variations in romanechite X-ray diffraction patterns on that basis. Several of my samples have infrared spectra intermediate between those of romanechite and hollandite (Figure 7). This may be the result of intimate structural intergrowth although it could be explained by a simple physical mixture. I found no evidence for mixed phases under the scanning electron microscope. The intensities of the water absorption bands in the 4000 cm^{-1} to 1400 cm^{-1} do not follow the trend set by the absorption bands in the 1400 cm^{-1} to 200 cm^{-1} region, which are due to vibrations of the ring framework of MnO_6 octahedra. This reflects the variable amounts of water in romanechite and suggests that water is not important in controlling the mineralogy.

At the Cady Mountain locality I found desert varnish (#10) and crack deposits (#36) developed within a meter of each other. Several meters away were manganese dendrites (#22). The varnish has birnessite and the crack deposit and dendrites are romanechite-hollandite intergrowths (Figure 7). Clay minerals are not detectable

Figure 7. Infrared spectra illustrating the range between pure romanechite and pure hollandite structures

A. Cryptomelane (hollandite group) standard #28, 90% intensity

B. Crack deposit # 36, 105% intensity (sample has contaminating silicates)

C. Manganese dendrite #22, 94% intensity

D. Romanechite standards # 38 (4000 cm^{-1}-1400 cm^{-1}) and #34 (1400 cm^{-1}-200 cm^{-1}) 100% intensity

Figure on following two pages.

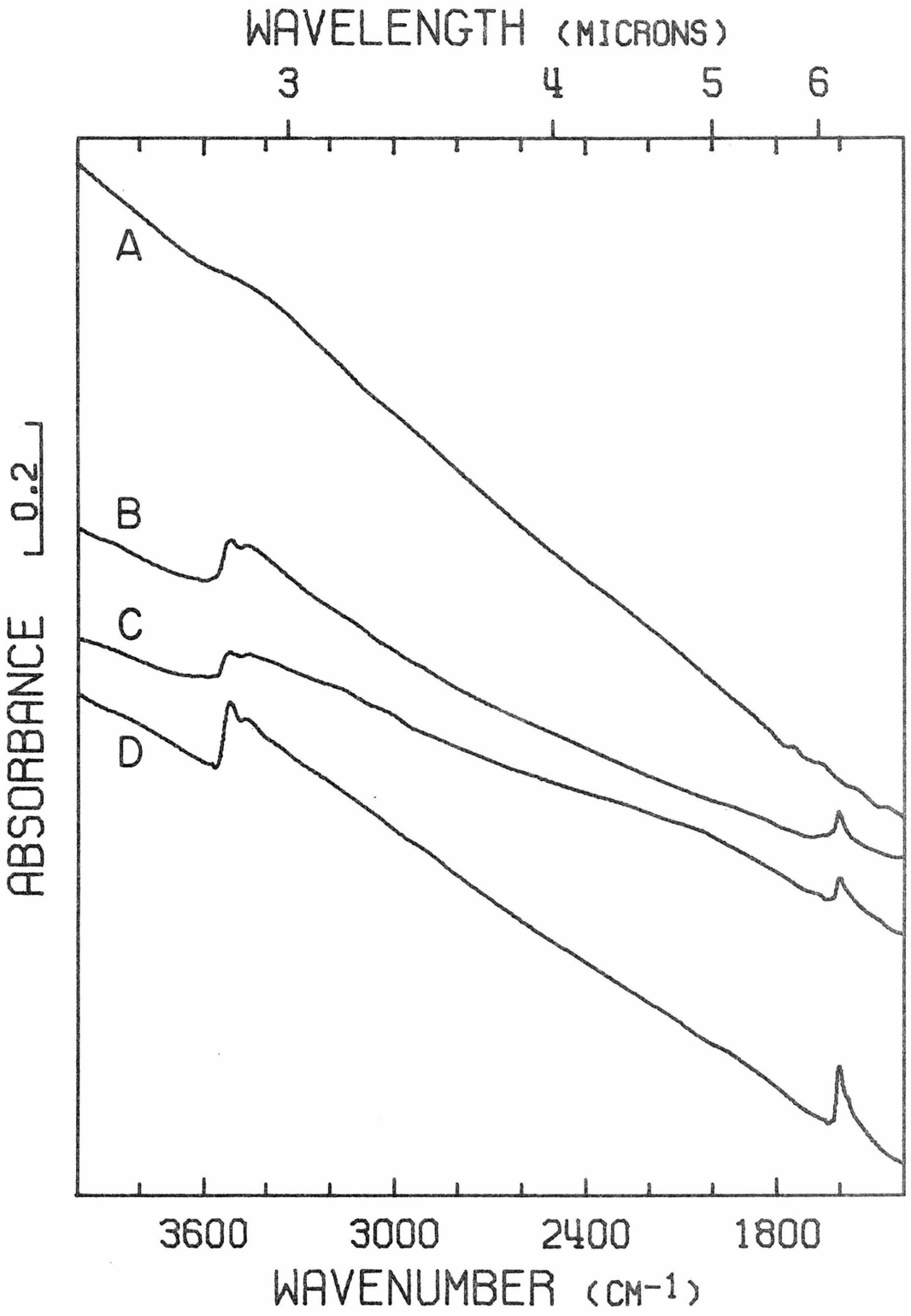
WAVELENGTH (MICRONS)
3
4
5
6
A
B
C
D
0.2
ABSORBANCE
3600
3000
2400
1800
WAVENUMBER (CM-1)

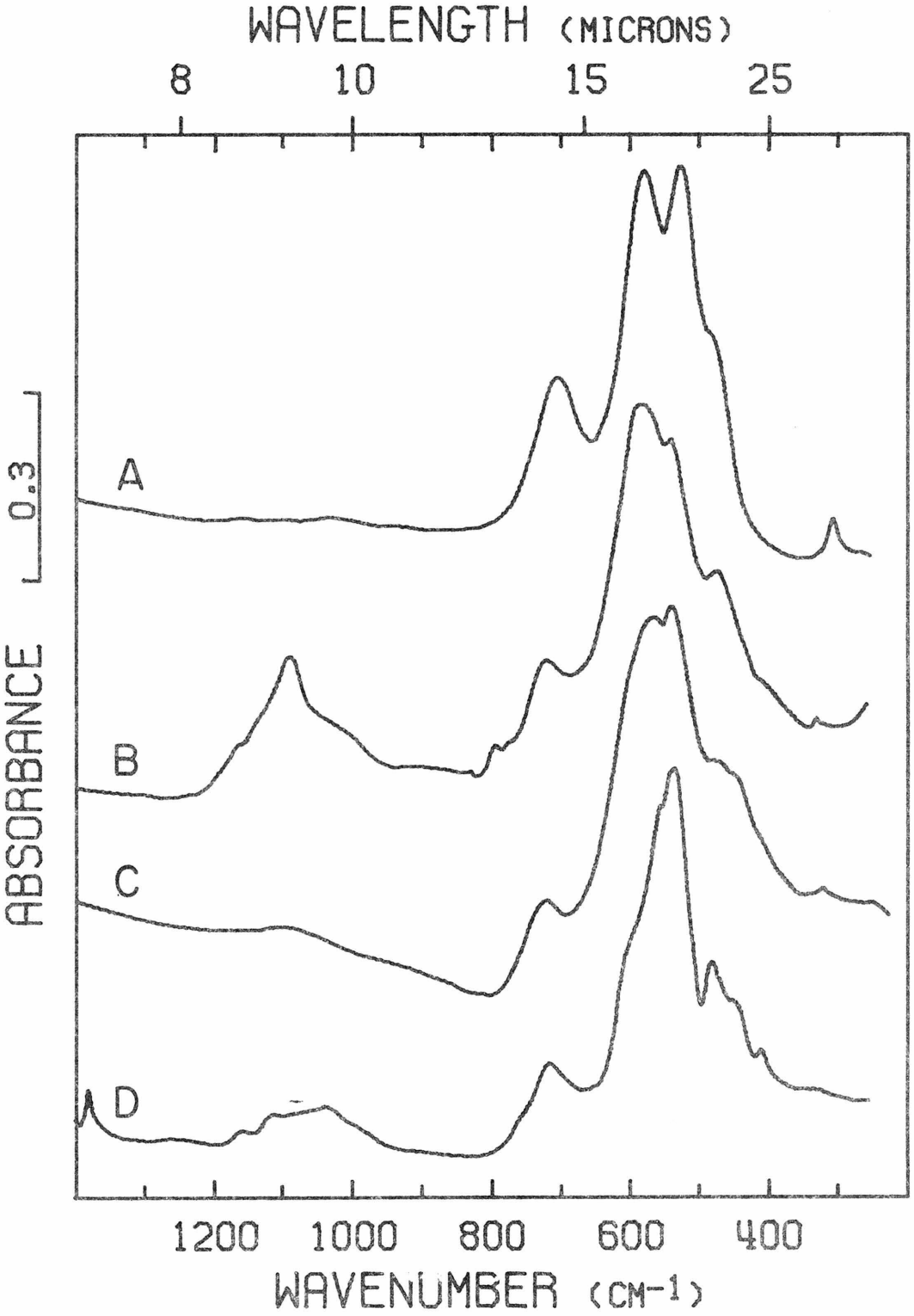

Figure 7. Continued from preceding page

in either the crack deposit or the dendrites. It is not known how far below the ground surface or at what time the crack deposits and dendrites formed, but the occurrence in close proximity of manganese oxide concentrations which differ markedly in manganese oxide mineralogy suggests that the accessory clay minerals may be an important factor in controlling manganese oxide mineralogy. Although the presence of clay minerals is not a sufficient condition for birnessite formation (some manganese dendrites have appreciable clay associated with hollandite or romanechite) it appears to be necessary. Clay minerals are an integral part of desert varnish, which invariably has birnessite. All stream deposits with birnessite mineralogy are associated with clay minerals. The only stream deposit lacking clay minerals is the nsutite from Pyrite Creek. Environmental conditions do not appear to be responsible for the distinctive mineralogy of the Pyrite Creek deposit. The Shawn Creek deposit has the normal birnessite mineralogy. These two streams are within 20 km of each other in western Maine and differ only in water trace element chemistry (Nowlan, 1976); Pyrite Creek water is anomalously high in lead and zinc. I know of no reason why this should lead to nsutite formation.

Burns and Burns (1977) have suggested that epitaxial growth on iron oxides may be responsible for the occurrence in marine manganese nodules of δ-MnO_2, which is a disordered birnessite. With the exception of some birnessite soil concretions (Taylor et al., 1964), there is a good correlation between birnessite mineralogy and iron content in manganese oxide deposits of the terrestrial weathering

environment.

Infrared spectroscopy has provided mineralogical information on deposits which are too poorly crystalline, too finely particulate or too highly contaminated with other crystalline phases for successful study by X-ray diffraction. It is hoped that infrared spectroscopy will find wider application to more detailed investigation into the genetic nature and relationships of the various manganese oxide concentrations.

PART 2

In a study of the chemical remanent magnetization of sediments in Baja California, Larson and Walker (1975) reported the presence of manganese-rich concretions which were found to carry remanent magnetization in numerous sedimentary horizons of late cenozoic age. They informally named the manganese oxide phase "hydropsilomelane" due to similarities in both chemistry and X-ray diffraction pattern to the manganese oxide romanechite (psilomelane). I have studied these concretions as part of the survey concerned with the mineralogy of manganese oxides in the terrestrial weathering environment.

Samples for infrared and qualitative chemical analysis are from a locality 56 km. south of San Felipe, Baja California, Mexico, and consist of weakly cemented siltstone in which the concretions are dispersed. The siltstone was disaggregated by immersion in water and the concretions hand-picked from the coarse fraction of the sediment. Removal of the manganese by chemical extraction (Mehra and Jackson, 1960) showed that the bulk of each of the concretions consists

Figure 8. (Following two pages) Infrared spectra of hydropsilomelane concretions compared to reference manganese oxide spectra

A. Reference spectrum of chalcophanite

B. Reference spectrum of aurorite

C. Difference spectra attributable to the manganese oxide phase in the concretion

D. Whole concretion showing bands attributable to calcite (c), kaolinite (k), mica (m), and quartz (q)

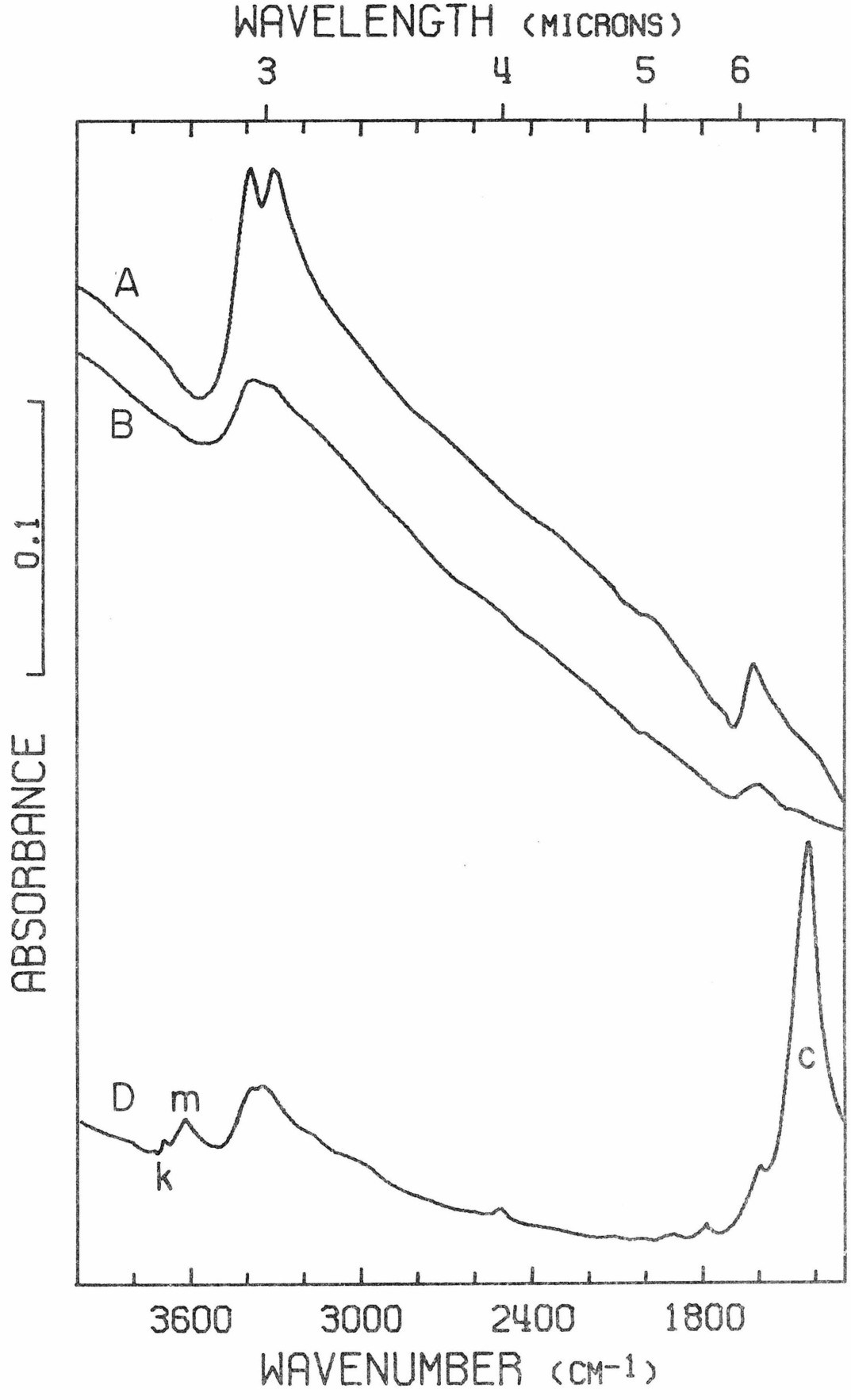
WAVELENGTH (MICRONS)
3
4
5
6
A
B
0.1
ABSORBANCE
D
m
k
c
3600
3000
2400
1800
WAVENUMBER (CM-1)

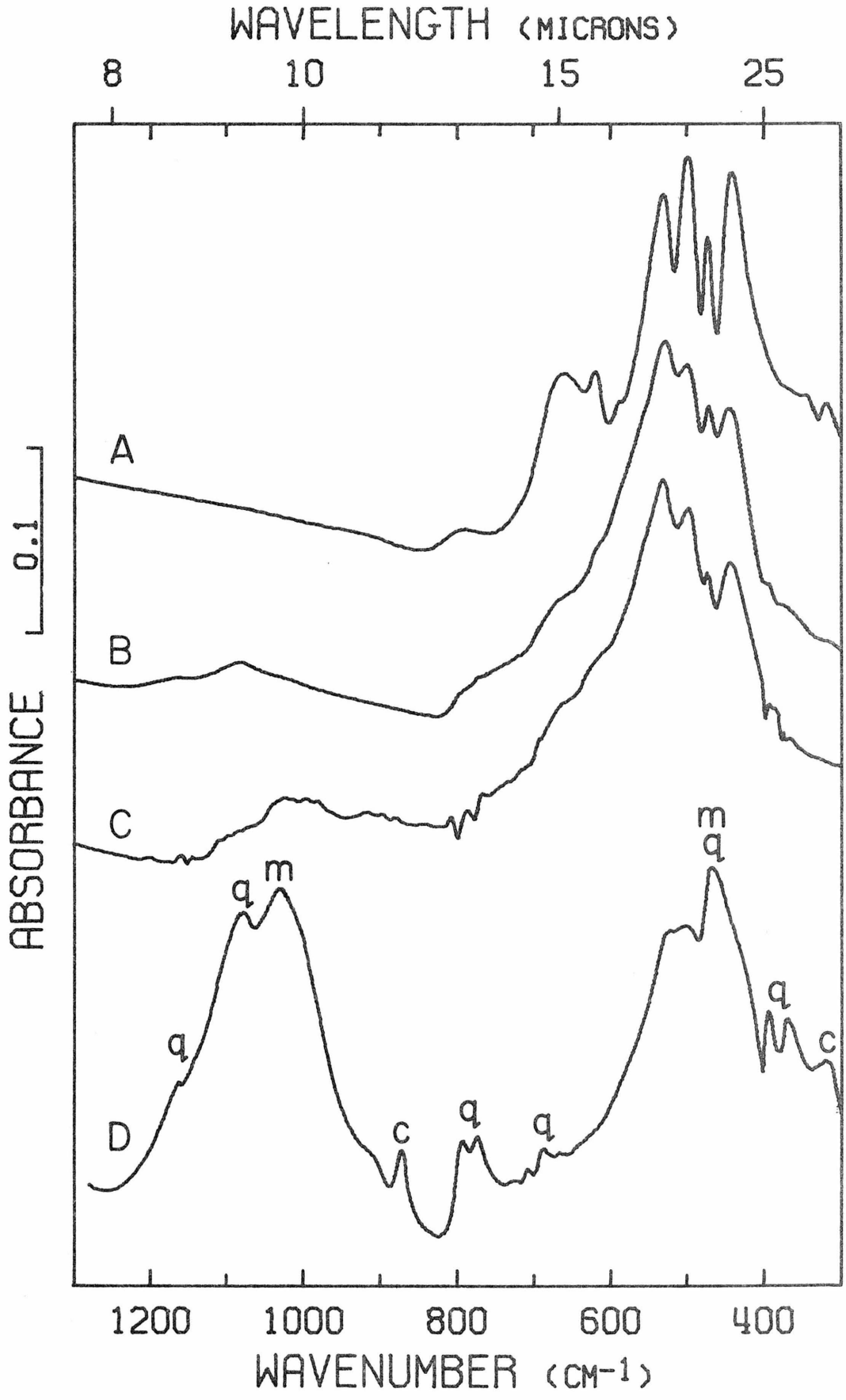
WAVELENGTH (MICRONS)
8
10
15
25
A
B
C
D
0.1
ABSORBANCE
q
m
c
1200
1000
800
600
400
WAVENUMBER (CM-1)

of the siltstone matrix minerals, calcite, quartz, kaolinite, and mica. This is in agreement with the infrared spectra of whole concretions (Figure 8D) obtained by methods reported in Part 1 of this chapter. Its spectrum is dominated by absorption due to the siltstone matrix minerals.

In order to investigate the manganese oxide mineralogy, powdered concretions were washed with 1.0 M acetic acid to remove the calcite, and difference infrared techniques (Part 1, this chapter) were then applied to produce infrared spectra of the pure manganese oxide phase in the concretions. In the 4000 cm^{-1} to 1400 cm^{-1} region of the spectrum absorption due to the hydrous components of the manganese oxide can be seen without interference from the contaminating silicates and strongly suggests a chalcophanite structure based on comparison to standard chalcophanite and aurorite spectra (Figure 8). Absorption in the 1400-200 cm^{-1} region confirms that the manganese oxide has the chalcophanite structure. The positions and number of absorption bands in Figure 8 are diagnostic for minerals of the chalcophanite structure (Chapter 2). Two such minerals are known, chalcophanite and aurorite. These differ in the nature of the cations between the layers of manganese octahedra but are indistinguishable on the basis of their X-ray diffraction and infrared absorption patterns. Chemical analysis of manganese rich areas of the concretions using energy dispersion X-ray analysis under a scanning electron microscope indicated manganese as a major component with lesser amounts of silicon, potassium, calcium, aluminum, magnesium, and sodium. I could find no areas as rich in oxide as that analyzed by

Larson and Walker.

The X-ray and chemical data of Larson and Walker (1975) are in agreement with my infrared results. These X-ray data are a significantly better match to chalcophanite and aurorite than to romanechite (Table 2). Larson and Walker report that heating at 550°C caused the 6.95 Å X-ray peak to disappear and a new one to develop at 4.87 Å. This is strongly reminiscent of the behavior of chalcophanite on heating (Dasgupta, 1974), in which the 6.96 Å chalcophanite line disappears and an intense 4.76 Å line is produced. Larson and Walker's chemical data yield the following formula on the basis of 7 oxygens (excluding water) with all of the Mn in the +4 oxidation state:

$$(Mg_{0.6}Ba_{0.1}Fe_{0.1})(Mn_{3.0}Al_{0.1})O_7 \cdot 2H_2O$$

This is in agreement with the formula of a predominantly magnesian chalcophanite, $MgMn_3O_7 \cdot 3H_2O$ if allowance is made for uncertainty in water content, which was determined by difference of the microprobe analysis from 100 percent. If some manganese is present as Mn^{2+}, as seems probable from chalcophanite analyses (Palanche et al., 1944), the agreement would improve. This would increase the interlayer site population, decrease the manganese octahedra layer site population, and increase the water content. The chemical data do not yield a recognizable romanechite formula when calculated on the basis of 10 non-water oxygens. The mutually supporting results of infrared spectroscopy, X-ray diffraction, and chemical analysis leaves little doubt that the manganese oxide in the hydropsilomelane concretions has the chalcophanite structure.

Table 2. X-ray diffraction data for chalcophanite, aurorite, hydropsilomelane, and romanechite*

chalcophanite**		aurorite**		"hydropsilomelane"		romanechite**	
d(A)	I	d(A)	I	d(A)	I	d(A)	I
						9.68	3
6.96	10	6.94	10	6.92	10	6.95	6
4.08	5	4.06	5				
3.50	6	3.46	7	3.48	4	3.48	6
						3.32	3
						3.23	3
		2.76	3			2.88	4
2.57	4	2.54	5				
		2.45	4			2.42	3
		2.40	4	2.40	1	2.41	10
						2.37	5
2.24	5	2.23	5	2.23	4	2.26	4
						2.19	8
		2.13	3			2.15	4
1.90	3	1.90	4	1.89	1	1.82	4
		1.80	3				
1.60	5	1.56	5	1.59	1	1.56	3
1.43	3	1.43	5	1.38	2	1.42	3

*Data from the following sources: chalcophanite, J.C.P.D.S. File Card No. 15-807; aurorite, Radtke et al., 1967; hydropsilomelane, Larson and Walker, 1975; romanechite, J.C.P.D.S. File Card No. 14-627.

**Lines with intensity lower than 3 have been omitted.

This manganese oxide phase differs from all other previously reported minerals with the chalcophanite structure in the nature of the substitution for the interlayer cation. My reformulation of the chemical data of Larson and Walker indicates that Mg^{+2} is the cation predominantly substituting for Zn^{+2} although some Mn^{+2} is probably present. There is no evidence for any Zn^{+2} or Ag^{+} in the structure. This lends support to the idea that wide compositional variations exist for chalcophanite (Radtke, et al., 1967). I suggest that variation in the nature of interlayer cations in minerals of the chalcophanite structure is sufficiently large to justify the designation of a chalcophanite group.

The paragenesis of the phase I am describing is different from that of other occurrences of manganese oxides with the chalcophanite structure and may indicate a significantly larger range of occurrence than has previously been recognized. Chalcophanite group minerals have been thought to be relatively rare and of secondary origin associated with extensive manganese mineralization. In Baja, the occurrence is as a primary mineral formed authegenically in silt deposits with no relation to any other manganese mineralization (Larson and Walker, 1975). Larson and Walker suggest that these manganese concretions may be a common feature of continental playa sediments. Their report that the concretions carry remanent magnetization makes the study of the effect of interlayer cation substitution on the magnetic properties of chalcophanite group minerals a matter of importance to paleomagnetic investigations.

REFERENCES

Burns, R.G., and Burns, V.M. (1977) Chapter 7, Mineralogy. In G.P. Glasby, Ed., Marine Manganese Deposits, p. 185-248. Elsevier, Amsterdam.

Buser, W., Graf, P., and Feitknecht, W. (1954) Beitrag zur Kennthis der Mangan(II)-manganite und des δ-MnO_2. Helvetica Chim. Acta, 37, 2322-2333.

Carpenter, R.H., Pope, T.A., and Smith, R.L. (1975) Fe-Mn oxide coatings in stream sediment geochemical surveys. J. Geochem. Exploration, 4, 349-363.

Dasgupta, D.R. (1974) Oriented transformation of chalcophanite during thermal treatment. Z. Kristallogr., 139, 116-128.

Fleischer, M. (1960) Studies of manganese oxide minerals. III. Psilomelane. Am. Miner., 45, 176-187.

Gallaher, R.N., Perkins, H.F., Tan, K.H., and Radcliffe, D. (1973) Soil concretions: II. Mineralogical analysis. Proc. Soil Sci. Soc. Am., 37, 469-472.

Larson, E.E., and Walker, T.R. (1975) Development of chemical remanent magnetization during early stages of red-bed formation in late Cenozoic sediments, Baja California. Geol. Soc. Am. Bull., 86, 639-650.

Mehra, O.P., and Jackson, M.L. (1960) Iron oxide removal from soils and clays by a dithionite-citrate system buffered with sodium bicarbonate. In A. Swineford, Ed., Proc. of the Seventh Natl. Conf. on Clays and Clay Miner., p. 317-327. Pergamon, Oxford.

Moore, G.W., and Nicholas, G. (1964) Speleology. D.C. Heath and Company, Boston.

Nowlan, G.A. (1976) Genesis of manganese-iron oxides in stream sediments in Maine. United States Geological Surv. Open-File Report 76-878.

Palanche, C., Berman, H., and Frondel, C. (1944) Dana's System of Mineralogy, Vol. 1, Elements, Sulfides, Sulfosalts, Oxides. John Wiley and Sons, Inc., New York.

Radtke, A.S., Taylor, C.M., Hewett, D.F. (1967) Aurorite, argentian todorokite, and hydrous silver-bearing lead manganese oxide. Econ. Geol., 62, 186-206.

Ross, Jr., S.J., Franzmeier, D.P., and Roth, C.B. (1976) Mineralogy and chemistry of manganese oxides in some Indiana soils. Proc. Soil Soc. Am., 40, 137-143.

Taylor, R.M., McKenzie, R.M., and Norrish, K. (1964) The mineralogy and chemistry of manganese in some Australian soils. Aust. J. Soil Res., 2, 235-248.

Turner, S., and Buseck, P.R. (1979) Some manganese oxide tunnel structures and their intergrowth. Science (in press).

CHAPTER 4 APPENDIX A

This appendix contains infrared spectra of those manganese oxide concentrations listed in Table 1 which are not shown in figures included in the text. These spectra are the basis for identification of the manganese oxide mineralogy. In those cases in which silicate contamination is negligible, the spectrum of the whole concentration is presented. In those cases in which the infrared difference technique was used for manganese oxide identification, the difference spectrum, in which the silicate absorption has been removed, is presented. For two manganese dendrite samples, it was not possible to use the difference technique because too little material was available. In these instances the spectrum of the rock matrix, which probably reflects the mineralogy of the silicate contamination, is included for comparison with the spectrum of the whole manganese dendrites (Figure 4A). All spectra are presented at the measured concentration of the 0.5 mg KBr pellets. Where applicable, that fraction of the extracted residue spectrum necessary to null the silicate absorption in the spectrum of the untreated material is noted in the figure caption as a percentage in parentheses. The difference of this number from 100 is roughly proportional to the amount of oxide present in the deposit. Samples are identified in the figure captions by their Table 1 sample numbers.

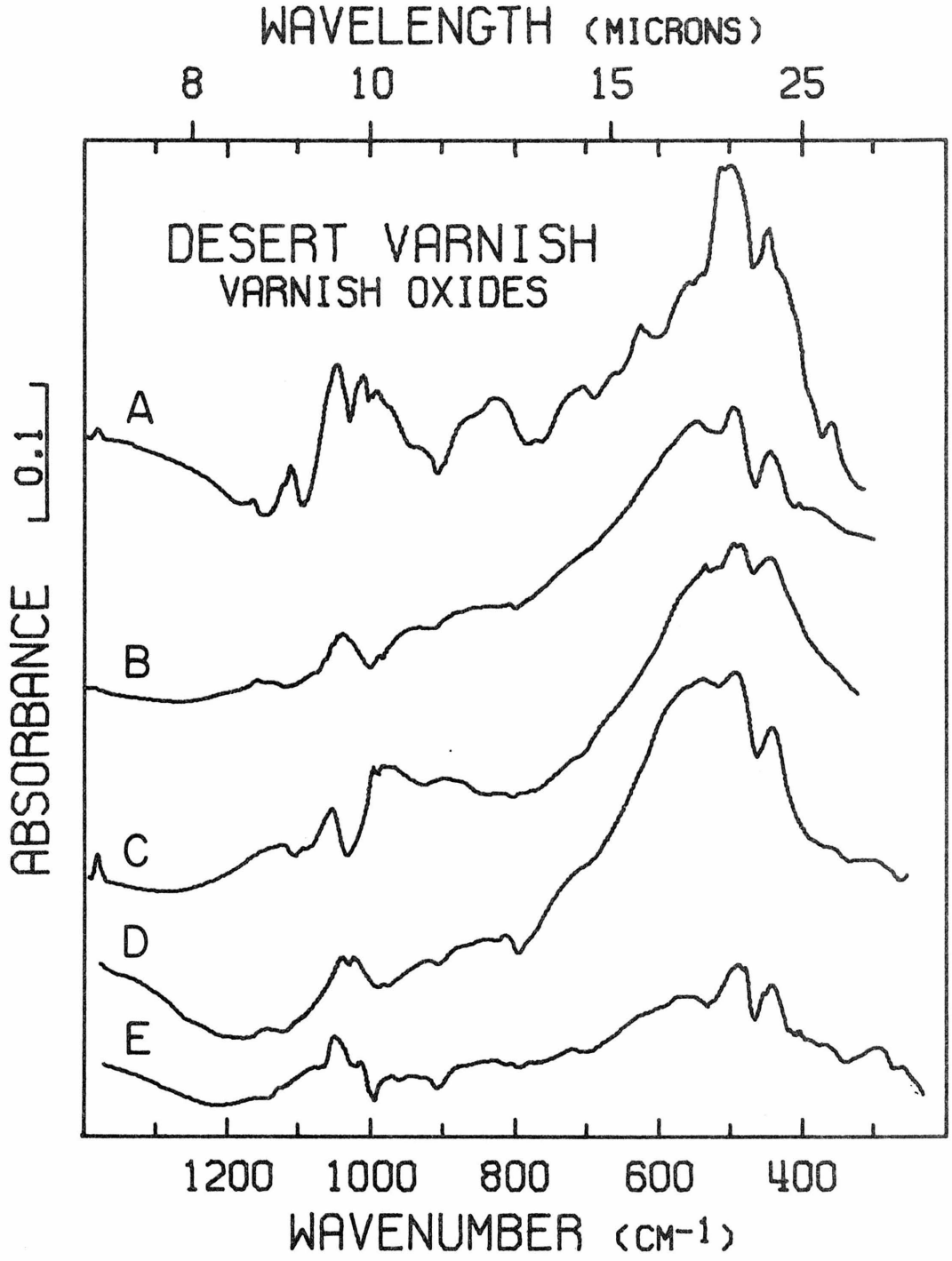

Figure 1A. Desert varnish difference spectra: A. #4 (107%); B. #7 (55%); C. #10 (70%); D. #11 (78%); E. #13 (89%)

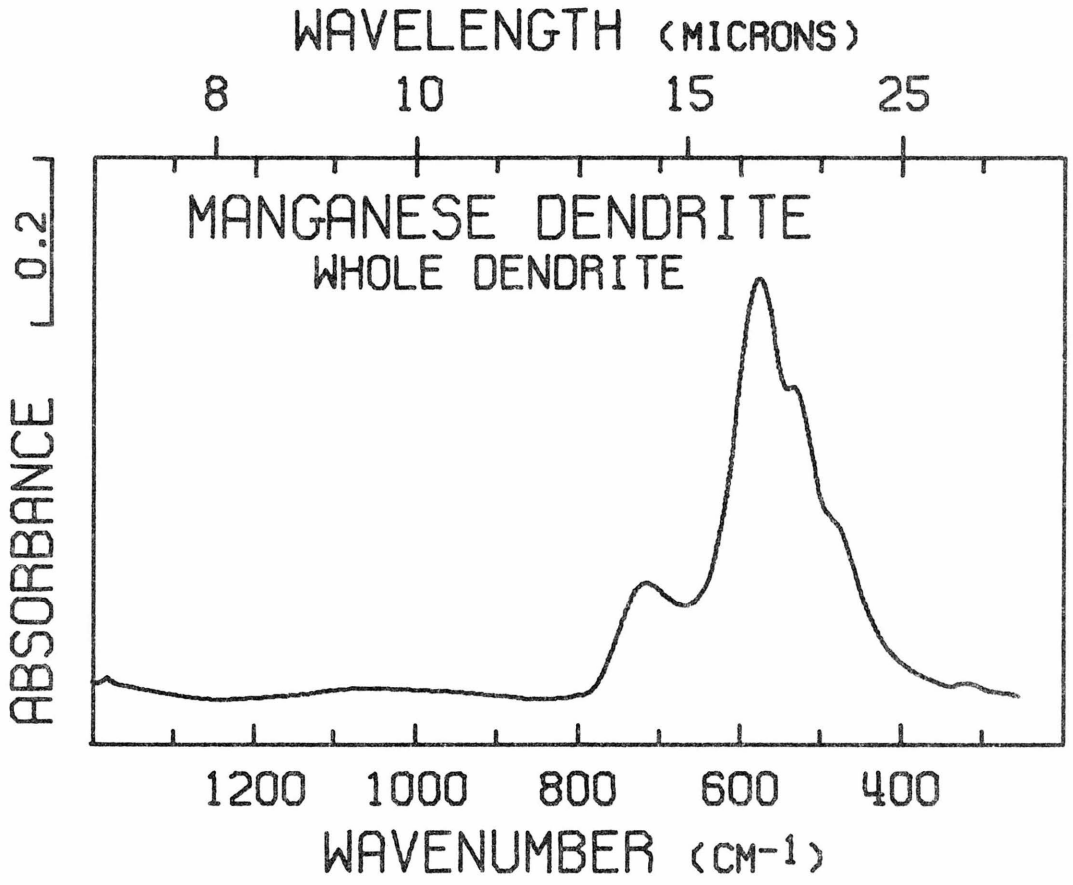

Figure 2A. Manganese dendrite #15.

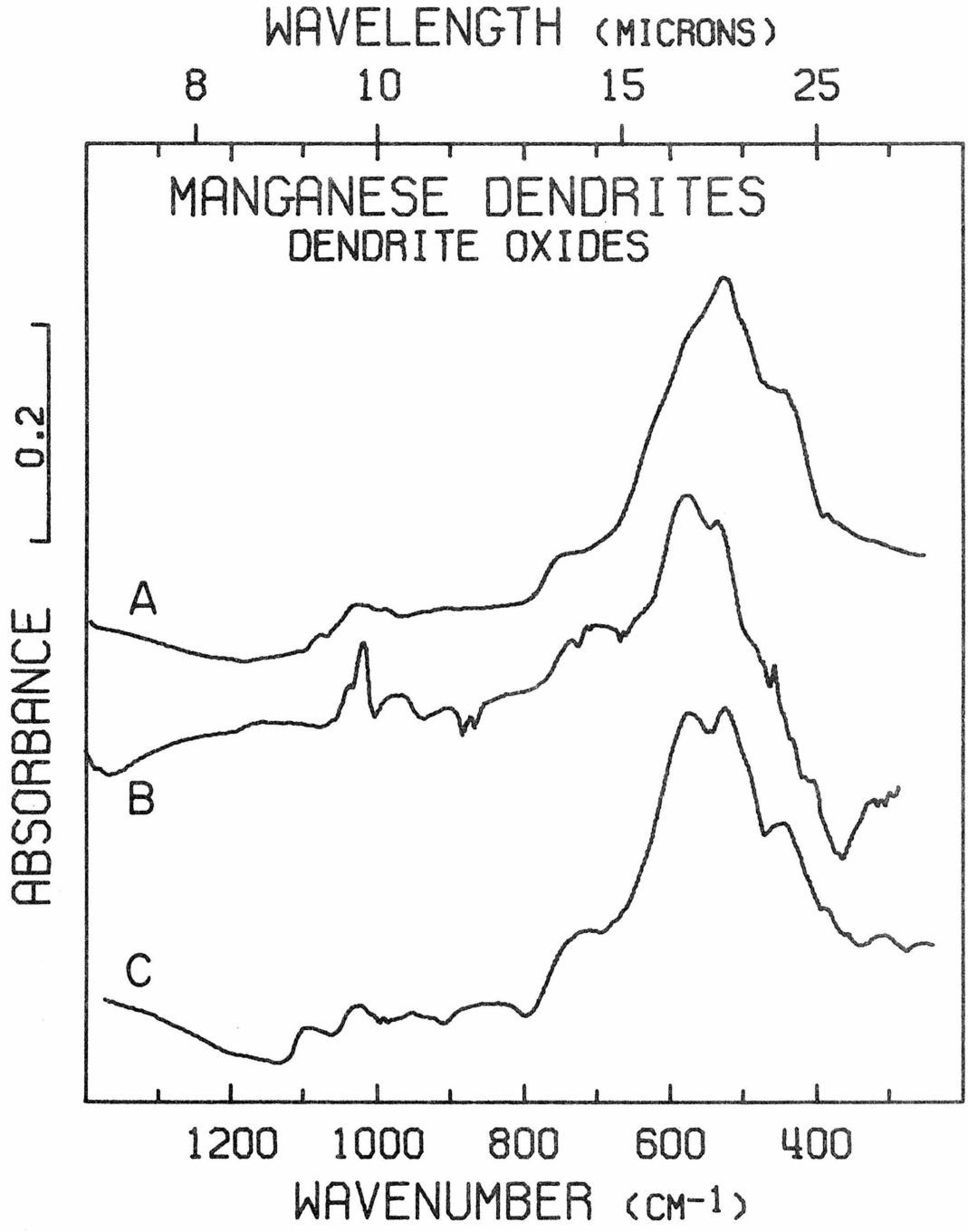

Figure 3A. Manganese dendrite difference spectra: A. #19 (48%); B. #21 (70%); C. #23 (49%)

Figure 4A. Manganese dendrites compared to their rock matrices:

A. Manganese dendrite #20

B. Rock matrix of manganese dendrite #20

C. Manganese dendrite #16

D. Rock matrix of manganese dendrite #16

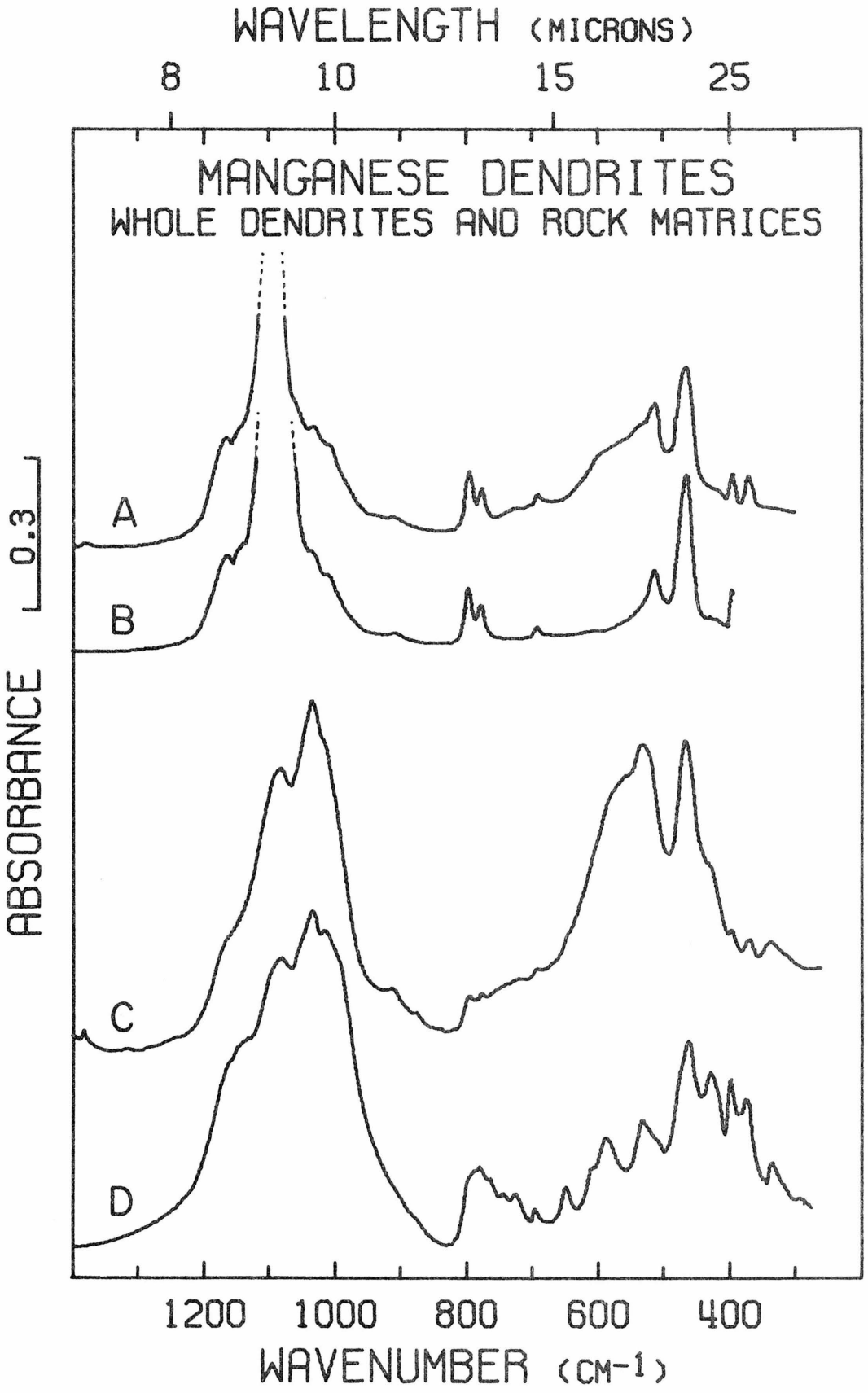
WAVELENGTH (MICRONS)
8
10
15
25
MANGANESE DENDRITES
WHOLE DENDRITES AND ROCK MATRICES
A
B
C
D
0.3
ABSORBANCE
1200
1000
800
600
400
WAVENUMBER (CM-1)

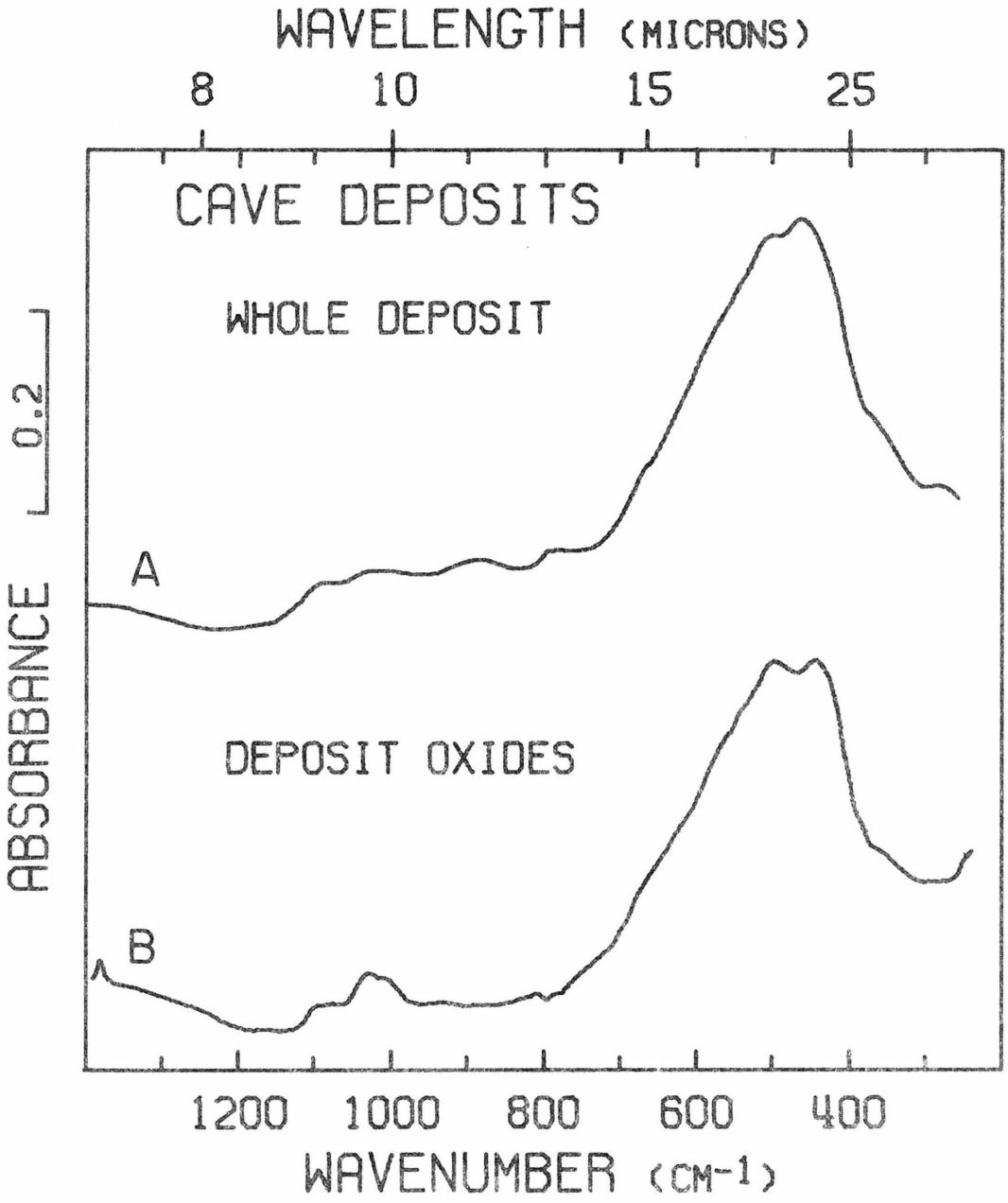

Figure 5A. Manganese cave deposits: A. #25; B. Difference spectra; #26 (33%)

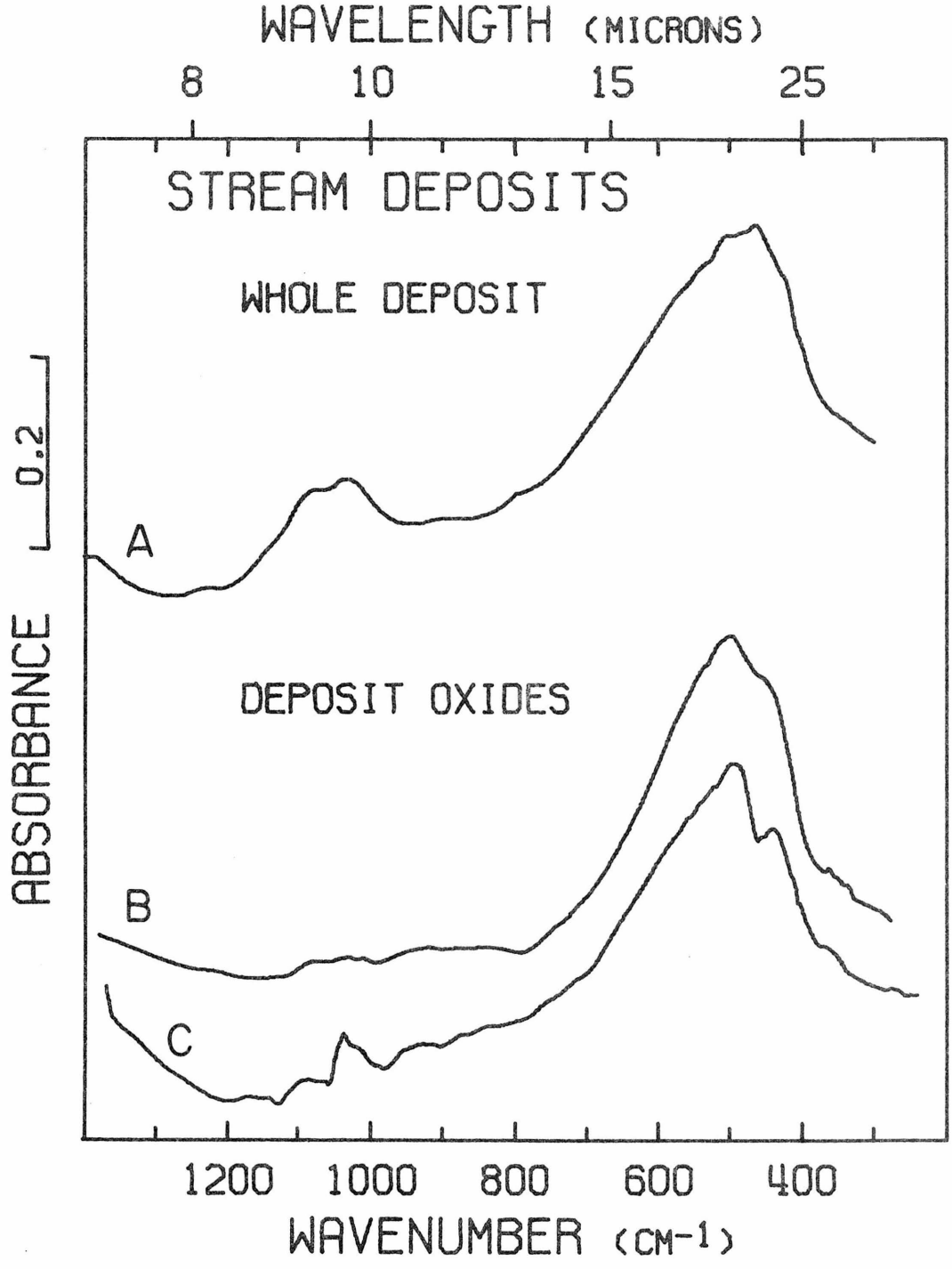

Figure 6A. Manganese stream deposits: A. #27; B. Difference spectra; #28 (27%); C. Difference spectra; #29 (99%)

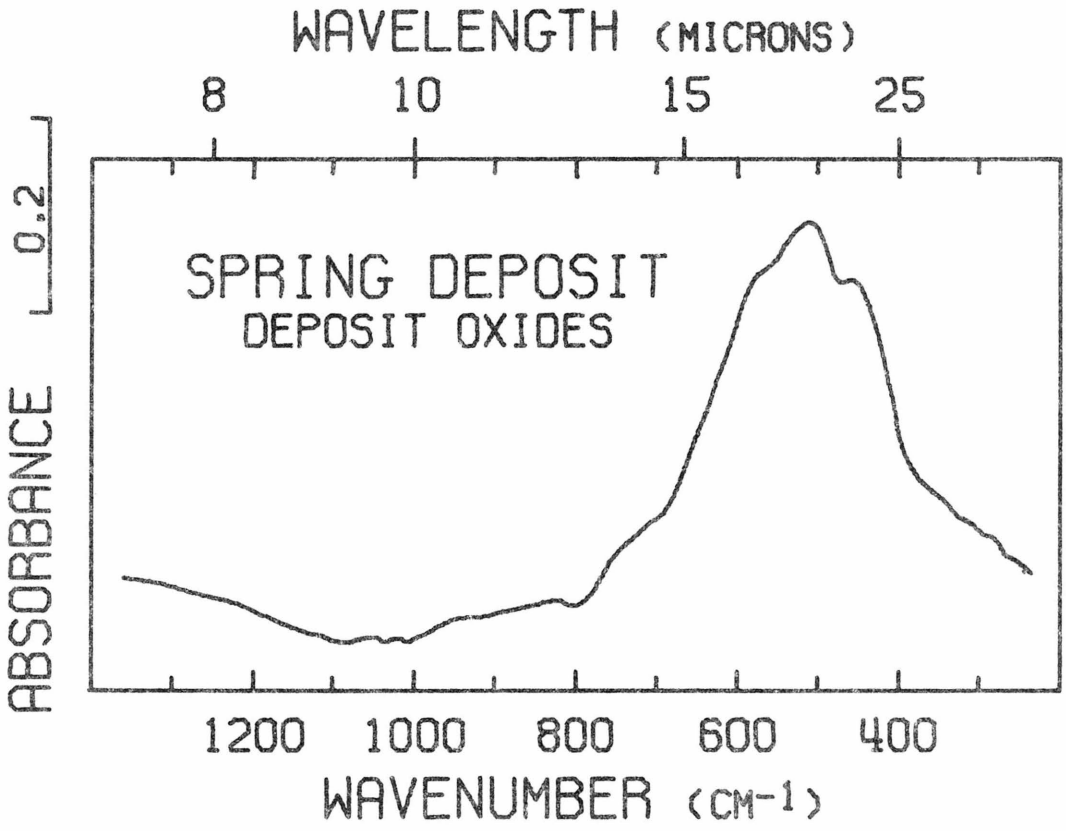

Figure 7A. Manganese spring deposit difference spectrum #32 (27%)

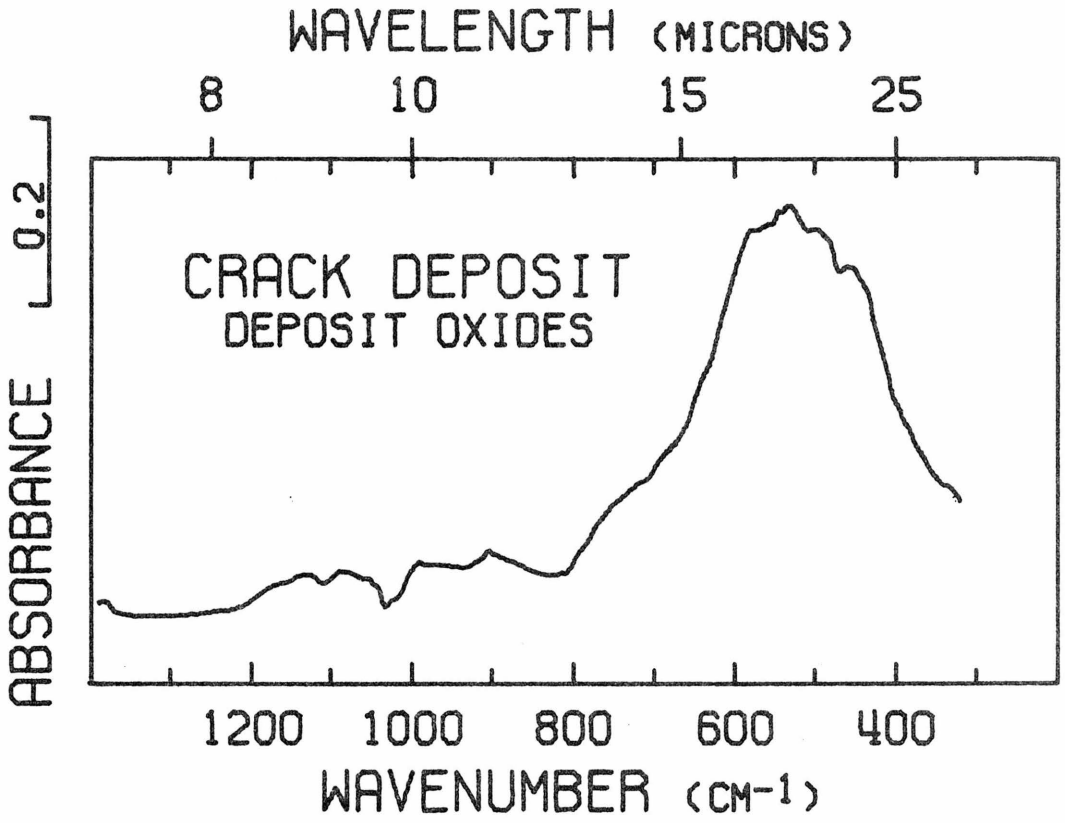

Figure 8A. Manganese crack deposit difference spectrum #35 (45%)

CHAPTER 4 APPENDIX B

This appendix contains more detailed information on the sample localities of Table 1.

Desert varnish #1: Four Buttes, California. Detailed information is found in Chapter 3.

Desert varnish #2: Salt Spring, California. Detailed information is found in Chapter 3.

Desert varnish #3: Stoddard Wells, California. Detailed information is found in Chapter 3.

Desert varnish #4: Little Colorado Canyon, Arizona. Collected by the author. Cameron Quadrangle, Arizona, 1955 ed.; in the southeast corner of Section 22, T.29 N., R.9 E. Samples are from streaks of varnish (manganese veils) on the canyon walls just to the east of the bridge carrying U.S. Route 89 over the canyon at Cameron, Arizona.

Desert varnish #5: Biklabito, New Mexico. Collected by the author. Rattlesnake Quadrangle, New Mexico, 1937 ed.; near 36° 1' N. Lat., 109° W. Long. Samples are from several localities just north of New Mexico Highway 504 approximately 2 km. west of Biklabito, New Mexico.

Desert varnish #6: Petroglyph Park, New Mexico. Samples were collected by the author from outcrops just south of Indian Petroglyph State Park , which is located near Albuquerque, New Mexico, west of Arizona Highway 448.

Desert varnish #7: Thunderbird Park, Arizona. Collected by R. Perry, University of Washington. Hedgepeth Hills Quadrangle,

Arizona, 1957 ed.; near the center of the quadrangle. Sample is from a locality about 2.5 km. north of Thunderbird State Park, New Mexico.

Desert varnish #8: Funeral Peak, California. Collected by the author. Funeral Peak Quadrangle, California, 1951 ed.; near 36° 7' N.Lat., 116° 44' W. Long. Samples are from a colluvial cone on the east wall of Death Valley, California, approximately 100 m. east of California Highway 178.

Desert varnish #9: Olo Canyon, Arizona. Collected by R.P. Sharp, California Institute of Technology. Samples are from along the Colorado River near Lava Falls, where Olo Canyon intersects the Grand Canyon.

Desert varnish #10: Cady Mountains, California. Collected by G.R. Rossman, California Institute of Technology. Broadwell Lake Quadrangle, California, 1955 ed. Samples are from a single locality in the vicinity of sections 21, 27, and 28, T.8 N., R.78.

Desert varnish #11: Lake Pleasant, Arizona. Samples collected by M. Furst, California Institute of Technology, from an outcrop of the Pike's Peak iron-formation approximately 10 km. west of Lake Pleasant, Arizona.

Desert varnish #12: Eetza Mountain, Nevada. Collected by J.C. Bard, Lawrence Berkeley Laboratory. Carson Lake Quadrangle, Nevada, 1951 ed. Samples are from parts of sections 28 and 29, T.18 N., R.30 E.

Desert varnish #13: Negev Desert, Israel. Collected by A.J. Jelinek, University of Arizona, from a locality about 155 km

south of Beershiva, Israel, on the road to Eilat.

Desert varnish #14: Fort Davis, Texas. Sample collected by J.D. Hayden, Tucson, Arizona, from a locality near Davis Mountain, northwest of Fort Davis, Texas.

Manganese dendrite #15: Soda Mountains, California. Sample collected by the author near 35° 20' N. Lat., 116° 10' W. Long. from a stream cobble of undetermined bedrock source.

Manganese dendrite #16: Southwestern United States. No more detailed geographical information available.

Manganese dendrite #17: South Dakota. No more detailed geographical information available.

Manganese dendrite #18: Pala, California. Collected by G.R. Rossman, California Institute of Technology. Pechanga Quadrangle, California, 1949 ed.; section 24 T.9 S., R.2 W. Sample is from within the White Queen Mine.

Manganese dendrite #19: Barstow, California. Collected by G.R. Rossman, California Institute of Technology. Lane Mountain Quadrangle, California, 1948 ed.; section 9, T.11N., R.1 W. Samples are from along the Ransburg-Barstow Road.

Manganese dendrite #20: Argus Peak, California. Collected by the author. Trona Quadrangle, California, 1949, ed.; in the south-central part of section 33, T.22 S., R.23 E. Samples are from just to the west of California Highway 178.

Manganese dendrite #21: Afton Canyon, California. Collected by G.R. Rossman, California Institute of Technology. Cave Mountain Quadrangle, section 21, T.11 N., R.6 E. Sample is from an alluvial

boulder of undetermined source.

Manganese dendrite #22: Cady Mountains, California. Samples collected by G.R. Rossman, California Institute of Technology, from within several meters of desert varnish #10.

Manganese dendrite #23: Beechworth, Australia. No more detailed geographical information available.

Manganese dendrite #24: Oro Preto, Brazil. No more detailed geographical information available.

Cave deposit #25: Southeastern United States. Sample provided by K. Nealson, Scripps Institution of Oceanography.

Cave deposit #26: Southeastern United States. Sample provided by K. Nealson, Scripps Institution of Oceanography.

Stream deposit #27: Ladysmith, Wisconsin. Sample provided by R.H. Carpenter, University of Georgia, from the Flambeau River, 1.5 km. south of Ladysmith, Wisconsin.

Stream deposit #28: Athens, Georgia. Sample collected by R.H. Carpenter, University of Georgia, from Turkey Creek (Carpenter et al., 1975).

Stream deposit #29: Pilar, New Mexico. Collected by the author. Taos SW Quadrangle, New Mexico, 1964 ed. Samples are from the splash zone of the Rio Grande River just north of the bridge carrying New Mexico Highway 96 across the river.

Stream deposit #30: Long Pond Quadrangle, Maine. Sample collected by G.A. Nowlan, U.S. Geological Survey, from Pyrite Creek (Nowlan, 1976).

Stream deposit #31: The Forks Quadrangle, Maine. Sample

collected by G.A. Nowlan, U.S. Geological Survey, from Shawn Creek (Nowlan, 1976).

Spring deposit #32: Montezuma, Colorado. Sample provided by G.A. Nowlan, U.S. Geological Survey, from a mountainside deposit believed to be a fossil spring and located approximately 0.5 km. east of Montezuma, Colorado.

Subglacial deposit #33: Jackson Glacier, Montana. Sample collected by B. Hallet, Stanford University, from the base of Jackson Glacier, Glacier National Park, Montana.

Subglacial deposit #34: Khumbu Region, Nepal. Sample collected by B. Hallet, Stanford University.

Crack deposit #35: Sierra National Forest, California. Collected by G.R. Rossman, California Institute of Technology. Giant Forest Quadrangle, California, 1956 ed.; near the center of section 12, T.13 S., R.27 E. Sample is from near California Highway 180 just outside the national forest.

Crack deposit #36: Cady Mountains, California. Sample collected by G.R. Rossman, California Institute of Technology, from within a meter of desert varnish sample #10.

Counterfeit Mn deposit #37: Sierra National Forest, California. Sample collected by G.R. Rossman from a water seep within several meters of crack deposit #35.

Counterfeit Mn deposit #38: Rock Creek, California. Collected by the author. Casa Diablo Mountain Quadrangle, California, Section 2, T.5 S., R.30 E., 1953, ed. Samples are from cobbles in the stream bank.

Counterfeit Mn deposit #39: Summit Meadow Lake, California.

Collected by R. Stoessel, Exxon Production Research, Houston, Texas. Silver Lake Quadrangle, California, 1956 ed.; the southwest corner of section 11, T.9 N., R.17 E. Samples are from the outlet streambed of Summit Meadow Lake.

Counterfeit Mn deposit #40: Meteor Crater, Arizona. Sample collected by G.R. Rossman, California Institute of Technology.

Counterfeit Mn deposit #41: Antarctic. Sample provided by A.J. Bauman, Jet Propulsion Laboratory.

CHAPTER 5
A GENERAL SUMMARY
WITH IMPLICATIONS FOR FUTURE WORK

The purpose of this chapter is to provide a concise summary of the more important conclusions of the work presented in earlier chapters; to consider how it has modified current thought on the subject and where it leads.

Recent research on manganese oxides has been centered on the disordered phases due to their geochemical importance and the poor understanding of their structures. It is becoming increasingly clear, however, that understanding of the commonly well-crystallized, stoichiometric phases such as pyrolusite and ramsdellite is by no means complete. I have found that pyrolusite exhibits not only an orthorhombic distortion of the tetragonal unit cell, but also a large, unexplained variation in its infrared spectrum. Ramsdellite is not stoichiometric MnO_2 but contains water inherent in its structure in a specific crystallographic site. Such unexpected discoveries are grounds for skepticism regarding the supposedly well-known manganese oxide structures and suggest that a careful examination of their structures by modern X-ray crystallographic techniques might prove fruitful.

Much of the confusion concerning the relation of natural phases to each other and to their presumed synthetic analogs is a direct result of the poor response of X-ray diffraction to finely-particulate phases of poor crystalline order. The sensitivity of infrared spectroscopy to short range order makes it ideal for

clarification of these relationships. Todorokite is a valid mineral species which bears no relation to the synthetic phase buserite or to any cation-exchanged derivatives of buserite. Buserite appears to be a highly-hydrated form of birnessite. Birnessite, todorokite, and rancieite all appear to have structures based on layers of manganese octahedra. These structures are distinct from one another although those of birnessite and rancieite appear closely related. Infrared spectroscopy is an effective means for identifying the mineralogy of manganese oxide both in pure form and when highly contaminated by silicates or carbonates. The infrared spectra reflect differences in the organization of the manganese octahedral framework and in the structural nature of the hydrous components and thereby distinguish manganese oxides of different structural groups from one another. Well-crystallized samples of different manganese oxide minerals clearly differ in their infrared spectra, but as crystalline order decreases these differences become more subtle. This raises the practical question of how a mineral is defined. A few small domains of well-crystallized material in a matrix of extreme disorder due to poor crystallinity or small particle size could cause different interpretations of the material's mineralogy. X-ray diffraction would reflect the mineralogy of the small, well-crystallized domains while infrared spectroscopy would reflect the structural nature of the material as a whole. Both present valid, but incomplete, structural descriptions of the material, and this should be borne in mind whenever X-ray diffraction and infrared spectroscopy are applied to poorly-crystalline materials. These considerations have important consequences for my interpretation of the relationship between

birnessite, todorokite, and rancieite. I have suggested that as these minerals become disordered their structural distinctions become less pronounced so that a continuum may exist among them in their disordered forms. The structural homogeneity of the samples on which this interpretation is based needs to be proven before it can be considered as anything more than a suggestion. The morphologic information of conventional transmission electron microscopy and the detailed structural information of high resolution transmission electron microscopy would provide this important addition to the information obtainable by infrared spectroscopy and X-ray diffraction. The integrated use of these four techniques promises to be a powerful method for more detailed investigation of many of the structural variations and relationships which I have suggested.

My work on the tetravalent manganese oxides has provided a solid foundation for an understanding of the mineralogy of manganese oxide concentrations in the terrestrial, weathering environment. The detailed chemical, mineralogical, and structural characterization of desert varnish has significantly altered the prevalent conception of this phenomenon. It is not a stain of manganese and iron oxides in a surficial weathering rind of the rock. It is a distinct entity distinguished from the rock by abrupt changes in chemistry, mineralogy, and morphology. Desert varnish has a characteristic mineral assemblage and overall structural organization: finely-particulate birnessite and hematite are intimately mixed with illite-montmorillonite clays or, more rarely, kaolinite. This characterization constrains some elements of the formation mechanism. Clay minerals in

desert varnish are of external origin and are transported to the rock surface in particulate form by wind and, probably, by water. Manganese and iron are of external origin and water is involved in their transport. The processes of oxide concentration and deposition at the varnish site are not yet fully understood. Clay minerals appear to be necessary for the formation of an oxide stain and I have suggested that this is due to topotactic growth of birnessite on clay minerals. This is supported by the fact that birnessite is invariably associated with clay minerals in all manganese oxide concentrations. The possibility of such a topotactic relationship should be carefully examined since it has important consequences for the formation of desert varnish, marine manganese nodules, and a number of other types of manganese oxide concentrations. Desert varnish does not show great promise as a dating tool; however, the best possibility for this lies in the chemistry of the oxide phases.

The classification of manganese oxide concentrations of the terrestrial weathering environment on the basis of morphology, physical properties, and environment of deposition generally reflects basic differences in manganese oxide and silicate mineralogy. On the basis of manganese oxide mineralogy alone, two groups have emerged: (1) Desert varnish, stream deposits, and a variety of deposits associated with glaciers, caves, and springs are characterized by poorly-crystallized layer-structure manganese oxides such as birnessite and todorokite; (2) Manganese dendrites and crack deposits are characterized by romanechite and the hollandite group minerals, which are ring-structure (channel-structure) manganese

oxides. Except for desert varnish, manganese dendrites, and river deposits, a larger sampling is needed to determine the validity of this grouping and the implications it has for genetic relationships among the concentrations. The results of my work on desert varnish suggest that characterization of other types of manganese oxide concentrations in similar detail would prove extremely fruitful in developing a deeper understanding of the products of the weathering environment and the processes forming them.